Experimental characterization and modeling of the mechanical behavior of filled rubbers under cyclic loading conditions

Yannick Merckel

N° d'ordre : 186

THESE

présentée en vue
d'obtenir le grade de

DOCTEUR

en

Spécialité : Mécanique

par

Yannick Merckel

DOCTORAT DELIVRE PAR L'ECOLE CENTRALE DE LILLE

Titre de la thèse :

Experimental characterization and modeling of the mechanical behavior of filled rubbers under cyclic loading conditions

Caractérisation expérimentale et modélisation du comportement mécanique d'élastomères
chargés sous conditions de chargement cycliques

Soutenue le 26 Juin 2012 devant le jury d'examen :

Président	Laurent Chazeau	Professeur, MATEIS, INSA de Lyon
Rapporteur	Denis Favier	Professeur, 3SR, Université de Grenoble
Rapporteur	Erwan Verron	Professeur, GeM, Ecole Centrale de Nantes
Membre	Julien Caillard	Ingénieur de Recherches, MICHELIN, Ladoux
Membre	Nicolas Saintier	Maître de conférences, LAMEFIP, Arts et Métiers ParisTech
Directeur de thèse	Mathias Brieu	Professeur, LML, Ecole Centrale de Lille
Directeur de thèse	Julie Diani	Directeur de Recherche, PIMM, Arts et Métiers ParisTech

Acknowledgements

First and foremost, I would like to express my deepest gratitude to my supervisors Mathias Brieu and Julie Diani who have both believed in me and have guided me through this work with an extraordinary brio. They have provided me with numerous valuable advices, suggestions and recommendations that have greatly helped me to achieve this work. There incredible enthusiasm and very supportive temperament have encouraged me not only academically, but also professionally and personally.

My sincerest thanks to Denis Favier and Erwan Verron for their valuable time and efforts for having accepted to act as reviewers for this thesis. I also wish to thank Julien Caillard, Laurent Chazeau and Nicolas Saintier for having accepted to take part of the jury as examinators.

I am very grateful to the Michelin company for having initiated this project and for having given me the great opportunity to play a part in it. In particular, I would like to deeply thank Daniel Berghezan, Julien Caillard, Christophe Moriceau, Maude Portigliatti and Fabien Vion-Loisel. They have supported my research from its beginning and have provided me with valuable knowledge and expertise. I also wish to thank the other members of the project AMUFISE, with whom I had numerous fruitful discussions that have contributed to significantly enhance this work.

I would like to thank the members of the Equipe Mécanique et Matériaux of the Ecole Centrale de Lille for their support and the useful discussions that greatly help me to achieve this work.

Contents

Introduction

This thesis is part of a project named AMUFISE (*Analyse MUltiéchelle de la FISsuration des Elastomères chargés*) that is supported by the French *Agence Nationale de la Recherche*. The project aims at improving the quality and the design of tires, what means building lighter tires and increasing their endurance and their safety. For this purpose a thorough understanding of the fatigue damage mechanisms is required. We are interested in the filled rubber part of the tire. Within such materials, the fatigue damage may be characterized by the crack growth. Currently, fatigue crack growth is still not well understood and remains a critical issues. Therefore, the project objective is to develop an experimental and theoretical understanding of multi-scale damage mechanisms at the crack tip and their dependencies to the material microstructure.

Background and aims of this thesis

Up to now, numerous researches on rubber materials have been drawing their attention to fatigue damage under cyclic loading conditions. However, its understanding is still an ongoing issue and there is no general agreement about crack growth mechanisms. Most studies are based on empirical and phenomenological approaches. They aim at capturing the major parameters connected to the crack growth under cyclic loading conditions. The results put in light the main factors driving the fatigue damage, such as the chemical nature of the rubber molecular network, the crosslink density, the amount of fillers, the type of fillers,... However, these studies did not assess the physical and chemical origins of the phenomenon. Currently, the model proposed 40 years ago by Lake and Thomas (1967) is the most reliable model able to relate the physical nature of the rubber network to the fatigue failure properties. However, its use is limited. For instance, the model is well suited for unfilled rubber networks, but it does not account for the filler effect. Let us note that fillers induce a significant reinforcement of the mechanical behavior.

The crack growth within rubber materials submitted to cyclic loading conditions may be decomposed in two issues: the crack initiation and the crack propagation. Fatigue life in tires is driven by propagation, therefore, the project focus on crack propagation. The crack propagation during fatigue loading is characterized by submitting a pure shear sample with a single edge crack to a cyclic loading. The crack propagates along the number of cycles. Experimental results reported by Mzabi (2010) in his PhD thesis reveals that the zone near the crack tip is highly strained and may undergo several hundred percent of strain. Under such a loading intensity, a damage unrelated to the crack growth occurs. Therefore, the material behavior in the highly strained local region changes before the crack propagates through. Currently, the size of the local region impacted by the crack propagation and the mechanical behavior evolution within this region are not clearly established.

Modeling the mechanical behavior of the material in the local highly strained region, in the vicinity of the crack tip, may be a key ingredient in the crack propagation understanding. Basic mechanical experiments at large strain illustrate the strongly non-linear stretch-stress responses of filled rubber materials. Moreover, they highlight a significant damage occurring under cyclic loading conditions. Experimental observations reveal two types of damage that may be studied

independently.

- Filled rubbers materials undergo a significant change in their mechanical behavior when first stretched. This property has been extensively studied by Mullins (1947, 1949, 1950, 1969) and is now referred to as the Mullins softening. The Mullins softening is a large stress-softening. It develops a residual stretch and induces an anisotropy for the mechanical behavior. Although it has been studied for more than six decades, it is still a major difficulty for modeling and understanding the mechanical behavior of rubber materials.

- Once the Mullins softening has occurred during the first cycle, a rubber material submitted to subsequent identical cycles undergo another type of damage. It evolves progressively with the number of cycles and it develops a stress-softening and a residual stretch. Although its evolution between two successive cycles may rapidly become unnoticeable, its cumulative effect when considering a large number of cycles cannot be neglected.

Contributions

The project contributors are the *Manufacture Française des Pneumatiques Michelin*, the *Laboratoire de Physico-chimie des Polymères et des Milieux Dispersés* (*Ecole Supèrieure de Physique et Chimie Industrielle de Paris*), The *Laboratoire de Mécanique et de Technologie* (*Ecole Normale Supérieure de Cachan*) and the *Laboratoire de Mécanique de Lille* (*Ecole Centrale de Lille*). Each contributors bring specific and complementary sets of skills. Our contributions to the project is firstly to perform the experimental characterization of the mechanical behavior of filled rubber material under cyclic loading conditions, and secondly, to develop constitutive equations in order to capture the mechanical behavior of the material and its evolution under cyclic loading conditions. This work will focus on the equilibrium responses, the issues of viscoelasticity are beyond the scope of this study. It is to emphasize that the purpose is not to develop crack growth models. It is rather to propose a model able to predict the mechanical behavior of the material in the local highly strained region in the vicinity of the crack tip, before the crack propagates through.

The requirements for the experimental characterization are now described.

- Perform cyclic tension tests according to various loading conditions in order to characterize the phenomena of stress-softening, residual stretch and induced anisotropy. The experimental work should allow to quantify the dependencies to the maximum loading intensity and to the number of cycles.

- Assess the effects of the material microstructure on the stress-softening phenomenon. For this purpose, materials with various compositions will be considered.

- The region in the vicinity of the crack tip undergoes significant changes in loading conditions. The multiaxiality of the loading path evolves while the crack propagates through the sample. Therefore, experiments accounting for biaxial loading conditions should be considered.

The experimental works should provide a complete experimental basis for the constitutive model definition. The mechanical modeling of the material behavior should account for the phenomena brought to light by the experiments (stress-softening, residual stretch, anisotropy) and for the loading parameters (type of loading, loading intensity, number of cycles).

Layout of this thesis

This thesis is organized as follows. Chapter 1 proposes a literature review on the mechanical behavior of rubber-like materials submitted to cyclic loading conditions. During this review, some modeling issues are highlighted. An experimental strategy is defined in order to assess experimental evidences allowing to improve the constitutive equations. Finally, testing devices and general experimental techniques are described within this chapter. Chapter 2 introduces the materials studied during the thesis. In order to investigate the effect of the material microstructure, several carbon-black filled styrene-butadiene rubbers with various compositions are considered. Monotonic and cyclic uniaxial tension tests are performed in order to illustrate few basic mechanical properties according to the material composition. Chapter 3 proposes an original parameter to qualitatively characterize the Mullins softening occurring under cyclic uniaxial loading conditions. The proposed parameter is used to study the effect of the material composition on the Mullins softening. Chapter 4 aims at providing a criterion for the Mullins softening activation able to account for general loading conditions. Unconventional experimental procedures are used in order to apply cyclic non-proportional loadings. Then an original experimental analysis is defined to assess the Mullins softening criterion. Chapter 5 proposed an original constitutive modeling for filled rubber materials in order to capture the anisotropic softened behavior induced by general non-proportional loading histories. The constitutive equations are grounded on a thorough analysis of original experimental data. The proposed framework is built in order to provide a model versatile that applies for a wide range of materials. For this purpose, the chapter also provided an identification procedure. In order to extend the understanding and to accurately predict mechanical behavior changes occurring during cyclic loading conditions, Chapter 6 is addressing the cyclic softening that evolves with the number of cycles. Firstly, an original method is proposed for the cyclic softening characterization and the effects of the material composition are studied. Secondly, the method is extended for modeling the stress-softening of filled rubbers occurring during proportional cyclic tests.

Finally the next chapter concludes the thesis. We summarize the key-points of our works. In addition, we discuss the results and we present few possible directions for future works.

Appendix A is addressing a side issue regarding the hyperelastic modeling for filled rubber mechanical behavior accounting for an anisotropic damage. A full-network approach with directional damage is used. The framework is rewritten using spherical harmonics in order to provide an efficient numerical implementations. It is to be noticed that such a formalism may be extended on the model proposed in Chapter 5. Such a work was not carried out during the thesis because we chose to focus on the mechanical behavior modeling and the material understanding instead on numerical issues. Nevertheless, this work was shown to perform well and to drive to a publication.

Chapter 1

Literature review and experimental setup

This first chapter aims at providing basis for the entire thesis works developed in subsequent chapters. Firstly, a literature review on rubber-like materials submitted to cyclic loading conditions is proposed. Three main topics are addressed within this review: rubber-like materials, Mullins softening and cyclic softening. Experimental observations, physical interpretations and mechanical modeling are considered. It is to be noticed that works published after the beginning of the thesis are not included in this first chapter. The review will highlight some insufficiencies in the models currently used and a lack of experimental data within the literature. Secondly, the experimental setup used to assess the needed data is given. The testing devices and general experimental techniques are described with details when needed.

Contents

1.1 Introduction

Rubber-like materials are commonly used in various industrial applications. Their complex microstructures consist of long flexible molecular chains randomly arranged in space and linked together to form large molecular networks. Such a microstructure gives to rubber-like materials some extraordinary elastic properties. In order to increase their stiffness, fillers are usually added to the rubber compounds. The main drawback of such reinforcements is to induce some material stress-softening when submitted to cyclic loading conditions. The larger part of the stress-softening occurs during the first loading and is known as the Mullins softening (Mullins, 1969). During subsequent cycles, the mechanical behavior evolves very slowly and becomes rapidly unnoticeable between two successive cycles. However, when considering a large number of cycles, this evolution cannot be neglected. The literature reports a significant amount of work addressing the behavior of rubber-like materials under cyclic loading conditions. However, there are still numerous major issues that need to be addressed. Building an efficient constitutive model for the behavior rubber-like materials with an account of the cyclic softening remains a significant challenge.

The first objective of this chapter is to review and discuss the literature dedicated to the topic. An analysis of the previous works will highlight some modeling insufficiencies and a lack of experimental data within the literature. Then an experimental strategy will be proposed in order to assess the required data. The second objective is to introduce the experimental setup and to provide details regarding testing devices, and experimental techniques and procedures used in the sequel.

This chapter is organized as follows. The next section gives a basic description of rubber-like material microstructure and mechanical modeling. Then, the literature dedicated to the Mullins softening and to the cyclic softening is reviewed in Sections 1.3 and 1.4, respectively. Literature reviews synthesis and analysis are given in the following section. Finally, the experimental setup is introduced and concluding remarks close the chapter.

1.2 Rubber-like materials

1.2.1 Material description

Originally and for more than a hundred years, the only elastomer used for industrial application was the natural rubber (NR). Natural rubber is extracted from latex produced by the Hevea braxiliensis tree. Hevea commercial plantations are mainly located in India. During World War II, the United States were cut off from rubber-growing areas and developed synthetic alternates for natural rubber applications. One of the most widely used synthetic rubbers is Styrene Butadiene Rubber (SBR). SBR is the type of gum used to manufacture the materials studied in this thesis. Most of synthetic rubbers are processed from petroleum raw products, however, their microstructure and mechanical properties are very comparable to natural rubber ones.

At a smaler scale, elastomers are made of very long macromolecular chains. The chain consists into repeated units called monomers. The monomer is a specific arrangement of atoms connected by covalent bonds. Due to thermal agitation, rotations along the macromolecular chain backbone are free rendering easy the changes of chain configurations, which favors large strains. Raw rubbers, consisting of uncrosslinked macromolecular chains, show very limited elasticity due to unrestrained chain slipping. Within a raw rubber, long chains are only connected by weak bonds and entanglements. Hence, when submitted to a mechanical solicitation chain reptations occur and material flows like a highly viscous fluid. To reach mechanical properties suitable for industrial applications, raw rubbers are submitted to a vulcanization process. Vulcanization is a chemical process usually carrying out in a mold under high pressure and high temperature. Raw rubber is mixed with sulfur and during the process atomic covalent bonds

between polymer chains are created by sulfur atoms. Those bonds are usually called crosslinks. A vulcanized rubber microstructure is shaped as a network, therefore chain reptations are no longer possible and material can withstand large deformations.

Pure vulcanized rubber materials are able to undergo quasi-reversible large deformations. However, other mechanical properties, such as stiffness, are too weak for practical use. In order to significantly improve the mechanical properties, filler particles are incorporated within rubber compounds to act as reinforcement. Even though the filler rubber interactions are still not well understood, it is commonly known that adding fillers to rubbers increase their stiffness significantly (Mullins and Tobin, 1965; Bergström and Boyce, 1999) and delay the crack propagation (Auer et al., 1957; Mars and Fatemi, 2004a; Mzabi, 2010). Two main types of fillers are widely used, carbon black and silica. Materials studied in this thesis are SBR compounds filled with carbons black. Within a filled rubber, the elementary carbon black particles are aggregates. Even for the same type of carbon black, aggregates may have numerous shape, their structure can be more or less branched and some rubber gum, usually refer as occluded rubber, may be trapped within aggregates (Medalia, 1970).

A filled rubber micrograph is shown in Figure 1.1a. This figure highlights aggregates formed by grouped carbon black particles. The aggregates of various shapes are randomly dispersed. The microstructure of filled rubbers is schematized in Figure 1.1b. Relevant and average dimensions for filled rubber description are the following: a monomer size is 0.15 nm; a chain cross section is 0.5 nm^2; a crosslinks diameter is 3 nm; the elementary carbon black particle diameter is of 10 to 90 nm; the aggregate is composed by 10 to 100 particles reading a size between 100 to 500 nm (Leblanc, 2002).

(a)   (b)
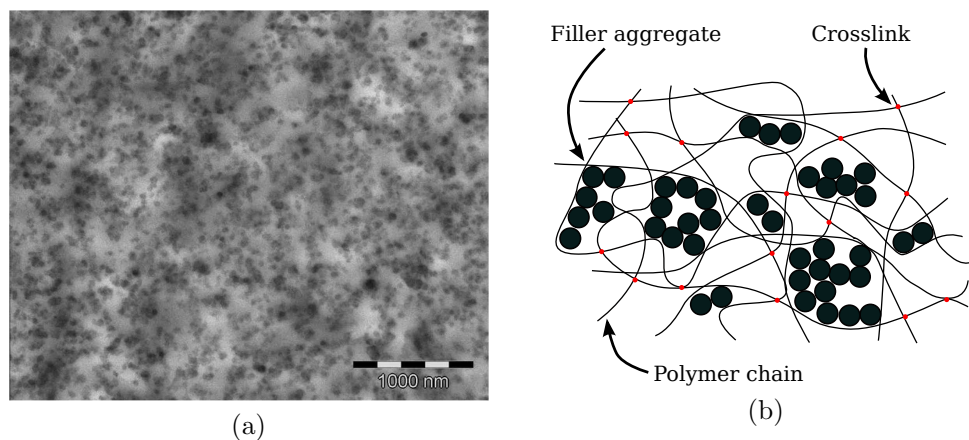
Figure 1.1: Material physical description. (a) Micrograph of a SBR filled with 50 phr of N347 carbon black. (b) Schematic filled rubber microstructure.

1.2.2 Material behavior modeling

Rubber-like materials may undergo large elastic strains and strongly non-linear stretch-stress responses. In order to accurately model the material mechanical behavior, large strain formalism and the hyperelastic framework are prefered. Therefore, a strain energy density $\mathcal{W}$ is introduced from which the constitutive equations devive. The deformation of a material from an initial (undeformed) configuration to a current (deformed) configuration is described by the deformation gradient tensor $\boldsymbol{F}$. The strain is given by the right Cauchy-Green deformation tensors $\boldsymbol{C} = \boldsymbol{F}^t\boldsymbol{F}$ (superscript ^{t} denotes transposition). In what follows, two stress tensors are used. The second Piola-Kirchoff stress tensor $\boldsymbol{S}$ and the Cauchy stress tensor $\boldsymbol{\sigma}$ defined on the initial and the

current configurations, respectively. They are both related through

$$\boldsymbol{\sigma} = J\boldsymbol{F}\boldsymbol{S}\boldsymbol{F}^t \tag{1.1}$$

with $J = \det(\boldsymbol{F})$ the Jacobian determinant. It is noteworthy that $J = V/V_0$ with V the current volume and V_0 the initial volume. Therefore, for incompressible materials, J remains equal to 1. From the laws of thermodynamics, the Clausius Duhem inequality for an isothermal process can be written as

$$\frac{1}{2}\boldsymbol{S} : \dot{\boldsymbol{C}} - \dot{\mathcal{W}} \geqslant 0. \tag{1.2}$$

The state of the material is assumed to be described by the strain energy density $\mathcal{W}$ expressed in term of $\boldsymbol{C}$. Then the Clausius Duhem inequality gives

$$\left(\frac{1}{2}\boldsymbol{S} - \frac{\partial \mathcal{W}}{\partial \boldsymbol{C}}\right) : \dot{\boldsymbol{C}} \geqslant 0 \tag{1.3}$$

hence, to satisfy any arbitrary deformation,

$$\boldsymbol{S} = 2\frac{\partial \mathcal{W}}{\partial \boldsymbol{C}}. \tag{1.4}$$

Taking into account the incompressibility assumption, the Cauchy stress tensor yields

$$\boldsymbol{\sigma} = 2\boldsymbol{F}\frac{\partial \mathcal{W}}{\partial \boldsymbol{C}}\boldsymbol{F}^t - p\boldsymbol{I} \tag{1.5}$$

where p is an arbitrary hydrostatic pressure.

It must be emphasized that proposing a relevant expression of $\mathcal{W}$ remains a major issue. Some reviews about this topic were proposed by Boyce and Arruda (2000); Marckmann and Verron (2006); Vahapoğlu and Karadeniz (2006). There is currently no model reported in the literature able to build a direct link between the filled rubber microstructure and its experimental stress-stretch responses. Therefore, in order to define the strain energy density, two main approaches may be considered. One of them is based on a mathematical development of the strain energy density without any physical considerations. Within this approach, proposed models are phenomenological, usually based on strain invariants and with parameters without any physical meaning. A well-known phenomenological development has been proposed by Rivlin (1948)

$$\mathcal{W} = \sum_{i,j=0}^{\infty} C_{ij}(I_1 - 3)^i(I_2 - 3)^j \tag{1.6}$$

with C_{ij} defining the material parameters and I_1 and I_2 been the first and second invariants of the right Cauchy–Green deformation tensor.

The second approach aims at proposing models built with a strain energy density grounded on physical motivations. The material is considered as a network constituted of long molecular chains randomly oriented in all directions of space. A unidirectional elementary strain energy density w is defined for a single chain. A three-dimensional framework is obtained by considering elementary strain energy density contributions along several directions. Meyer et al. (1932); Meyer and Ferri (1935) were first to consider rubber microstructure composed of flexible chain rather than a rigid molecule and to propose a theory assuming that rubber elasticity is governed by changes in configurational entropy. They also realized that internal rotation between successive monomers are free and random, therefore end-to-end chain distance is related to statistical considerations. Using a statistical mechanics approach, the entropy of a single chain, s, is

$$s = k \ln P \tag{1.7}$$

with k the Boltzmann's constant and P the probability of end-to-end chain distance. Considering both laws of thermodynamics and assuming that the internal energy is independent of the chain extension (full details may be found in Treloar (1973, 1975)), the chain energy density, w, reads

$$\mathrm{d}w = T\mathrm{d}s \qquad (1.8)$$

with T the temperature. In order to account for molecular chain extensibility limit, the elementary strain energy density proposed by Kuhn and Grün (1942) is mainly used. It is based on a probability of end-to-end distance distribution P defined by the Langevin function, $\mathcal{L}(x) = \coth(x) - 1/x$, and yields

$$w(\Lambda_{\mathrm{chain}}) = NkT \left[\frac{\Lambda_{\mathrm{chain}}}{\sqrt{N}} \beta_{\mathrm{chain}} + \ln\left(\frac{\beta_{\mathrm{chain}}}{\sinh \beta_{\mathrm{chain}}} \right) \right] \qquad (1.9)$$

with $\beta_{\mathrm{chain}} = \mathcal{L}^{-1}(\Lambda_{\mathrm{chain}}/\sqrt{N})$, N the number of chain bonds and Λ_{chain} the chain elongation. Finally, the global strain energy density $\mathcal{W}$ is the summation of all elementary contributions and an idealized representation introduced by Treloar and Riding (1979) is the full-network model. Considering a continuous spatial distribution of w, integration on the unite sphere leads to

$$\mathcal{W} = \frac{n}{4\pi} \int_{\varphi=0}^{2\pi} \int_{\theta=0}^{\pi} w \, \sin(\theta)\mathrm{d}\theta\mathrm{d}\varphi \qquad (1.10)$$

with n the active chain density and (θ, φ) the polar angles. Let us note that the number of considered directions may be limited, for instance a well-known "8-chain" model was proposed by Arruda and Boyce (1993).

Constitutive equations introduced in this section are able to capture a very idealized rubber mechanical behaviors, *i.e.* a perfectly reversible and isotropic hyperelastic material response. Unfortunately, actual filled rubber behaviors are far more complicated. Some experimental observations putting in light this complexity are presented in the next section.

1.3 Review on the Mullins softening

1.3.1 Experimental observations of the Mullins softening

Filled rubbers exhibit highly non-linear and time-dependent mechanical responses. Moreover, the material loading history induces some behavior changes. Among the latter, a significant stress softening occurs when stretched for the first time. This phenomenon, first reported by Bouasse and Carrière (1903) is now commonly referred to as the Mullins softening du to the amount of work addressed on this specific issue by Mullins (1947, 1949, 1950, 1969). Over the following decades numerous contributions investigated the Mullins softening, but it is well known that there is still no general agreement on its experimental characterization, its physical understanding or its mechanical modeling. Experimental observations are shown in this section, then physical interpretations and modeling are discussed in subsequent sections. Further details may be found in a recent review on the topic proposed by Diani et al. (2009).

In order to illustrate the Mullins softening main features, a filled rubber sample was submitted to a cyclic uniaxial tension. The stress-stretch response for a cyclic loading test with increasing maximum stretch every 10 cycles is shown in Figure 1.2. This classic experiment highlights the stress softening occurring when the material is first loaded to a level of stretch never undergone. One may notice that when stretched beyond the maximum intensity previously applied, the stretch-stress response returns on the monotonous uniaxial tension response path and the material softens significantly. To the contrary, once the Mullins softening is evacuated and during subsequent cycles, the material behavior evolves very slowly with respect to

the number of cycles. Since changes between two successive cycles may rapidly become unnoticeable (Mullins, 1949), they are usually neglected. While material softens, one may notice a residual stretch that increases and seems to mainly evolve with the applied maximal stretch. Along with the softening, the residual stretch was intensively studied by Mullins (1947, 1949) and very similar changes were observed for both phenomena. However, the residual stretch is very dependent on the material viscoelasticity and it shows a significant and rapid recovery even at room temperature (Mullins, 1949; Diani et al., 2006a). On the contrary the Mullins softening is commonly reported in the literature as an irreversible damage phenomenon and, at least at room temperature, no softening recovery was observed by Mullins (1947); Rigbi (1980); Hanson et al. (2005); Diani et al. (2009). Let us note that a large softening recovery may occur at high temperatures (in vacuo) or by swelling (Harwood and Payne, 1966a,b).
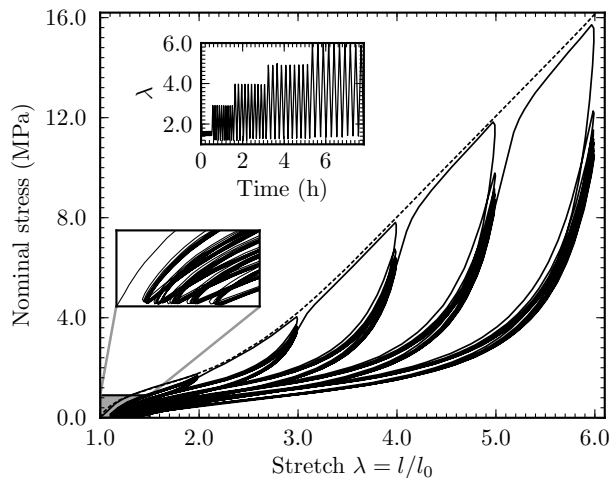
Figure 1.2: Mullins softening: Stress-stretch response of a filled rubber under cyclic uniaxial conditions.

The early experimental works aiming at studying the Mullins softening (Bouasse and Carrière, 1903; Mullins, 1947, 1949) were performed on filled natural rubbers. A Mullins softening was also reported for unfilled natural rubber by Dannenberg and Brennan (1965); Harwood et al. (1965); Harwood and Payne (1966a) for very high level of strains. However, natural rubber is known to crystallize upon stretching and its mechanical response is significantly impacted by this phenomenon. Recently Trabelsi et al. (2003a) showed that in natural rubbers, a major part of hysteresis between the loading and the unloading responses may be related to crystallization and melting. By measuring the amount of crystallinity Trabelsi et al. (2003b) showed that crystallization is identical during the first and the second cycles while the softening evolves significantly. Hence, behavior changes are not related to a crystallization decrease with the number of cycles and strain-induced crystallization is not significantly affected by the Mullins softening. Mullins softening occurrence for synthetic filled rubbers has been reported many times in the literature and for various type of gums. However, the dependence of the Mullins softening to the type of gum or to the type of fillers is not clearly established. Nevertheless, it is clearly known that the softening increases with the amount of fillers, one may cite Mullins and Tobin (1957); Klüppel and Schramm (2000); Dorfmann and Ogden (2004); Luo et al. (2004) among others. Finally, Mullins softening has never been observed in unfilled non-crystallizing rubber (see for instance Meunier et al. (2008) for a silicone rubber).

Experimental contributions aiming at investigating the Mullins softening usually focus on proportional loadings, *i.e.* successive loadings with the same multiaxial nature of the stretching and the same principal directions of stretching. Uniaxial tension tests are mostly used for

technical simplicity, numerous references may be found in Diani et al. (2009) review. Only few studies applied more complex loading conditions, for instance a Mullins softening has been reported in pure shear (James and Green, 1975; Moreau et al., 1999; Machado et al., 2010), biaxial tension (Johnson and Beatty, 1995; Li et al., 2008; Palmieri et al., 2009; Machado et al., 2010), and uniaxial compression (Bergström and Boyce, 2000; Amin et al., 2002; Qi and Boyce, 2005; Webber et al., 2007), among others. All last-cited contributions highlight strong effects of loading conditions on rubber hyperelastic stress-stretch responses. But, since materials are only submitted to proportional loadings, the Mullins softening features are similar to those presented in Figure 1.2 for a simple uniaxial tension test. To the contrary, applying non-proportional loadings reveal another interesting Mullins softening feature. During his early work, Mullins (1947, 1949) brought to light the induced anisotropy of both the softening and the residual stretch by submitting a material to successive non-proportional loadings. However, this particular aspect was not investigated further until very recently (Laraba-Abbes et al., 2003; Hanson et al., 2005; Diani et al., 2006a,b; Itskov et al., 2006; Dargazany and Itskov, 2009). The latter contributions report considerable and coupled softening's dependencies on the pre-loading intensity, the direction and multiaxiality of the loadings, without reaching an understanding of the anisotropic phenomenon and its evolution.

1.3.2 Physical interpretations of the Mullins softening

Assessing the physical origins of the Mullins softening is relevant in many aspects, like providing a better understanding of the phenomenon in order to build ground for physically motivated mechanical models. Along the last decades, many physical interpretations have been proposed in order to explain the Mullins softening occurrence in rubber materials. However, as previously pointed out, there is still no general agreement about this issue. An early review about this topic was proposed by Mullins (1969) then more recently by Diani et al. (2009). Only few of them are presented in the following.

In order to propose a physical interpretation, for the Mullins effect, Blanchard and Parkinson (1952) attributed the softening to bond ruptures induced by stretching at rubber-particle interfaces. A similar approach considering ruptures of the shorter chains linking two particles when distance between particles expended was proposed by Bueche (1960). However, many experimental observations disagree with such an interpretation. When chain ruptures occur, the amount of carbon radicals increases within the material and carbon radicals may be measured by electron spin resonance. Using this method Suzuki et al. (2005) reported that chain scissions happen either for filled or unfilled SBR and the latest does not exhibit any Mullins softening. Therefore, even if chain scissions contribute to the Mullins softening, they are not the main source. Another drawback of this interpretation has been put in light by Dannenberg and Brennan (1965); Kraus et al. (1966). These authors carried out some swelling tests on pre-stretched filled rubbers, they measured no significant changes in rubber networks and concluded that bond ruptures cannot be the main source of the Mullins softening. Finally, the Mullins softening recovery pointed out in the previous section (Harwood and Payne, 1966a,b) does not agree with the bond rupture interpretation.

Another physical interpretation initially proposed by Houwink (1956), then supported by Dannenberg and Brennan (1965); Clément et al. (2001), attributes the Mullins softening to chains slipping on the surface of filler particles. Let us note that an earlier theory of breaking and reforming adsorption bonds introduced by Alexendrov and Lazurkin (1944) is equivalent to chain slipping. This interpretation could explain the observed recovery and the insignificant change in the rubber network of stretched materials. However, the softening occurrence observed for unfilled natural rubber (Dannenberg and Brennan, 1965; Harwood et al., 1965; Harwood and Payne, 1966b) can not be justified.

A phenomenological interpretation proposed by Mullins and Tobin (1957) considers the ma-

terial to be a two-phase composite with a soft phase and a hard phase. The Mullins softening is acting like a rearrangement or a breakdown of the hard phase induced by localized high deformations and changing some hard phase into soft phase. The authors suggested that breakages of filler aggregates or rupture of polymer-filler bonds might be involved in this process. Kraus et al. (1966) performed electrical conductivity measurements on pre-stretched filled rubber samples and notice subsequent changes of material resistivity with the pre-stretch intensity. Therefore, the authors followed the idea of Mullins and Tobin (1957) and also attributed the main source of the stress-softening to ruptures of carbon-black aggregates. It is worth pointing out that Mullins and Tobin (1958); Kraus et al. (1966) look at volume changes and measured a rather small volume expansion for large stretch (usually less than 2 % for $\lambda = 2$). Hence the authors concluded that vacuoles formation could not be the main cause of the Mullins softening. Later, Klüppel and Schramm (2000) used the same interpretation of filler cluster breakdowns for the Mullins softening. Main drawbacks of this physical interpretation are the reversibility of the process and its extension for unfilled crystallizing rubbers Mullins softening.

Harwood and Payne (1966a,b) studied the Mullins softening in filled and unfilled vulcanized natural rubbers, respectively. They attributed the Mullins softening to a quasi-irreversible rearrangement of the molecular network due to local non-affine deformations resulting from a complete extension of the short chains. During the first extension, local non-affine deformations within the material result in non-affine displacements of molecular network junctions from their initial random state. Then when the material is stretched a second time, the network is already in a "preferred" configuration. Harwood and Payne (1966a,b) also addressed the issue of the Mullins recovery in pure and filled natural rubbers. They observed a slow and limited recovery of the stress softening at room temperature but a substantial and sometimes almost complete recovery by heating or by swelling. Finally, the proposed interpretation of molecular network rearrangements for the Mullins softening agrees with a possible recovery.

Let us notice that physical interpretations of the Mullins softening presented below are very different (bond ruptures, chains slipping, ruptures of filler aggregates, rearrangement of molecular networks). But they all have in common the idea that when a vulcanized filled rubber (or unfilled natural rubber) is stretched, some regions of the material are highly strained even at low extension. In any case, the phenomenona occurring within the highly strained zones leads to the softening. The finite extensibility of molecular chains within those regions leads to the rapid upturn of the material stress-stretch response for extensions approaching the maximum previous extension (Mullins, 1969).

1.3.3 Modeling the Mullins softening

At room temperature, the Mullins softening is generally considered as an irreversible damage and therefore is modelled by damage parameters and their evolutions. Many models reported in the literature are designed to reproduce rubber-like material behaviors accounting for the Mullins softening. Nevertheless, as for the physical interpretations, there is still no general agreement on the modeling (Diani et al., 2009). In order to build a constitutive model for filled rubbers behavior accounting for the Mullins softening, one may identified five major issues to be addressed:

- Mullins softening features → What are the material characteristics resulting form the Mullins softening?

- Hyperelastic law → What is the reference material behavior?

- Account for the Mullins softening → How does the Mullins softening act?

- Mullins softening activation criterion → When does the Mullins softening activate and evolve?

- Softening evolution rule → <u>How does the softening evolve?</u>

The couple first questions were previously discussed in Section 1.3.1 and 1.2.2, respectively. The current section focuses on the third and fourth issues, namely the account of the Mullins softening and of the definition of a criterion. Finally, the Mullins softening evolution rule is usually chosen in order to fit experimental data. In what follows, I review the Mullins softening criterion already introduced in the literature. Then, three approaches relevant to account for the Mullins softening are detailed.

Mullins softening activation criterion

In there early work on the Mullins softening, Mullins and co-workers (Harwood et al., 1965; Harwood and Payne, 1966a; Mullins, 1969) noticed that when filled and unfilled natural rubber were first loaded to the same stress[1], materials experience various maximal stretches due to different stiffness but undergone the same degree of softening between the first and the second extension[2]. According to this observation, the authors attributed the softening to localized non-affine deformations. Therefore, it seems relevant to relate the evolution of the Mullins softening to the maximal stretch rather than to the maximal stress. This path is mostly followed ever since.

Most Mullins softening activation criteria are proposed in order to develop an isotropic softening. One may find in the literature the maximum of the higher eigenvalue of the deformation gradient tensor (Laiarinandrasana et al., 2003), the maximum of some deformation tensor invariants (Lion, 1996; Krishnaswamy and Beatty, 2000; Chagnon et al., 2004; Elías-Zúñiga, 2005), the maximum free energy (Simo, 1987; Ogden and Roxburgh, 1999) or other scalar quantities ... Only few models account for an anisotropic Mullins softening driven by an anisotropic criterion. One may cite the maximum directional free energy (Göktepe and Miehe, 2005) and the maximum directional stretch (Diani et al., 2006a,b).

All pre-cited criteria may be able to be used within three-dimensional frameworks considering or not the observed anisotropy. The model will probably give good agreement with experimental data provided by proportional cyclic loadings. However, for such loading conditions, the Mullins softening changes when the maximal loading intensity (whatever its definition) is overcome. With such criteria the mechanical quantity driving the Mullins softening evolution under non-proportional loading conditions remains unclear (Diani et al., 2009; Machado et al., 2010). Therefore, many models are based on critical assumptions and, for most of them, predictive capabilities for different and successive loading paths or loading directions can not be expected.

Accounting for the Mullins softening by strain energy density penalization

In order to account for the Mullins softening the concept of continuum damage variable (Kachanov, 1958) was extended by Simo (1987) for rubber-like materials. Undamaged strain energy density $\mathcal{W}_0$ is penalized by a damage parameter D according to

$$\mathcal{W} = (1 - D)\mathcal{W}_0. \tag{1.11}$$

Such an account for the Mullins softening has been widely used and many references may be found in Diani et al. (2009) review. It is noteworthy that most proposed models based on this approach are mainly phenomenological and any physical phenomena may be considering within parameter D. Furthermore, the used strain energy densities $\mathcal{W}_0$ are also usually phenomenological and may for instance be based on constitutive equation similar to the development introduced in Eq. (1.6). Let us note that the well-known concept of pseudo elasticity proposed by Ogden

---

[1]Notes that nominal (Piola) stress is used, *i.e.* not the Cauchy stress.
[2]Characterized by the difference between stresses at the same stretch.

and Roxburgh (1999), is part of this class of model. In order to increase experimental fitting accuracy, the penalization method was improved by Ogden and Roxburgh (1999) considering a strongly non linear form of damage parameter depending on both the current and the maximal loading states. The framework was later improved by Dorfmann and Ogden (2004) to account for residual stretch, but the softening remains isotropic. Recently, Itskov et al. (2010) proposed an anisotropic model accounting for the Mullins softening via a strain energy density penalization. However, despite good agreement with experimental data for uniaxial proportional loadings, such a general penalized strain energy densities fail at predicting uniaxial responses after non-proportional uniaxial loading histories.

Accounting for the Mullins softening by strain amplification

A different class of models accounting for the Mullins softening is based on the early phenomenological interpretation provided by Mullins and Tobin (1957). The authors observed that uniaxial stress-stretch responses of materials submitted to various pre-loading stretches had the same characteristic shapes and were able to collapse into a single master curve. They built a constitutive model on this experimental observation. For this purpose, the material is described as a two-phase composite made of a hard phase and a soft phase. The hard phase is assumed rigid, therefore the strain in the soft phase ϵ^{soft} is assumed to be the macroscopic (or applied) strain $\epsilon^{\mathrm{macro}}$ magnified by a strain amplification factor X, leading to

$$\epsilon^{\mathrm{soft}} = X.\epsilon^{\mathrm{macro}} \tag{1.12}$$

or equivalently to $\lambda^{\mathrm{soft}} = 1 + X(\lambda^{\mathrm{macro}} - 1)$ in term of stretches. The Mullins softening is accounted for by considering a decrease of the hard phase volume fraction (*i.e.* an increase of X from an undamaged state) with the maximum stretch. The strain amplification factor is applied according to

$$\sigma(\epsilon^{\mathrm{macro}}) = \sigma(\epsilon^{\mathrm{soft}}). \tag{1.13}$$

Later, the strain amplification factor concept was used by Klüppel and Schramm (2000) and related to the physical interpretation that the Mullins softening results from an irreversible breakdown of filler clusters. Such an account of the Mullins softening may be found in many models proposed in the literature, for instance Johnson and Beatty (1993); Heinrich et al. (2002); Klüppel (2003); Luo et al. (2004); Meissner and Matějka (2006, 2008). Then, the strain amplification concept was reviewed by Qi and Boyce (2004) and extended to directional models as definded in Eq. (1.10). For this purpose, the strain amplification is applied to the elementary strain energy densities w according to

$$w(\epsilon^{\mathrm{macro}}) = w(\epsilon^{\mathrm{soft}}). \tag{1.14}$$

The model proposed by Qi and Boyce (2004) provides good approximation of experimental data, nevertheless, it does not aim at reproducing either the material anisotropy or the residual stretch induced by the Mullins softening. Let us note that the difference between Eqs. (1.13) and (1.14) is highlighted Eq. (1.5). When considering Eq. (1.14), $\boldsymbol{F}$ and $\boldsymbol{F}^t$ on both sides of $\partial \mathcal{W}/\partial \boldsymbol{C}$ in Eq. (1.5) are unaffected by the amplification. On the contrary, they are both amplified when using Eq. (1.13).

Accounting for the Mullins softening by strain energy density parameter alteration

Ideally, an hyperelastic model should be built with a strain energy density grounded from physical motivations and a physical interpretation of the Mullins softening. Hence, the Mullins softening can be accounted for by altering the strain energy density parameters. Many physically based models are reported in the literature, but only few induce anisotropic softening. For

instance, Govindjee and Simo (1991) interpreted the Mullins softening as the rupture of chains links between particles. Killian et al. (1994) defined the Mullins softening by irreversible chain slippages. Marckmann et al. (2002) assumed that the softening is caused by the breakage of network crosslinks. All pre-cited models are isotropic and in order to reproduce the anisotropy induced by the Mullins softening some improvements were initially proposed by Göktepe and Miehe (2005); Diani et al. (2006b) and more recently used by Dargazany and Itskov (2009). In the following, more details are given for the second one (Diani et al., 2006b).

In order to account for anisotropic Mullins softening, Diani et al. (2006b) proposed an extension of the isotropic physically-based model introduced by Marckmann et al. (2002). As a starting point, a directional framework built from the statistical mechanics and a limited set of m directions is used. Eqs. (1.9) and (1.10) combined in

$$\mathcal{W}(\boldsymbol{F}) = \sum_{i=1}^{m} \omega_i n_i N_i kT \left[\frac{\Lambda_i}{\sqrt{N_i}}\beta_i + \ln\left(\frac{\beta_i}{\sinh\beta_i}\right) \right] \tag{1.15}$$

where ω_i are the directional weights for numerical integration, $\beta_i = \mathcal{L}^{-1}(\Lambda_i/\sqrt{N_i})$ and $\Lambda_i = \sqrt{\boldsymbol{u}_i.\boldsymbol{C}.\boldsymbol{u}_i}$, the unit vector $\boldsymbol{u}_i$ being oriented in chain i direction. At first, an isotropic approach was proposed by Marckmann et al. (2002). The Mullins softening is accounted for by changing the active chain densities n_i and the number of bonds N_i with the maximal applied stretch intensity characterized by $\sqrt{I_1/3}$ with the deformation invariant $I_1 = \boldsymbol{C} : \boldsymbol{I}$. According to experimental observations, the initial stiffness (n_i) decreases and the extension limit (N_i) increase with the maximal stretch increase. Moreover, assuming that the number of monomers remains constant, the following condition is used

$$N_i n_i = \text{constant}. \tag{1.16}$$

Hence only one damage evolution law needs to be defined for both parameters. It is worth noticing that using an isotropic activation criterion, such as the maximum of $\sqrt{I_1/3}$, leads to an isotropic evolution of the Mullins softening. Therefore, n_i and N_i remain even over all material directions and no anisotropic change occurs. In order to account for anisotropy, the material parameters n_i and N_i are initially chosen even for all directions, then the parameters change independently for each direction i according to the maximum stretch Λ_i applied along direction $\boldsymbol{u}_i$. The anisotropic model proposed by Diani et al. (2006b) is able to induce both anisotropic Mullins softening and residual stretch. The model provides fair estimate of experimental data considering non-proportional stretching.

1.4   Review on the cyclic softening

The previous section, focused on the softening occurring during the first cycle and related to the Mullins softening. However, experimental results presented in Figure 1.2 show that the material behavior keeps softening when loading cycles are repeated at the same maximal stretch. Throughout the thesis, this secondary softening is defined as "cyclic softening". This section reviews the (short) literature dedicated to this topic.

1.4.1   Experimental observations of the cyclic softening

Once the Mullins softening evacuated during the first cycle, the softening occurring during subsequent identical cycles is very small and decreases rapidly with the number of cycles (Mars and Fatemi, 2004a). Therefore, the material behavior change may rapidly become unnoticeable between two successive cycles (Mullins, 1949) and is usually neglected. Nevertheless, when considering the cumulative softening induced by a large number of cycles, this change cannot

be neglected anymore. Contributions on rubbers-like materials submitted to a large number of cycles address mostly the issues of fatigue life, lifetime criterion and crack propagation (Beatty, 1964; Lake and Thomas, 1967; Mars and Fatemi, 2002; Abraham et al., 2005; Kim and Jeong, 2005; Mars and Fatemi, 2006; Le Cam et al., 2008; Saintier et al., 2006; Harbour et al., 2008; Verron and Andriyana, 2008; Andriyana et al., 2011; Mzabi et al., 2011; Saintier et al., 2011). Actually, only few works have been drawing their attention to material mechanical behavior changes under cyclic loading conditions (Derham and Thomas, 1977; Shen et al., 2001; Gentot et al., 2004; Mars and Fatemi, 2004a; Yu et al., 2008; Brieu et al., 2010; Yan et al., 2010). Figure 1.3a shows the stress-stretch response of a filled rubber submitted to a cyclic loading with repeated cycles at the same maximal stretch. This figure illustrates the Mullins softening during the first load characterized by a large hysteresis and a substantial residual stretch. It also shows the very slow cyclic softening occurring during subsequent cycles. One may notice also that the residual stretch slowly increases with respect to the number of cycles.
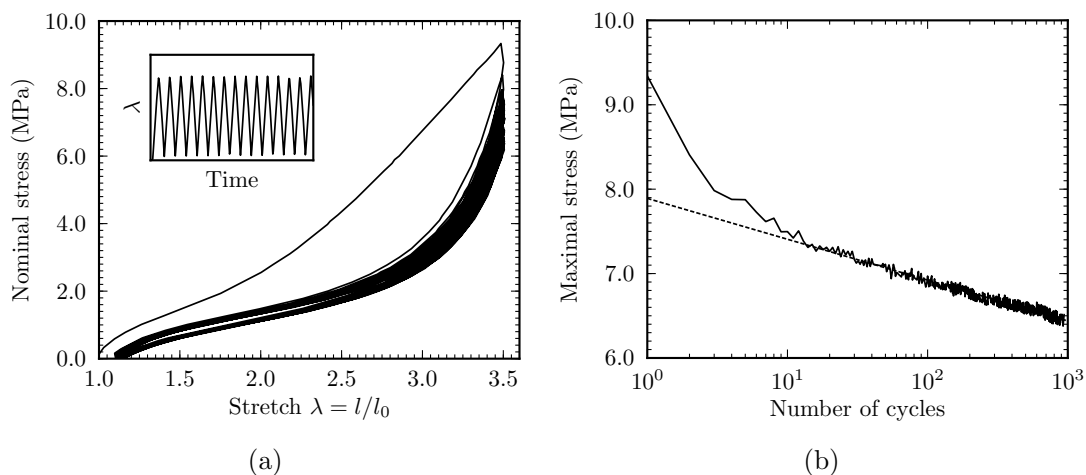
Figure 1.3: Cyclic softening: (a) Stress-stretch response of a filled rubber to a uniaxial tensile cyclic test of one thousand cycles at a constant maximum stretch. (b) The maximal stress decreases with respect to the number of cycles.

In order to characterize the cyclic softening according to the number of cycles, a solution commonly used in the literature, is to follow the decrease of the maximal stress with respect to the number of cycles (see for instance Shen et al. (2001); Gentot et al. (2004); Mars and Fatemi (2004b); Asare et al. (2009); Berrehili et al. (2010); Brieu et al. (2010); Yan et al. (2010); Saintier et al. (2011) among others). Figure 1.3b shows the maximal stress evolution according to the number of cycles for the stress-stretch experimental response illustrated in Figure 1.3a. One may note that the evolution becomes linear with respect to the logarithm of the number of cycles after a relatively low number of cycles. A similar observation has been reported by Gentot et al. (2004); Mars and Fatemi (2004a); Brieu et al. (2010).

Mars and Fatemi (2004a); Brieu et al. (2010) showed that the cyclic softening is strongly affected by an initial overload (*i.e.* few pre-loading cycles applied at larger stretch before the cyclic loading). After an overload, the maximal stress does not decrease anymore with the number of cycles, but remains constant. Moreover, Brieu et al. (2010) reported that for non-crystallizing rubbers the cyclic softening evolution changes with the maximal stretch but does not change with the stretching amplitude[3]. These observations suggest that both the Mullins softening and the cyclic softening are strongly dependent to the maximal stretch ever applied.

---

[3]Difference between maximal and minimal cycle stretches.

1.4.2 Modeling the cyclic softening

As discussed in Section 1.3.2, many physical interpretations have been proposed for the Mullins softening, but, very few exists for the cyclic softening. Moreover, the few existing interpretation conclude that both stress-softening are related to the same physical mechanisms, the cyclic softening being a residual part of the first cycle Mullins softening. Such a suggestion was initially proposed by Derham and Thomas (1977) and the authors suggest the bond ruptures mechanism. Later, this explanation was supported by Mars and Fatemi (2004a). More recently, Brieu et al. (2010) studied the effect of an overload and showed that a very small overload is sufficient to "freeze" the cyclic softening. The authors concluded that such an experimental observation proves that both softening have the same physical origin.

Bear in mind that Mullins softening physical interpretations are still not clearly established, so neither the cyclic softening ones. Therefore, physical motivations cannot be used to build a cyclic softening model. Only few models accounting for the cyclic softening may be found in the literature and they are all based on an amplification of the Mullins softening with the number of cycles. A common method (Shen et al., 2001; Gentot et al., 2004) is to extend the stress penalization initially proposed for the Mullins softening by Simo (1987), see Eq. (1.11), to the cyclic softening. The stress σ^N at the cycle N is related to the stress at the first cycle according to

$$\sigma^N = (1 - D)\sigma^{N=1} \qquad (1.17)$$

with D a phenomenological damage parameter evolving with the number of cycles.

1.5 Literature review

Hitherto, the thesis proposed a literature review aiming at providing all elementary basis that will be useful in the sequel. Section 1.3 and Section 1.4 focus on the Mullins softening and the cyclic softening, respectively. Those reviews highlight that for both phenomena, their experimental characterizations, their physical interpretations and their mechanical modelings present issues still to be solved.

The current section provides an outcome of the literature review in order to clearly identify the insufficiencies of the existing models. Then knowing those insufficiencies, the related experimental data lead to the definition of an experimental strategy and an experimental setup. At this point, it worth emphasized that the thesis work focuses on equilibrium responses. Therefore viscoelastic aspects are beyond the scope of this study.

1.5.1 Model insufficiencies

Regarding modeling the filled rubber behavior, one may notice the large number of models proposed in the literature and the current activity aiming at developing new models providing a better and accurate representation of material behavior (see the reviews Muhr (2005); Diani et al. (2009)). It appears that even basic and common assumptions such as the incompressibility are questionable (Le Cam, 2010). In the author's opinion, the goal is to find a balance between complexity necessary to accurately feature the filled rubber's stress-stretch responses and simplicity required for parameter identification and numerical implementation.

This thesis aims at developing a constitutive model able to capture the behavior of rubber resulting from a cyclic loading. In order to do so, it must account for the cyclic softening, the Mullins softening and an hyperelastic framework. The modeling insufficiencies regarding the three aspects are now detailed (citations are voluntarily omitted).

- Cyclic softening: All existing models accounting for the cyclic softening define it as an amplification of the Mullins softening by increasing either the governing parameter or the

softening evolution rule. Therefore, there is no specific model developed for the cyclic softening. Some specific governing parameters, evolution rules are still needed.

- <u>Mullins softening</u>: There is still no general agreement on its modeling. A significant drawback of most existing models is that they are built considering only material responses to proportional loadings. As a first consequence, the material behavior and the Mullins softening evolution may be assumed to be isotropic. There are now ample evidences for the anisotropy induced by the Mullins softening. Therefore, constitutive equations capable to capture the anisotropy are needed. As a second consequence, the Mullins softening is observed to evolve with the maximal loading intensity, but any parameter may be used for characterizing the loading intensity. The definition of a general Mullins softening activation criterion has not been yet assessed.

  Another problem is due to the difficulties for assessing the physical interpretations related to the Mullins softening occurrence. Physically motivated models cannot be easily built. Therefore, various assumed solutions for accounting for the Mullins softening are proposed in the literature. A proper method needs to be defined still.

  Finally, because the softening evolution rule is also related to physical interpretations, its definition remains to be defined. Moreover, its rate should be dependent of the material microstructure. Therefore, in order to provide constitutive equations suitable for a large range of materials such a dependence should be studied.

- <u>Hyperelastic framework</u>: As a consequence of the isotropic Mullins softening assumption, most hyperelastic constitutive equations were developed considering an isotropic behavior. Therefore, anisotropic framework suitable for the Mullins softening account is needed.

  Ideally, a hyperelastic model should be build with a strain energy density grounded from physical motivations. Moreover, constitutive equations should be related to material microstructure. However, the relationship between the filled rubber microstructure and its experimental stress-stretch responses is still an issue and demands further studies.

  Few observations reported in the literature seem to significantly disagree with the incompressibility assumption commonly used for rubber materials. Therefore, this aspect requires more investigation.

1.5.2 Experimental strategy

In order to provide a complete experimental basis necessary for the constitutive model definition, a global experimental strategy has been developed. It is now described.

- <u>Material strategy</u>: In order to study the effect of the material microstructure on the hyperelastic response, on the Mullins softening, and on the cyclic softening, several materials with various compositions were chosen. The material strategy was to vary the filler amount and the crosslink density within carbon black filled SBRs.

- <u>Uniaxial tensile loading</u>: Basic monotonic or cyclic proportional tests are sufficient for most issues that will be addressed. Uniaxial tensile loading was chosen for its simplicity and its reliability.

- <u>3D deformation measurements</u>: In order to investigate the material incompressibility upon stretching and to study the material anisotropy, all three principle stretches are needed during uniaxial tests. Therefore, an original experimental setup was established.

- <u>Non-proportional loadings</u>: Significant model insufficiencies regarding the Mullins softening are due to the lack of experimental data resulting from non-proportional loadings.

Therefore, an original experimental protocol was defined to acquire such data. For this purpose, two different types of non-proportional loadings were used. The first one is composed of two successive uniaxial tension experiments applied in two different material directions. For the second one, biaxial tension tests are performed prior to an uniaxial loading. A biaxial testing device has been built for this specific problem.

1.6 Experimental developments

The experimental strategy was previously established according to the literature review. This section aims at introducing the experimental setup used throughout the thesis. In order to perform experiments on rubber-like material, a particular experimental setup is required. The main components are presented in what follows as well as specific experimental procedure used in the sequel.

Experimental notations

For clarity, all notations used for experimental characterization are introduced here. Those notations will be unchanged along the thesis. In order to characterized the loading, principal components of the deformation gradient tensor $\boldsymbol{F}$ are used and organized such as F_{11} in the main tension direction, F_{22} in the secondary or transverse direction and F_{33} in the sample thickness direction. For uniaxial loading, λ may conveniently stand for the principal stretch in the tension direction. The Cauchy stress $\sigma = F/S$ is mostly used for uniaxial tension responses, with F the force and S the current sample cross-section. Let us note that incompressibility is commonly assumed when computing the Cauchy stress and gives $S = \lambda^{-1}S_0$ with S_0 the initial sample cross-section.

1.6.1 Deformation measurement

Because of the large extensibility and the low stiffness exhibited by our materials, the deformation measurements is a key component demanding good accuracy for successful experiments. In the following, the deformation measurement setup and the testing methods are detailed. Few issues that can significantly alter the experimental results are also illustrated.

Deformation measurement setup

The deformation gradient tensor, $\boldsymbol{F}$, is the link between the initial material configuration and the current deformed material configuration. In order to acquire local measures and to avoid any contact with the sample, strain measures are performed by video extensometry. The same method, setup and image analysis algorithm are used for every experiment and every sample geometry. Sample face is pinpointed with two or four painted marks. During test, mark motions are captured by a CCD camera. Images are analyzed in real time using a homemade algorithm programmed in C/C++ with OpenCV libraries for image processing. Tensor $\boldsymbol{F}$ components are computed from mark barycenters considering image grey levels. Such a video extensometer method may seemed obsolete with the wide development of digital image correlation (DIC) and integrated digital image correlation (IDIC) to follow large strains as encountered for rubber-like materials. However, only homogeneous strains are considered for experiments presented in what follow and video extensometry is more convenient and reliable. Moreover, neither DIC nor IDIC are currently able to be used for real time control testing devices due to image processing duration. Strain computation is usually post-processed, hence cannot be used for accurately control the experiment.

CCD Elphel NC353L cameras were used. Cameras capture 2592×1936 pixels images. However, the sensor size may be reduced to focus on a reduced zone, leading to smaller image and higher number of frames per second (fps). 100 fps may easily be reached, which is very interesting for real time control testing applications. According to the experimental setup, two focal lengths were chosen, a Linos MeVis-C with a fixed focal length of 35 mm and a Zeiss Makro-Planar T ZF with a fixed focal length of 50 mm. Both are high quality lenses designed for no distortion across the full field. Note that optical distortions can induce significant errors on deformation measurements. In order to illustrate optical distortion effect, Figure 1.4a shows a chessboard pattern captured by a low quality lens. Image barrel distortion appears to be very important. It was tested that such distortion leads to a $\Delta\lambda = 0.1$ error for a $\lambda = 5$ measure. The chessboard pattern captured by the Linos MeVis-C lens is shown in Figure 1.4b. No significant image distortion is observed, hence no correction is needed.

(a)   (b)
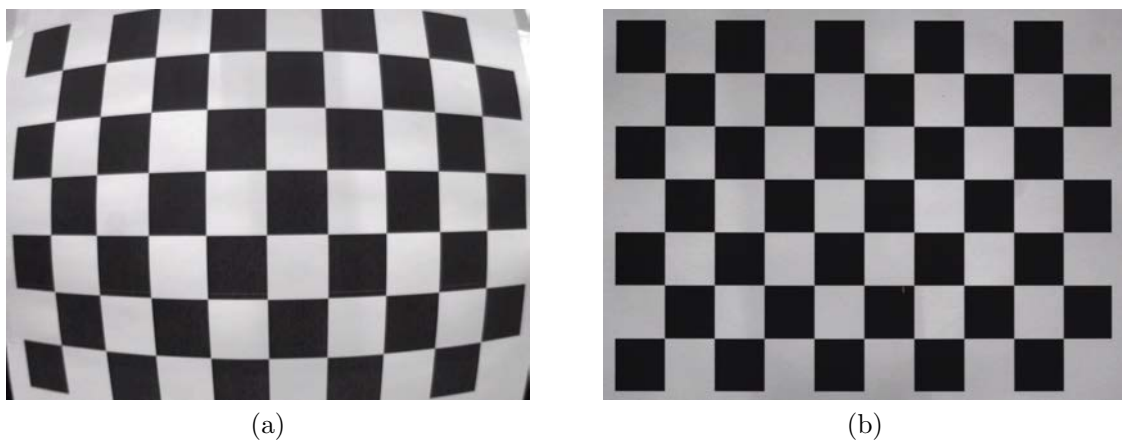
Figure 1.4: Chessboard pattern used for controlling and eventually correcting the optical aberrations. (a) Low quality lens. (b) High quality lens.

Initial configuration

The Mullins softening evolves from the very beginning of the stretching. Therefore, its experimental study requires an accurate measurement of stretches characterizing the state of strain between the <u>virgin material</u> configuration and the current configuration. For this purpose, initial configuration characterization is extremely important and might induce some critical experimental data miscalculation because even a slight error in the initial state is amplified at large strains by the stretching.

For instance, in uniaxial tension the stretch undergone by the material is $\lambda = l/l_0$ The difference with the measured stretch is given by $\Delta\lambda = \lambda^{\text{meas}} - \lambda$. An error $\Delta l_0 = l_0^{\text{meas}} - l_0$ on the initial length measurement may be characterized by $\lambda_{\text{err}} = 1 + \Delta l_0/l_0$. Such an error acts as a factor on the stretch λ undergone by the material and leads to a measured stretch $\lambda^{\text{meas}} = \lambda \times \lambda_{\text{err}}$. Therefore, even a small initial difference, Δl_0, on the initial configuration may become very significant at large stretches because $\Delta\lambda = \lambda \times \Delta l_0/l_0$. Figure 1.5 illustrates the stretch difference, $\Delta\lambda$, according to the error on the initial configuration, $\Delta l_0/l_0$, and the applied stretch, λ. Let us note that when performing uniaxial experiment on a soft material, $\Delta l_0/l_0$ may easily reach 5% if the sample is clamped without care. This error is enlarged for a plane biaxial experiment due to the four grids to clamp.

Experimental protocol has been developed to ensure initial configuration characterization accuracy. The studied materials are very soft. Hence, sample clamping induces uncontrolled and non-predictive deformations. To overcome this problem, initial material configuration character-
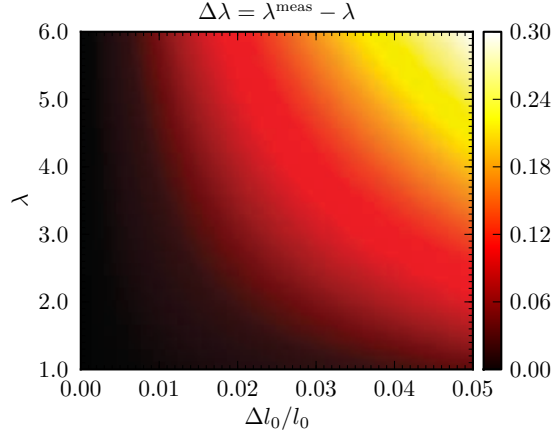
Figure 1.5: Error $\Delta\lambda$ induced by a mismeasurement Δl_0 of the initial configuration for an uniaxial tension test.

ization is performed while sample is only clamped to the upper grip. Then, once measurement is acquired, sample is fully connected to the testing machine. It is noteworthy that suitable sample grips are required to efficiently test rubber-like materials. Such grips were engineered by my own to improve ease of use and testing repeatability, they are described in Section 1.6.2.

Principal loading basis

Material deformation is characterized by the non-symmetric deformation gradient tensor $\boldsymbol{F}$ and for its computation the symmetric right Cauchy-Green deformation tensor, $\boldsymbol{C} = \boldsymbol{F}^t\boldsymbol{F}$, is used. In the sequel, experiments are performed with at least one sample plane face being free of stress. Direction 3 being normal to this surface, it can reasonably be assumed that such a direction is also a principal tensor $\boldsymbol{C}$ direction ($C_{13} = C_{23} = 0$ may be assumed because no sample surface out of plan distortions are observed). Then C_{11}, C_{22} and C_{12} components can be computed from length and orientation changes of two vectors "drawn" on the sample surface. Thus, two vectors $\boldsymbol{a}$ and $\boldsymbol{b}$ with initial lengths a_0 and b_0, and there current lengths a and b are introduced. Initial and current angles between $\boldsymbol{a}$ and $\boldsymbol{b}$ are defined as α_0 and α, respectively. For practical reasons, $\boldsymbol{a}$ is given by the upper and the lower marks, and $\boldsymbol{b}$ by the left and the right marks. It is to be notice that vectors $\boldsymbol{a}$ and $\boldsymbol{b}$ are not necessarily orthogonal either in the initial configuration or in the current one. At any time, α read

$$\alpha = \arccos\left(\frac{\boldsymbol{a}.\boldsymbol{b}}{ab}\right) \tag{1.18}$$

among other expressions. According to the right Cauchy-Green deformation tensor definition (*i.e.* $\boldsymbol{x}.\boldsymbol{y} = \boldsymbol{x}_0.\boldsymbol{C}.\boldsymbol{y}_0$ with vectors $\boldsymbol{x}$ and $\boldsymbol{y}$ evolving from $\boldsymbol{x}_0$ and $\boldsymbol{y}_0$, respectively), its components expressed in an orthogonal material basis oriented according to direction 3 and vector $\boldsymbol{a}$ direction, and labelled m read

$$_mC_{11} = \left(\frac{a}{a_0}\right)^2, \tag{1.19}$$

$$_mC_{12} = \frac{ab\cos(\alpha) - a_0b_0\cos(\alpha_0)\ _mC_{11}}{a_0b_0\sin(\alpha_0)} \tag{1.20}$$

and

$$_mC_{22} = \frac{b^2 - \left(b_0\cos(\alpha_0)\right)^2\ _mC_{11} - 2b_0^2\cos(\alpha_0)\sin(\alpha_0)\ _mC_{12}}{\left(b_0\sin(\alpha_0)\right)^2}. \tag{1.21}$$

Tensor $\boldsymbol{C}$ components in the principal loading basis are assessed by computing eigenvalues through

$$C_{ii} = \frac{{}_m C_{11} + {}_m C_{22} \pm \sqrt{({}_m C_{11} - {}_m C_{22})^2 + 4 \ {}_m C_{12}^2}}{2} \qquad \text{(no sum)}. \qquad (1.22)$$

Finally, the tensor deformation gradient $\boldsymbol{F}$ eigenvalues come as

$$F_{ii} = U_{ii} = \sqrt{C_{ii}} \qquad \text{(no sum)} \qquad (1.23)$$

since in regard to the experiments performed during this thesis, the rigid rotation $\boldsymbol{R}$ defined by the polar decomposition $\boldsymbol{F} = \boldsymbol{RU}$ does not affect the experimental results.

Figure 1.6 illustrates the importance of using relations Eq. (1.18) to Eq. (1.23) instead of computing the normalized distances between marks to estimate the values of F_{11} and F_{22}. Four mark positions are acquired during a cyclic uniaxial tension test and both methods are used to compute stretches F_{11} and F_{22}. Results are compared in Figure 1.6a. It can be observed that differences along the loading direction are limited to few percent of strain even when $\lambda = 6$, therefore length ratio l/l_0 from a two mark measure provides a fairly good approximation for machine controlling. On the contrary, it is to be stressed that differences along the transverse direction are significant. In order to explain such unrealistic results, a numerical sample is presented in Figure 1.6b. The sample is computed with transverse marks oriented in a 5-degree angle from the horizontal axis. The left sample shows the initial state, and then changes induced by a perfect uniaxial tension are computed. During loading beginning, transverse marks become closer due to incompressibility, see mid sample stretched up to $\lambda = 2.6$. But for larger stretching, the transverse marks vertical displacement becomes predominant and the distance between the marks increases. That can be noticed for $\lambda = 6$ on the right picture. Therefore, stretches computed from length ratios may lead to erroneous strain characterization and should be avoided.

(a) (b)
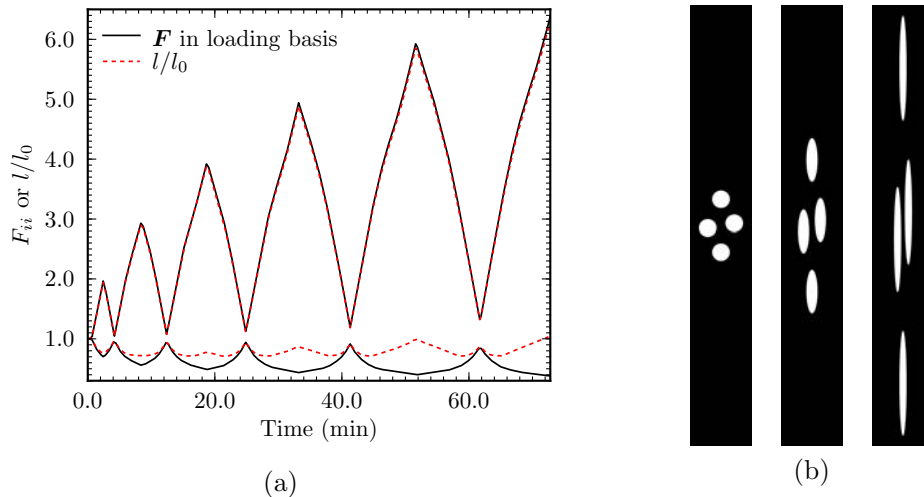
Figure 1.6: (a) Experimental stretch measurements and normalized distences between marks during a cyclic uniaxial test. (b) Numerical (Matlab computing) samples in initial configuration then uniaxialy stretched up to $\lambda = 2.5$ and 6.

As a side issue, It is noteworthy that numerical samples showed in Figure 1.6b were originally computed to be compiled in a movie for testing and controlling each components of the deformation measurement setup as well as the whole chain.

1.6.2   Sample gripping

In addition to stretch measurements, the connexion between sample and testing machine is a crucial component of the experimental setup. The design of such a connection is challenging for rubber-like materials. As explained in the previous section, for soft materials, the sample gripping is determinant regarding the initial material configuration characterization. Moreover, studied materials are able to undergo very large strains (up to $\lambda = 8$). Thus, during an experiment, sample thickness decreases with the applied stretch. For instance, when $\lambda = 6$ is reached in uniaxial tension, sample thickness is divided by 2.4 when considering the material incompressibility assumption. Therefore, using classical grips, sample need to be tight very strong to avoid slippage. Hence material will be locally damage and out of plan sample deformations will occur. Furthermore, initial configuration will not be accurately characterized and during a cyclic loading, assessing the relaxed configuration, *i.e.* via $F = 0$ measurement will be inaccurate. Finally, as a matter of fact, samples will slip anyways and stretch to failure will be unreachable.

In order to avoid such troubles, two main gripping solutions are available for plane samples. Pneumatic action grips are the preferred solution for industrial application. They are very efficient, but expensive and an air compressor is required. As a value-priced efficient alternate, self-tightening grips can be used. Such self tightening grips suitable for the studied materials were engineered. Figure 1.7 illustrates the pincer shape grips chosen design. The principle of operation is basic and efficient. The sample does not need any preparation and its insertion is extremely easy. An initial clamping force is provided by springs action. Then the clamping force increases with the loading tensile force. Moreover, the jaws tighten themselves when the sample thickness decreases with stretching. Therefore, the sample cannot slip and do not need to be strongly tight at the beginning of the test. Over time and experiments, such a design has proved to be very efficient and easy to use. Initially engineered for 150 mm large pure shear samples, pincer shape grips were finally used of all uniaxial and biaxial experiments.

1.6.3   Uniaxial tests

The uniaxial tension tests were conducted on an Instron 5882 uniaxial testing machine operating at room temperature. The force was measured by a 2 KN load cell. All tests were run at constant crosshead speed and local stretches were used to control the loading. In order to evaluate all three principal stretches, a second camera was added when needed, each one of them positioned in front of one orthogonal sample free face. The two cameras setup is illustrated in Figure 1.8. Samples and machine are connected by two pincer shape self tightening grips detailed in Figure 1.7a. Because only one grip is mobile and the other is fixed, substantial displacement of the sample central zone used for deformation measurement occurs during a tension test. Therefore, the camera needs to be repositioned to avoid moveing out of the field view. For this purpose, both cameras are fixed on a homemade vertical motorized adjustable support. Vertical position is automatically adjusted and controlled by the video extensometer in order to align the center field camera sensor with the mid length between upper and lower marks.

During the study, various sample geometries were used for uniaxial tension tests. Normalized sample beeing dumbbell shape 30 mm long and 4 mm wide, punched in 2.5 mm tick sheets. Two other specific sample geometries were necessary, a larger dumbbell 25 mm wide and 60 mm long, and a smaller one 4 mm wide and 10 mm long.

1.6.4   Biaxial tests

According to the experimental strategy introduced Section 1.5.2, material samples submitted to non-proportional loadings including biaxial loading paths are used. Biaxial experiments were carried out on a house-built planar biaxial testing device built with four perpendicular electromechanical actuators. The testing device is shown in Figure 1.9. It must be notice
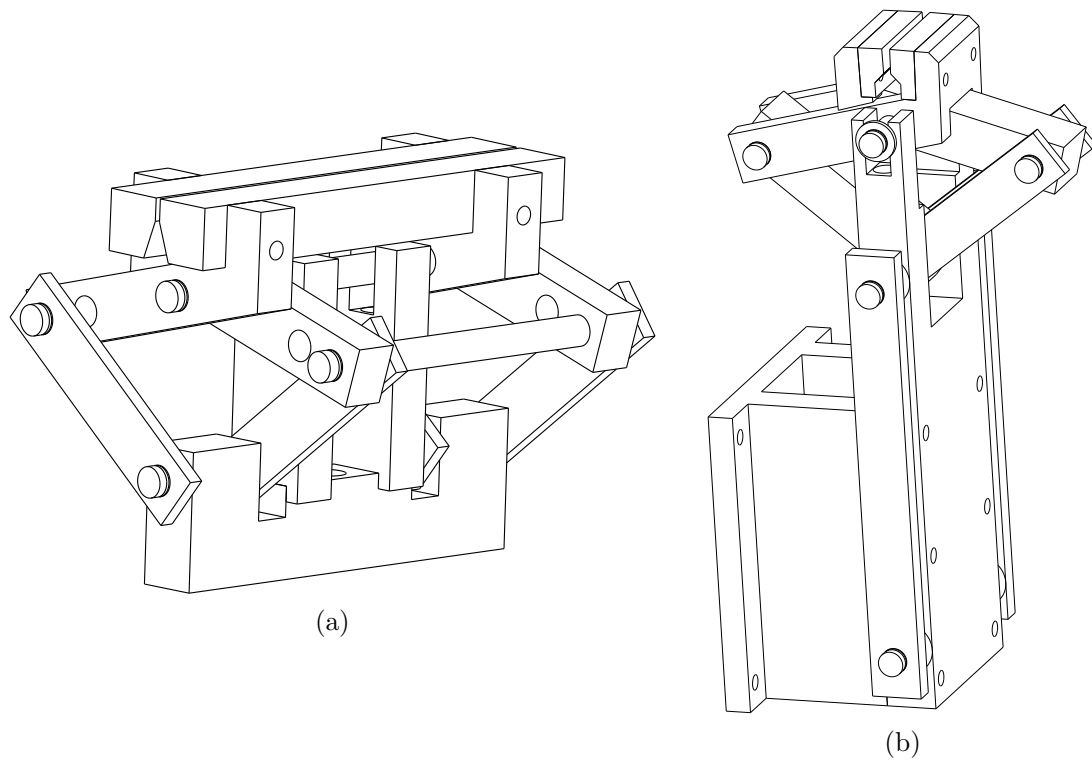
Figure 1.7: Pincer shape self tightening grips. (a) Design for uniaxial experiments. (b) Design for biaxial testing device.
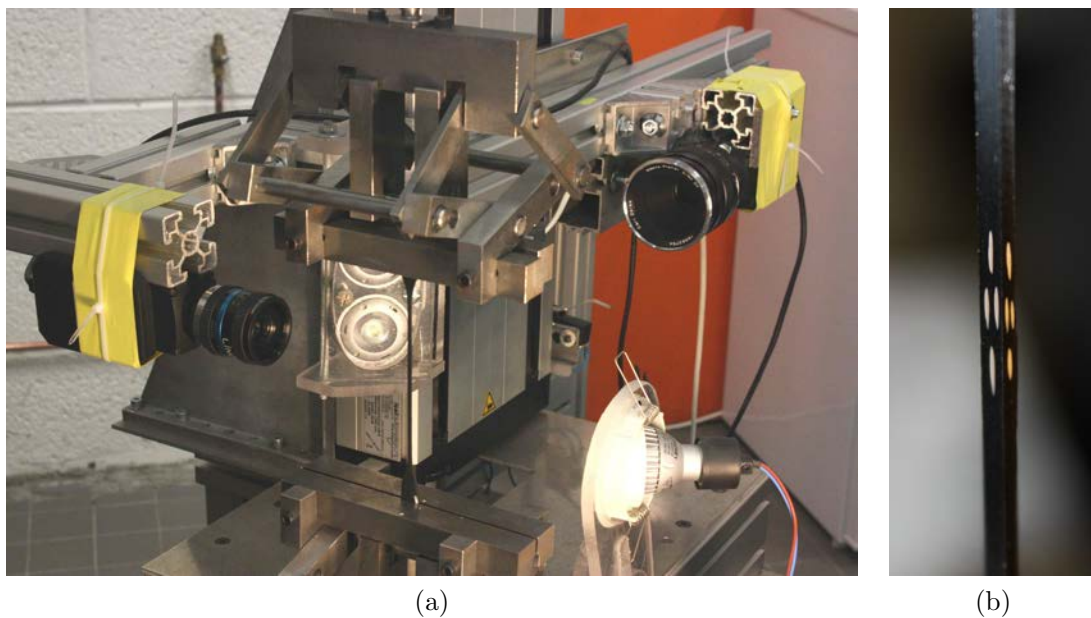
Figure 1.8: Uniaxial testing. (a) Device with two cameras in front of two orthogonal sample free faces. (b) Stretched sample with one sets of 4 paint marks on each free faces. Initial sample cross-section is 4×2.5 mm^2.

that the biaxial testing device has been designed and engineered from scratch within the thesis duration. Cross shape biaxial samples were designed and optimized for a largest central zone

with homogeneous strains (Brieu et al., 2007). Sample and machine are connected by four pincer shape self tightening grips detailed in Figure 1.7b. Theses grips were designed in order to allow them to be very close along the 4 directions as shown in Figure 1.9a and still permit an easiness of use avoiding any local sample damage. Each grip is fixed to an electromechanical actuator. An electromechanical actuators is composed of few elements, a linear table, a gearheads, a servomotor and a servo drive. The linear positioning table has a mobile carriage guided along a translation axis and controlled in motions by an integrated ball screw. Such a positioning table ensures an accurate displacement for the grip (fixed to the carriage) along a 600 mm travel range. For safety, adjustable limit sensors on each side of the travel range are used to prevent overtravel of the carriage. The ball screw shaft is connected to a servomotor via an intermediate gearhead for torque reduction (hence a lower motor capacity). The servomotor is a brushless motor. It is commanded by a servo drive and command modes might be torque, velocity, position, among others. The servo drive can be connected to a computer and be programmed via a standard serial communication. Finally, once communication parameters have been setup, basic communication instructions can be used to command the servo drive, hence the carriage (or grip) motion. More importantly, such instructions can easily be incorporated within a C/C++ programming code. Therefore, the four actuators are controlled independently using an algorithm programmed in C/C++.

| (a) | (b) |
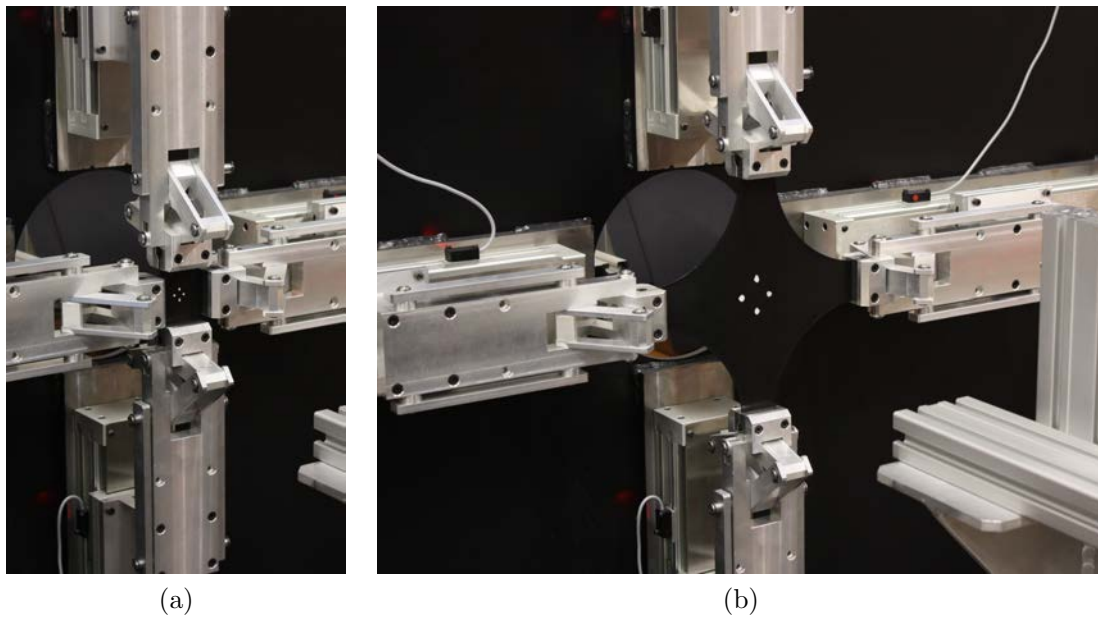
Figure 1.9: Biaxial testing device (a) before and (b) during stretching. Both pictures are at the same scale.

In order to accurately applied multiaxial loading paths, the servomotors are commanded in velocity mode and control in real time by the stretches measured on the sample by video extensometry (see Figure 1.9b). Image processing is performed in real time according to details provided in Section 1.6.1. Both, the servo drive communication and the image processing are performed on the same computer, using the same environment and the same programming code. Therefore, using the local stretches measured from 4 paints marks to control the actuators is not very challenging and do not required any additional hardware. Actuators are controlled by pair for all experiments. Using this method, any biaxial tension condition is reachable and the sample marked zone barely moves from the center of the camera sensor field. Therefore, there is no need for an adjustable support, the camera can be fixed. For biaxial tests, a master direction is chosen, usually the vertical direction, and tests are run at constant "crosshead" or grip speed

along this specific direction. To ensure that the desired loading path is accurately applied, stretch along second direction is controlled in real time using video extensometry measurements.

1.6.5 Experimental procedure

In the sequel, an original experimental procedure will be used in order to investigate the mechanical response of materials submitted to successive non-proportional loadings. This section provides technical details and the procedure is synopsized in Figure 1.10.
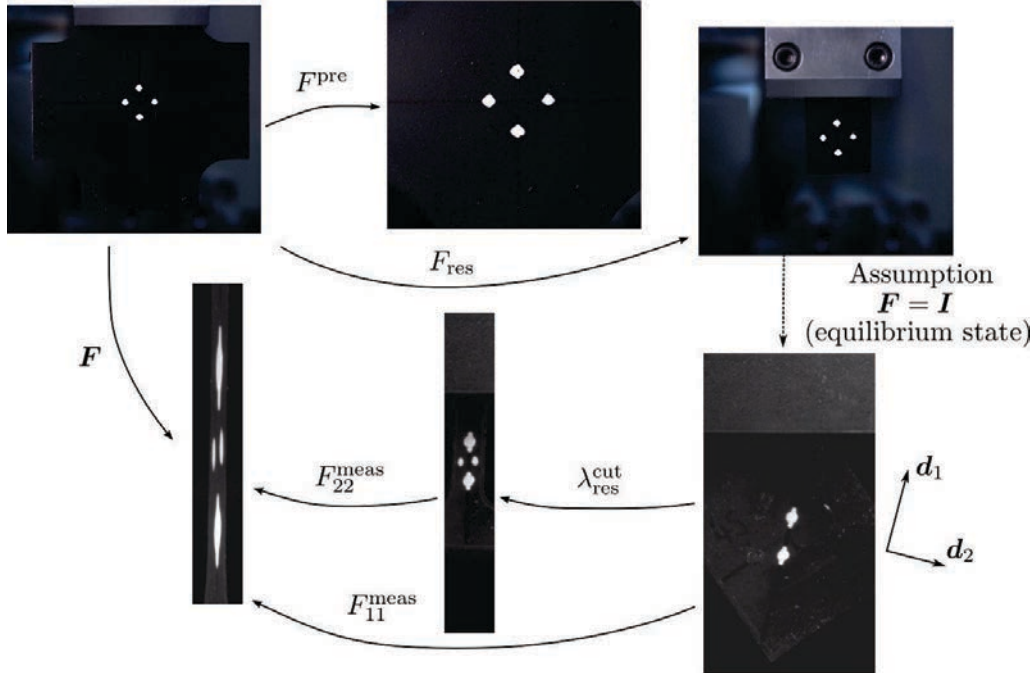
Figure 1.10: Experimental procedure and configuration characterizations.

The developed experimental protocol aims at applying a complex stretching history to a material and for this purpose, various sample geometries are required. Therefore, the first pre-stretched sample need to be unclamped then a smaller sample will be punched in, before being submitted to a uniaxial tension test. According to Mullins softening experimental observations (see Section 1.3.1), the residual stretch evolves with the softening during the first stretching. When applying a biaxial pre-loading, the sample is softened non-homogeneously and buckling occurs. Figure 1.11 (left) shows a 2.5-equibiaxially pre-stretched sample and one may notice the buckling. In order to allow the sample recovery towards an equilibrium state, the zone of interest is cut apart from useless sample parts as illustrated in Figure 1.11.

After a 24 hours rest to ensure the viscoelastic quasi-stabilization, the remaining sample part is clamped to the upper testing machine grip and a camera is used to acquire marks positions. Deformation from material virgin configuration to the current residual configuration is characterize by the tensor $\boldsymbol{F}_{\text{res}}$. Then all four paint marks are removed and two new marks are painted along the next loading direction defined by the unit vector $\boldsymbol{d}_1$. The two mark positions are measured via a camera acquisition and small uniaxial tension dumbbell is punched along $\boldsymbol{d}_1$ (see Figure 1.11 on the left). It is to emphasized that punching a small sample with four marks cannot be considered seriously. Two marks position before cutting is the initial configuration used for the last uniaxial tension test and relation between the measured stretch λ^{meas} and the
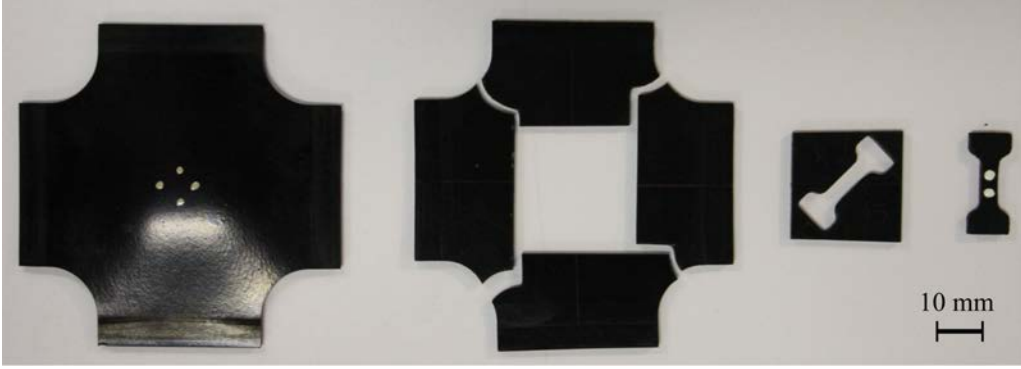
Figure 1.11: Uniaxial dumbbell samples cut from biaxially stretched specimens.

overall stretch λ expressed form material virgin configuration reads

$$\lambda = \lambda^{\mathrm{meas}}\sqrt{\boldsymbol{d}_1.\boldsymbol{C}_{\mathrm{res}}.\boldsymbol{d}_1}. \tag{1.24}$$

When transverse stretch F_{22} is also needed, an additional step is required. After the small dumbbell punching, left and right marks are painted. The current four marks configuration is characterized by video and at the same time, sample strains undergone during cutting, $\lambda_{\mathrm{res}}^{\mathrm{cut}}$, are computed only from two marks assuming material incompressibility and transverse isotropy. It is to be noted that $\lambda_{\mathrm{res}}^{\mathrm{cut}}$ is very small, few percents only, hence errors induced by the latter assumptions are very limited. Finally, F_{22} expressed form material virgin configuration is given by

$$F_{22} = F_{22}^{\mathrm{meas}}\sqrt{\frac{\boldsymbol{d}_2.\boldsymbol{C}_{\mathrm{res}}.\boldsymbol{d}_2}{\lambda_{\mathrm{res}}^{\mathrm{cut}}}} \tag{1.25}$$

with unit vector $\boldsymbol{d}_2$ normal to $\boldsymbol{d}_1$.

After pre-loading, the sample thickness varies due to the residual stretches $F_{11\,\mathrm{res}}$ and $F_{22\,\mathrm{res}}$. Assuming material incompressibility, $i.e.$ $\det(\boldsymbol{F}_{\mathrm{res}}) = 1$, all principal $\boldsymbol{F}_{\mathrm{res}}$ components are known. Therefore, the Cauchy stress during the last loading can be expressed as

$$\sigma = \frac{F}{S} = \frac{F\lambda^{\mathrm{meas}}}{S_0 \ F_{33\,\mathrm{res}}} \tag{1.26}$$

with S_0, the cross-section if sample was punched in a virgin material ($i.e.$ considering initial sheet thickness).

1.7   Conclusion

This chapter aimed at providing basis and motivations on objectives for the entire thesis works. For this purpose, a literature review on the mechanical behavior of rubber-like material submitted to cyclic loading conditions was given. By analyzing the existing works, it was noticed that significant modeling issues still needed to be addressed. Therefore, an experimental strategy was established in order to assess the required experimental data. The experimental strategy leaded to develop original testing procedures and setup for characterizing the mechanical behavior of rubber-like materials.

Several experimental parts were engineered and built within the thesis duration. Therefore, this chapter also aimed at illustrating some key components to successfully test rubber-like materials and to acquire reliable experimental data. The strain measurements, the sample gripping,

the uniaxial testing machine and the biaxial testing device were described. An uncommon testing procedure that will be used in subsequent chapters was also introduced in order to provide data processing details.

During the following chapters, the experimental strategy is applied and results are analyzed in order to provide answers to modeling issues highlighted by the literature review.

Chapter 2

Materials

Some parts of this chapter have been published and can be found in reference:

- *Yannick Merckel, Mathias Brieu, Julie Diani, Daniel Berghezan, 2011. Effect of material and mechanical parameters on the stress-softening of carbon-black filled rubbers submitted to cyclic loadings, Proceedings of the 7th European Conference on Constitutive Models for Rubber, ECCMR 2011, 253-257.*

Several carbon-black filled styrene-butadiene rubbers (SBRs) were studied during the thesis. They are introduced and their compositions are given in this chapter. The material preparation is described and its initial anisotropy is studied. Uniaxial tension experiments were performed. Firstly, volume changes are shown to be significant upon monotonic stretching, but material incompressibility assumption remains consistent when considering cyclic uniaxial loading. Secondly, monotonic tension were used in order to characterize few basic mechanical properties according to the material composition. Finally, cyclic tensions were applied to illustrate basic observations of the Mullins softening and the cyclic softening.

Contents

2.1 Introduction

The mechanical behavior of rubber-like materials depends strongly on its microstructure. A wide variety of filled rubbers are used in industrial and research fields. The literature review in Chapter 1 highlights that the three main mechanical characteristics addressed during the thesis, *i.e.* hyperelastic response, Mullins softening and cyclic softening, are strongly impacted by the material composition and microstructure. Moreover, the relationship between the rubber composition and the mechanical response is not clearly established and remains an ongoing issue. In order to study that, several materials with various compositions were chosen. The material strategy was to vary the filler amount and the crosslink density. It is clearly established in the literature that the filler amount has a significant effect on the material behavior (see the review of Kohls and Beaucage (2002)) and also on the softening (see the review of Diani et al. (2009)). To the contrary, it is known that the crosslink density modifies the material behavior (stiffness, stretch at failure, for instance), but its effect on the softening is yet undetermined.

For a better understanding of the mechanical behavior of the chosen materials, a basic experimental characterization is performed. The first experimental objective of this chapter is to investigate the incompressibility commonly assumed for rubber-like materials. Actually, it appears that many contributions report significant volume changes within filled rubbers upon stretching. A recent review on the topic was proposed by Le Cam (2010). Moreover, volume changes evolution with the applied stretch is not clearly established and they are some disagreements between the few published experimental results. Therefore, volume changes are studied in order to validate or invalidate the incompressibility assumption for specific materials and loading conditions considered. The second experimental objective is to investigate the hyperelastic stress-stretch response dependencies to the material compositions. For this purpose, samples were submitted to monotonic uniaxial tension loadings. The material stiffness and the stretch to failure, were studied. Finally, the third experimental objective is to illustrate few basic features of the material softening when samples are submitted to cyclic loading conditions. Dependencies to material composition will be discussed in order to introduce some works developed in subsequent chapters.

This chapter is organized as follow. In the next section all materials used in the sequel are introduced and described. Then, the material incompressibility is studied and discussed in Section 2.3. Section 2.4 addresses material stress-stretch responses under monotonic loadings. Section 2.5 illustrates basic experimental observations regarding the stress-softening induced by cyclic loadings. Finally, concluding remarks close the chapter.

2.2 Materials

2.2.1 Material composition

For this study, several carbon black filled vulcanized rubbers were manufactured by the french manufacture of tires Michelin. The material labelled NR is a natural rubber, the others are synthetic styrene-butadiene rubbers (SBR). The SBR gum is a random copolymer with a 15% styrene molar fraction. NR gum density is 0.91 g/cm^3 and SBR gum density 0.94 g/cm^3. N347 carbon-black fillers were used, which morphology is characterized by the fineness of elementary particles and by the aggregate structure. Fineness corresponds to the specific surface area of fillers, which was found close to 90 m^2/g by nitrogen absorption using the Brunner Emmet Teller (BET) analysis. Aggregate structure characterizes the branching of aggregates, and is measured at 120 ml/100g by dibutyl-phthalate absorption (DBP absorption). Fillers density is 1.8 g/cm^3. A classical crosslinking system based on sulfur and CBS is used. Sulfur and CBS densities are 2.05 and 1.3 g/cm^3, respectively. For material labeled R the crosslinking reaction is activated by Struktol ZEH and for the other materials by zinc oxide and stearic acid. Struktol ZEH, zinc

oxide and stearic acid densities are 1.2, 5.7 and 0.85 g/cm^3, respectively. A 6PPD antioxidant with a 1.07 g/cm^3 density is added. All material compositions are listed in Table 2.1.

Ingredient	R	A4	B4	C1	C2	C3	C4	C5	C6	D4	E4	NR
SBR	100	100	100	100	100	100	100	100	100	100	100	-
NR	-	-	-	-	-	-	-	-	-	-	-	100
Carbon-black (N347)	40	40	40	-	5	30	40	50	60	40	40	40
Antioxidant (6PPD)	1.0	1.9	1.9	1.9	1.9	1.9	1.9	1.9	1.9	1.9	1.9	1.9
Stearic acid	-	2.0	2.0	2.0	2.0	2.0	2.0	2.0	2.0	2.0	2.0	2.0
Zinc oxyde	-	2.5	2.5	2.5	2.5	2.5	2.5	2.5	2.5	2.5	2.5	2.5
Struktol ZEH	3.0	-	-	-	-	-	-	-	-	-	-	-
Accelerator (CBS)	1.5	4.7	2.3	1.6	1.6	1.6	1.6	1.6	1.6	1.2	1.0	1.6
Sulfur	1.5	4.7	2.3	1.6	1.6	1.6	1.6	1.6	1.6	1.2	1.0	1.6

Table 2.1: Material compositions in parts per hundred rubber (phr).

The material labeled R is the study's main material, it will be used to give grounds for experimental procedures and for modeling frameworks. Material R contains 40 phr of fillers which corresponds to a volume fraction $\Phi = 0.16$. The crosslink density N_c was measured by Michelin by swelling using the Flory-Rehner theory and is $N_c = 5.08 \times 10^{-5}$mol/cm^3.

Several comparable materials were defined in order to investigate the relation between material composition and mechanical behavior. The material strategy was to vary the filler volume fraction Φ and the crosslink density N_c. From a reference material C4, materials C1, C2, C3, C5 and C6 were obtained by varying the filler amount from 40 phr to 0, 5, 30, 50 and 60 phr, resulting in 0, 0.13, 0.16, 0.19 and 0.23 volume fractions, respectively. Materials A4, B4, D4 and E4 contain the same amount of fillers than material C4 but their crosslink densities vary. Figure 2.1 illustrates the material strategy. The lists of filler volume fractions and of crosslink densities appear in Table 2.2.

Finally, the natural rubber named NR is similar to material C4 in term of filler amount and crosslink density but the resulting stress-stretch response exhibiting a substantial crystallization during stretching. It was only used when a very different behavior from SBR is wanted.

	R	A4	B4	C1	C2	C3	C4	C5	C6	D4	E4	NR
Φ	16.71	16.18	16.54	0.00	2.43	13.03	16.65	19.98	23.06	16.72	16.75	16.23
N_c	5.08	15.53	10.55	7.00	6.53	8.16	7.38	8.26	7.71	5.42	3.63	7.03

Table 2.2: Filler volume fraction Φ in % and crosslink density N_c in 10^{-5}mol/cm^3 for each material.

2.2.2   Material preparation

Compounds were mixed in two steps. The first step was performed in an internal mixer with a mixing chamber of 7000 ml. The starting temperature was 50°C. Elastomer, fillers, antioxidant and activator were introduced at the beginning and the dump temperature close to 165°C was chosen as the main parameter to release the compound. In a second step, curing agents, *i.e.* accelerators and sulfur, were added using a two-roll mill. Once mixed and still uncured the material is calendered and transformed into sheets of 2.8 mm thickness (typically 180 mm wide and 1 m long). Next, plates of $150 \times 150 \times 2.8$ mm^3 are punched out of these sheets. They are finally put into a mold of dimensions $150 \times 150 \times 2.5$ mm^3, where they are cured at 150°C under a 100 Bar pressure. Significant material amounts were used during the study and mechanical properties repeatability between subsequent batches were ensure by Michelin company knowledge.
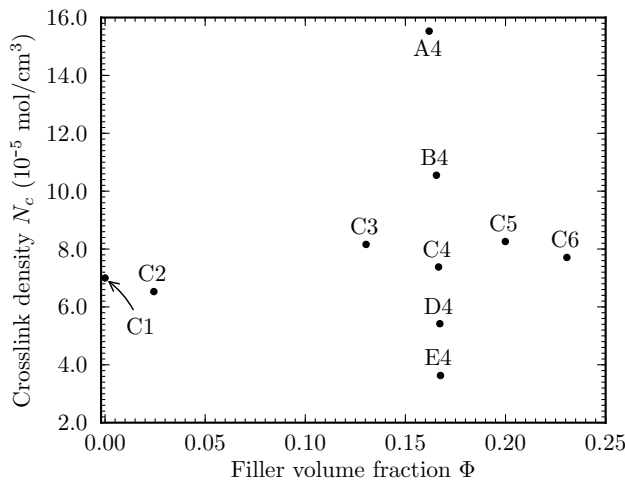
Figure 2.1: Material strategy.

2.2.3 Material anisotropy

All materials are sheet shape manufactured with a 2.5 mm thickness. In-plane isotropy was verified by testing in uniaxial tension samples punched in various directions. Material R stress-stretch responses in two orthogonal directions are shown in Figure 2.2a and are quasi-perfectly superimposed. Therefore, no sample punching direction has to be privileged.

In order to study the material anisotropy along the thickness direction, deviations from transverse isotropy may be used. During a uniaxial tension test in direction 1, boundary conditions $\sigma_{22} = \sigma_{33} = 0$ are given by the stress free faces. Therefore, the in-plan (2,3) anisotropy may be characterized by comparing stretches F_{22} and F_{33}, with $F_{22} = F_{33}$ being the particular transverse isotropy case. Material R ratio F_{22}/F_{33} evolution with λ is presented in Figure 2.2b. As expected because of the manufacturing process using a two-roll mill and a final curing in a mold, material anisotropy is observed along the sheet thickness direction.

(a)

(b)
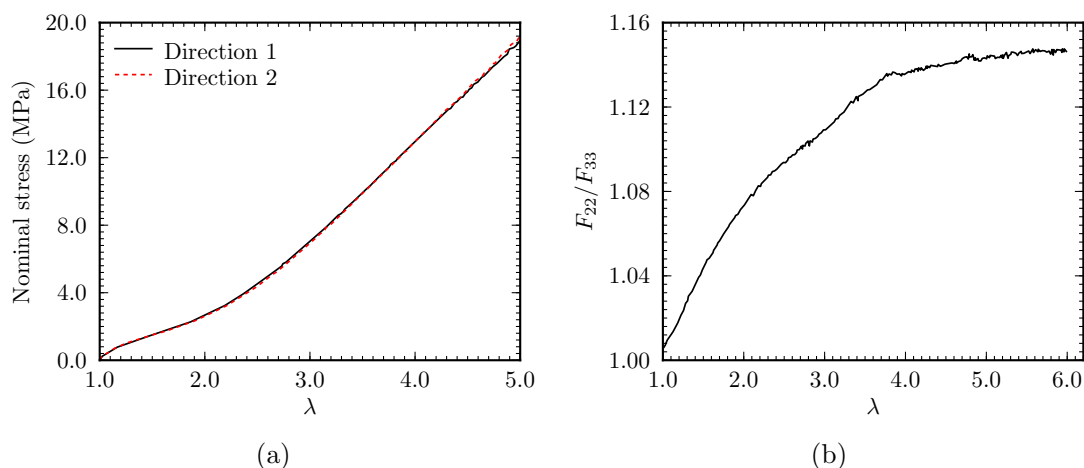
Figure 2.2: Material R initial anisotropy. (a) Comparison between uniaxial tension stress-stretch responses along two orthogonal directions. (b) F_{22}/F_{33} evolution during monotonic uniaxial tension test.

2.3 Material incompressibility

Incompressibility is widely used as an assumption for testing and modeling the mechanical behavior of rubber-like materials. Nevertheless, substantial volume changes have been reported within filled rubbers when stretched (see for instance Jones and Yiengst (1941)). These Volume changes are attributed to decohesion at the rubber-filler interface and to vacuole formation in the rubber matrix (Jones and Yiengst, 1941; Ramier et al., 2007). A review on the topic has been recently proposed by Le Cam (2010).

This section aims at investigating the significance of volume changes upon stretching within studied materials. Macroscopic measurements of material volume changes will provide true Cauchy stress-stretch responses, which will highlight the error generated by the incompressibility assumption when processing experimental data or when modeling the mechanical behavior. Volume changes may also lead to a better understanding of the physical mechanisms related to the Mullins softening.

2.3.1 Volume changes within stretched filled rubbers

Few methods have been used to assess at a macroscopic scale the volume changes within rubbers upon stretching. They have been firstly carried out using dilatometry measurements (Holt and McPherson, 1936; Jones and Yiengst, 1941; Gee et al., 1950; Mullins and Tobin, 1957; Shinomura and Takahashi, 1970; Kumar et al., 2007). Such a technique consists in immersing samples in a liquid (often water) which volume change is measured when the rubber is stretched. An alternative is to place the sample in a gas chamber and to deduce the volume changes from gas pressure measurements (Chenal et al., 2007; Ramier et al., 2007). The dilatometer measurements seem to be very accurate, nonetheless several minutes are required for each measurement in order to reach the dilatometer equilibrium rendering impossible dynamic measurements. Using dilatometry technique, Jones and Yiengst (1941) measured volume expansions in filled natural rubbers when stretched. They showed that volume changes are due to vacuoles forming at the rubber-particle interface. To the contrary unfilled natural rubbers exhibit very small volume changes for similar stretching conditions (Gee et al., 1950). The difficulty with natural rubber is that both vacuoles formation and crystallization contribute with opposite effects to volume change, rendering any interpretation delicate. Shinomura and Takahashi (1970) measured volume change in filled butyl rubber and filled SBR during stretching. They studied the effect of the type of fillers, the filler amount and the curing. They reported an increase of volume changes with the amount of fillers, 0.07 and 0.25 volume expansions for $\lambda = 4$ stretched samples with 20 phr and 50 phr fillers amounts, respectively. More importantly they noticed stretch thresholds of approximately 2.4 and 1.6 below which volume changes were unnoticeable for 20 phr and 50 phr filled samples, respectively.

Later, with the increase of video analysis for the local stretch measurements in stretched rubber-like materials, the video extensometry technique was extended to volume variation measurements (G'Sell et al., 1992; Wu and Liechti, 2000; Layouni et al., 2003; Addiego et al., 2006; Starkova and Aniskevich, 2010) as well as digital image correlation techniques (Le Cam et al., 2008; Le Cam and Toussaint, 2009). Nevertheless, for all pre-cited contribution longitudinal and transverse stretches are measured on one face of the samples only. Then, volume changes are estimated assuming material transverse isotropy. It is noteworthy that results obtained by video analysis coupled to the transverse isotropy assumption are in disagreement with the earlier dilatometry measurements. For instance, Le Cam and Toussaint (2009) used such a method to assess volume changes in a 34 phr carbon black filled SBR submitted to a cyclic uniaxial tension test. They reported a 0.09 volume expansion for $\lambda = 3$ stretched samples. The measured volume evolution is merely linear with respect to the applied stretch and no significant differences in volume changes are observed between the first cycle and subsequent cycles. However, according to

Shinomura and Takahashi (1970), for a SBR with such an amount of fillers, a material stretched up to $\lambda = 3$ should experience quasi-incompressibility at moderate stretches and the volume expansion should appear for stretching above a threshold depending on the amount of fillers. Moreover, it was shown by Mullins and Tobin (1957) that volume changes are different between a virgin material and a pre-stretched material. Therefore, the transverse isotropy assumption used by the previous authors is questionable. Bear in mind that, according to the results shown in Figure 2.2b, the transverse isotropy assumption was not validated for our materials. In some experimental works reported in the literature, cross-section changes are assessed during uniaxial tension tests by video analysis avoiding the transverse anisotropy assumption (Gloaguen and Lefebvre, 2001; Parsons et al., 2004, 2005; De Almeida et al., 2008; Fang et al., 2009; Grytten et al., 2009). For this purpose, stretches are measured on two orthogonal sample free faces using two cameras or using a single camera and a right-angle optical prism. However, these contributions mainly addressed the issue of determining the true stress during necking, hence do not focus on volume changes.

2.3.2 Materials and experiments

Mechanical tests were performed on the uniaxial testing machine described in Section 1.6.3. Thanks to the use of two cameras (see Figure 1.8), every principle stretch is measured. F_{11}, or equivalently λ, denotes the stretch in the tensile direction and F_{22} and F_{33} are the stretches along both transverse directions. The volume change is defined by $V/V_0 = \det(\boldsymbol{F})$, with V the current volume and V_0 the initial volume. Because 2.5 mm is large enough for a set of 4 paint marks, normalized dumbbell samples with a cross section of 4×2.5 mm^2 and a 30 mm length were considered. All tests were run in displacement control at a constant crosshead speed of 10 mm/min. Monotonic loadings up to failure and cyclic loadings with a maximal stretch increasing at each cycle with a step of $\Delta\lambda = 1$ were applied.

In this study, the reference material R is used to illustrate the loading path effect. Moreover, in order to investigate the volume change dependence to the amount of fillers, materials C2 to C6 with a filler amount ranging from 5 to 60 phr were chosen.

2.3.3 Results

Volume changes measured during uniaxial monotonic loadings are illustrated in Figure 2.3a for materials C2 to C6. First of all, in agreement with the experimental observations reported in the literature, this figure evidences that volume changes induced by stretching may be very large within a filled rubber. The results illustrate the strong impact of the filler amount on volume changes. It appears that the 5 phr filled material may fairly be considered as incompressible, and the volume expansion increases with the amount of fillers. Maximal volume expansions are very significant for materials with large amount of fillers. For instance, $V/V_0 \approx 1.2$ is undergone by the material filled with 60 phr. One may also notice that the volume does not expand at all until the material stretching reaches a threshold λ_t which depends on the filler amount. The stretching threshold decreases with increasing the filler amount. The values of λ_t are approximately equal to 2.5, 3, 3.5 and 4 for materials filled with 60, 50, 40 and 30 phr, respectively. These observations agree with earlier dilatometry results reported by Shinomura and Takahashi (1970).

To access the uniaxial Cauchy stress, the current cross-section S has to be measured while stretching the sample. The relation between current and initial sample cross-sections S_0 is given by $S = F_{22}F_{33}S_0$. In order to lighten the experimental setup, incompressibility is conventionally assumed and leads to $S = \lambda^{-1}S_0$. Cauchy stress responses computed with and without the incompressibility assumption are compared in Figure 2.3b for materials C2 to C6. As expected, differences occur over the threshold λ_t and become very significant at large stretches for materials

with the larger amount of fillers.
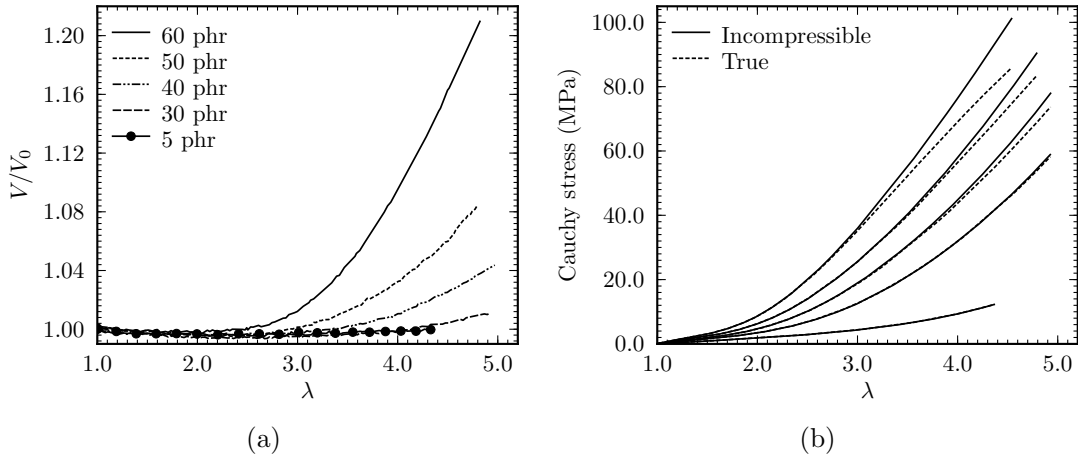
Figure 2.3: Materials with similar crosslink densities $N_c \approx 7 \times 10^{-5}$ mol/cm^3 and various amounts of carbon-black. (a) Uniaxial monotonic tension volume changes. (b) Effect of incompressibility lost on material Cauchy stress-stretch response to a uniaxial monotonic tension test.

Figure 2.4a shows the volume changes occurring within material R (40 phr) during a cyclic loading with an increasing maximal stretch. During the first cycles, no significant deviations form the V/V_0 monotonic path may be notice. For a larger cycle, when the stretch pass λ_t for the first time, volume changes expand during the loading and retract during the unloading with a noticeable hysteresis. For subsequent cycles, results put in light that no significant volume changes occur as far as the previous maximum stretch is not reached. It may be noticed that after a volume expansion, all re-loading curves seem to follow the same V/V_0 path. Then, when the previous maximal stretch is passed, volume expands significantly with a large hysteresis between loading and unloading. Figure 2.4a reveals that for a given maximum stretch, the cumulative volume expansion experienced by the material during a cyclic loading is comparable to the volume expansion measured during a monotonic loading. Cauchy stress comparison is shown in Figure 2.4b. One may notice that the difference between stresses estimates is noticeable when the load exceeds the maximum stretch previously applied, but may fairly be neglected during unloadings or re-loadings responses as far as stretching remains below the maximum stretch ever applied.

2.3.4 Discussion

First, it is to notice that the results presented here are among the first obtained by video measurement that reproduce the volume changes measured by dilatometry reported in the literature. Results show that for a filled rubber submitted to uniaxial tension, volume expands when the rubber is stretched above a stretch threshold. Moreover, it was noticed that this stretch threshold decreases with the increase of fillers and for very low filler amount, sample failure occurs before noticing any volume expansion. Very recently, most of the materials studied in this thesis were submitted to monotonic uniaxial tension and probed by synchrotron X-ray radiation for small angle X-ray scattering (SAXS). Experiments and results are reported by Zhang et al. (2012). The authors showed that cavities appear above a similar stretch threshold for our materials filled with 30, 40, 50 and 60 phr, and that no cavity appear for the 5 phr filled material. Moreover, the volume fraction of voids extracted from SAXS measurements corroborates the macroscopic volume changes.

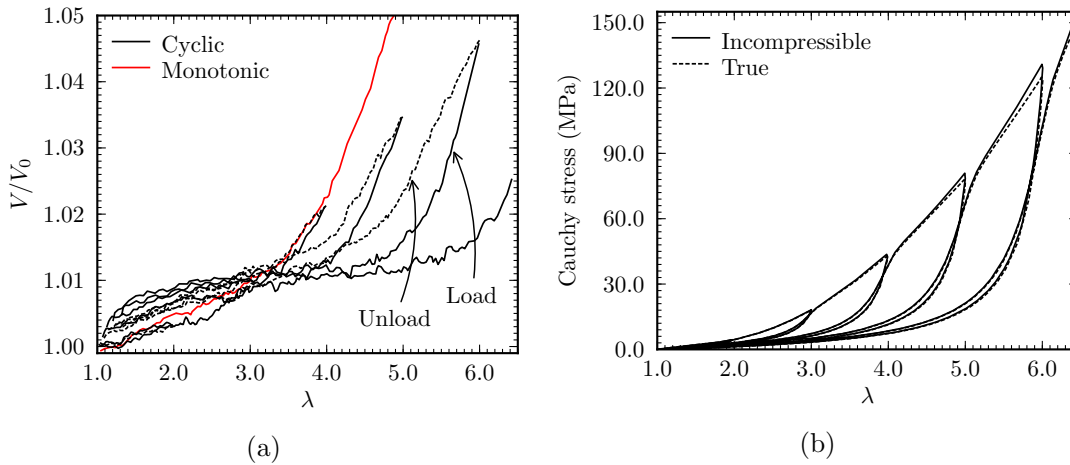Figure 2.4: Material R. (a) Uniaxial tension volume changes (data were smoothed for a clearer reading). (b) Effect of incompressibility lost on material Cauchy stress-stretch response to a uniaxial tension test.

Under cyclic uniaxial loading conditions, the full strain history plays an important role on the volume changes. Results put in light that for moderately to highly filled rubbers, the volume expands when the rubber is stretched beyond the maximum stretch ever applied but remains insignificant while the rubber is stretched below this maximum stretch. The latest observations are supported by SAXS analysis (not yet published), but up to now are not clearly established in the literature. Mullins and Tobin (1957) performed similar measurement by dilalometry on natural filled rubbers but crystallization induces a significant volume contraction. It is noteworthy that Le Cam and Toussaint (2009) submitted a 34 phr filled SBR to cyclic uniaxial tension and do not reported such observations, neither the stretch threshold before volume expansion. However, the latest authors measured stretches on one face of the samples only, and then estimate volume changes by assuming material transverse isotropy. Processing our own data with the same assumption for the material C3 filled with 30 phr leads to changes very similar to those reported by Le Cam and Toussaint (2009). That supports the experimental setup presented Section 1.6.3 with two cameras in front of two orthogonal sample free faces.

Figure 2.4 illustrates few similar features between the volume change and the Mullins softening. Firstly, they are both triggered when the material is stretched above the maximal stretch ever applied. Then, they both require a minimum amount of fillers to occur and both effects are amplified by the amount of fillers. However, Figures 2.3 and 2.4 show that a stretch threshold must be reached before volume changes while the Mullins softening is observed for stretches well below those thresholds. Therefore, one cannot draw a direct link between the appearance of cavities and the Mullins softening. Even if cavitation might contribute to the Mullins softening, it could not be the main cause. Such an observation was already reported by Mullins and Tobin (1958); Kraus et al. (1966).

In terms of filled rubbers stress-stretch responses, the generally accepted incompressibility assumption introduce an overestimate of the Cauchy stress. Nonetheless, results show that under cyclic loading conditions, no significant volume changes occur as long as the stretching remains below the maximum stretch ever applied. Therefore, while assuming incompressibility seems unrealistic upon the first stretch, it shows to be a fair assumption for subsequent stretching below the maximum stretch ever applied (Figure 2.4b). In what follows, cyclic loadings are mainly used, hence the Cauchy stress resulting from uniaxial tension will be computed within incompressibility assumption and models will be proposed within an incompressible framework.

2.4 Material behaviors under monotonic loading conditions

This section aims at illustrating basic properties of the filled rubber mechanical behavior according to the material composition.

2.4.1 Materials and Experiments

For this study, all materials detailed in Figure 2.1 are considered in order to highlight the effects of the filler amount and the croslinking density on the mechanical behavior. Uniaxial monotonic tension tests up to failure are performed at a constant low crosshead speed of 10 mm/min. Because a dispersion is expected, the experiment was performed on seven virgin samples for each material composition. According to the results discussed in Section 2.3, the incompressibility assumption cannot be used to compute the Cauchy stress at large strain during a monotonic uniaxial tensile test. Therefore, the resulting stress used Figure 2.5 to illustrate the materials responses is the nominal stress defined by F/S_0.

The effect of the filler volume fraction on the stress-stretch response is shown in Figure 2.5a by comparing materials with similar crosslink densities, $N_c \approx 7 \times 10^{-5}$ mol/cm^3, and various filler amounts from 0 to 60 phr. The last one is equivalent to a $\Phi = 0.23$ filler volume fraction. One may notice the strong impact of the filler amount on the material stiffness. On the contrary, the stretch to failure appears to significantly increase when fillers are added in the compound, but the main changes seem to occurred when the amount of fillers is moderate. Moreover, this figure illustrates that a substantial amount of fillers is required within the material to show the stress-stretch response upturn classically observed for filled rubber materials. The effect of the crosslink density is evidenced in Figure 2.5b by comparing materials with the same filler amount of 40 phr, equivalently $\Phi \approx 0.16$, and a crosslink density ranging from 3 to 15×10^{-5} mol/cm^3. Results show a strong effect of the crosslink density on both the stretch to failure and the stiffness. It is noteworthy that a large increase of the crosslink density leads to a catastrophic fall of the mechanical properties. The material with $N_c = 15 \times 10^{-5}$ mol/cm^3 can barley withstand any mechanical solicitations due to a very low stretch to failure.
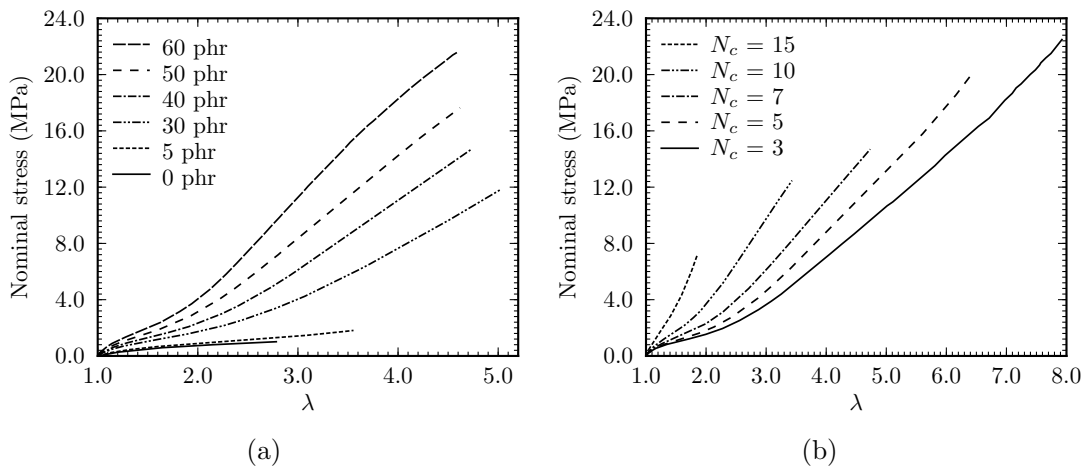
Figure 2.5: Materials stress-stretch responses to monotonic uniaxial tensile tests. (a) Effect of the amount of fillers for materials with various amounts of carbon-black and similar crosslink densities $N_c \approx 7 \times 10^{-5}$ mol/cm^3. (b) Effect of crosslink density for materials with various crosslink densities and similar filler volume fractions $\Phi \approx 0.16$ (40 phr).

In next sections, dependencies between material compositions and mechanical properties are

closely studied. Two mechanical properties are considered, the stiffness and the stretch to failure.

2.4.2 Stiffness and reinforcement

The stiffness is characterized at small strain by the Young modulus, E, defined by

$$E = \frac{\mathrm{d}\sigma}{\mathrm{d}\lambda}\bigg|_{\sigma=0}. \tag{2.1}$$

The latest is estimated by computing the tangent modulus of the Cauchy stress-stretch response for stresses below 0.2 MPa. Such a limit has been chosen to preserve the linearity of the mechanical behavior and to provide enough experimental data for computation. It is worth pointing out that E is computed assuming the material incompressibility. At small strain, such an assumption is fair and is supported by the results discussed in Section 2.3.

Figure 2.6a illustrates the effect of the filler volume fraction on the modulus by comparing materials with similar crosslink densities ($N_c \approx 7 \times 10^{-5}$ mol/cm^3). The modulus is strongly dependent on Φ. The reinforcement of rubber materials when compounded with fillers is commonly known (Mullins and Tobin, 1965; Medalia, 1978; Bergström and Boyce, 1999; Heinrich et al., 2002; Kohls and Beaucage, 2002; Bokobza, 2004, 2007; Chazeau et al., 2010; Gherib et al., 2010). In order to capture such a dependence, an early quantitative approach has been proposed by Guth and Gold (1938),

$$\frac{E}{E_0} = 1 + 2.5\Phi_{\text{eff}} + 14.1\Phi_{\text{eff}}^2 \tag{2.2}$$

with E_0 the Young modulus of the pure gum and Φ_{eff} the effective volume fraction of fillers in the rubber gum. In order to account for the occluded rubber trapped in branched structure of the filler aggregates, Medalia (1970) proposed the following relationship based on the absorption of DBP measurement

$$\Phi_{\text{eff}} = \frac{\Phi}{2}\left(1 + \frac{1 + 0.02139.\text{DBP}}{1.46}\right) \tag{2.3}$$

where Φ is the actual volume fraction of filler reported in Table 2.2. The reinforcement computed with Eqs. (2.2) and (2.3) is illustrated in Figure 2.6a by the dashed line. The experimental results are accurately predicted for the lower volume fractions, up to $\Phi \approx 0.16$, but the filler reinforcement is clearly underestimated for higher volume fractions. Such an observation is expected. According to Medalia (1970), Eq. (2.3) provided an accurate estimate of Φ_{eff} up to a maximal volume fraction $\Phi = 0.15$. For higher Φ, additional effects due to interactions between aggregates may induce an increase of the reinforcement. Therefore, Eqs. (2.2) and (2.3) are not suitable anymore and a model with a higher level of analytical sophistication must be used.

The effect of the crosslink density on the modulus is shown in Figure 2.6b by comparing materials with similar amount of fillers (40 phr). The modulus, E, increases with N_c. Previous studies have reported a similar observation (Smith, 1977; Diani et al., 2008; Dijkhuis et al., 2009; Fukahori, 2010). However, it seems that an analytical relation for such a dependence is not clearly established. According to the statistical theory of rubber elasticity (Treloar, 1973), the elastic modulus of an unfilled rubber should be proportional to the number of bonds of the chain. The latest being himself proportional to the crosslink density. Therefore, when comparing materials with the same amount of fillers, one may expect $E \propto N_c$. However, such a linear relation between E and N_c is not observed in Figure 2.6b.

In the next section, the effects of the material composition on the stretch to failure are discussed.

2.4.3 Stretch to failure

The effect of the filler volume fraction on the stretch to failure, λ_{fail}, is shown in Figure 2.7a by comparing materials with similar N_c. Results put in light that the stretch to failure
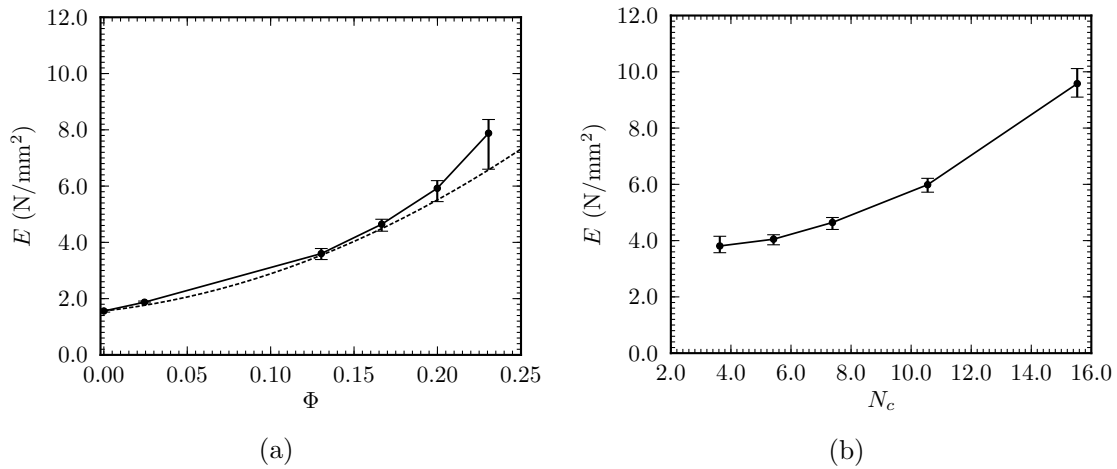
Figure 2.6: Evolution of the Young modulus, E, according to the material composition. (a) Dependence to the filler volume fraction for $N_c \approx 7 \times 10^{-5}$ mol/cm^3. (b) Dependence to the crosslink density for $\Phi \approx 0.16$.

exhibits an optimum according to Φ. For low amounts of fillers, λ_{fail} increases with the increase of fillers. Such a phenomenon has been observed by Hamed (1994); Zhao and Ghebremeskel (2001); Gauthier et al. (2005). The failure of a rubber material may be related to cracks growth mechanisms. The failure occurs when a critical threshold condition, still not clearly identified, is reached. The presence of fillers within the rubber gum acts as obstacles and stops or reduces the crack growths. Therefore, they delay the threshold of failure for the material. However, this phenomenon seems to be limited to the lower value of Φ. One may notice in Figure 2.7a that the stretch to failure appears to pass through a maximum and then, for $\Phi > 0.12$, decreases with the increase of Φ. Similar observations have been reported by Krauss (1971); Bokobza (2007). For significant filler volume fractions, the carbon black filler aggregates may agglomerate into large clusters. They provide defects from which some cracks can more easily initiate and propagate under stretching, leading to the material failure (Zhao and Ghebremeskel, 2001). Let us note that a comparable observation is reported by Auer et al. (1957) for works addressing the fatigue of rubbers under cyclic loading conditions. It appears that the resistance to crack growth is maximal for an optimal amount of fillers.

Figure 2.7b illustrates the dependence of the stretch to failure with the crosslink density. Results show that the stretch to failure is strongly impacted by N_c. By increasing the crosslink density, one significantly decreases λ_{fail}. This observation is in good agreement with several results reported in the literature (Bueche, 1959; Smith and Magnusson, 1961; Fedors and Landel, 1966; Smith, 1977; Ortega et al., 2008; Dijkhuis et al., 2009; Wang et al., 2009). However, the relationships between N_c et λ_{fail} is not clearly established. For instance, Smith and Magnusson (1961) proposed a quantitative proportional relation of the form $\lambda_{\text{fail}} \propto N_c^{-1}$, while adding that in some cases, the exponent might be less than unity. Bueche and Halpin (1964) proposed the proportional relation $\lambda_{\text{fail}} \propto N_c^{-1/2}$. The latest is also observed by Smith (1967). It is noteworthy that such a relation is supported by the statistical theory of rubber elasticity according to which the chain extensibility limit is proportional to the square root of the number of links in the chain (Treloar, 1975). The dashed line in Figure 2.7b shows the approximate of the λ_{fail} dependence to N_c according to the proportional relation $\lambda_{\text{fail}} \propto N_c^{-1/2}$. It can be notice that such a relation provides a very good fit of the λ_{fail} values over the whole studied range of crosslink densities.

Previously, it was noticed that the failure under monotonic loadings and the fatigue crack growth under cyclic loading conditions undergo a comparable dependence to the amount of fillers.
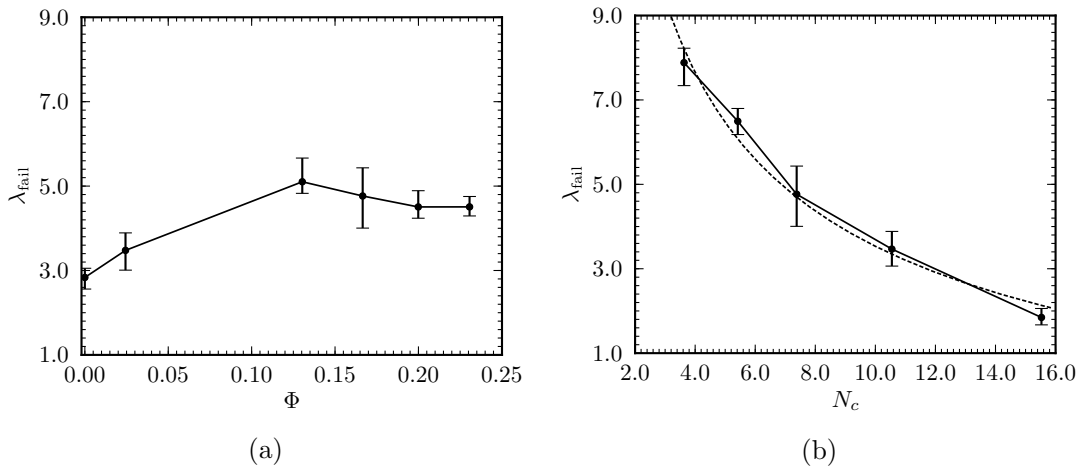
Figure 2.7: Evolution of the stretch to failure according to the material composition. (a) Dependence to the filler volume fraction for $N_c \approx 7 \times 10^{-5}$ mol/cm^3. (b) Dependence to the crosslink density for $\Phi \approx 0.16$.

The strain energy release rate or tearing energy, G, proposed by Lake and Thomas (1967) is usually used in order to study cracks propagations within rubber-like materials submitted to cyclic loading conditions. It is established that G is substantially dependent to the crosslink density and its threshold value, G_0, below which the crack does not grow, may read

$$G_0 = K M_c^{1/2} \tag{2.4}$$

with K a parameter that depends on the bond rupture energy and M_c the molar mass between crosslinks (Lake and Thomas, 1967; Smith, 1977; Gent et al., 1994; Lake, 1995; Tsunoda et al., 2000). According to Eq. (2.4), the relationship with the crosslink density is of the form $G_0 \propto N_c^{-1/2}$. Therefore, the results shown Figure 2.7 appears to support a significant correlation between the fatigue crack growth and the stretch to failure.

2.5 Material behaviors under cyclic loading conditions

This thesis addresses the issue of material mechanical behavior changes under cyclic loading conditions and in the following, only cyclic tests are considered. Hence, this section aims at illustrating basic material response features under cyclic loadings. It is to be stressed that the current section is restricted to basic experimental observations and does not attempt to produce original results. Its purpose is to introduce and to illustrate dependencies between material compositions and material behaviors during cyclic loading conditions.

All materials detailed in Figure 2.1 are considered as well as the natural rubber material labeled NR in Section 2.2.1. The experimental setup is similar to the one used in the previous section. The Cauchy stress, σ, is computed assuming the material incompressibility. Section 2.5.1 aims at highlighting the Mullins softening and Section 2.5.2 the cyclic softening.

2.5.1 Basic experimental observations of the Mullins softening

In this section, a cyclic loading path is considered in order to highlight the Mullins softening. Therefore, except when mentioned, samples were submitted to cyclic loadings with an increasing maximal stretch of $\Delta \log(\lambda) = 0.1$ at each cycle until failure. The minimum of cycles was set to a null force. All tests were run at a constant crosshead speed of 10 mm/min.

Pure gum

According to the literature reviewed in Chapter 1, until now, a Mullins softening has never been reported for unfilled non-crystallizing rubbers. In this section, this particular aspect is investigated. The pure gum material (0 phr of carbon black fillers) stress-stretch response to a cyclic loading is shown in Figure 2.8a. One may notice that a small hysteresis appears between loading and unloading curves as well as a small residual stretch increasing with the maximal stretch applied. However, these changes are strongly affected by the material viscoelasticity (Diani et al., 2006b). In order to avoid such effects, a first cycle is performed with a 2.5 maximal stretch, and the sample is unclamped 24 hours in order to allow a viscoelastic recovery. Then, the sample is submitted to a second cycle up to $\lambda = 2.5$. Results shown in Figure 2.8b clearly illustrates that both loading curves are quasi-perfectly superimposed. Therefore, no Mullins softening has occurred during the first cycle.
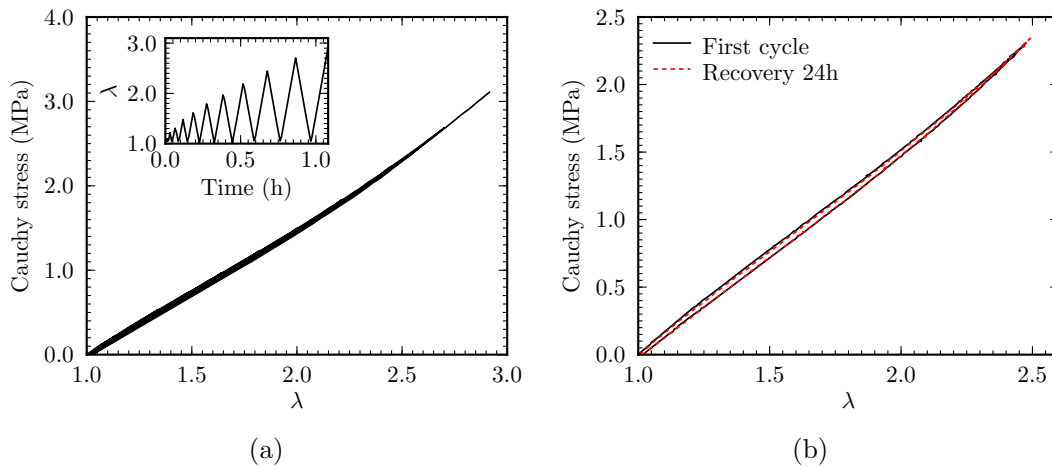
Figure 2.8: Pure SBR gum submitted to a cyclic loading. (a) Cycles with an increasing maximal stretch. (b) Two cycles at a same maximal stretch with a 24 hours recovery at null force in between.

Dependencies to filler amount

In the previous section it was shown that an unfilled SBR material behavior does not change significantly during a cyclic loading. The influence of fillers on the material stretch-stress cyclic response is now investigated. For this purpose, two SBR materials filled with 30 and 60 phr are submitted to a cyclic loading. Stress-stretch responses are shown in Figure 2.9a and 2.9b, respectively. Results highlight that the amount of fillers has a strong impact on the Mullins softening. Hysteresis between loading and unloading curves significantly increases with the filler amount as well as the residual stretch. The dependence of the Mullins softening to the amount of fillers is well-known and has already been reported by Mullins and Tobin (1957); Klüppel and Schramm (2000); Dorfmann and Ogden (2004); Luo et al. (2004) among others.

It is noteworthy that the Mullins softening dependence to the crosslink density is not as obvious as its dependence to the filler amount. Moreover, it cannot be extrapolate from material stress-stretch responses observation. A procedure, unavailable in the literature, is proposed in Chapter 3.
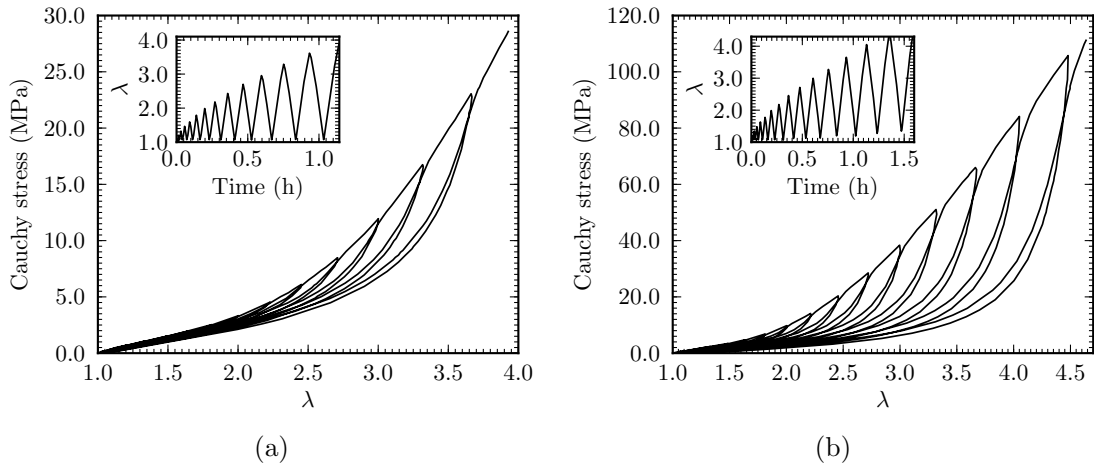
Figure 2.9: Stress-stretch response of filled SBR submitted to a cyclic loading with an increasing maximal stretch. Materials filled with (a) 30 phr and (b) 60 phr of carbon black ($N_c \approx 7 \times 10^{-5}$ mol/cm^3).

Residual stretch

In order to easily compare behavior changes occurring for various materials, residual stretch evolution with the maximal applied stretch may be used. Such a feature is usually associated with the Mullins softening (as a matter of fact, no contribution proposing otherwise has been found). Therefore, samples were submitted to cyclic loadings and the resulting residual stretch, λ_{res}, was monitored at the end of each unloading.

Figure 2.10a shows the dependencies of λ_{res} to the filler amount by comparing material with similar crosslink densities, $N_c \approx 7 \times 10^{-5}$ mol/cm^3, and various filler amounts from 0 to 60 phr. One may notice the strong impact of the filler amount on the residual stretch. λ_{res} increases with the increase of the filler amount. This observation was already reported by Dorfmann and Ogden (2004). It is worth noticing that material C1 with 0 phr of carbon black (pure gum) shows a noticeable residual stretch increase, whereas, it was highlighted in Figure 2.8 that a pure gum material does not undergo any Mullins softening. The λ_{res} induced by the cyclic loading entirely vanished after a 24 hour recovery, evidencing its viscoelastic nature.

The dependence of the residual stretch to the crosslink density is shown in Figure 2.10b by comparing material containing the same amount of fillers, 40 phr ($\Phi \approx 0.16$), and different crosslink densities from 3.65 to 10.55 $\times 10^{-5}$ mol/cm^3. Figure 2.10b shows a minor effect of N_c compared to the effect of the filler amount. It can be noticed that the effect of N_c is less obvious than the effect of the filler amount. For moderate maximal stretches ($\lambda_{\text{max}} < 3$), it appears that for the high crosslink densities ($N_c > 7$) the residual stretch does not depend of N_c, but for low crosslink densities, the residual stretch increases when N_c decreases.

Effect of crystallization

This thesis does not address the issue of crystallization phenomenon occurring within natural rubber upon stretching. Nevertheless, such a material labelled NR will be used in order to extend the validity of some experimental procedures and some modeling aspects proposed in the following chapters. Therefore, in order to emphasize significance of the crystallization effect influence on the material behavior, "similar" SBR and NR materials (*i.e.* same amount of filler and same crosslink density) are compared under identical cyclic loading conditions. Figure 2.11a and 2.11b illustrate the material stress-stretch responses of the SBR and the NR, respectively.
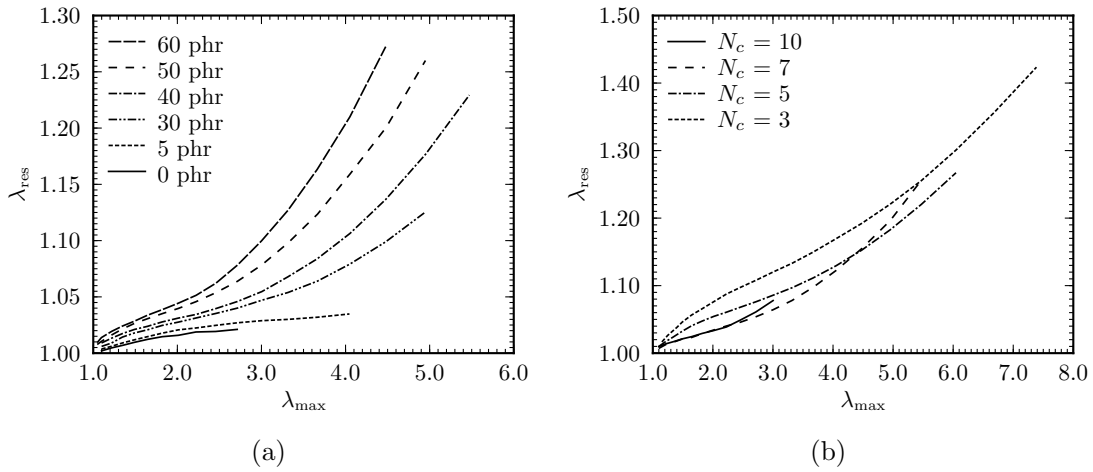
Figure 2.10: Residual stretch evolution during cyclic uniaxial loadings with an increasing maximal stretch. (a) Effect of the amount of fillers for materials with various amounts of carbon-blacks and similar crosslink densities $N_c \approx 7 \times 10^{-5}$ mol/cm^3. (b) Effect of the crosslink density for materials with various crosslink densities and similar filler volume fractions $\Phi \approx 0.16$ (40 phr).

One may notice that in the case of natural rubber, certain Mullins features differ significantly to those observed for the SBR materials. First of all, when the natural rubber is stretched beyond the maximum stretch previously applied, the stress-stretch response does not return on the monotonous response. Therefore, there is no obvious "return point" on re-loading path when the previous maximal stretch is reached. A second important difference is a significant hysteresis between loading and unloading curves even when the material has been already softened. Such a feature is related to crystallization induced by stretching (Treloar, 1941). The crystallization being unaffected by the Mullins softening, it still occurs after the first cycle (Trabelsi et al., 2003b).
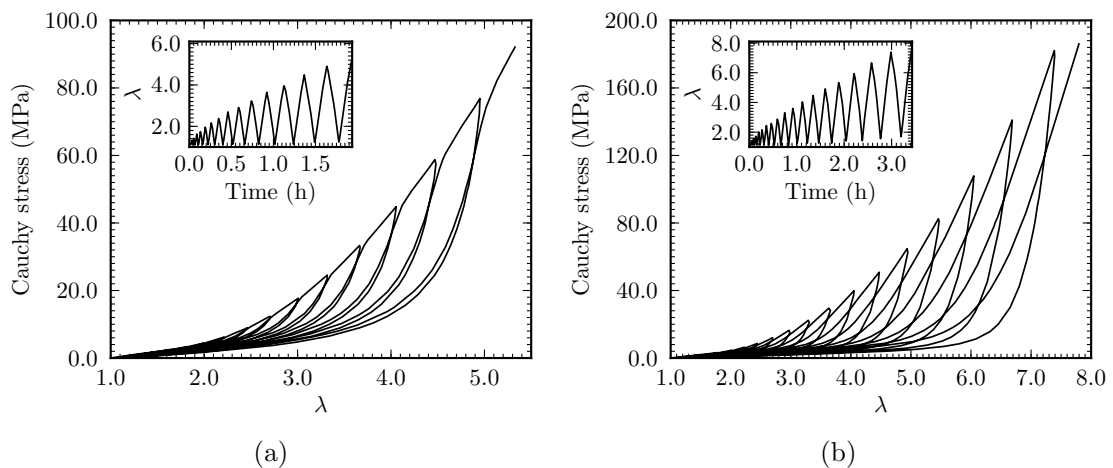
Figure 2.11: Stress-stretch responses to a cyclic loading. The loading appears in the inset graph. (a) SBR gum and (b) NR gum filled with 40 phr of carbon-blacks and $N_c \approx 7 \times 10^{-5}$ mol/cm^3.

2.5.2 Basic experimental observations of the cyclic softening

The Mullins softening occurring during the first cycle was previously discussed. This section is addressing the cyclic softening evolving during subsequent cycles. For this purpose, cyclic loadings with a thousand cycles from zero stress up to a maximum stretch of $\lambda_{max} = 3$ were performed. In order to reduce test duration, all experiments were run at a constant crosshead speed of 180 mm/min. The typical stress-stretch response of filled SBR materials under such a loading condition was illustrated and discussed in Section 1.4.1 for the thesis reference material R.

Evolution of the maximal stress

To characterize the softening during cyclic loadings, a method commonly used in the literature, is to follow the decrease of the maximal stress, σ_{max}, measured at the peak stretch with respect to the number of cycles (Shen et al., 2001; Gentot et al., 2004; Mars and Fatemi, 2004b; Asare et al., 2009; Berrehili et al., 2010; Brieu et al., 2010; Yan et al., 2010). To make easier the comparison between materials, the maximal stress value at cycle N may be normalized by the maximal stress at the first cycle. Figure 2.12 shows the evolution of the normalized maximal stress with the number of cycles for every material. One may notice that plots become linear with respect to the logarithm of the number of cycles after a relatively low number of cycles. A similar trend has been reported by Gentot et al. (2004); Mars and Fatemi (2004b); Brieu et al. (2010).

Figure 2.12a presents the change of the normalized maximal stress for materials with similar crosslink densities, $N_c \approx 7 \times 10^{-5}$ mol/cm^3, and different amounts of fillers. This figure shows a significant impact of the amount of fillers on the stress-softening. Adding fillers significantly increase the cyclic softening. Figure 2.12b shows the effect of the crosslink densities by comparing materials with similar filler amount, 40 phr, and different crosslink densities. It appears that the crosslink density has a negligible influence on the maximal stress evolution.
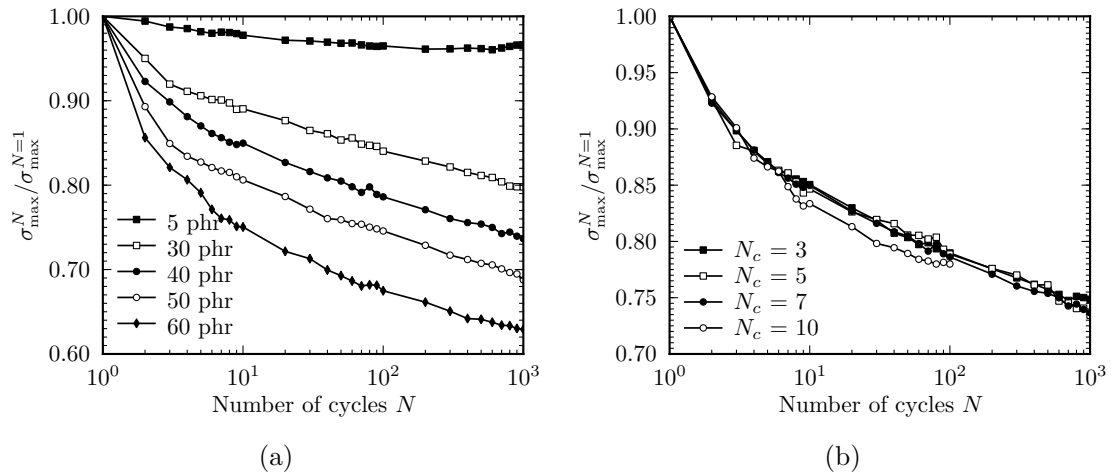
Figure 2.12: Evolution of the normalized maximal stress with respect to the number of cycles N. (a) Materials with similar crosslink densities $N_c \approx 7 \times 10^{-5}$ mol/cm^3 and varoius amounts of fillers. (b) 40 phr filled SBRs characterized by different crosslink densities.

Evolution of the residual stretch

As the cyclic softening evolves, the residual stretch increases with the number of cycles. Therefore, the residual stretch may, as well as the maximal stress, be used to characterize the cyclic softening. The residual stretch measured at the end of the cycle N can also be normalized by the residual stretch at the first cycle end.

Figure 2.13a presents the normalized residual stretch evolution with respect to the number of cycles for materials with similar N_c and various amount of fillers. One may notice that normalized residual stretch increases faster with the increase of filler amount. Therefore, such results are consistent with those obtained by using the maximal stress (see Figure 2.12a). Figure 2.13b shows the evolution of the normalized residual stretch with respect to the number of cycles for material filled with 40 phr of carbon black and different crosslink densities. It appears that the normalized residual stretch increases when the crosslink density decreases for $N_c \geqslant 7 \times 10^{-5}$ mol/cm^3 only. This quantity seems insensitive to N_c for higher values of N_c. One may notice that the later result does not agree with the previous observation obtained by using the maximal stress and illustrated in Figure 2.12b.

As a consequence, characterizing mechanical behavior changes during cyclic loadings using the maximal stress evolution is not satisfying. Therefore, in order to get a more accurate and reliable representation of the material softening, an original characterization of the mechanical behavior evolution during cyclic loadings will be proposed in Chapter 6.
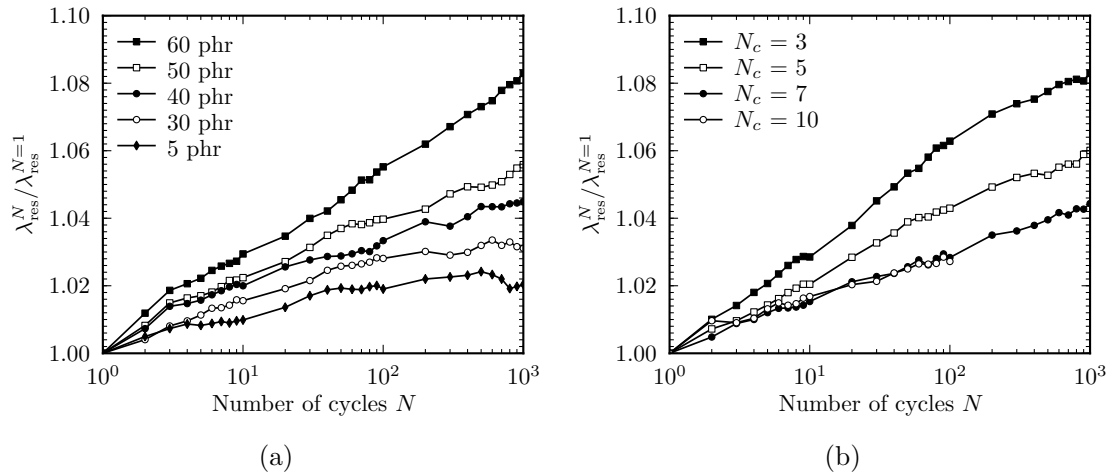
Figure 2.13: Evolution of the residual stretch with respect to the number of cycles N. (a) materials with similar crosslink densities $N_c \approx 7 \times 10^{-5}$ mol/cm^3 and different amounts of fillers. (b) 40 phr filled SBRs characterized by different crosslink densities.

2.6 Conclusion

This chapter aimed at introducing all materials used during the thesis work. At first, material compositions were given and manufacturing process was detailed. Various materials were compounded in order to assess the effect of two microstructural parameters, the filler volume fraction and the crosslink density. Then, material mechanical behaviors were characterized using uniaxial tension tests.

The first characterization aimed at investigating the incompressibility assumption commonly done for rubber-like materials. Volume changes are shown to be significant upon monotonic stretching, but material incompressibility assumption remains consistent when considering cyclic

loading conditions. Therefore, in what follows, the Cauchy stress resulting from cyclic uniaxial tension will be computed within incompressibility assumption and models will be proposed within an incompressible framework. As a side issue, this investigation highlights that stretches measurement on two orthogonal sample free faces is necessary to acquire volume changes. Lighten the experimental setup by measuring stretches on one sample face and estimate volume changes by assuming material transverse isotropy leads to erroneous results.

In order to link the material compositions to basic mechanical properties, samples were submitted to monotonic uniaxial tension tests up to failure. Results showed that the material stiffness increases with the increase of the filler amount and of the crosslink density. The stretch to failure increases with the crosslink density decrease and is barely affected by the filler amount.

The material softening when samples are submitted to cyclic loading conditions was studied. Regarding the Mullins softening, results showed that a pure SBR gum does not undergo any stress-softening after a pre-loading cycle. To the contrary, Mullins softening was observed for filled SBR. The "softening intensity" increased significantly with the filler amount. Regarding the cyclic softening, the maximal stress decrease and the residual stretch increase with the number of cycles were used to characterize the softening evolution. Results showed a significant influence of the filler amount on the softening. The effect of the crosslink density remained unclear. Therefore, validity of the softening parameter commonly used in the literature is questionable and a more reliable softening characterization will be proposed in Chapter 6.

Chapter 3

Mullins softening characterization

Most of this chapter has been published and can be found in references:

  - *Yannick Merckel, Julie Diani, Mathias Brieu, Pierre Gilormini, Julien Caillard, 2011. Characterization of the Mullins effect of filled rubbers, <u>Rubber Chemistry and Technology</u>, 84(3), 402-414.*
  - *Yannick Merckel, Julie Diani, Mathias Brieu, Pierre Gilormini, Julien Caillard, 2011. Effect of the microstructure parameters on the Mullins softening in carbon-black filled SBRs, <u>Journal of Applied Polymer</u>, 123(2), 1153-1161.*

Several carbon-black filled styrene-butadiene rubbers showed different sensitivities to the Mullins softening when submitted to cyclic uniaxial tension. In order to quantify this softening, a damage parameter is introduced. It is defined by a classic damage approach and it can be estimated by either the strain amplification factor method or the tangent modulus at zero stress. The proposed parameter is used to study the effect of the crosslink density and of the filler amount on the Mullins softening. The latter is shown to remain unaffected by a change of crosslink density and to increase with an increase of filler amount. The damage parameter exhibits linear dependencies to the maximum Hencky strain applied and to the filler volume fraction. Finally, the damage parameter provides a quantitative analysis of the Mullins softening and a quantitative analysis of its physical understanding.

Contents

3.1 Introduction

Adding fillers in a non-crystallizing rubber changes its mechanical behavior in many ways (Bergström, 1999). The fillers are understood to act as reinforcements at a continuum scale, which explains the stiffening effect (Kohls and Beaucage, 2002). At a molecular level, their influence is still debated, but it is clear that they introduce a local evolution of the strain state when the material is first stretched, which results in the development of the Mullins softening (Mullins, 1969; Diani et al., 2009). According to Chapter 1, the literature reports a large amount of experimental evidence of the phenomenon. Several mechanical modelings emerged during the past three decades in order to reproduce the stress-strain responses of rubbers exhibiting Mullins softening (Simo, 1987; Klüppel and Schramm, 2000; Marckmann et al., 2002; Dorfmann and Ogden, 2004). Nonetheless, these contributions lack to define an objective quantitative parameter that would allow the comparison of one material to others. Such a parameter would also permit to study the influence of the material composition on the Mullins softening (see Section 2.5.1 for some examples). The aim of the present chapter is to propose such an objective parameter.

Mullins and Tobin (1965) introduced the concept of strain amplification in filled rubbers in order to account for the reinforcement at large strains of an elastomer when filler particles and particle clusters are included into the gum. The fillers and the gum are described as hard and soft domains, respectively. The hard domains are assumed to remain undeformed, therefore the soft ones undergo a larger strain than the average strain applied to the material. The strain in the soft regions is then the applied strain amplified by a factor which is increasing with the increase of filler volume fraction. This strain amplification concept has been widely used to account for the filler reinforcement within the context of hyperelasticity (Mullins and Tobin, 1965; Govindjee and Simo, 1991; Bergström and Boyce, 1999; Dargazany and Itskov, 2009). Later, the strain amplification factor was extended to the case of hyperelasticity with Mullins softening, using an early idea suggested by Mullins and Tobin (1957), where the amount of hard phase depends on the strain history. The Mullins softening is then understood as an irreversible breakdown of filler-clusters, which results in a decrease of the "active" volume fraction of fillers. This physical interpretation of the Mullins softening was used in a number of contributions (Johnson and Beatty, 1993; Klüppel and Schramm, 2000; Luo et al., 2004; Qi and Boyce, 2004; Meissner and Matějka, 2006, 2008), where an amplification factor, decreasing with the maximum applied strain, is defined.

In this chapter, we will extend and apply the amplification factor concept in order to propose a damage parameter that quantifies the effect of the microstructure on the Mullins softening. The damage parameter will be proved to provide results that can be corroborated by the study of the evolution of the Young's modulus at small strain. Several carbon-black filled styrene butadiene rubbers characterized by their crosslink densities and their carbon-black volume fractions were submitted to cyclic uniaxial tension tests. The introduced damage parameter was estimated for each material and showed a linear dependence on the maximum strain applied. This simple dependence allows a direct comparison of the parameter for various materials.

The chapter is ordered as follows. The next section presents the material strategy and the mechanical tests that were conducted. Then, in Section 3.3 the basic idea and the method to estimate the Mullins softening are exposed. Results are reported and analyzed in Section 3.4. Finally, the reinforcing part of the strain amplification factor is discussed and concluding remarks close the chapter.

3.2 Materials and Experiments

For this study, various carbon-black filled SBR, described in Section 2.2.1, were considered. Material R was used to illustrate the experimental procedures. In order to identify the effect of the material composition on the Mullins softening, the material strategy was to vary the amount of fillers and the crosslink density N_c. According to Figure 2.1, from the reference material C4, materials C3, C5, and C6 were obtained by changing the filler amount from 40 phr to 30, 50, and 60 phr, respectively. Materials B4, D4, and E4 contain the same amount of fillers than material C4 but their crosslink densities vary. Resulting fillers volume fractions, Φ, and crosslink densities, N_c, were given in Table 2.2.

Mechanical tests were performed on the uniaxial testing machine described Section 1.6.3. Except when mentioned, tests were run in displacement control at a constant crosshead speed of 18 mm/min. Samples were submitted to cyclic loading up to failure. At each cycle, the maximum strain was increased with a step of $\Delta h = \Delta \log(\lambda) = 0.1$ (λ being the sample uniaxial stretch), the minimum of the cycles was set to a null force. Figure 3.1 illustrates the stress-strain response of material R during the cyclic uniaxial tension test. As expected for filled rubbers, the material shows a substantial stress softening when first loaded to an amount of strain never applied before. The materials evidence a clear Mullins softening.
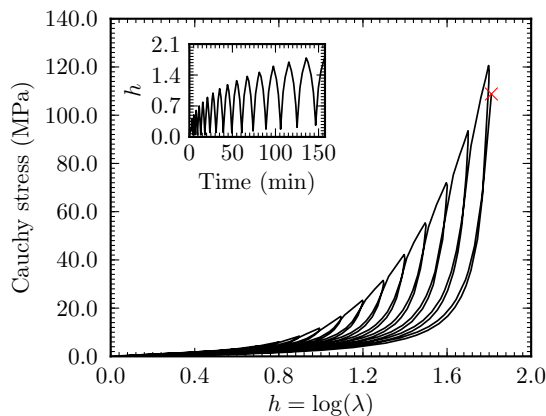
Figure 3.1: Material R stress-strain response to a uniaxial tensile cyclic test with an increasing maximum strain at each cycle.

The interest of such a loading as used in Figure 3.1 stands mainly in its simplicity. But the resulting Mullins softening is difficult to quantify and, worse, its quantitative comparison from one material to another is almost impossible without processing the data.

3.3 Characterization of the Mullins softening

3.3.1 Basic idea

The effects of adding fillers to a non-crystallizing rubber gum is first to increase its stiffness and second to introduce some stress-softening when first loaded due to the Mullins effect. One way to account for both effects is to compare the mechanical behavior of the actual material to the mechanical behaviors of the pure gum and of a virtual composite of pure gum with fillers that does not undergo any softening. This virtual composite is referenced as virgin material, and the mechanical behavior of the actual composite results from the softening of the virgin material. Many experimental contributions showed that, in uniaxial tension, the Mullins softening depends mainly on the maximum strain ever applied to the material. Figure 3.2 gives a schematic

representation of the three mechanical behaviors (gun, virgin, composite) and how they relate to each other. Our goal is to compare the mechanical behaviors of carbon-black filled rubbers according to the maximum strain undergone and their compositions (filler volume fraction and crosslink density).
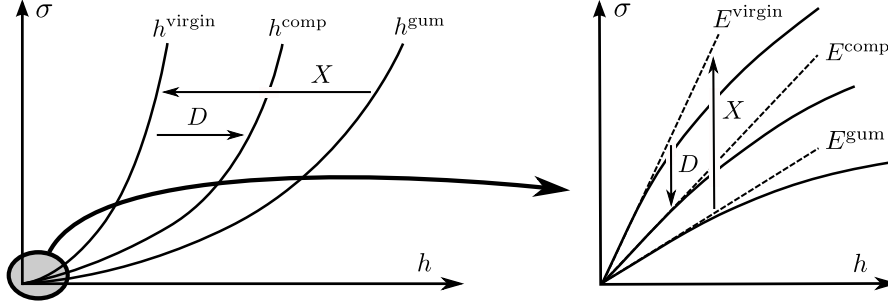
Figure 3.2: Schematic representation of the stress-strain response of a filled rubber undergoing Mullins softening (comp) in comparison with the idealistic behaviors of a filled rubber without Mullins softening (virgin) and of the same rubber without fillers (gum). On the right: magnified representation of the behaviors near the origin, characterized by the initial tangent modulus.

At large strain, the reinforcing effect of fillers may be accounted for by using the Mullins and Tobin (1965) strain amplification factor concept, according to which the mechanical response of the filled gum stretched to λ is similar to the mechanical response of the pure gum stretched to $1 + X(\lambda - 1)$. Here, we extend the strain amplification factor concept to the Hencky strain measurement, $h = \log(\lambda)$. The strain experienced by the gum is assumed as being the strain in the material virgin of any load magnified by a strain amplification factor X:

$$h^{\text{gum}} = X.h^{\text{virgin}}. \tag{3.1}$$

Since it is a reinforcing factor, $X \geqslant 1$. The parameter X is known to depend mainly on the volume fraction of fillers Φ. It is commonly assumed that $X = 1$ when $\Phi = 0$, which asserts that the virgin material and the gum coincide when no filler is added. Adopting the model proposed by Klüppel and Schramm (2000) based on a physical understanding of the Mullins softening by an irreversible breakdown of filler clusters and chain desorption at the filler-gum interface, the strain amplification factor is assumed to be altered by the maximum strain applied. These authors defined the variable X as dependent on the maximum strain ever applied, $X(h_{\text{max}}^{\text{comp}})$. The problem with such a definition of X is that it is difficult to isolate the softening effect from the reinforcing effect. For this reason, we introduce a damage parameter D, depending on the maximum strain and on the material parameters, acting as a penalization of the strain amplification in the composite material due to the Mullins softening. This is expressed by the relation

$$h^{\text{virgin}} = (1 - D)h^{\text{comp}}, \tag{3.2}$$

the parameter D characterizes the Mullins softening intensity.

At small strain, the mechanical behavior resulting from a uniaxial tensile test is characterized by the Young modulus E. The stress and strain measurements used in this study are the Cauchy stress with incompressibility assumption $\sigma = F\lambda/S_0$ (F and S_0 being the force and the initial cross-sectional area) and the Hencky strain $h = \ln(\lambda)$, respectively. The modulus is defined by

$$\sigma = E.h. \tag{3.3}$$

A quantitative account of the stiffening effect of rigid fillers in a rubber gum was first proposed by Smallwood (1944) who extended the theoretical results obtained by Einstein (1911) regarding

the hydrodynamic effect resulting from the addition of rigid particles in a fluid. The tensile modulus of the filled gum is related to the tensile modulus of the pure gum through a factor X depending on the amount of fillers,

$$E^{\text{virgin}} = X.E^{\text{gum}}. \tag{3.4}$$

One notes that within the small strain assumption, Eqs. (3.1) and (3.4) are strictly equivalent. A short review of the various expressions of X applying in Eq. (3.4) may be found in Bergström (1999).

The consequence of the Mullins softening on the Young modulus of filled rubbers was generally appraised from a qualitative point of view (Mullins, 1969). In order to precisely compare the softening at large strain and at small strain, we introduce the damage variable D in the very same way as previously done for the strain amplification factor Eq. (3.2). This damage parameter depends on the maximum strain already applied to the material and on the material parameters. It provides a link between the actual material stiffness E^{comp} and the virgin composite stiffness E^{virgin}:

$$E^{\text{comp}} = (1 - D)E^{\text{virgin}}. \tag{3.5}$$

At this point, Eqs. (3.2) and (3.5) define a similar parameter D, uniaxial tensile tests are now used to determine the changes of D according to the maximum strain applied, the applied strain rate or the material compositions (amount of fillers and crosslink density). Details of the procedure determining D are provided in what follows.

3.3.2 Loading versus unloading stress-strain responses

During a cyclic loading-unloading-reloading, the viscoelastic effect of the material is more pronounced on the reloading path than on the unloading path, since most of the viscoelastic stress contribution is evacuated at the beginning of the unloading observed in Figure 3.3a.
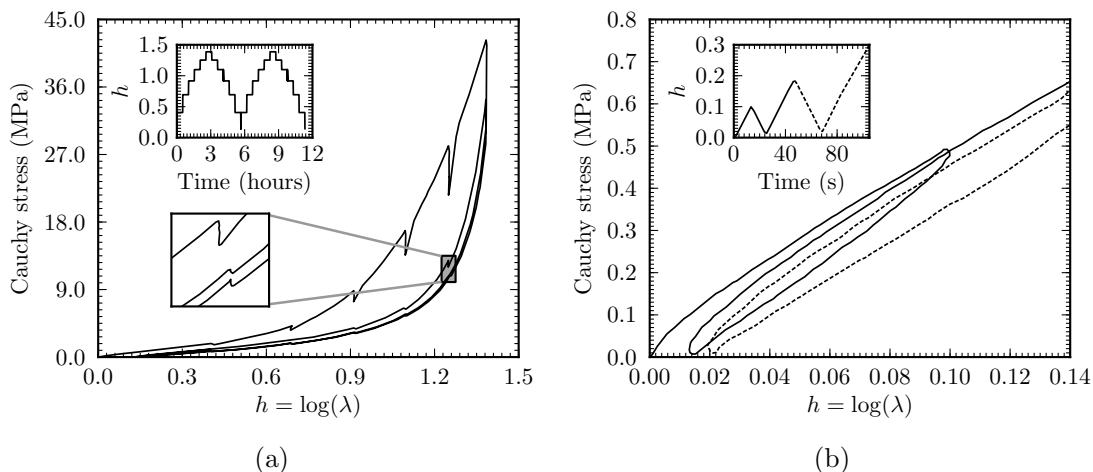
Figure 3.3: (a) Material R stress-strain response during a cyclic test with a 30 min relaxation step every 50% strain step. (b) Material R stress-strain response at the first few cycles of the cyclic tensile test. Experimental data have been smoothed by a moving window average for a clearer reading.

The viscoelastic effect is even more critical at small strain, when the initial modulus is estimated. Actually, when changing from the unloading to the loading, the loading strain rate changes from negative to positive. The large change in the strain rate introduces a viscoelastic contribution to the stress that affects the measurement of the tensile modulus. Figure 3.3b shows

the stress-strain response of material R during the first few cycles. One recognizes a substantial increase in the modulus at the very beginning of reloading. This increase does not appear at the end of the unloading, since the strain rate is stabilized when the stress goes to zero. In order to avoid the possible disturbance introduced by viscoelasticity, we adopt the unloading stress-strain responses as the material softened responses in the next sections.

3.3.3 Estimate of the softening parameter D

We start with explaining how values of the parameter D defined in large strain by Eq. (3.2) are extracted from the experimental data consisting of the unloading stress-strain responses measured during cyclic uniaxial tension. These stress-strain responses are convenient because fast to obtained during a cyclic test, but they do not picture the stress-strain responses that would be measured by a user ignorant of the loading history. Actually, one may notice a substantial residual stretch, λ_{res}, at the end of each unloading, which increases with the maximum strain applied. This residual stretch lowers the actual strain undergone by the material. Therefore, in order to reach the stress-strain response $(\lambda^{\text{comp}}, \sigma)$, that a user unaware of the loading history would measure experimentally, we need to change the data $(\lambda^{\text{meas}}, \sigma)$ into $(\lambda^{\text{comp}}, \sigma)$ using the relation:

$$\lambda^{\text{comp}} = \frac{\lambda^{\text{meas}}}{\lambda_{\text{res}}}. \tag{3.6}$$

Let us note that when using the Hencky strain, the latter relation transforms into $h^{\text{comp}} = h^{\text{meas}} - h_{\text{res}}$. Therefore, accounting for the residual stretch simplifies into a mere horizontal shift of the material unloading responses. Figure 3.4a illustrates the stress-strain responses of material R that are finally used after the residual stretch horizontal shift has been applied on the data reported in Figure 3.1.

According to Eq. (3.2), each softened stress-strain response is linked to the same virtual virgin material behavior through the constant parameter $D(h_{\text{max}}^{\text{comp}})$. The stress-strain response of the virgin material defines a master curve that is obtained by superimposing the unloading stress-strain responses thanks to Eq. (3.2). When the material is virgin $h_{\text{max}}^{\text{comp}} = 0$ and $D = 0$; for any other value of $h_{\text{max}}^{\text{comp}}$, the values of D are computed by a superimposition fit using a least squares minimization. Figure 3.4b shows the results of the superimposition method on the stress-strain responses of material R (Figure 3.4a). First, one notes that good superimposition is obtained, except near the maximum strain of the unloading responses. The observed discrepancy is partly due to the large relaxation experienced at the beginning of the unloadings by materials undergoing some Mullins softening. This discrepancy could be reduced by using the second cycle unloading responses. The observed superimposition justifies the use of Eq. (3.2) and supports the concept of a virtual virgin material behavior. Second, the inset figure in Figure 3.4b presents the values of D versus $h_{\text{max}}^{\text{comp}}$ resulting from the fitting procedure. These values increase with the maximum strain applied, and they show a linear trend that favors the use of the Hencky strain as the strain measurement. This linear trend is in good agreement with previous results (Klüppel and Schramm, 2000) that show an exponential evolution of D versus the maximum stretch.

Another way to estimate D is to use the tangent modulus. The Young modulus defined by Eq. (3.3) is estimated by calculating the initial tangent modulus,

$$E^{\text{comp}} = \left. \frac{\mathrm{d}\sigma}{\mathrm{d}h^{\text{comp}}} \right|_{\sigma=0}. \tag{3.7}$$

Values of this modulus are obtained from the unloading stress-strain responses by determining the slopes of the linear approximations as it is shown in Figure 3.5a for material R. The stress upper limit was chosen to 0.2 MPa and it is materialized in Figure 3.5a by a dashed line. This limit provides a good compromise between the need for having enough experimental data for
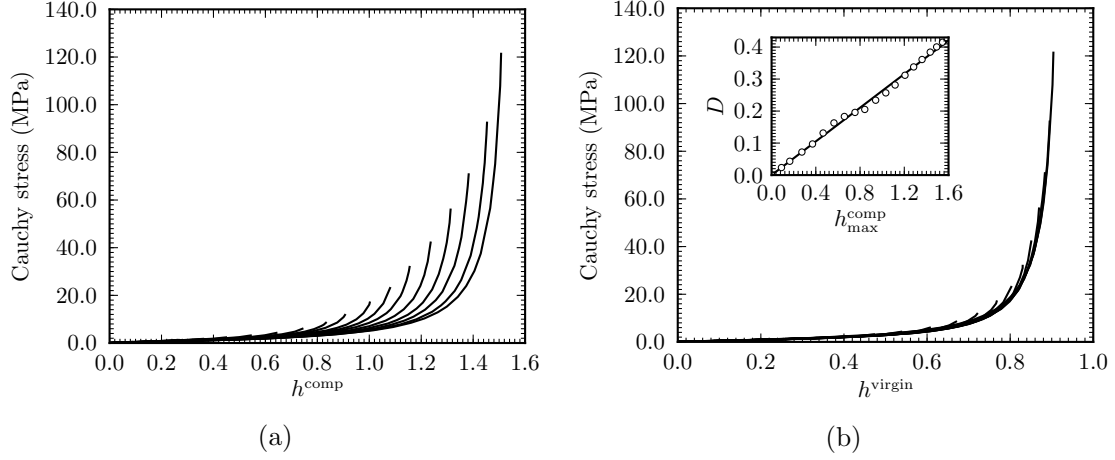
Figure 3.4: (a) Stress-strain responses of material R softened by previous loadings to various strain levels. (b) Material R master curve obtained by superimposition of the stress-strain responses plotted in Figure 3.4a. In the inset figure, the values of the damage parameter D that provide superimposition are shown.

an accurate estimate of the modulus and the need for preserving the linearity of the mechanical behavior.
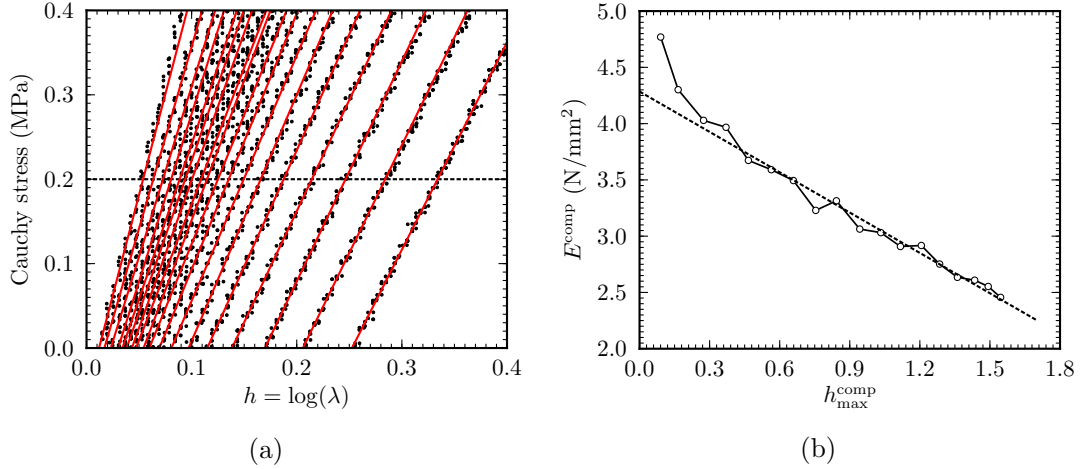
Figure 3.5: (a) Plot of the material R stress-strain unloading responses at small strains and their linear approximations used to estimate the initial tangent modulus. The dashed line materializes the upper stress limit used for the linear approximation. (b) Evolution of the tangent modulus at zero stress for the filled rubber R vs. maximum strain applied.

Figure 3.5b presents the values of the initial tangent modulus for the unloading stress-strain responses characterized by the maximum strain applied $h_{\text{max}}^{\text{comp}}$. One notes that the initial tangent modulus is linearly dependent of $h_{\text{max}}^{\text{comp}}$ except for the very few cycles corresponding to low maximum strains. The discrepancy observed for the first few cycles may result from the viscoelastic effect which hardly stabilize due to the short duration of the unloading for these short cycles. Therefore, we always neglected the first few cycles and assumed that the initial tangent modulus is linearly dependent of $h_{\text{max}}^{\text{comp}}$. The linear approximation of the evolution of the initial tangent modulus of material R versus $h_{\text{max}}^{\text{comp}}$ is represented by a dashed line in Figure

3.5b. This linear approximation provides an estimate for the tangent modulus of the virtual virgin material, which is defined by $E(h_{\max}^{\mathrm{comp}} = 0)$. From this approximation and Eq. (3.5), values of parameter D are computed according to

$$D = 1 - \frac{E^{\mathrm{comp}}}{E^{\mathrm{virgin}}}. \tag{3.8}$$

3.3.4   Comparison of the estimates of the softening parameter D

In theory, considering Eqs (3.2) and (3.5), the damage parameter D values obtained from both methods should coincide. In practice, both methods do not use the same data. The tangent modulus is limited to the data covering a very limited range of the stress-strain response, while the strain amplification factor method uses the entire stress-strain response, which covers several hundred percent strain. Figure 3.6 shows a comparison of the values of parameter D for the experimental data provided by the cyclic test conducted on material R. Due to the large amount of data processed with the strain amplification factor method, results obtained by the latter appear smoother but both methods display similar results. The values of parameter D show similar linear changes versus the maximum strain applied when either the tangent modulus method or the strain amplification factor method is used. Therefore, the softening parameter D introduced here defines an objective mean to characterize the Mullins softening quantitatively. We now use this parameter to examine how the Mullins softening of our materials evolves.
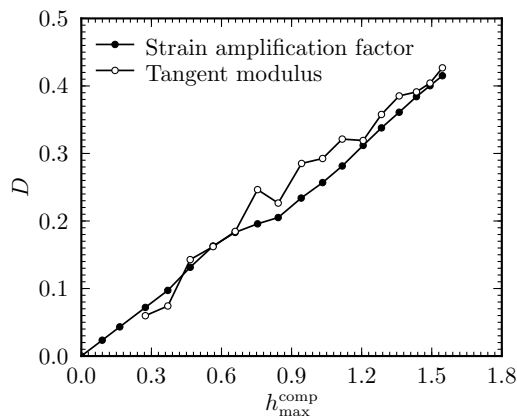
Figure 3.6: Comparison of the damage parameter D *vs.* the maximum strain applied, obtained by using either the strain amplification factor or the tangent modulus for material R.

3.4   Results and analysis

3.4.1   Effect of Material Viscoelasticity

Filled rubbers are known to be viscoelastic materials. Previous contributions (Kraus et al., 1966; Cheng and Chen, 2003; Amin et al., 2010) reported the strain rate effect on the stress-strain responses of filled rubbers but without proposing an objective comparison of the Mullins softening. In this section we want to investigate the impact of the viscoelastic properties of filled rubbers on the Mullins softening. For this purpose, we have submitted material C4 to cyclic loading tensile tests at various constant crosshead speeds, 1.8 mm/min, 18 mm/min, and 180 mm/min that provided strain rates close to 10^{-3} s^{-1}, 10^{-2} s^{-1}, and 10^{-1} s^{-1}, respectively. The strain rate-dependent stress-strain responses appear in Figure 3.7a. The damage D was

estimated according to the procedure described above and results are shown in Figure 3.7b. The Mullins softening appears to be strain rate dependent at large strain, increasing with the strain rate. In what follows, in order to study the impact of the amount of fillers and crosslink densities on the Mullins softening of filled SBRs, we will set the crosshead speed to 18 mm/min for every test.
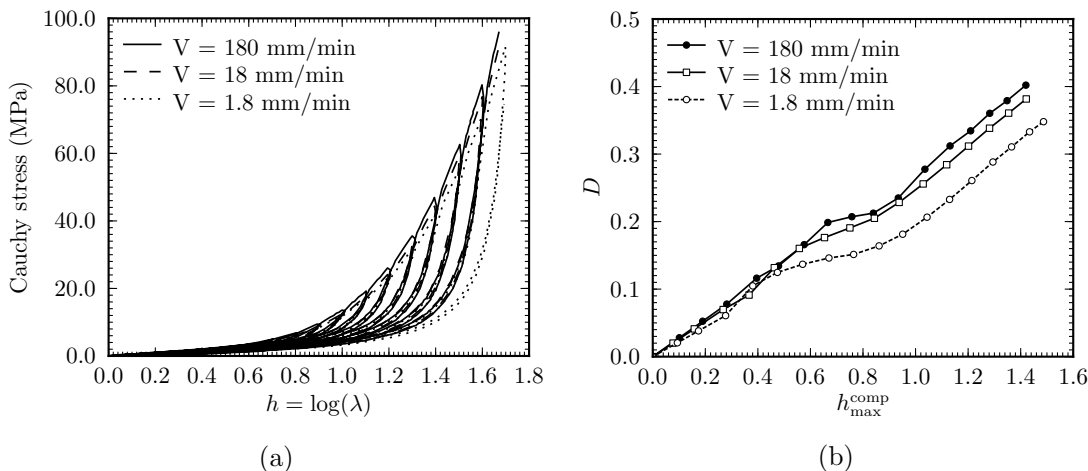
Figure 3.7: (a) Effect of strain rate on the stress-strain response of material C4 during cyclic uniaxial tension. (b) Estimate of the Mullins softening according to the strain rate.

3.4.2 Comparing Materials of Different Compositions

The Mullins softening parameter, D, was estimated according to the maximum strain applied, h_{max}^{comp}, for materials B4, C4, D4, and E4, which contain the same amount of fillers (40 phr) but have different crosslink densities (from 3.65 to 10.55×10^{-5} mol/cm^3) and for materials C3, C4, C5, and C6, which contains 30, 40, 50, and 60 phr of carbon-black, respectively, and similar crosslink densities ($N_c \approx 7 \times 10^{-5}$ mol/cm^3). Figures 3.8 and 3.9 present the change of D computed by both methods for each material. As expected, both methods provide very similar results.

One notes in Figure 3.8 that changing the crosslink density did not affect significantly the Mullins softening. This result might be due to the fact that, with the entanglement density ($\approx 42 \times 10^{-5}$ mol/cm^3) and the range of crosslink densities considered (between 3.63 and 10.55×10^{-5} mol/cm^3), these networks are sufficiently crosslinked (physically and chemically) to evidence a similar softening. Here, the softening is characterized by the initial tangent modulus, which may be linked to the material crosslink density that may be measured by swelling and to the material entanglement density. Bokobza and Rapoport (2002) carried out measurements of swelling on pre-stretched filled rubbers and showed an increase of the swelling ratio with the increase of the pre-stretch, which is equivalent to a decrease in the modulus. The decrease of the Young modulus is due to a reduction of the number of active physical and/or chemical crosslink. It is relevant to notice that the crosslink density was tuned by adding or withdrawing sulfur, and therefore without affecting the interface filler-matrix much.

In Figure 3.9, the amount of fillers is shown to have a considerable impact on the Mullins softening. By increasing the amount of fillers, one increases drastically the Mullins softening. This result is in good agreement with several qualitative data that appear in the literature (Mullins and Tobin, 1957; Harwood et al., 1965; Harwood and Payne, 1966a; Luo et al., 2004; Kar and Bhowmick, 1998; Bergström and Boyce, 1999; Klüppel and Schramm, 2000; Dorfmann and Ogden, 2004). Let us notice that even though unfilled crystallizing rubbers like pure natural

Figure 3.8: Effect of crosslink density on the Mullins softening: Evolution of the damage parameter D *vs.* h_{max}^{comp} for materials with various crosslink densities and similar filler volume fractions $\Phi \approx 0.16$ (40 phr). (a) Results obtained by using the strain amplification factor. (b) Results obtained by using the tangent modulus at zero stress.

rubber gum may show a clear Mullins (Harwood et al., 1965), the softening is observed for a substantially lower strain level when the material is filled. As shown Figure 2.8, non-crystallizing rubbers like SBR break before Mullins softening appearance when unfilled (Harwood et al., 1965) therefore, the presence of a rigid phase is a requirement to observe some Mullins softening. Moreover, when uniformly dispersed in the rubber gum, fillers induce some Mullins softening when added over a threshold. Tests conducted on our reference SBR gum filled with 5 phr ($\Phi = 0.024$) resulted in close to null Mullins softening (Figure 3.11). This threshold is lowered when the rigid phase is structured, the structure increasing the strain heterogeneities (Coquelle et al., 2006). Atomic Force Microscope (AFM) observations of the local strain in stretched filled rubbers showed a highly heterogeneous strain field and higher strains in regions where distances between aggregates are shorter (Lapra et al., 2003). Bokobza (2004) compared the Mullins softening of SBR gums filled with silica with and without a silane coupling agent. Silane builds strong covalent bonds at the silica-gum interface and one notes that a strong filler-gum interface enhances the Mullins softening. Therefore, Mullins softening appears when the material microstructure favors highly strained regions. Moreover, the fact that strong bonding creates more Mullins softening than weak bonding shows that Mullins softening is not only due to the rupture of bonds at the filler-gum interface since the rupture is expected to be substantially larger for weak covalent bonds than strong ones. Bond ruptures at the gum-filler interface probably occur but other changes must take place.

Another interesting aspect of the parameter D is that it also provides a quantitative access to the phenomenon. Figures 3.8 and 3.9 show that for our materials, the softening parameter is well approximated by

$$D = \alpha.h_{max}^{comp} \tag{3.9}$$

where the parameter α depends on the filler volume fraction only. Values of α may be reached from results reported in Figures 3.8 and 3.9, by a simple linear approximation. Results, in regard to the filler fraction, appear in Figure 3.10. Interestingly, the values of α versus the filler fraction can be approximated by a linear law. The linear plot shown in Figure 3.10 corresponds to the relation:

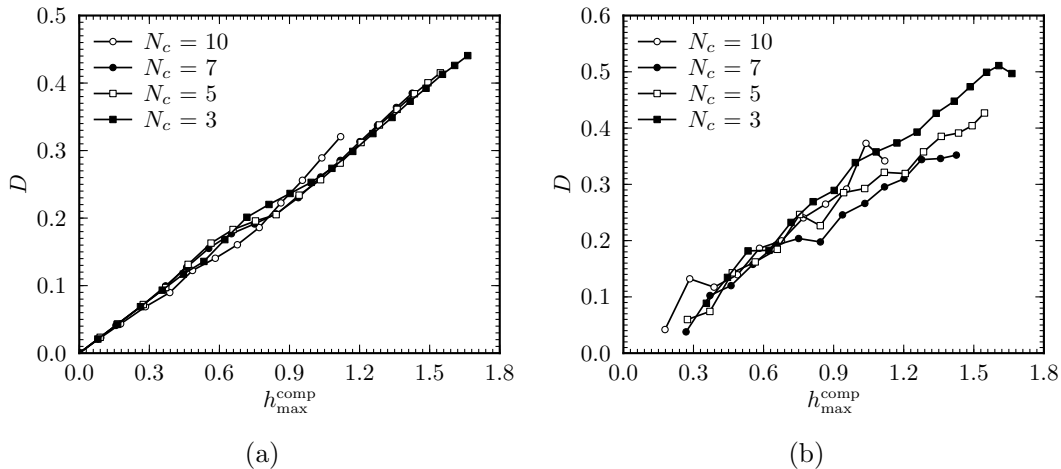$$\alpha(\Phi) = 2.25(\Phi - 0.05). \tag{3.10}$$
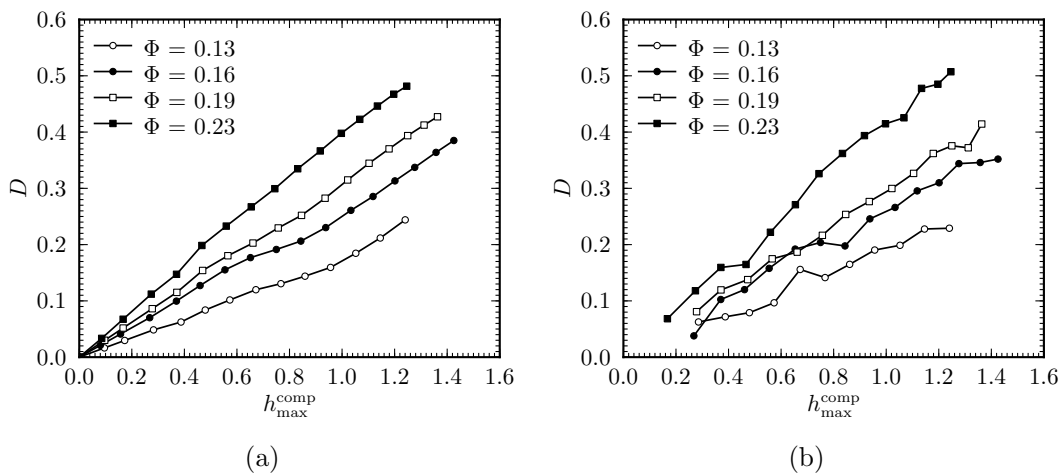
Figure 3.9: Effect of the amount of filler on the Mullins softening: Evolution of the damage parameter D vs. h_{max}^{comp} for materials with various amounts of carbon-black and similar crosslink densities $N_c \approx 7 \times 10^{-5}$ mol/cm^3. (a) Results obtained by using the strain amplification factor. (b) Results obtained by using the tangent modulus at zero stress.
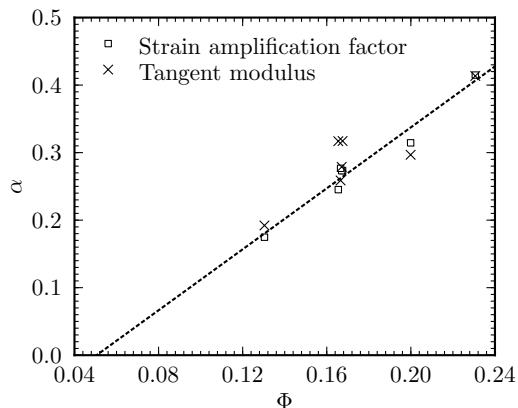
Figure 3.10: Evolution of parameter α vs. the filler volume fraction for all materials.

Such an approximation defines a filler volume fraction threshold $\Phi_0 \approx 0.05$, below which the Mullins softening is expected to be negligible. We have not been able to access materials containing this amount of fillers exactly, but we have checked that material C2 containing 5 phr, or equivalently a volume fraction of 0.024, shows barely any Mullins softening (Figure 3.11). Equations (3.9) and (3.10) combine into a surprisingly simple form for D,

$$D = \beta(\Phi - \Phi_0)h_{max}^{comp}. \tag{3.11}$$

Let us note that parameters β and Φ_0 are probably dependent of the gum type, and of the filler nature and geometry, but this aspect was not investigated here. Equation (3.11) closes our quantitative estimate of the Mullins softening. Once its two parameters are determined, relation (3.11) authorizes the prediction of the Mullins softening for mixes with amounts of fillers not yet tested.
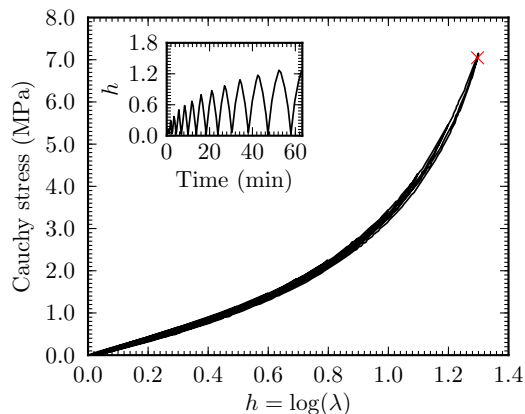
Figure 3.11: Stress–strain responses of materials C2 to a cyclic uniaxial tensile test.

3.5 Dependence of strain amplification to filler reinforcement

In previous sections we studied how the strain amplification is evolving according to the maximum stretching applied. This provided us with the evolution of the softening parameter D (Section 3.4). This process involved a master curve, see Figure 3.4, which defined the stress-strain behavior of the virgin material and was obtained for $D = 0$, for each material. In this section, we are interested in how the behavior of the virgin material relates to the behavior of the gum, which is disclosed by the reinforcement parameter X according to Eq. (3.1).

3.5.1 Method

The strain amplification factor X accounts for the initial reinforcing effects of fillers and filler aggregates embedded in the gum. As defined by Eq. (3.1), this factor relates the mechanical behavior of a filled rubber without softening to the mechanical behavior of the gum. It allows comparing the behavior of materials with a similar gum and various amounts of fillers, corresponding to various fractions of hard domains, to the behavior of the soft domains, without considering the induced damage. Reading the material strategy shown in Figure 2.1, one distinguishes a set of materials C1, C2, C3, C4, C5 and C6 where crosslink density does not vary. Therefore, in order to extend the filler volume fraction range for a gum characterized by a crosslink density of 7×10^{-5} mol/cm^3, materials C1 and C2 were also considered. These materials have null or low (5 phr) filler contents that make them likely to exhibit a mechanical behavior close to the mechanical behavior of the soft domain. They both present a very limited Mullins softening as shown in Figures 2.8 and 3.11 for C1 and C2, respectively. Figure 3.12a shows the master curves for the stress-strain responses of virgin materials corresponding to materials C1 to C6. As expected, adding carbon-black stiffens the materials.

For this set of materials, values of the amplification factor X are computed according to Eq. (3.1) in order to obtain the best superimposition of the stress-strain responses of virgin materials containing various amounts of fillers. This procedure is identical to the procedure used in order to assess parameter D but instead of comparing the stress-strain responses of the same material submitted to various levels of maximum strain, one compares the stress-strain responses for $D = 0$ for materials made with the same crosslink density and with different filler amounts. Figure 3.12b shows the superimposition of the mechanical behaviors of virgin virtual materials C1 to C6. Results are fairly good and supply values of the strain amplification factor X for all filler fractions.

71
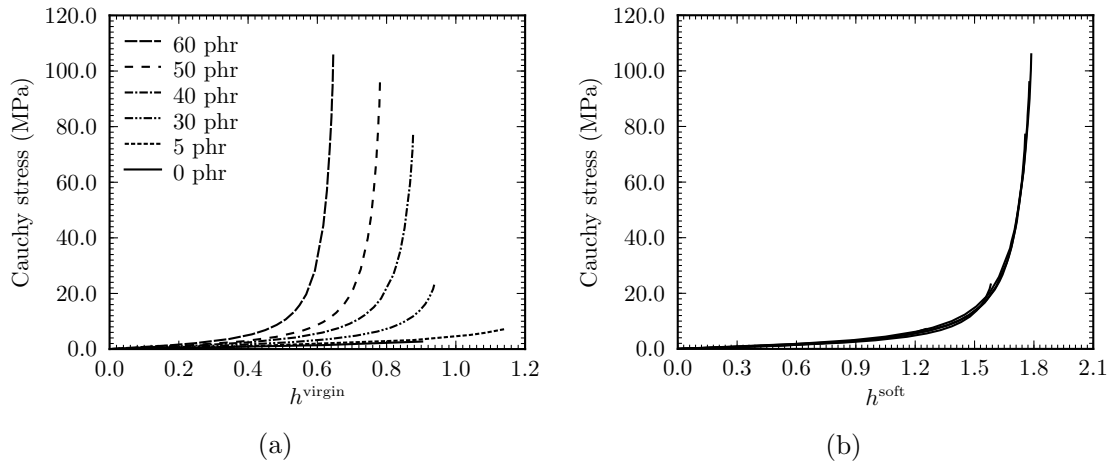
Figure 3.12: (a) Uniaxial tension stress–strain responses of virtual virgin materials compared with material C1 to C6. (b) Superimposition of the virgin material master curves onto the stress-strain behavior of the soft domains by using the strain amplification factor X defined in Eq. (3.1).

3.5.2   Results and analysis

Figure 3.13 displays the values of X obtained when producing Fig. 3.12b for various filler volume fractions Φ. It may be noted that X shows a quadratic dependence on Φ. This supports former quadratic results from the literature (Bergström and Boyce, 1999; Qi and Boyce, 2004) inspired by the Guth and Gold (1938) quadratic infinitesimal strain model. It is remarkable to read in Figure 3.13 that a quadratic function defined as:

$$X(\Phi) = 1 + a \; \Phi + b \; \Phi^2 \tag{3.12}$$

provides a good fit of the X values. The parameter $a = 2.5$ derives from a simple account of spherical filler particles at low concentrations (Smallwood, 1944). In Figure 3.13, the dashed line fit is obtained for $b = 21.3$.
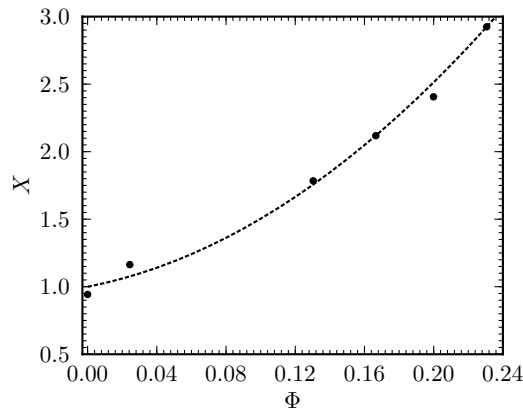
Figure 3.13: Evolution of parameter X with the filler volume fraction Φ.

3.6 Conclusion

In this chapter, we have proposed a way to characterize the Mullins softening in order to quantitatively compare this specific damage observed in filled rubbers according to the material composition. For this purpose, we revisited the strain amplification concept and proposed a decomposition of the strain amplification factor into a softening part D and a reinforcing part X. The damage parameter D, which can be reached using the strain amplification factor by considering the material stress-strain response over the entire strain range or equivalently using the tangent modulus at zero stress, provides an objective quantity to estimate and compare the Mullins softening. It was used to reflect the strain rate dependence of the Mullins softening and to study the effects of crosslink density and filler amount on the Mullins softening of SBR mixes. The crosslink density displayed a negligible impact on the Mullins softening, while increasing the filler fraction appeared to enhance the Mullins softening. Finally, the proposed softening parameter was shown to exhibit a mere linear change according to the maximum strain applied and also according to the filler volume fraction. This led to a simple expression of the softening parameter that may predict the Mullins softening for other compounds that were not tested experimentally. We have investigated the effects of crosslink density and filler amount. But one may consider, using the parameter D, to examine the consequences of changing the gum nature or the filler type and geometry. The reinforcing character of the fillers was also evaluated through the definition of suitable virgin virtual materials, which are assumed to behave like equivalent filled rubbers without Mullins softening. Comparison between the various materials showed that the reinforcing factor, X, depends quadratically on the filler volume fraction, which corroborates former results of the literature.

Within this chapter, a method was proposed in order to characterize the Mullins softening. One may notice that only uniaxial proportional tension tests were considered. For this type of loading, it is clearly established that the Mullins softening is activated by the maximum stretch $\lambda_{\max}$ (or any other strain measurement) ever undergone by the material. In order to propose a general three-dimensional framework for modeling the material behavior, an "equivalent" of this $\lambda_{\max}$ for general loading remains to be defined. Therefore, this specific issue is addressed in the next chapter.

Chapter 4

Mullins softening criterion for general loading conditions

Most of this chapter has been published and can be found in reference:

  - *Yannick Merckel, Mathias Brieu, Julie Diani, Julien Caillard, 2012. A Mullins softening criterion for general loading conditions, Journal of the Mechanics and Physics of Solids, In press.*

Samples of carbon-black filled styrene butadiene rubbers were submitted to successive non-proportional loadings in order to define a general criterion for the Mullins softening. For this purpose, each sample was initially submitted to uniaxial or biaxial pre-loadings followed by a cyclic uniaxial tension test. An original experimental analysis aimed at defining the activation threshold for the Mullins softening during cyclic uniaxial loadings. The experimental data provide substantial evidences establishing the surface of the maximum directional stretch undergone by the material as a relevant Mullins softening criterion. The latter was used to successfully predict the Mullins softening surfaces for additional loading cases. Finally, it was shown to apply to crystallizing carbon-black filled natural rubbers also.

Contents

4.1 Introduction

The literature reviewed in Chapter 1 highlights that despite numerous contributions on the Mullins softening, no general agreement has been found yet on the activation criterion of this phenomenon for general loading conditions. The objective of this chapter is to provide such a criterion essential for filled rubber constitutive modeling.

Mullins (1947, 1949) conducted extensive experimental studies on filled rubbers softening and residual stretch. The author revealed the anisotropy of both the Mullins softening and the residual stretch by applying successive non-proportional loadings. Subsequent experimental studies focused mainly on proportional loadings, and only a few authors (Laraba-Abbes et al., 2003; Hanson et al., 2005; Diani et al., 2006a,b; Itskov et al., 2006; Dargazany and Itskov, 2009; Machado et al., 2009; Machado, 2011) conducted non-proportional loadings showing the anisotropy induced by a preloading. Such a result is illustrated in Figure 4.1 for samples submitted to identical uniaxial tension pre-loadings and subsequent uniaxial stretchings according to various directions.
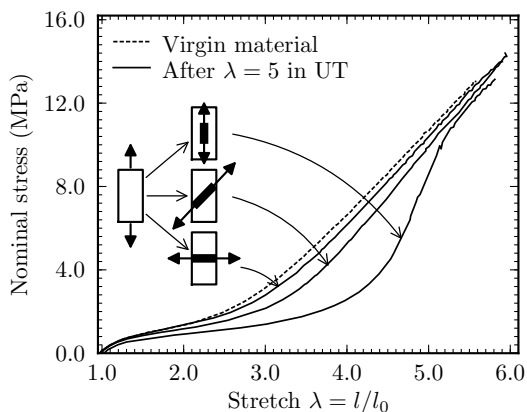
Figure 4.1: Evidence of uniaxial tension pre-loading induced anisotropy.

Most models proposed for the Mullins softening use an isotropic damage definition (see Diani et al. (2009) for a review) and very few models deal with an anisotropic criterion. One may cite Göktepe and Miehe (2005) accounting for directional damage parameters depending on the maximum directional free energy, Diani et al. (2006a,b) considering directional maximum stretches as directional criterion of damage activation, and Itskov et al. (2010) using the maximum stretches in the principal directions of the current deformation gradient tensor only. In what follows, an original analysis of non-proportional loading tests provides experimental evidences that the maximum directional stretch surface defines a relevant three-dimensional criterion for the Mullins softening activation. The next section presents the experimental setup and the mechanical tests that were conducted. Section 4.3 aims at describing the original method used to detect the Mullins softening activation. This section also provides experimental results obtained under non-proportional loading conditions. In section 4.4, the Mullins softening criterion is defined, validated for additional loading cases and extended to crystallizing filled natural rubber. Finally, concluding remarks close the chapter.

4.2 Experiments

4.2.1 Experimental setup

For this study, we used the material R processed into final plates of 2.5 mm thickness. The material in-plane isotropy was verified (Figure 2.2). In order to submit the material to uniaxial and biaxial loading conditions, both testing machines detailed Sections 1.6.3 and 1.6.4 were used. The uniaxial tension tests were conducted at a constant crosshead speed which was chosen in order to reach an average strain rate close to 10^{-2} s^{-1}. Biaxial tests were characterized by the biaxial ratio R,

$$R = \frac{F_{22} - 1}{F_{11} - 1} \tag{4.1}$$

with F_{11} and F_{22} the longitudinal and transverse stretchings, respectively. Biaxial tension conditions were set such as $F_{11} \geq F_{22}$ and R ranging from 0 (pure shear) to 1 (equi-biaxial tension) (Figure 4.2). All biaxial tests were run at constant crosshead speed corresponding to an average strain rate close to 10^{-2} s^{-1} in direction 1. They were used for pre-loadings only, and stresses were not recorded.
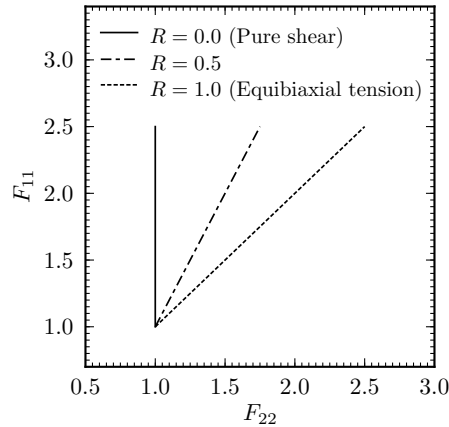
Figure 4.2: Biaxial loading paths

4.2.2 Mechanical test descriptions

When proportional loadings are considered, the Mullins softening is triggered when the stretching exceeds the maximum stretch applied during the loading history. In order to extend such a criterion to non-proportional loadings, a specific protocol was used consisting into applying a tensile pre-loading varying in nature and intensity followed by a uniaxial tension applied on a sample punched in the preloaded specimens. During the latter loading, the tensile stretch is measured using two paint marks and is defined as $\lambda = l/l_0$, with l_0 being the initial distance between the paint marks for the material virgin of any loading. In order to measure λ properly, the residual stretches were carefully tracked during the various steps of sample testing and sample cuting. Protocol details are provided Section 1.6.5.

Former contributions studying the mechanical response of filled rubbers when submitted to successive non-proportional loadings focused mainly on the induced anisotropy (Laraba-Abbes et al., 2003; Hanson et al., 2005; Diani et al., 2006a; Itskov et al., 2006; Dargazany and Itskov, 2009; Machado, 2011). For this purpose, pre-loadings are followed by a monotonic uniaxial tension loadings in various directions. The resulting stress-stretch responses are always compared to the response of a virgin material. Figure 4.1 illustrates such responses for a uniaxial pre-loading.

Such an experimental procedure reveals the Mullins softening induced anisotropy and the softening dependence to the direction of pre-loadings. Figure 4.3 shows the stress-stretch responses of pre-loaded samples uniaxially stretched in the direction of maximum pre-stretch according to the pre-loading biaxiality. In this Figure one may notice the significant increase of softening with the pre-loading biaxiality characterized by R. The stress-stretch response of the equi-biaxially pre-loaded sample is affected far beyond the maximum pre-stretch ($F_{11} = 2.5$). Moreover, the material stress-stretch response does not return on the virgin stress-stretch response necessarily, and using such a criterion for the detection of the Mullins softening activation appears hazardous. For this reason, instead of applying monotonous uniaxial tensions post pre-loading, we propose to apply cyclic uniaxial tensions. Figure 4.4 brings to light the interest of such a cyclic
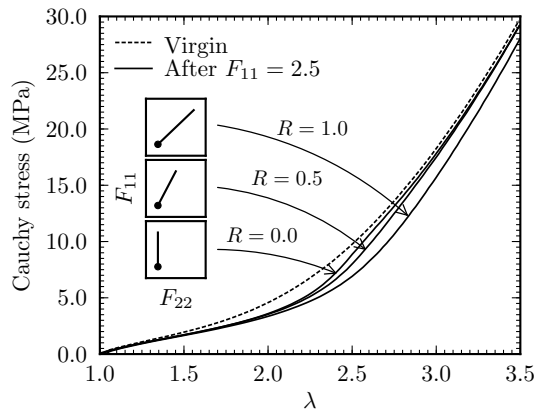
Figure 4.3: Comparison between the stress-stretch response of a virgin sample and the stress-stretch responses of samples previously submitted to pure shear ($R = 0$), $R = 0.5$ biaxial tension or equibiaxial tension ($R = 1$) with a $F_{11} = 2.5$ loading intensity, and cut in the maximal stretch direction.

loading.

In Figure 4.4, we compare the stress-stretch response of a virgin material submitted to a cyclic uniaxial tension test (left) to the stress-stretch response of a material first stretched up to $\lambda_{pre} = 3.5$ and then submitted to the same cyclic tension test (right). For the virgin material, the Mullins softening evolves gradually at each cycle while for the pre-stretched sample the Mullins softening is first triggered when the stretching exceeds the pre-stretch λ_{pre} only. Actually, the comparison of the stress-stretch responses in between two successive cycles may provide an objective criterion for the Mullins softening activation as it is demonstrated in the next section.

Let us clarify some notations that will be used along the study, biaxial pre-loadings are characterized by the ratio R and the maximum value of stretching denoted F_{11}, uniaxial pre-loadings are characterized by the applied maximum pre-stretch λ_{pre} and each cycle of the subsequent cyclic uniaxial tension loadings is characterized by the maximum stretch λ_{max} reached during the latter.

4.3   Determination of the Mullins softening activation

4.3.1   Residual stretch

Along with Mullins softening materials show substantial residual stretch increasing with the applied maximum stretch. Therefore, one may want to use the increase of residual stretch as a Mullins threshold activation. Several samples were uniaxially pre-stretched to various values λ_{pre} then submitted to cyclic uniaxial tension in the same direction. Figure 4.5a shows the
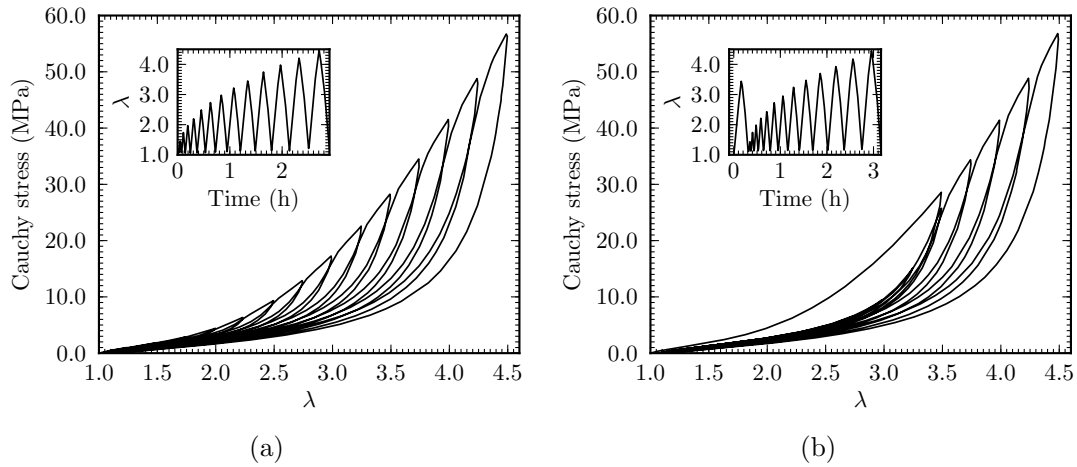
Figure 4.4: Material stress-stretch response to a uniaxial tensile cyclic test. (a) Virgin sample. (b) 3.5-uniaxialy pre-stretched sample.

evolution of the residual stretch during the cyclic tension. One notes that the residual stretch remains fairly constant until reaching the pre-stretch λ_{pre}, then it increases with the maximum applied stretch. According to this figure, the residual stretch could be a useful parameter for the Mullins activation. Unfortunately, as evidenced by Mullins (1949) and Diani et al. (2006a) the residual stretch is perturbed by the filled rubber viscoelasticity and shows partial rapid recovery when samples are unclamped (see Figure 4.5b). For this reason, it is preferable to define an indicator built on the entire stress-stretch material response.
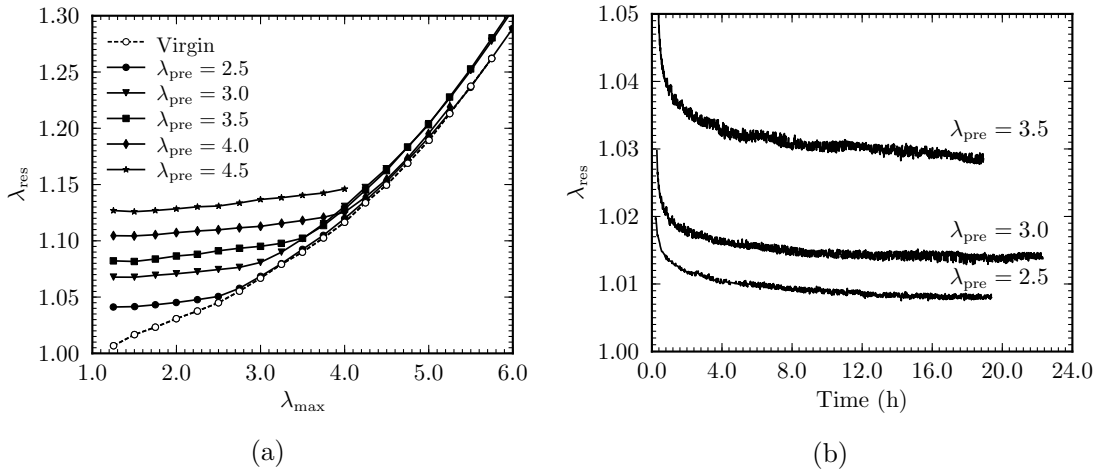
Figure 4.5: (a) Residual stretch evolution during cyclic uniaxial loadings for sample uniaxialy pre-stretched up to λ_{pre}. (b) Residual stretch recovery *vs.* time during a creep test at zero stress.

4.3.2 Parameter for the Mullins softening evolution

In this section, the stress-stretch responses of softened materials, measured during cyclic uniaxial tension tests are analyzed in order to propose an original indicator for Mullins softening activation.

In Figure 4.4, the material exhibits a significant hysteresis when loaded above the maximum

stretch yet undergone. When loaded below the maximum stretch $\lambda_{\max}$, the material shows fairly close loading and unloading responses. Therefore any of these responses may be used to characterize its softened behavior, and the loading responses were privileged in the sequel. It was noticed that the Mullins softening introduces a residual stretch that is partly recovered in between successive loadings when samples are unclamped (Figure 4.5b). In order to limit interferences between the residual stretch and the material softening, it seems better to correct the actual stretch λ according to,

$$\lambda^{\mathrm{cor}} = \frac{\lambda}{\lambda_{\mathrm{res}}} \tag{4.2}$$

in order to withdraw the residual stretch contribution in the cyclic uniaxial tension stress-stretch responses.

In order to illustrate the benefit of such a correction, the cyclic loading responses of a uniaxial sample pre-stretched to $\lambda_{\mathrm{pre}} = 2.5$ are plotted in terms of stress *vs.* amended stretch, λ^{cor} , in Figure 4.6a. One notes that the loading responses coincide as long as the Mullins effect is not re-activated. When the Mullins effect is re-activated, the next loading response exhibits a clear softening. As a consequence, one only needs to compare the difference between two successive loading responses to recognize a possible evolution of the Mullins softening. The gap between the loading responses of cycle (i) and the previous one (cycle $(i-1)$) may be estimated by calculating the difference between the stresses for stretches ranging from 1 to $(\lambda_{\max})_{(i-1)}$ or reversely by calculating the difference between stretches for stresses ranging from 0 to $(\sigma(\lambda_{\max}))_{(i-1)}$. In order to remain consistent with Merckel et al. (2011c) (or Chapter 3, equivalently), we use the latter option and we introduce the parameter α,

$$\alpha_{(i)} = \max_{0 \leq \sigma \leq \max(\sigma_{(i-1)})} \left(\frac{\lambda^{\mathrm{cor}}_{(i)}(\sigma)}{\lambda^{\mathrm{cor}}_{(i-1)}(\sigma)} \right). \tag{4.3}$$

quantifying the difference between the stress-stretch responses of two successive cycles. Nonetheless, other mathematical forms characterizing the difference between two successive cycles are possible and would lead to the same results. Examining Eq. (4.3), one may notice that α will remain close to 1 as long as the Mullins softening is not activated and α will be different from 1 when the Mullins softening occurs.

Figure 4.6b shows the evolution of α according to the maximum stretch applied at each cycle (i) for a virgin sample and for a sample already stretched up to $\lambda_{\mathrm{pre}} = 2.5$. For the virgin sample, α is above 1 for each cycle which shows the constant increase of the material softening. For the pre-stretched sample, α remains constant to 1 as long as the sample stretching remains below the maximum pre-stretch, then α evolves suddenly and return onto the α-curve provided by the virgin sample. In this figure, the parameter α appears as a relevant and obvious indicator of the Mullins activation. In order to assess the interest of the parameter α compared to the residual stretch λ_{res}, we have submitted several samples to various uniaxial proportional tension loading histories. The objective is to apply several loading histories characterized by the same maximum pre-stretch ($\lambda_{\mathrm{pre}} = 2.5$) and various resulting residual stretches. Therefore four loadings are considered, the material is pre-stretched then (i) submitted to the cyclic uniaxial loading, (ii) unclamped during 72 hours and submitted to the cyclic uniaxial loading, (iii) maintained at the pre-stretch during 12 hours and submitted to the cyclic uniaxial loading, (iv) submitted to 100 successive cycles up to the pre-stretched followed by the cyclic uniaxial tension. Loading case (ii) induces a recovery of λ_{res}, while loadings (iii) and (iv) result in an increase of λ_{res}. Figure 4.7a presents the residual stretch changes during the cyclic uniaxial tension tests for the four pre-cited cases added of the residual stretch changes for a virgin sample submitted to the cyclic uniaxial tension test only. One may notice that in every case the residual stretch returns to the residual stretch curve provided by the virgin sample, nonetheless the point of return varies according to the pre-loading histories. Figure 4.7b shows the evolutions of parameter α during
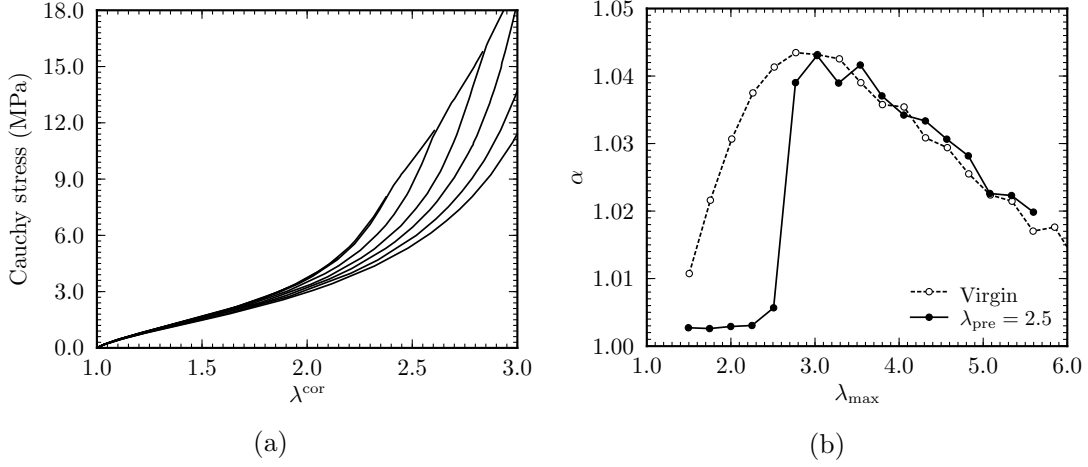
Figure 4.6: (a) $(\lambda^{\mathrm{cor}}, \sigma)$ cyclic uniaxial response of samples uniaxialy pre-stretched up to $\lambda_{\mathrm{pre}} = 2.5$. (b) Parameter α evolution during a cyclic uniaxial tension loading for a virgin sample and for a 2.5-uniaxialy pre-stretched sample.

the cyclic uniaxial tension tests for the same loading cases. For all the pre-stretched samples, the softening evolution parameter α appears to diverge from the value 1 at the same maximum stretch $\lambda_{\mathrm{max}} = \lambda_{\mathrm{pre}}$. Hence, the various loading histories are shown to change the residual stretch without affecting the softening activation threshold. This original result proves that even though residual stretch and material softening occur simultaneously during the so-called Mullins effect, they are not necessarily correlated. The material residual stretch may evolve while the Mullins softening remains constant. As a consequence, Figure 4.7 demonstrates the relevance of computing α on the amended stress-stretch responses $(\lambda^{\mathrm{cor}}, \sigma)$, to characterize the threshold of Mullins softening activation.
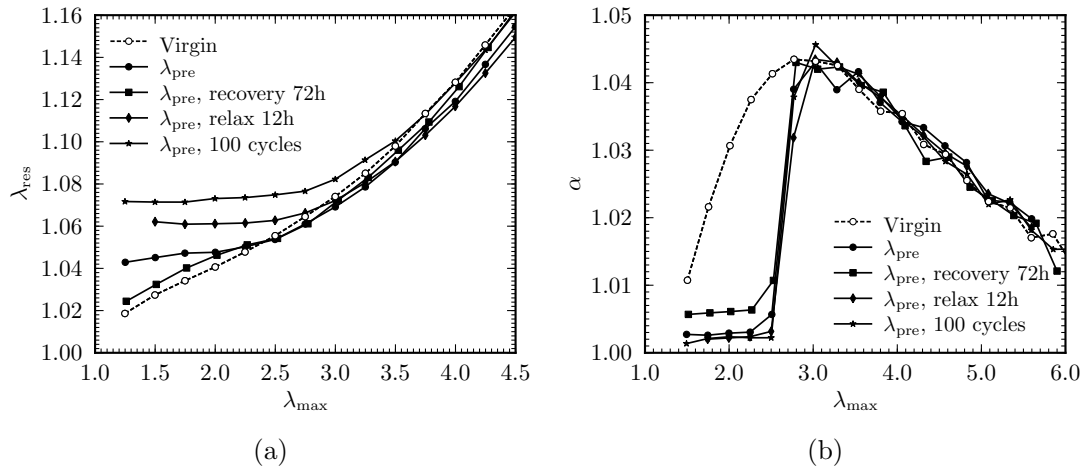
Figure 4.7: Estimate of the (a) residual stretch and (b) parameter α during a cyclic unixial tension loading for samples submitted to similar pre-loaded stretch $\lambda_{\mathrm{pre}} = 2.5$ but different loading histories.

4.3.3 Results

The softening evolution parameter α defined above is now applied to non-proportional loadings. First, large uniaxial dumbbell samples are submitted to a $\lambda_{\text{pre}} = 2.5$ pre-stretch and small dumbbell uniaxial tension samples are punched in the large samples with a direction of 0, 45 and 90 degrees with respect to the pre-stretch direction. The small specimen are then submitted to cyclic uniaxial tension tests. Figure 4.8 presents the parameter α computed on the cyclic uniaxial tension stress-stretch responses according to the angle of cut. One notices the strong dependence of the Mullins softening evolution according to the direction of second loading. As one could expect, for the sample cut along the direction of pre-stretch the Mullins softening re-activates when the material is stretched beyond the pre-stretch, but for the other two samples, cut at 45 and 90 degrees with respect to the pre-stretch direction, the Mullins softening is activated from the first cycle. It is also interesting to note, that for the sample stretched in the direction of pre-stretching, once the maximum stretch passed the pre-stretch values, the parameter α returns instantaneously on the evolution of α provided by the virgin sample. For the other samples, during the first cycles, the softening evolves but at a lower rate than for the virgin material, evidencing a softening evolution but from an already pre-damaged state. Finally, the sample cut at 90 degrees and the virgin material show similar softening evolutions.
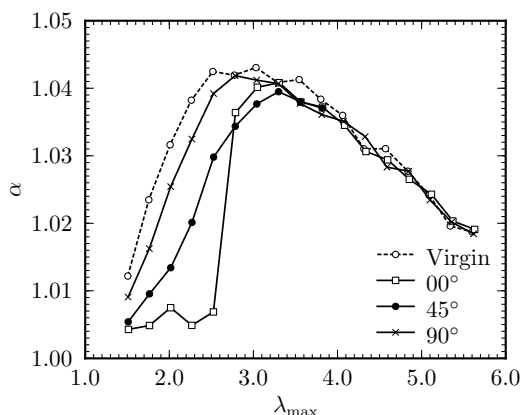
Figure 4.8: Parameter α evolution for uniaxially pre-stretched ($F_{11} = 2.5$) samples submitted to a cyclic uniaxial tensions in directions tilted of an angle 0, 45 or 90 degrees from the first direction of stretching.

Biaxial samples were submitted to a biaxial tension pre-loading defined by $R = 0.5$ and $F_{11} = 2.5$, the resulting stretch in direction 2 being $F_{22} = 1.75$. Uniaxial dumbbell samples were cut along various directions. Figure 4.9a shows the evolutions of α for samples cut in directions displaying angles of 0, 45 and 90 degrees with respect to the direction 1. These evolutions are progressive for every direction and even though it is not obvious to spot the accurate value of λ_{max} exhibiting Mullins-softening re-activation due to 0.25 stretch steps in between the successive cycles, directions 1 (0 degree) and 2 (90 degrees) stretch of Mullins activation seem close to the pre-stretch applied in these directions.

Other biaxial samples were submitted to equi-biaxial tension ($R = 1$) stretching up to $F_{11} = 2.5$. For these samples, it was verified that the cyclic uniaxial tension sample cutting direction had no effect on the softening evolution, the Mullins softening exhibiting in-plane isotropy. Figure 4.9b compares the parameter α for a virgin material sample, the uniaxially pre-stretched sample cut along direction of pre-stretching and the equi-biaxially pre-stretched sample. Both pre-stretched samples show the same threshold of softening activation which corresponds to the pre-stretching. Nonetheless once this threshold passed, the return of α on the virgin material
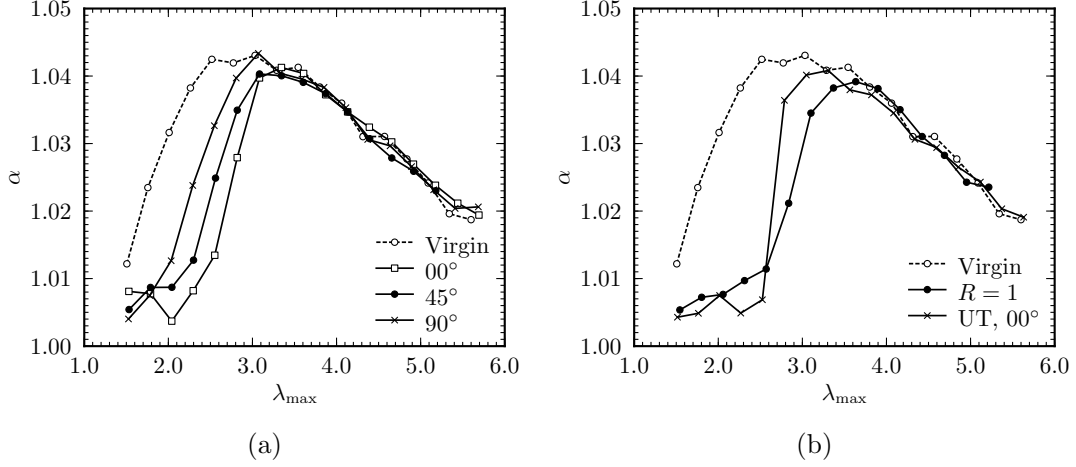
Figure 4.9: Parameter α evolution during cyclic unixial tension loadings according to the direction of stretching (which compares to the direction of maximum pre-stretch) for biaxially pre-stretched samples up to $F_{11} = 2.5$. (a) $R = 0.5$. (b) Equibiaxial ($R = 1$).

α-curve is more gradual for the equi-biaxially pre-stretched sample.

These original results are now used to define a three-dimensional Mullins softening criterion.

4.4 Mullins softening criterion

4.4.1 Definition

Considering the directional dependence of the Mullins softening activation evidenced in the previous section and its well-known dependence to the maximum stretching, we introduce directional stretching scalars along directions $\boldsymbol{u}$ according to,

$$\Lambda(\boldsymbol{u}, \boldsymbol{C}) = \sqrt{\boldsymbol{u}.\boldsymbol{C}.\boldsymbol{u}} \tag{4.4}$$

with $\boldsymbol{C} = \boldsymbol{F}^t \boldsymbol{F}$ being the right Cauchy-Green tensor, $\boldsymbol{F}$ the deformation gradient tensor and $\boldsymbol{u} = (\cos(\theta), \sin(\theta)\cos(\varphi), \sin(\theta)\sin(\varphi))$ unit vectors characterized by their polar angles (θ, φ). We observed that the Mullins softening was evolving when at least one direction was stretched above its maximum stretch already undergone, therefore we propose the following criterion for the activation of the Mullins softening,

$$\exists \boldsymbol{u}(\theta, \varphi) \mid (\Lambda - \Lambda_{\max}) = 0 \tag{4.5}$$

with $\Lambda_{\max}$ being the maximum stretch along direction $\boldsymbol{u}$ over the loading history, which writes:

$$\Lambda_{\max}(\theta, \varphi) = \max_{0 \to t} \left[\Lambda(\theta, \varphi, \boldsymbol{C}(t)) \right]. \tag{4.6}$$

Let us note that such a Mullins softening activation criterion has been already applied by Diani et al. (2006a,b), Dargazany and Itskov (2009), Merckel et al. (2011e) and studied by Itskov et al. (2010), though without any experimental evidences supporting its use.

According to Eq. (4.6), the Mullins criterion may be represented by the three-dimensional surface defined by $\Lambda_{\max}$. For proportional loadings, one may write analytical expressions specifying the Mullins threshold surface. For non-proportional loadings, the surface contour is reached through numerical computations. Figure 4.10 shows the three-dimensional representations of
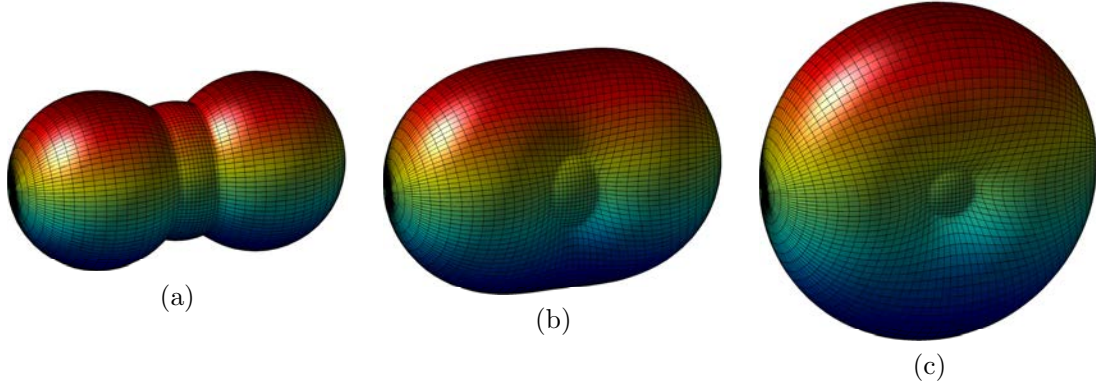
Figure 4.10: Three-dimensional representation of the surface defined by $\Lambda_{\max}(\theta, \varphi)$ for a $F_{11} = 2.5$ loading in (a) uniaxial tension, (b) $R = 0.5$ biaxial tension, and (c) equibiaxial tension ($R = 1$).

the surfaces resulting from uniaxial, biaxial ($R = 0.5$) and equi-biaxial loading conditions, which are the pre-loading conditions of our study.

The criterion proposed in Eq. (4.5) is now confronted to the experimental results.

4.4.2 Analysis

Figure 4.11 presents the evolution $\Lambda_{\max}(\theta, \varphi)$ with the applied loading for $\lambda_{\mathrm{pre}} = 2.5$ uniaxially pre-stretched samples cut in directions 0, 45 and 90 degrees and submitted to a cyclic uniaxial tension with maximum stretch increasing of $\Delta \lambda = 0.25$ at each cycle. This figure corresponds to the evolution of $\Lambda_{\max}$ for the Mullins softening progression experimentally studied in Figure 4.8. In order to ease the understanding, the evolution of $\Lambda_{\max}$ is plotted in the specimen stretching plane. The dashed line draws the pre-loading surface, the solid lines result from the post uniaxial tension cycles when increase the dimension of the $\Lambda_{\max}$ surface.

Figure 4.11a, corresponding to proportional uniaxial tension loading, shows that the surface defined by $\Lambda_{\max}$ evolves when the pre-stretched is passed only. Moreover, when evolving, a substantial number of directions are affected. For samples cut at 45 degrees (Figure 4.11b), the maximum stretching surface evolves from the first cycle and the number of directions affected starts low and grows gradually at each cycle. The $\Lambda_{\max}$ surface corresponding to samples cut at 90 degrees with respect to the pre-stretching direction, evolves from the very first cycle as demonstrates Figure 4.11c.

Figure 4.12 shows the evolution of $\Lambda_{\max}$ for a biaxial pre-loading characterized by $R = 0.5$ and $F_{11} = 2.5$, followed by a cyclic uniaxial tension at 0, 45 and 90 degrees with respect to direction 1. This figure compares with Figure 4.9a. For this pre-loading, one may notice that the $\Lambda_{\max}$ surface evolves after reaching direction-dependent values of stretching. For samples cut at 0, 45 and 90 degrees, the surfaces evolve after cycle 6, 4 and 3 respectively (corresponding to $\lambda_{\max}$ equals to 2.5, 2 and 1.75 respectively), which corroborates the Mullins softening activation thresholds given by Figure 4.9a. A similar analysis worked well for the equi-biaxial pre-loading case also.

The former qualitative analysis may be reinforced by a quantitative analysis of the surface created at each cycle. For this purpose, we introduce the parameter

$$\gamma = \frac{1}{4\pi} \iint_{\mathcal{S}} \gamma^{\boldsymbol{u}} \sin(\theta) \mathrm{d}\varphi \mathrm{d}\theta \tag{4.7}$$

with $\gamma^{\boldsymbol{u}}(\theta, \varphi) = 1$ when $\partial \Lambda_{\max}/\partial t > 0$ et $\gamma^{\boldsymbol{u}}(\theta, \varphi) = 0$ when $\partial \Lambda_{\max}/\partial t = 0$, t being the time.
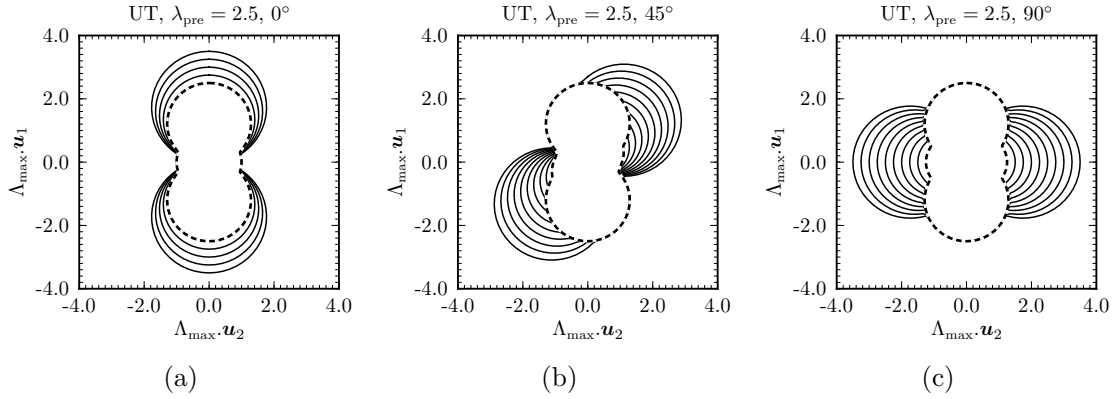
Figure 4.11: Projection of the $\Lambda_{\max}(\theta, \varphi)$ surface in the sample plane. Dashed line: uniaxial pre-stretch up to $\lambda_{\mathrm{pre}} = 2.5$. Solid line: surface evolution during cyclic uniaxial loadings performed in directions (a) 0, (b) 45 and (c) 90 degrees compared to direction of pre-stretching.
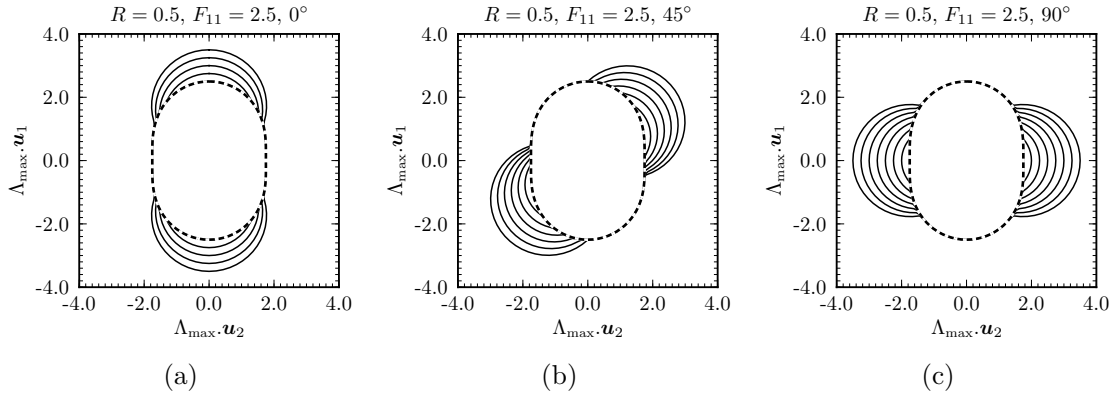
Figure 4.12: Projection of the $\Lambda_{\max}(\theta, \varphi)$ surface in the sample plane. Dashed line: $R = 0.5$ biaxial pre-stretch up to $F_{11} = 2.5$. Solid line: surface evolution during cyclic uniaxial loadings performed in direction (a) 0, (b) 45 and (c) 90 degrees compared to direction of pre-stretching.

Parameter γ, inspired by former work by Diani and Gilormini (2005), computes the fraction of directions stretched above their maximum stretch already undergone. Figure 4.13 shows values of γ continuously computed for $\lambda_{\max}$ ranging from 1 to 5, for the loading histories studied in Section 4.3.3. We marked by symbols each cycle of the actual cyclic uniaxial tension tests. This figure is to be compared with Figures 4.8 and 4.9. These figures reveal a strong correlation between α and γ characterizing the increase of material softening and the increase of the $\Lambda_{\max}$ surface respectively, and they provide solid evidences supporting the relevance of criterion Eq. (4.5).

4.4.3 Validation

We presented a number of experimental results leading to the definition Eq. (4.5) of a Mullins softening criterion. The criterion is now tested in other conditions. For this purpose, biaxial samples were submitted to different loading histories leading to the same $\Lambda_{\max}$ surfaces. Then uniaxial tension samples were cut at 0, 45 and 90 degrees and submitted to cyclic uniaxial tension tests. During the latter tests, the Mullins softening activation was estimated with the
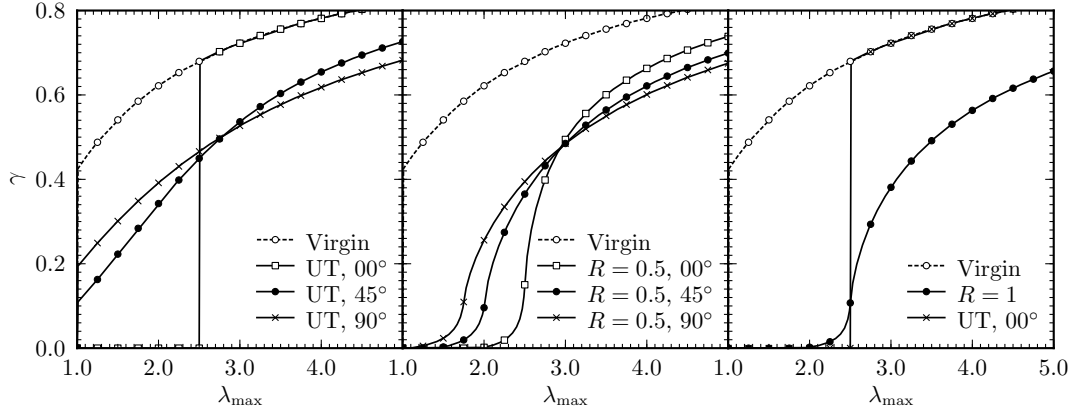
Figure 4.13: Fraction of active elongated chains γ evolution during cyclic uniaxial loadings performed in different directions for pre-stretched samples with a $F_{11} = 2.5$ loading intensity. Pre-loading paths are grouped according to Figures 4.8 and 4.9.

parameter α and compared according to the loading history.

The two loading histories are sketched in Figure 4.14a. The first one from A to $B1$, is made of two successive perpendicular pure shear loadings. The second loading from A to $B2$ adds a biaxial compression-tension to the pure shear according to direction 1 (A). Both loading paths cause the identical maximum stretch surface drawn in Figure 4.14b. These paths were chosen specifically for several reasons. First, the resulting maximum stretch surface exhibit an interesting change of convexity at 45 degrees, second, during pre-loading from A to $B2$, direction 1 is first stretched and then quite severely compressed ($F_{11} = 0.62$), which puts to test the criterion when some directions are stretched and then compressed.

(a)

(b)
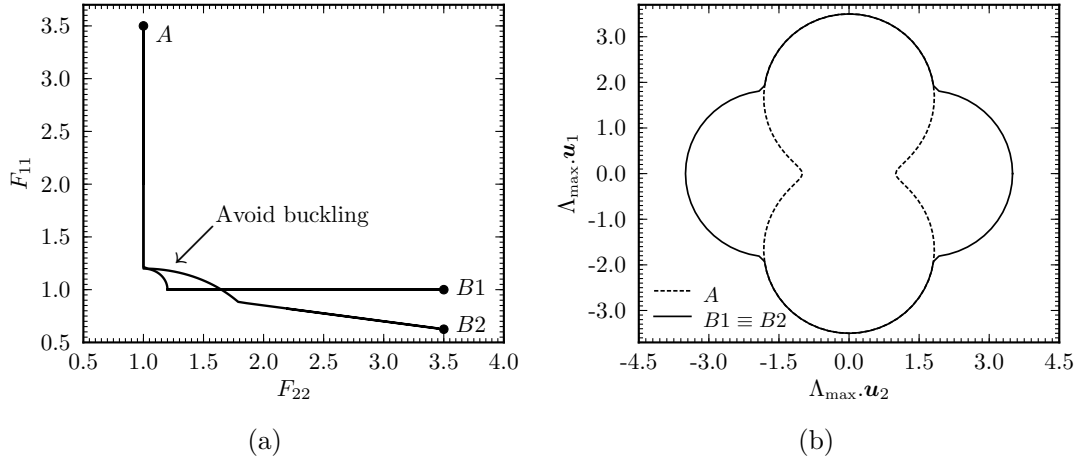
Figure 4.14: (a) $F_{11} - F_{22}$ plane schematic representation of two specific loading paths: A to B1 and A to B2. (b) Projection of $\Lambda_{\max}(\theta, \varphi)$ surfaces for both loading paths.

Figure 4.15 shows the parameter α computed during the cyclic uniaxial tension for samples cut at 0, 45 et 90 degrees for both pre-loading cases. One notices that both pre-loading cases lead to the same evolution of the softening parameter α, therefore both pre-loading cases are identical in terms of Mullins softening. Finally, Figure 4.15 shows that Mullins softening activates earlier for samples cut at 45 degrees compare to samples cut in directions 1 and 2, and Figure 4.15b illustrates that the post-stretching compression in direction 1 does not change the evolution of α

which is similar for both directions 1 and 2. Both results reinforce the well-grounded of criterion Eq. (4.5).
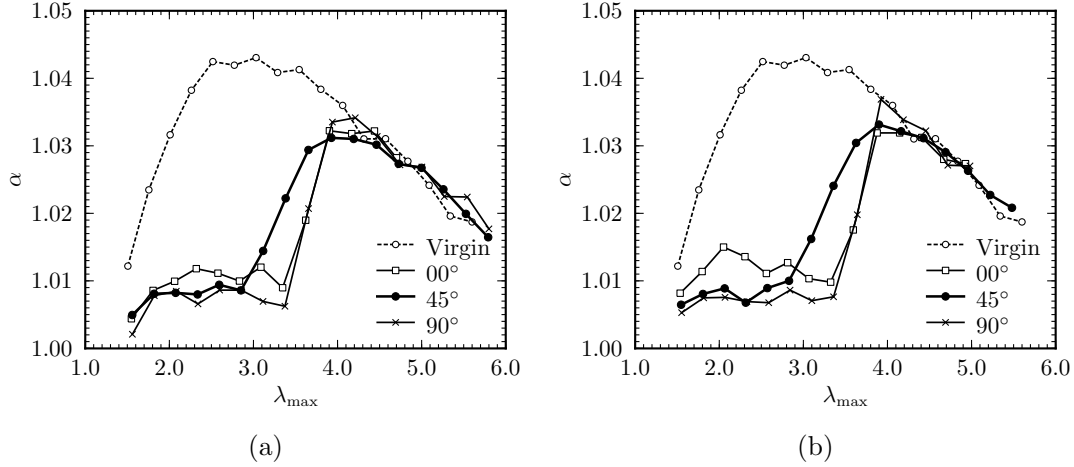
Figure 4.15: Parameter α evolution during cyclic uniaxial loadings for (a) path A to $B1$ and (b) path A to $B2$ pre-loaded samples.

At last, in order to prove the general nature of the proposed criterion, we tested it on the 40 phr carbon-black filled natural rubber detailed and labelled NR in Section 2.2.1, exhibiting substantial crystallization during stretching. Figure 4.16a illustrates the stress-stretch behavior of the filled natural rubber. The stress-stretch responses of the natural rubber differ from the SBR stress-stretch responses for the substantial hysteresis existing at any cycle (during and post Mullins effect) due to the crystallization. This material was submitted to the pre-loading A and $B1$ (Figure 4.14a). The parameter α was estimated for samples cut in directions 0, 45 and 90 degrees as it was done for the SBR. Figure 4.16b displays the evolution of α with respect to the the cyclic maximum stretch and the angle of cut. Results are very similar to the results obtained on the SBR material in Figure 4.14a. As a consequence, the activation of the Mullins softening is not affected by the crystallization and its criterion extends to crystallizing natural rubber.
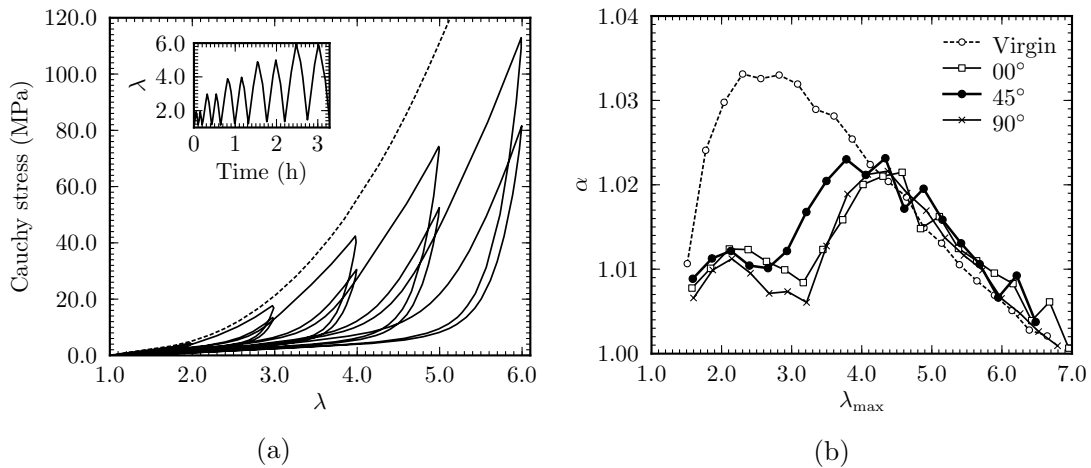
Figure 4.16: (a) Stress-stretch response of a filled natural rubber under monotonic and cyclic uniaxial conditions. (b) Parameter α evolution during a cyclic unixial tension loading for path A to $B1$ pre-loaded samples.

4.5 Conclusion

This chapter aims at defining a Mullins softening activation criterion for filled rubbers submitted to general loading conditions, including non-proportional loadings. The criterion is grounded on an original analysis of unconventional experimental data. By comparing the stress-stretch responses of successive uniaxial tension cycles with increasing maximum stretch, a softening evolution parameter is defined. According to this softening parameter evolution, it is possible to recognize the Mullins softening activation. The method applies for pre-loaded samples, and allows the definition of the directional stretch necessary to re-activate the Mullins softening in the direction of cyclic uniaxial stretching. The method has been applied to several samples uniaxially or biaxially pre-loaded, including proportional and non-proportional post cyclic uniaxial loadings. Results provide solid evidences for the definition of a Mullins softening activation criterion as the three-dimensional surface of maximum directional stretch submitted to the material along the loading history. Also, two specific loading cases involving different loading paths with identical maximum direction stretch surfaces were considered in order to test the criterion predictive ability. The Mullins softening activation threshold was well predicted by the criterion. Finally, the criterion was shown to apply to crystallizing filled natural rubber. The definition of such a valid experimentally-based criterion is a critical point for constitutive modeling of the Mullins softening, it should open new perspectives in terms of mechanical modeling. The next chapter will use the criterion in order to propose a constitutive model for filled rubbers accounting for Mullins softening induced anisotropy.

Chapter 5

Constitutive modeling of the anisotropic behavior of Mullins softened filled rubbers

Most of this chapter has been submitted for publishing within reference:

Original constitutive modeling is proposed for filled rubber materials in order to capture the anisotropic softened behavior induced by general non-proportional pre-loading histories. The hyperelastic framework is grounded on a thorough analysis of cyclic experimental data. The strain energy density is based on a directional approach. The model leans on the strain amplification factor concept applied over material directions according to the Mullins softening evolution. In order to provide a model easily versatile that applies for a wide range of materials, the proposed framework does not require to postulate the mathematical forms of the elementary directional strain energy density and of the Mullins softening evolution rule, and a computational procedure is defined to build both functions incrementally from experimental data obtained during cyclic uniaxial tensile tests. Successful comparisons between the model and the experiments demonstrate the model abilities. Moreover, the model is shown to accurately predict the non-proportional uniaxial stress-stretch responses for uniaxially and biaxially pre-stretched samples. Finally, the model was efficiently tested on several materials and proves to provide a quantitative estimate of the anisotropy induced by the Mullins softening for a wide range of filled rubbers.

Contents

5.1 Introduction

In terms of modeling, one may find a significant number of models in the literature designed to reproduce the behavior of Mullins softened rubber-like materials. However, most of them are developed for idealized isotropic softening and very few aim at capturing the softening induced anisotropy. A first representation for anisotropic hyperelastic behavior was proposed by Weiss et al. (1979), based on a strain invariants which limits its applicability to simple anisotropies (transverse isotropy or orthotropy) and excludes its extension to the Mullins softening. An alternative approach based on directional behavior laws was proposed by Pawelski (2001), Göktepe and Miehe (2005) and Diani et al. (2006b). The directional laws were shown to capture the Mullins softening induced anisotropy without major difficulties by considering that damage evolves independently along each material direction. Nonetheless, in the existing directional laws, the residual stretch is constrained by the anisotropy induced by the Mullins softening, and this is not in complete agreement with the experimental observations. Actually, experimental evidences detailed in the following section support a decoupling of the residual stretch with the Mullins softening. Therefore, both should be accounted for independently.

The pre-cited directional models are based on a physical interpretation of the Mullins softening. They generally depend on physically motivated elementary strain energy densities and the Mullins softening is accounted for by altering the strain energy density parameters. In order to accurately fit original experimental data, the elementary strain energy density and the Mullins softening evolution rule may require substantial modifications according to the material behavior. Moreover, the strain energy density and the evolution rule must be guessed *a priori*, and no general procedure has been proposed to do so.

In this study, our main motivation is to propose a general framework easily versatile for the modeling of hyperelastic rubber-like material behavior with a realistic account of the anisotropic induced Mullins softening. For this purpose, a directional approach is considered with an anisotropic criterion for the Mullins softening activation. At first, according to experimental evidences, Mullins softening and residual stretch evolutions are decoupled. Then, in order to propose a modeling with the largest flexibility, the account for the Mullins softening is chosen to avoid assumptions on the elementary strain energy density or the softening evolution rule. This is made possible by using the strain amplification concept early proposed by Mullins and Tobin (1957) and developed in Chapter 3. Finally, an identification procedure is proposed to assess both the elementary strain energy density and the Mullins softening evolution rule without postulating their mathematical forms.

The chapter is organized as follows. In the next section, the experimental setup and experimental results are presented. The constitutive equations and the identification procedure are detailed in Section 5.3. Results are shown and discussed in Section 5.4. Finally, concluding remarks close the chapter.

5.2 Experiments

5.2.1 Experimental setup

The material labeled R is used as a reference material to illustrate experimental grounds of the model and to validate the model and the identification procedure. Materials C3 to C6 will be used to assess the general aspect of the model and to test its interest for comparing the mechanical behavior of various materials. Uniaxial and biaxial tension tests were conducted according to the experimental details provided in Chapter 4. In what follows, the states of stretch are characterized by the principal stretches which coincide with the eigenvalues F_{ii} of the deformation gradient $\boldsymbol{F}$. The direction of larger stretching will be referenced as direction 1, directions 2 and 3 are perpendicular to direction 1 and direction 3 lies along the sample thickness.

For uniaxial loadings, λ may conveniently denote the principal stretch in the tension direction. The Cauchy stress $\sigma_{11} = F/S$ is used for uniaxial tension responses, with F the force and S the current sample cross-section. According to results shown in Section 2.3, the Cauchy stress resulting from cyclic uniaxial tension will be computed within incompressibility assumption and the model will be proposed within an incompressible framework.

5.2.2 Mullins softening and residual stretch

When a filled rubber is submitted to cyclic loading conditions, one may notice along with the softening, a residual stretch that increases with the applied maximum stretch. Both features are usually pointed out as consequences of the Mullins effect. However, some experimental evidences show otherwise. The softening occurring upon first stretch is an irreversible damage phenomenon at room temperature (Mullins, 1947). To the contrary, the residual stretch is very dependent on viscoelasticity and shows an important and rapid recovery at room temperature (Mullins, 1949; Diani et al., 2006b). Other experimental observations prove that although residual stretch and material softening usually occur simultaneously, their evolutions are not necessarily correlated. Various loading histories with identical maximum stretch may result in substantial residual stretch changes while the Mullins softening remains unaffected. An example is presented in Figure 5.1. A $\lambda = 2.5$ uniaxialy pre-stretched sample is submitted to uniaxial cyclic loading with an increasing maximum stretch of $\Delta\lambda = 0.25$ at each cycle after a 72 hours stress free recovery. Figure 5.1a shows the loading responses resulting from the cyclic loading. One may notice that the stress-stretch responses evolve at each cycle from the very first cycle. However, while representing the loading stress-stretch responses applying a residual stretch correction, according to $\lambda_{\mathrm{cor}} = \lambda/\lambda_{\mathrm{res}}$, one notices that the loading responses are perfectly superimposed until the maximum previous stretch ($\lambda = 2.5$) is reached (Figure 5.1b). This demonstrates that in Figure 5.1a, the mechanical behavior of the material does not evolve for cycles below $\lambda = 2.5$, except for the residual stretches, evidencing a significant residual stretch evolution and a constant Mullins softening.
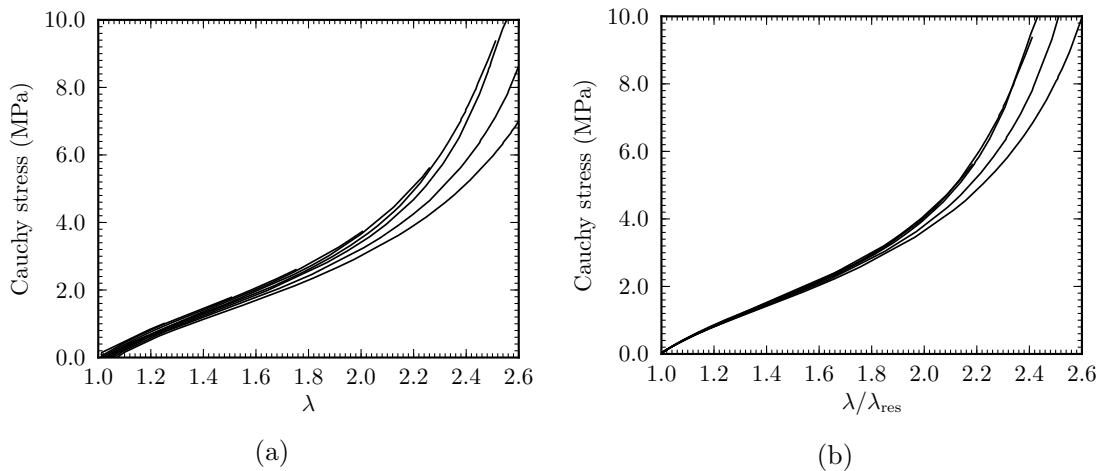
Figure 5.1: Uniaxial tensile cyclic test performed after a 72-hour stress-free recovery on a 2.5-uniaxialy pre-stretched material. (a) Stress-stretch (λ, σ) loading responses. (b) Residual stretch corrected stress-stretch $(\lambda/\lambda_{\mathrm{res}}, \sigma)$ loading responses.

Other experimental evidences support the uncorrelation of the residual stretch and of the Mullins softening. First, the Mullins softening and the residual stretch seem both quite dependent to the material composition but with different sensitivities (Mullins, 1949; Dorfmann and Ogden, 2004; Merckel et al., 2011b). Second, some materials may evidence some large

Mullins softening with very little residual stretch. For instance, a silicone filled rubber studied by Machado (2011) display significant Mullins softening and an unnoticeable residual stretch.

5.2.3 Anisotropy characterization

When submitting a sample to an uniaxial tension according to direction 1, its free faces are submitted to the boundary conditions $\sigma_{22} = \sigma_{33} = 0$, and when the measured stretches satisfy to $F_{22} = F_{33}$, the material shows transverse isotropy properties. Therefore in order to illustrate the material anisotropy, the ratio F_{22}/F_{33} resulting from a cyclic proportional uniaxial tension test is plotted with respect to the stretch λ in Figure 5.2a. The ratio F_{22}/F_{33} appears different from 1, highlighting the material initial anisotropy resulting from the manufacturing process. The material appears stiffer along the plate thickness direction than in any in-plane direction (bear in mind that the in-plane isotropy has been verified). More interestingly, the F_{22}/F_{33} evolution seems to follow the same path for every cycle, evidencing the same anisotropy throughout the test.
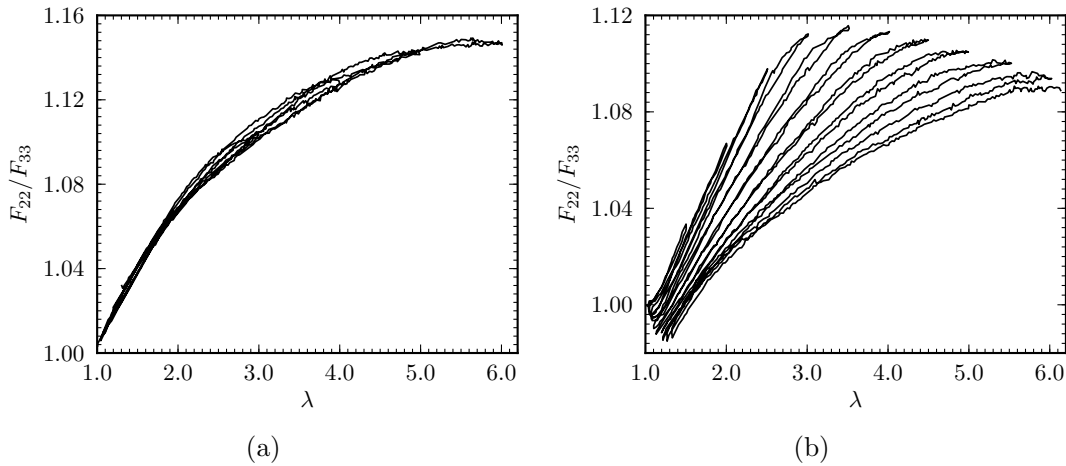
Figure 5.2: In-plane (2,3) anisotropy changes. (a) Proportional cyclic uniaxial tension loading. (b) Cyclic uniaxial tension loading performed on a 2.5-biaxially pre-stretched sample.

The anisotropy characterization method is now applied to a small uniaxial dumbbell sample punched in a $\lambda = 2.5$ equi-biaxially pre-stretched specimen. Results are shown in Figure 5.2b. The F_{22}/F_{33} evolution follows the same path as long as the sample is stretched below the maximum stretch previously applied ($\lambda = 2.5$). Then the anisotropy evolves at each cycle and the ratio F_{22}/F_{33} slowly evolves toward a similar path than the path displayed by the virgin material in Figure 5.2a. The introduced material anisotropy characterization will provide an additional element to validate the relevance of the modeling.

5.2.4 Equilibrium response

In the current work, the material viscoelasticity is not considered and our focus is set on the equilibrium responses only. Once the Mullins softening has been evacuated, the loading and the unloading responses are fairly close and both responses may be used to characterize the material softened behavior (Figure 5.3a). In order to remain consistent with previous modeling works proposed by the authors (Diani et al., 2006a,b), the unloading responses are favored, and the material mechanical behavior evolution due to the Mullins softening is illustrated by the stress-stretch responses in Figure 5.3b.
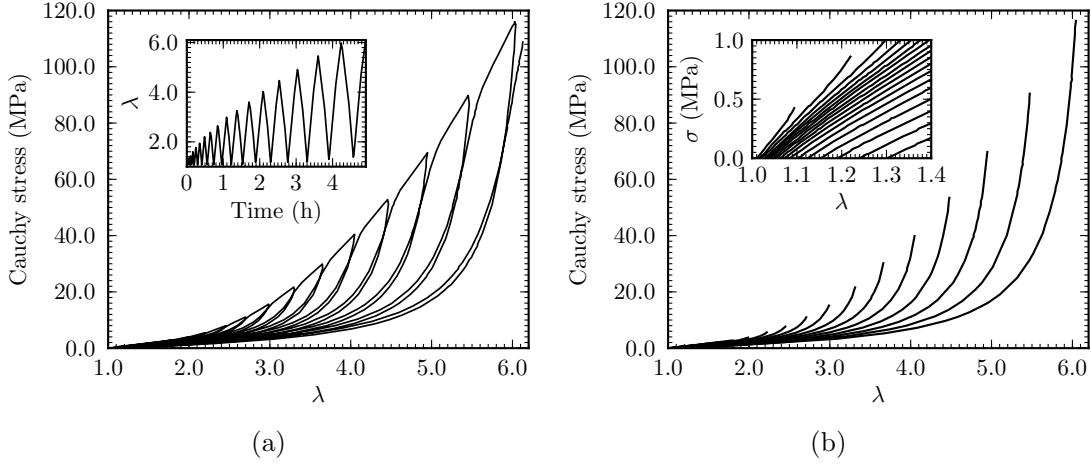
Figure 5.3: Material stress-stretch response to a uniaxial tensile cyclic test with maximum stretch increasing at each cycle. (a) Entire response. (b) Unloading responses.

The next section presents the theoretical and the computational aspects of the modeling.

5.3 Modeling

5.3.1 Hyperelastic framework

Experimental observations reported in Section 5.2.2 support a decoupling of the residual stretch from the Mullins softening. Therefore, we use a kinematic approach decomposing the total deformation gradient $\boldsymbol{F}$ into an elastic part $\boldsymbol{F}_e$ and an inelastic part $\boldsymbol{F}_p$,

$$\boldsymbol{F} = \boldsymbol{F}_e \boldsymbol{F}_p. \tag{5.1}$$

The inelastic deformation gradient tensor $\boldsymbol{F}_p$ changes the initial reference configuration into a stress-free intermediate configuration accounting for residual deformation, while the elastic deformation gradient tensor $\boldsymbol{F}_e$ changes the stress-free configuration into the current configuration and therefore accounts for the elastic deformation. It is assumed that $\boldsymbol{F}_p$ does not evolve during the unloading responses shown in Figure 5.3b.

In order to describe the material deformation, the right Cauchy-Green tensor $\boldsymbol{C} = \boldsymbol{F}^t \boldsymbol{F}$ and the left Cauchy-Green tensor $\boldsymbol{B} = \boldsymbol{F} \boldsymbol{F}^t$ are introduced. The state of the material is assumed to be described by the strain energy $\mathcal{W}$ written in terms of $\boldsymbol{C}_e$ and $\boldsymbol{B}_p$. Considering a strain energy with decoupled effects of the elastic and inelastic deformations leads to,

$$\mathcal{W}(\boldsymbol{C}_e, \boldsymbol{B}_p) = \mathcal{W}_e(\boldsymbol{C}_e) + \mathcal{W}_p(\boldsymbol{B}_p). \tag{5.2}$$

and the second Piola-Kirchhoff stress tensor in the stress-free configuration derives from the second law of thermodynamics,

$$\boldsymbol{S} = 2 \frac{\partial \mathcal{W}_e(\boldsymbol{C}_e)}{\partial \boldsymbol{C}_e}. \tag{5.3}$$

Elastomeric materials can be represented as three-dimensional networks of very long flexible macromolecules randomly oriented in all directions of space. In directional approaches, the strain energy density $\mathcal{W}_e$ is evaluated from the summation of elementary strain energy contributions w over all considered directions. An idealized representation introduced by Treloar and Riding

([1979](#)) is the full-network model, which considers a continuous spatial distribution of directions leading to an integration over the unite sphere,

$$\mathcal{W}_e(\boldsymbol{C}_e) = \iint_{\mathcal{S}} w(\boldsymbol{u}) \ \mathrm{d}\mathcal{S} \tag{5.4}$$

with unit vectors $\boldsymbol{u} = (\cos(\theta), \sin(\theta)\cos(\varphi), \sin(\theta)\sin(\varphi))$ characterized by the polar angles (θ, φ) and $\mathrm{d}\mathcal{S} = 1/4\pi \sin(\theta)\mathrm{d}\varphi\mathrm{d}\theta$.

In such a directional representation, anisotropy may be accounted for by considering uneven elementary strain energy contributions w, according to the direction $\boldsymbol{u}$. As previously noticed by Diani et al. (2004); Göktepe and Miehe (2005); Diani et al. (2006b), such an account for anisotropy may lead to uncontrolled residual stresses in the free strain state. Therefore, in order to circumvent such residual stresses, and to satisfy to a stress-free undeformed state, the constitutive equation, Eq. (5.3), is modified into (Diani et al., 2004),

$$\boldsymbol{S} = 2\frac{\partial \mathcal{W}_e(\boldsymbol{C}_e)}{\partial \boldsymbol{C}_e} - 2\frac{\partial \mathcal{W}_e(\boldsymbol{C}_e)}{\partial \boldsymbol{C}_e}\bigg|_{\boldsymbol{C}_e = \boldsymbol{I}}. \tag{5.5}$$

The elastic elongation along each direction $\boldsymbol{u}$, Λ_e, is obtained from the right elastic Cauchy-Green tensor as,

$$\Lambda_e = \sqrt{\boldsymbol{u}.\boldsymbol{C}_e.\boldsymbol{u}}. \tag{5.6}$$

Let us note that $\partial \Lambda_e / \partial \boldsymbol{C}_e = (\boldsymbol{u} \otimes \boldsymbol{u})/2\Lambda_e$, hence the elastic energy density partial derivative comes as

$$\frac{\partial \mathcal{W}_e}{\partial \boldsymbol{C}_e} = \frac{1}{2}\iint_{\mathcal{S}} \frac{\boldsymbol{u} \otimes \boldsymbol{u}}{\Lambda_e} \frac{\partial w}{\partial \Lambda_e} \ \mathrm{d}\mathcal{S}. \tag{5.7}$$

The Cauchy stress tensor $\boldsymbol{\sigma}$ is obtained by pushing forward the Piola Kirchhoff stress tensor $\boldsymbol{S}$ from the relaxed configuration to the current configuration via $\boldsymbol{F}_e$. Substituting Eq. (5.7) in Eq. (5.5) and assuming material incompressibility yield to the following expression for the Cauchy stress tensor,

$$\boldsymbol{\sigma} = \boldsymbol{F}_e \left(\iint_{\mathcal{S}} g(\boldsymbol{u}) \ (\boldsymbol{u} \otimes \boldsymbol{u}) \ \mathrm{d}\mathcal{S} \right) \ \boldsymbol{F}_e^t - p\boldsymbol{I} \tag{5.8}$$

where p is an arbitrary hydrostatic pressure introduced to account for incompressibility and $g(\boldsymbol{u})$ a directional scalar that writes,

$$g = \frac{f(\Lambda_e)}{\Lambda_e} - f(1) \tag{5.9}$$

with f the elementary force-elongation relation in the direction $\boldsymbol{u}$ defined as

$$f(\Lambda_e) = \frac{\partial w(\Lambda_e)}{\partial \Lambda_e}. \tag{5.10}$$

While the full-network initially proposed by Treloar and Riding (1979) uses a specific inverse Langevin function based form for f, the above formulation is not restricted and can be applied to any directional force-elongation $f(\Lambda_e)$. Therefore, we are not assuming any specific mathematical form for f since the latter will unfold upon experimental data fit.

The full-network framework is not efficient for numerical implementations due to the numerical integrations and in order to circumvent the time-consuming computational integration task, discrete integrations are usually preferred. For this purpose, a finite number of directions is considered. For instance, Göktepe and Miehe (2005) and Diani et al. (2006b) used sets of 42 and 32 directions respectively, based on Bažant and Oh (1986) numerical integration. We followed this path but many other methods may be found in the literature.

In the next section, account for the Mullins softening is introduced.

5.3.2   Mullins softening

Recently, Merckel et al. (2012a) conducted an extensive experimental study on the Mullins softening (see Chapter 4). It was shown that the latter evolves when at least one material direction is stretched above its maximum stretch. Therefore, the criterion proposed by Diani et al. (2006b) for anisotropic Mullins softening has been validated by Merckel et al. (2012a)'s experimental work. It writes as,

$$\forall \boldsymbol{u}(\theta, \varphi) \mid (\Lambda - \Lambda_{\mathrm{max}}) = 0 \tag{5.11}$$

with Λ being the total elongation along direction $\boldsymbol{u}$

$$\Lambda(\boldsymbol{u}) = \sqrt{\boldsymbol{u}.\boldsymbol{C}.\boldsymbol{u}} \tag{5.12}$$

and Λ_{max} the maximum of Λ over the loading history

$$\Lambda_{\mathrm{max}}(\boldsymbol{u}) = \max_{0 \to t} \left[\Lambda(\boldsymbol{u}, t) \right]. \tag{5.13}$$

It is noteworthy that the criterion Eq. (5.11) is based on the total elongation and not only on its elastic component. This particular aspect of the criterion is supported by the fact that a softened material may recover some of its residual stretch without recovering any of its Mullins softening as shown in Section 5.2.2. Once the criterion defined, the damage variable which provides the softening in the stress-strain responses remains to be introduced.

The strain amplification concept, early introduced by Mullins and Tobin (1957), and based on experimental evidences reproduced by Klüppel and Schramm (2000) and Merckel et al. (2011c) for instance, supports the idea that the stress-strain responses of softened filled rubbers evolve due to the amplification of the strain undergone in softened materials compared to the strain a virgin material would undergo at similar stress (see Chapter 3). This may be written as[1],

$$\log(\Lambda_e) = X \log(\Lambda_e^{\mathrm{virgin}}) \tag{5.14}$$

when the logarithmic strain is chosen. The strain amplification factor X satisfies to $X(\boldsymbol{u}) \geqslant 1$ along each direction $\boldsymbol{u}$. The stretches $\Lambda_e^{\mathrm{virgin}}$ and Λ_e characterize the directional stretch in the virgin material and the directional amplified stretch respectively. The strain amplification factor concept is introduced within the hyperelastic framework proposed in Section 5.3.1 by substituting Λ_e as a function of X and $\Lambda_e^{\mathrm{virgin}}$ (Eq. (5.14)), in g (Eq. (5.9)). Such a concept was already used in a similar fashion by Qi and Boyce (2004).

At this point, the model is fully defined. The residual stretches are captured by $\boldsymbol{F}_p$ in the decomposition Eq. (5.1). The Cauchy stress response, for a general full-network directional framework, is given by Eq. (5.8). The Mullins criterion is a directional criterion, defined by Eq. (5.11), providing possible induced anisotropy. Finally, the Mullins softening is accounted for by substituting Eq. (5.14) in g (Eq. (5.9)), the enhanced directional stretches Λ_e depending on the directional amplification factors $X(\boldsymbol{u})$. In order to describe and predict the material softening depending on the loading history, two material functions remain to be determined: X and f. Therefore the next section draws attention to the identification procedure.

---

[1]It worth emphasize that within Chapter 3, the strain amplification concept has been used in order to characterize the Mullins softening. For this purpose, we proposed a decomposition of the strain amplification factor into a softening part D and a reinforcing part X. The parameter D was then used to quantified the softening. In the current chapter, we do not pursue the same goal and we do not need to introduce the parameter D. Therefore, the classical factor X is used for the strain amplification. However, the reader may notice that X in Eq. (5.14) is equivalent to the definition of $1/(1-D)$ in Chapter 3.

5.3.3 Identification of the elementary force-elongation function f and the Mullins softening rule X

The elementary force-elongation function and the Mullins softening evolution rule are built incrementally in order to obtain a good fit of the experimental unloading responses from a cyclic uniaxial tension test with increasing maximum stretch at every cycle as shown in Figure 5.3. Since for every mechanical test, the material stress-stretch response depends on both f and X, an original method is defined guaranteeing simultaneous identification of both functions.

The main difficulty stands in the uneven evolution of the softening according to the spatial directions. Actually, the maximum directional stretch $\Lambda_{\max}(\boldsymbol{u})$ depends on the direction considered ranging from 1 to $\lambda_{\max}$ (the maximum stretch in the uniaxial stretching direction). Figure 5.4 illustrates $\Lambda_{\max}$ directional evolution for uniaxial tension tests.
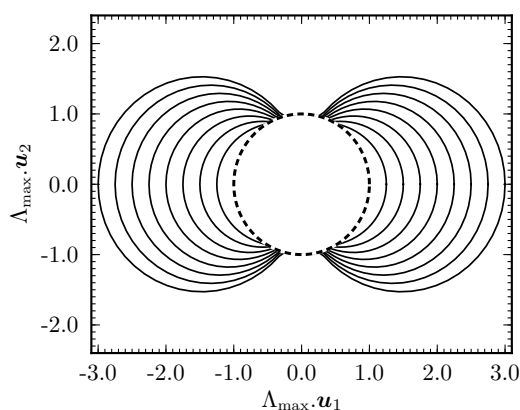
Figure 5.4: Directional evolution of $\Lambda_{\max}$ during a cyclic uniaxial loading, projected in the sample plane $(\boldsymbol{u}_1, \boldsymbol{u}_2)$. The initial state is emphasized by dashed line.

When unloading the sample, the Mullins softening and the residual stretch evolutions are both stabilized. The inelastic part $\boldsymbol{F}_p$ (see Eq. (5.1)) coincides with the residual stretch λ_{res} and the elastic part λ_e may be extracted from the measured stretch λ^{meas} using,

$$\lambda_e = \frac{\lambda^{\mathrm{meas}}}{\lambda_{\mathrm{res}}}. \tag{5.15}$$

The material anisotropy evolves upon stretching only. Therefore, when the incompressible material is assumed as initially isotropic, the relation $F_{22} = F_{33} = \lambda^{-0.5}$ is obtained for uniaxial stretching in direction 1. Constitutive equations Eq. (5.8), simplify into:

$$\sigma_{11} = \iint_{\mathcal{S}} g \left(u_1^2 \lambda_e^2 - \frac{u_2^2}{\lambda_e} \right) \mathrm{d}\mathcal{S} \tag{5.16}$$

with $g(\boldsymbol{u})$ depending on $\Lambda_e(\boldsymbol{u})$, $X(\boldsymbol{u})$ and f (Eqs. (5.14) and (5.9)).

On one hand X increases with the increase of the maximum stretch submitted and remains constant during unloadings. On the other hand, f is independent of the softening, and remains the same for any cycle. The identification strategy is based on a resolution of the implicit Eq. (5.16). From a given experimental couple (σ_{11}, λ_e) and knowing the Mullins softening governing parameter spatial density $\Lambda_{\max}(\boldsymbol{u})$ illustrated in Figure 5.4, local values X and f may be computed numerically. Therefore, discrete definitions for f and X may be built by putting into practice the procedure synopsized in Figure 5.5.

The identification procedure starts from the first (and smallest) cycle. Initial conditions $X(1) = 1$ and $f(1) = 0$ are naturally chosen, then X and f are progressively extended. In the
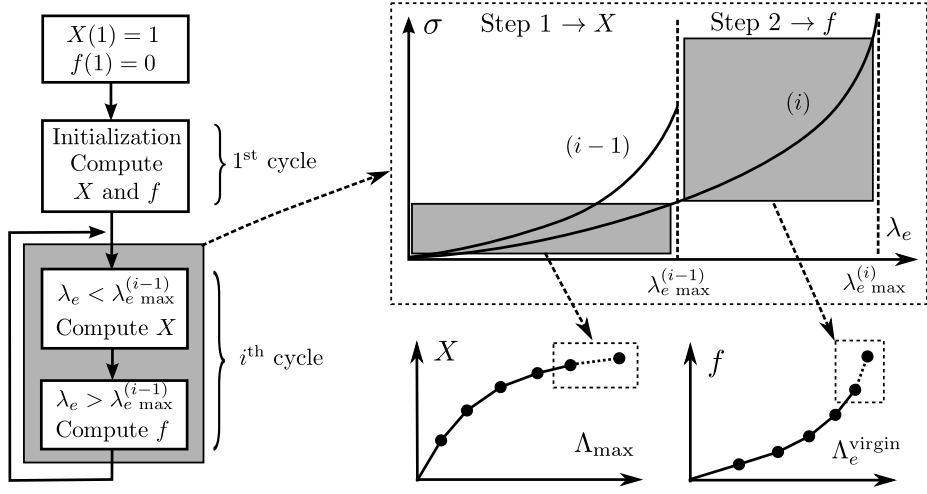
Figure 5.5: Identification procedure.

first cycle ($i = 1$), the identification process is initialized according to the procedure reported in Table 5.1 in order to compute X for $\Lambda_{\max} \in [1, \lambda_{\max}^{(i=1)}]$ and f for $\lambda_e \in [1, \lambda_{e\,\max}^{(i=1)}]$. It is worth noting that a small cycle is advised for the initialization.

Experimental data	First cycle maximum stretch $\lambda_{\max}^{(i=1)}$
	Couples (σ_{11}, λ_e)
Initial conditions	$X(1) = 1$
	$f(1) = 0$
Mullins criterion	Compute the directional governing parameter $\Lambda_{\max}(\boldsymbol{u})$
	$\Lambda_{\max}(\boldsymbol{u}) = \sqrt{\boldsymbol{u}.\boldsymbol{C}(\lambda_{\max}^{(i=1)}).\boldsymbol{u}}$
Model	Relationship between (σ_{11}, λ_e) and (X, f)
	$\sigma_{11} = \iint_{\mathcal{S}} g \left(u_1^2 \lambda_e^2 - u_2^2/\lambda_e \right) \mathrm{d}\mathcal{S}$
	with $g = f(\Lambda_e)/\Lambda_e - f(1)$, and $\log(\Lambda_e) = X \log(\Lambda_e^{\mathrm{virgin}})$
Numerical resolution	Compute $X(\Lambda_{\max})$ for $\Lambda_{\max} = \lambda_{\max}^{(i=1)}$ and $f(\Lambda_e^{\mathrm{virgin}})$ for $\lambda_e = \lambda_{e\,\max}^{(i=1)}$
	with a local square minimization of σ_{11}
	Compute few intermediate values of $f(\Lambda_e^{\mathrm{virgin}})$ for $\lambda_e \in [1, \lambda_{e\,\max}^{(i=1)}]$
	with a local square minimization of σ_{11} and the computed X value

Table 5.1: Identification procedure initialization

Once X and f have been initialized, they are extended by fitting each unloading response as illustrated in Figure 5.5. At cycle (i), the beginning of functions X and f have previously been determined, and the next identification action is performed in two steps. At first, the force-elongation f is known for values of $\Lambda_e^{\mathrm{virgin}}$ corresponding to macroscopic stretches ranging in $1 < \lambda_e < \lambda_{e\,\max}^{(i-1)}$, and therefore is used to compute $X(\Lambda_{\max}^{(i)})$. In a second step, $X(\Lambda_{\max})$ being defined for the entire cycle (i), f is extended for values of $\Lambda_e^{\mathrm{virgin}}$ corresponding to $\lambda_e \in [\lambda_{e\,\max}^{(i-1)}, \lambda_{e\,\max}^{(i)}]$. Computational details for both steps are provided in Tables 5.2 and 5.3 respectively. When both X and f have been determined for cycles up to (i), the identification strategy is iterated for cycle $(i+1)$. Let us note that intermediate values for f and X are given by a linear interpolation.

During the identification procedure described above, evolutions of X and f are defined by experimental data only. However, it was noticed that the following restriction,

$$f(\Lambda_e^{\mathrm{virgin}} \leqslant 1) = 0. \tag{5.17}$$

Experimental data	Cycle i maximum stretch $\lambda_{\max}^{(i)}$
	Couples (σ_{11}, λ_e) for $\lambda_e < \lambda_{\max}^{(i-1)}$
Initial conditions	$X(\Lambda_{\max})$ known for $\Lambda_{\max} \in [1, \lambda_{\max}^{(i-1)}]$
	$f(\Lambda_e^{\text{virgin}})$ known for $\lambda_e \in [1, \lambda_{e\,\max}^{(i-1)}]$
Mullins criterion	Compute the directional governing parameter $\Lambda_{\max}(\boldsymbol{u})$
	$\Lambda_{\max}(\boldsymbol{u}) = \sqrt{\boldsymbol{u}.\boldsymbol{C}(\lambda_{\max}^{(i)}).\boldsymbol{u}}$
Model	Relationship between (σ_{11}, λ_e) and (X, f)
	$\sigma_{11} = \iint_{\mathcal{S}} g\left(u_1^2 \lambda_e^2 - u_2^2/\lambda_e\right) \mathrm{d}\mathcal{S}$
	with $g = f(\Lambda_e)/\Lambda_e - f(1)$, and $\log(\Lambda_e) = X \log(\Lambda_e^{\text{virgin}})$
Numerical resolution	Compute $X(\Lambda_{\max})$ for $\Lambda_{\max} = \lambda_{\max}^{(i)}$ with a mean square minimization of σ_{11} on the interval $\Lambda_{\max} \in [\lambda_{\max}^{(i-1)}, \lambda_{\max}^{(i)}]$

Table 5.2: First identification step at cycle i

Experimental data	Couples (σ_{11}, λ_e) for $\lambda_e > \lambda_{\max}^{(i-1)}$
Initial conditions	$X(\Lambda_{\max})$ known for $\Lambda_{\max} \in [1, \lambda_{\max}^{(i)}]$
	$f(\Lambda_e^{\text{virgin}})$ known for $\lambda_e \in [1, \lambda_{e\,\max}^{(i-1)}]$
Model	Relationship between (σ_{11}, λ_e) and (X, f) using
	$\sigma_{11} = \iint_{\mathcal{S}} g\left(u_1^2 \lambda_e^2 - u_2^2/\lambda_e\right) \mathrm{d}\mathcal{S}$
	with $g = f(\Lambda_e)/\Lambda_e - f(1)$, and $\log(\Lambda_e) = X \log(\Lambda_e^{\text{virgin}})$
Numerical resolution	Compute few values of $f(\Lambda_e^{\text{virgin}})$ for $\lambda_e \in [\lambda_{e\,\max}^{(i-1)}, \lambda_{e\,\max}^{(i)}]$ with a local square minimization of σ_{11}

Table 5.3: Second identification step at cycle i

was favorable for a good comparison between the model and the experimental data in terms of induced anisotropy. While proof of such a restriction will be discussed in the next section, it may be noticed that this restriction may be interpreted as if directions in compression do not sustain the stress and only stretched directions do. Anyhow, accounting for Eq. (5.17) within the proposed framework does not lead to any adjustment in the constitutive equations or the identification procedure previously presented.

The proposed identification procedure was tested on material R. A first cycle is performed up to $\lambda_{\max}^{(i=1)} = 1.1$, then for each cycle, the maximum stretch was increased with a step of $\Delta \log(\lambda) = 0.1$. The interest of such a loading stands in smaller first few cycles before the difference between two successive cycles becomes significant. Therefore, the loading is well suited for the identification, with a short cycle for initialization (Table 5.1) and stretch intervals increasing at each cycle for the computation of f (Table 5.3). Model fit of the experimental unloading responses used for identification is shown in Figure 5.6. Experimental responses appear to be successfully represented.

Figure 5.7a shows the elementary force-elongation relation, $f(\Lambda_e^{\text{virgin}})$, resulting from the identification procedure. One may notice that f presents the classic features of a filled rubber behavior, with a low stiffness and a quasi-linear response at small stretch, then a sharp upturn followed by an asymptotic vertical at larger stretch when the material limit extensibility is reached.

The Mullins softening rule, $X(\Lambda_{\max})$, is shown in Figure 5.7b. The dependence of X to the maximum stretch is well approximated by,

$$X = \alpha \log(\Lambda_{\max}) \tag{5.18}$$

with α a material parameter characterizing the softening evolution rate. For material R, one
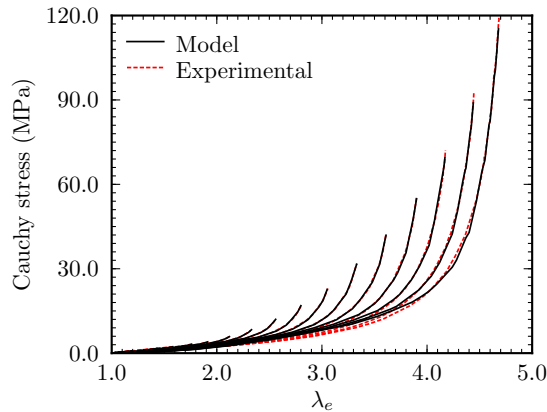
Figure 5.6: Model ability to fit the Mullins softened behavior of material R.
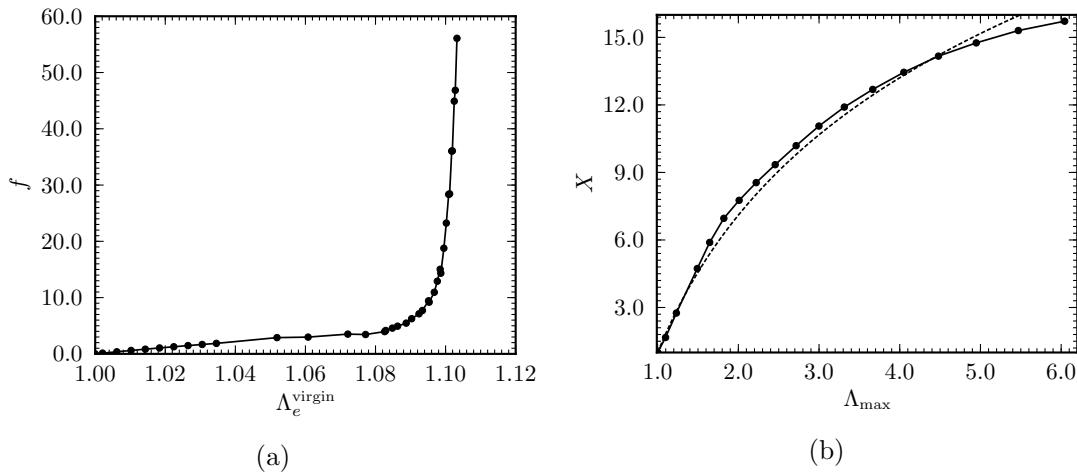
Figure 5.7: Identification results for material R. (a) Elementary force-elongation relation. (b) Mullins softening rule.

gets $\alpha = 8.8$. The logarithmic evolution of X with respect to the maximum elongation is consistent with previous results aiming at characterizing the Mullins softening (shown Chapter 3 and reported by Merckel et al. (2011c)). Furthermore, softening evolution rules defined in order to converge toward a saturation limit are used in other models, for instance Miehe and Keck (2000); Klüppel and Schramm (2000); Qi and Boyce (2004) among others. Let us note that models based on the Ogden and Roxburgh (1999) approach for the Mullins softening do not agree with this observation.

5.4 Results and discussion

5.4.1 Prediction of non-proportional loading resulting behavior

This section aims at illustrating the model predictive capabilities. For this purpose, the force-elongation relation, $f(\Lambda_e^{\mathrm{virgin}})$, and the Mullins softening law, $X(\Lambda_{\max})$, previously identified for the material R are used to represent the responses of material R when submitted to cyclic uniaxial tension post non-proportional pre-stretchings.

Samples submitted to cyclic uniaxial tension tests are now small dumbbell samples punched

in a larger sample already submitted to a uniaxial or biaxial pre-loading. Between both the pre-loading and the loading experiments, an important residual stretch recovery induced by the material viscoelasticity occurs. The material viscoelasticity is not accounted for here and the experimental data are corrected according to Eq. (5.15) and the modeling condition $\boldsymbol{F}_p = \boldsymbol{I}$ is set.

First, the experimental procedure is applied for $\lambda = 2.5$-uniaxial stretch pre-loading, and small dumbbell samples are cut at 45 and 90 degrees from the pre-loading stretching direction. The cyclic uniaxial tension is performed with maximum stretches increasing of $\Delta\lambda = 0.25$ at each cycle. According to criterion, Eq. (5.11), the Mullins softening is activated in some directions from the very first cycle, and it evolves differently according to the directions. Comparison between the experimental unloading responses and the model predictions are shown in Figure 5.8. One may notice that the experimental unloading curves are well approximated for small and large cycles and this without using any adjusting parameter or further identification but by using the material function f and X identified earlier on a virgin sample only (Section 5.3.3). Therefore, the model is able to capture the material anisotropy induced by the Mullins softening resulting from a uniaxial pre-loading. Let us note that such a Mullins softening observed at the very first cycles in Figures 5.8a and 5.8b, could not be represented with an isotropic Mullins criterion, which would have predicted Mullins reactivation at $\lambda = 2.5$ only.
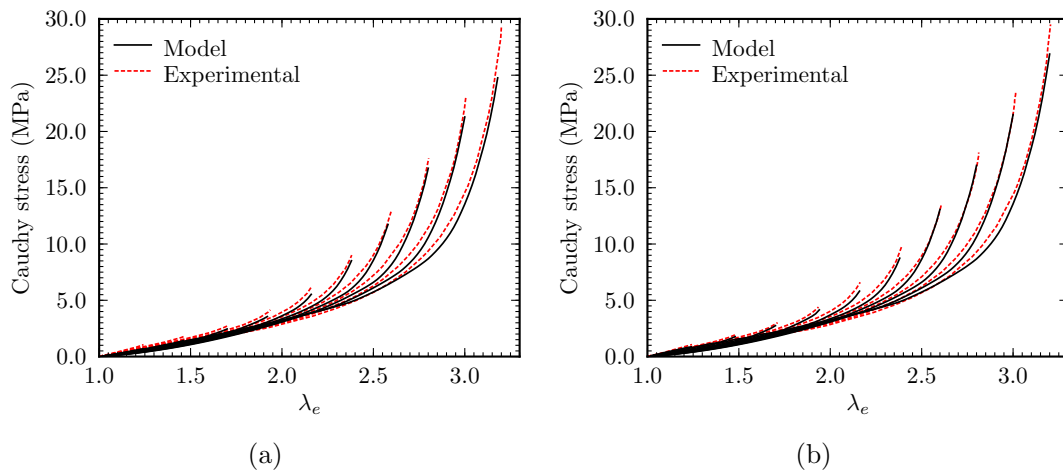
Figure 5.8: Model prediction for 2.5-uniaxially pre-stretched material. Sample cut in directions (a) 45 and (b) 90 degrees compared to direction of pre-stretching.

Second, the same experimental procedure is applied to samples submitted to biaxial pre-loads. Two pre-loading conditions were chosen, $F_{11} = F_{22} = 2.5$ equi-biaxial pre-stretching and $F_{11} = 2.5$ and $F_{22} = 1.75$ biaxial pre-stretching (loading condition characterized by $R = 0.5$ in Chapter 4). The small dumbbell samples were cut in the direction of maximum stretching (direction 1). According to criterion, Eq. (5.11), the Mullins softening will not activate until $\lambda = 2.5$ was reached. Experimental responses and model estimates are compared in Figure 5.9. Apart from the viscoelasticity exhibited by actual samples at the very beginning of the unloadings that cannot be reproduced, the model predictions appear to be accurate below and above the Mullins activation for both pre-loading conditions. The softening induced by a biaxial loading appears to be also well captured by the model.

Results shown in Figure 5.9 yield to important consequences in terms of material behavior modeling and identification. The mechanical tests performed in order to obtain the experimental data involved a multiaxial loading path, but the Mullins softening evolution rule $X(\Lambda_{\max})$ was chosen as dependent of the maximal directional stretch only. The prediction abilities shown by
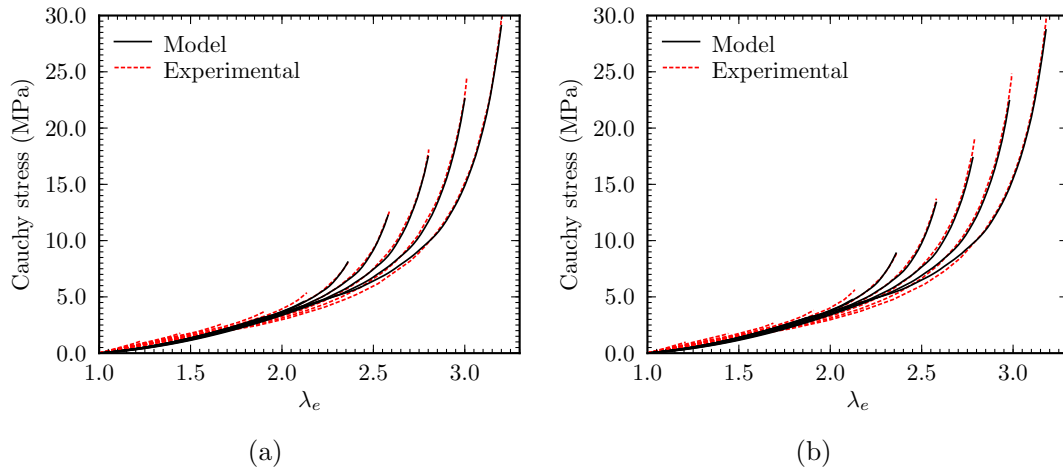
Figure 5.9: Model prediction of the uniaxial stress-stretch responses of samples biaxially pre-stretched material up to (a) $F_{11} = F_{22} = 2.5$ and (b) $F_{11} = 2.5$, $F_{22} = 1.75$ and cut along the the maximum pre-stretched direction.

the model proves that X does not require complex account of the loading multiaxiality and its complete identification may be performed on a mere cyclic uniaxial tension test.

The following section aims at studying the actual material anisotropy evolution and its model prediction. The anisotropy is then characterized by measuring and comparing the stretches according to the principal stretching directions.

5.4.2   Estimate of the induced anisotropy

The ratio F_{22}/F_{33} evolution was introduced Section 5.2.3 to characterize the anisotropy changes during cyclic uniaxial tests. Figure 5.10a shows the ratio F_{22}/F_{33} model prediction for a cyclic uniaxial loading performed on a 2.5-equi-biaxially pre-stretched material. As long as $\lambda = 2.5$ is not reached, the Mullins softening does not evolve and F_{22}/F_{33} path remains identical. Once the Mullins softening is re-activated, changes occurs and at each cycle, the path slowly converges on a proportional uniaxial loading path (*i.e.* $F_{22}/F_{33} = 1$). This modeling result is to be compared with experimental observations presented Figure 5.2b. Note that the discrepancies between Figure 5.2a and Figure 5.10 are due to the model initial isotropy assumption, which does not match the actual material initial anisotropy. Nonetheless, the trend of the material anisotropy evolution is well captured by the model.

In the modeling section, the condition Eq. (5.17) was introduced for the elementary force-elongation. When releasing this condition, the fitting procedure drives to a function f reaching negative values for $\lambda < 1$. The resulting ratio F_{22}/F_{33} computed with the function f obtained without applying condition Eq. (5.17) is shown in Figure 5.10b. During the equi-biaxial pre-loading, the material is softened in direction 2 while remaining virgin in direction 3. Since the material stiffness is higher in direction 3, boundary conditions $\sigma_{22} = \sigma_{33} = 0$ should yield to $F_{22}/F_{33} > 1$. This is obviously not the case in Figure 5.10b. Moreover, one may notice in Figure 5.10b that the anisotropy intensity increases with $\lambda_{\max}$ while it is expected to decrease. The result is obviously unrealistic and validate the condition Eq. (5.17), which supports the physical picture of directions in compression not sustaining the stresses.
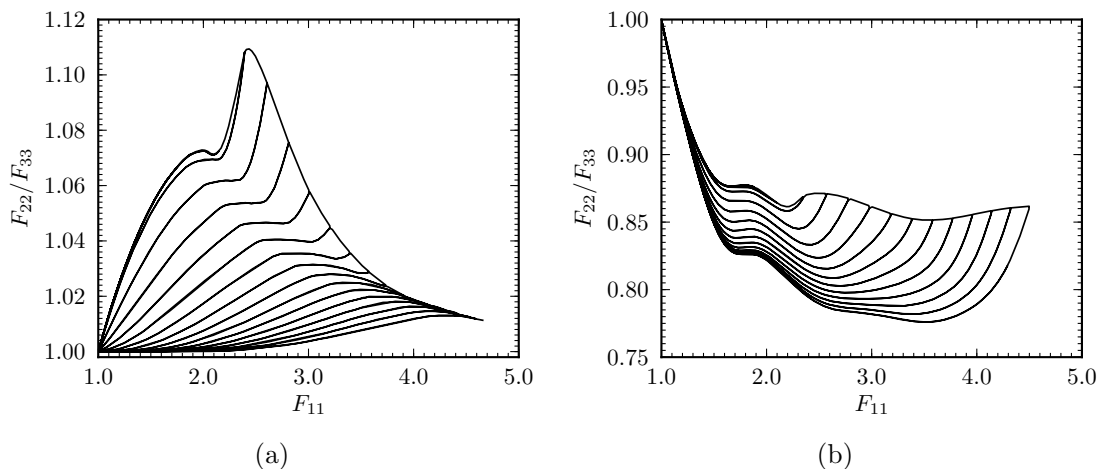
Figure 5.10: Model prediction for the anisotropy changes in-plane (2,3). (a) with Eq. (5.17) condition. (b) without Eq. (5.17) condition.

5.4.3 Other model interest: Study of the effect of filler amount

Hitherto, only the reference material labelled R was used to develop the mechanical behavior model and the identification procedure. This section aims at applying the model on various materials in order to validate the identification procedure and to investigate the effect of the filler amount on the Mullins softening. Materials C3, C4, C5 and C6 described in Table 2.1 were submitted to cyclic uniaxial loadings with a maximum stretch increasing at each cycle with of a $\Delta \log(\lambda) = 0.1$ step and up to failure. The evolution rules f and X were computed for each material performing the identification procedure detailed in Section 5.3.3. The model responses and experimental data are favorably compared in Figure 5.11. Therefore, the model and the identification procedure was successfully extended to several materials, exhibiting distinct mechanical behaviors and distinct sensitivities to the Mullins softening.

In order to investigate dependencies to the filler amount, evolution rules f and X are compared in Figure 5.12. Figure 5.12a shows the filler amount effect on the identified elementary force-elongation relations. Every material exhibits a quasi-linear virgin response followed by a plateau ended by a sharp upturn. The main dependences of f to the filler amount are the initial stiffness increase and the upturn stretch decrease with the filler amount. These observations are consistent with former results from the literature. Actually, the reinforcing effect of filler volume fraction on the initial stiffness is well known (Einstein, 1906; Guth and Gold, 1938).

The effect of the amount of fillers on X is illustrated Figure 5.12b. As expected, the Mullins softening rate increases with the amount of fillers, see for instance Mullins and Tobin (1957); Bergström and Boyce (1999); Klüppel and Schramm (2000); Dorfmann and Ogden (2004); Merckel et al. (2011c) among others. One may notice that for every material the evolution of X is quasi-linear with respect to the logarithm of the maximum directional stretch $\Lambda_{\max}$. The same property was observed and shown in Figure 5.7b for material R, therefore the Mullins softening evolution rule introduced Eq. (5.18) may well be general.

5.5 Conclusion

This chapter aimed at proposing a constitutive model for the mechanical behavior of filled rubbers with Mullins softening. The constitutive equations were grounded on an thorough analysis of original experimental data. Basic uniaxial tensile tests and unconventional non-proportional tensile tests including uniaxial and biaxial loading paths were used to produce the
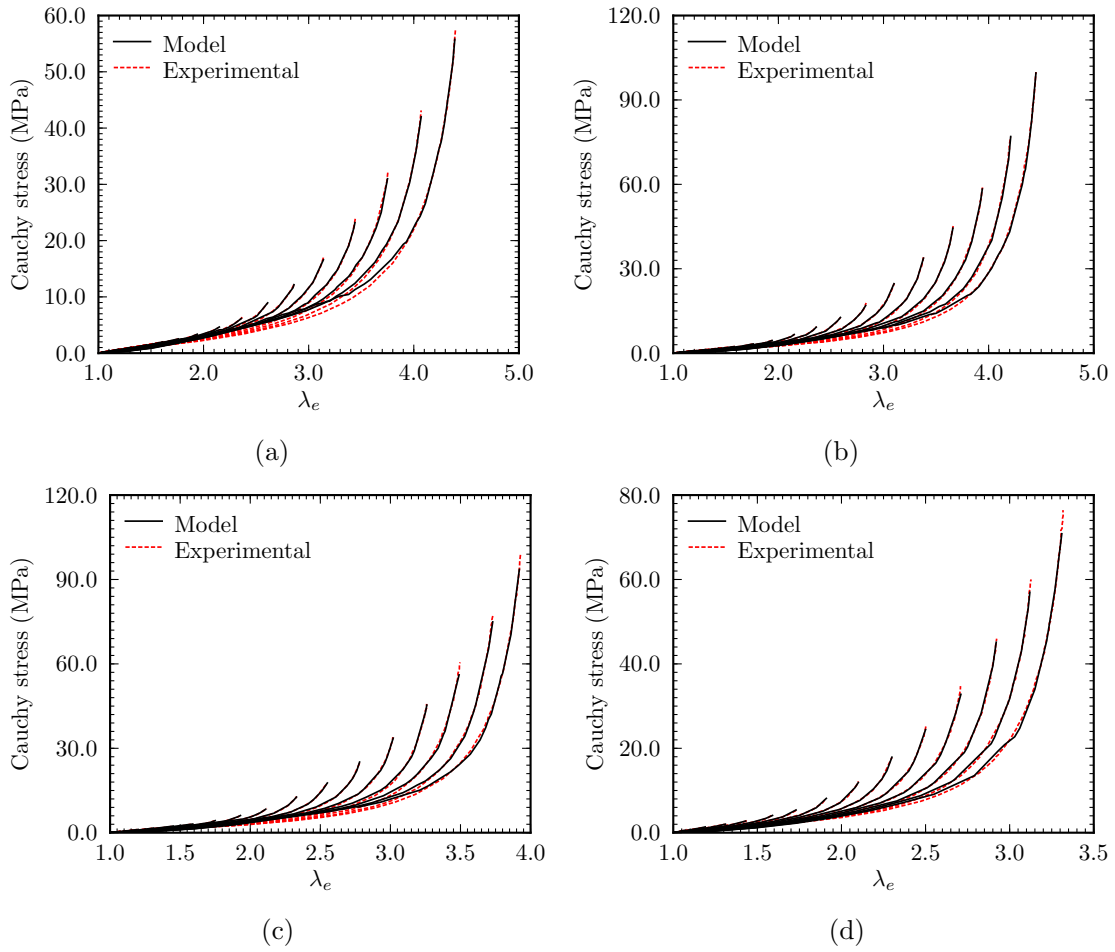
Figure 5.11: Model prediction for material (a) C3, (b) C4, (c) C5, (d) C6
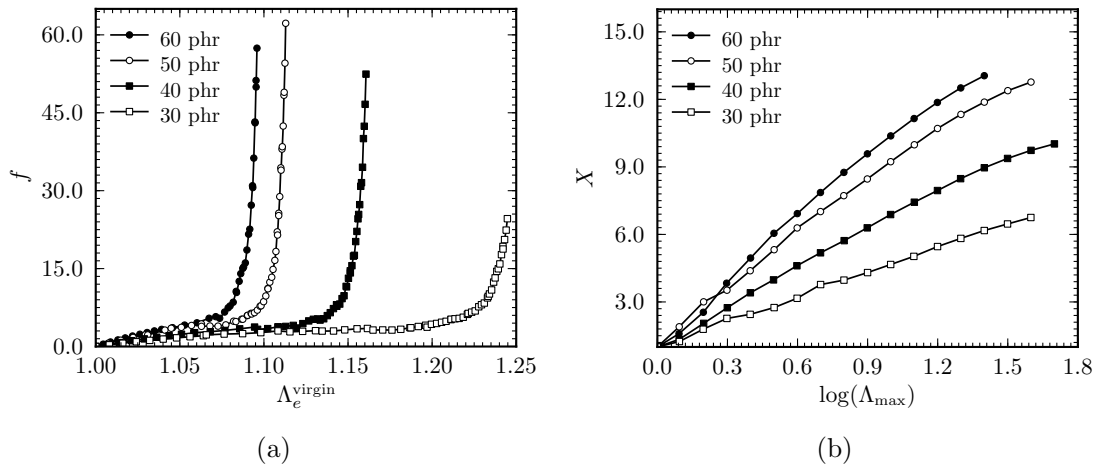
Figure 5.12: Identification results for material with different amount of fillers. (a) Elementary force-elongation functions. (b) Mullins softening rules.

necessary experimental data. The model was based on a directional approach in order to capture the anisotropy induced by general non-proportional pre-loading histories. The Mullins softening

was accounted for by the strain amplification concept and was activated by a directional criterion. The framework was developed in order to avoid any *a priori* assumption of the mathematical forms of the elementary strain energy density and of the Mullins softening evolution rule. An original identification procedure was proposed in order to build both functions from a cyclic tensile stress-stretch response. An accurate fit of the experimental data provided by a cyclic proportional uniaxial tensile test illustrated the model ability to capture the material stress-softening. Once identified on a proportional cyclic test, the model was shown to successfully and accurately predict uniaxial stress-stretch responses of non-proportional uniaxially or biaxially pre-stretched samples. Finally, the model and the identification procedure were applied on various filled rubber materials evidencing different mechanical behaviors and sensitivities to the Mullins softening. The results showed favorable comparisons and illustrated the model flexibility to apply to a wide range of rubber-like materials.

This current chapter closed the investigations on the Mullins softening reported within the thesis. In Chapter 3, a quantitative method to characterize the Mullins softening under uniaxial tension loading conditions has been proposed. The mechanical quantity driving the Mullins softening evolution under general loading conditions has been determined within Chapter 4. Finally, the current Chapter 5 has provided constitutive equations to model the mechanical behavior of filled rubbers accounting for the Mullins softening. In order to complete our study, the next chapter is addressing the cyclic softening that evolves with the number of cycles.

Chapter 6

Characterization and modeling of the cyclic softening

Most of this chapter has been published and can be found in reference:

- *Yannick Merckel, Julie Diani, Mathias Brieu, Daniel Berghezan, 2011. Experimental characterization and modelling of the cyclic softening of carbon-black filled rubbers, <u>Materials Science and Engineering A</u>, 528, 8651-8659.*

Several carbon-black filled styrene-butadiene rubbers were submitted to uniaxial tension cyclic tests at large strain to investigate filled rubbers cyclic softening. In order to study the effect of the material composition (amount of fillers and crosslink density) and of the stretch intensity, an original method for cyclic softening characterization is proposed. The softening is seen as an amplification of the stretch in the rubber gum, and a stretch amplification factor is then introduced as the softening parameter. The latter is evaluated for various materials and several levels of cyclic stretch intensity. Material softening is shown to increase with the loading intensity, the amount of carbon-black fillers and the decrease of the crosslink density. In terms of modeling, the introduced softening parameter provides access to the entire stress-stretch responses of the softened material for any cycle. Therefore, a model is written for the description and the prediction of the stress-stretch responses of filled rubbers during proportional cyclic tests.

Contents

6.1 Introduction

Rubber-like materials are used in various industrial applications. Elastomeric parts are particularly suitable for engineering applications designed to be submitted to cyclic loading conditions, like tires or vibration isolators. In order to increase their stiffness (Mullins and Tobin, 1965; Kohls and Beaucage, 2002) and delay crack propagation (Auer et al., 1957; Mars and Fatemi, 2004b; Mzabi, 2010), fillers are added to rubber compounds. Resulting from this adjunction, rubbers show an undesired stress softening known as the Mullins effect (Mullins, 1969) when first loaded. Considering proportional cyclic loadings, the Mullins softening may be linked to the maximum stretch applied to the material along the loading history. Once the latter softening occurred, the material softening evolves so slowly with respect to the number of cycles (Mars and Fatemi, 2004a; Brieu et al., 2010) that the changes of the mechanical behavior between two successive cycles may rapidly become unnoticeable. The stress softening occurring during the first cycle and attributed to the Mullins effect has been the focus of numerous contributions over the past decades (see Diani et al. (2009) for a review) while contributions on rubbers submitted to a large number of cycles usually aim at studying lifetime (see Mars and Fatemi (2002) for a review). Actually, only few papers have been drawing their attention to the evolving mechanical behavior of rubbers during cyclic loading conditions (Shen et al., 2001; Gentot et al., 2004; Mars and Fatemi, 2004a; Brieu et al., 2010), and yet, when used as structural parts submitted to cyclic loadings, one may be interested in rubber cumulative stress-softening induced by large number of cycles.

Moderate (few percent of strain) cyclic uniaxial tests on notched samples reveal that close to the crack, strains may reach several hundred percent (Mzabi, 2010; Mzabi et al., 2011). In this highly strained local region, the material undergoes a relatively low number of cycles (typically 1000) before the crack propagates through the highly strained region. Therefore, the study of rubber softening at large strain during a moderately large number of cycles, may be a key ingredient in the crack propagation understanding. In the current study, we will focus on the secondary stress-softening that begins after the first cycle when the major part of the Mullins softening had happened, at large strain and for a moderately large number of cycles. For this purpose, an original approach for rubber softening characterization is proposed based on the concept of stretch amplification due to material softening. Unlike the standard softening characterization method based on the observation of the maximum stress change (resp. strain) with respect to the number of applied cycles at constant maximum strain (resp. stress), this original approach introduces a softening parameter identified on the entire material stress-stretch responses. Such an approach provides an effective parameter for the comparison of the softening of materials of different compositions and for the prediction of the stress-stretch responses for any number of cycles. Hence, we will first compare the softening of styrene-butadiene rubbers according to the amount of fillers and the crosslink density, and second we will write constitutive equations for modeling the cyclic softening of filled rubbers.

In the following section, the material strategy and the experimental procedure are presented. Then in Section 6.3, we introduce the original softening parameter and highlight its interest. Section 6.4 shows the effect of mechanical and material parameters like the loading intensity, the amount of fillers and the crosslink density on the softening of SBR materials. In Section 6.5 we show how the introduced softening parameter provides a simple tool for modeling the softened stress-stretch responses of rubbers for large strain proportional loadings. Finally, concluding remarks close the chapter.

6.2 Materials and experiments

6.2.1 Materials

For this study, several filled SBRs were considered in order to investigate the relation between the material composition and the material cyclic softening. As in Chapter 3, the material strategy was to vary the filler volume fraction Φ and the crosslink density N_c. Therefore, we considered materials C2 to C6 for Φ changes and materials B4, C4, D4 and E4 for N_c changes. See Chapter 2 for detailed composition.

6.2.2 Experiments

Mechanical tests were conducted on the uniaxial tensile machine. All tests were run at a constant crosshead speed of 180 mm/min, which according to the sample dimensions is equivalent to an average strain rate close to 10^{-1} s^{-1}. For each test, a fresh sample was submitted to 1000 cycles from null force to a chosen maximum stretch measured locally. In order to illustrate the effect of the material compositions on their mechanical behavior, the material responses during the first cycle are shown in Figure 6.1. One notices the strong effect on the mechanical behavior of both the amount of fillers and the crosslink density.
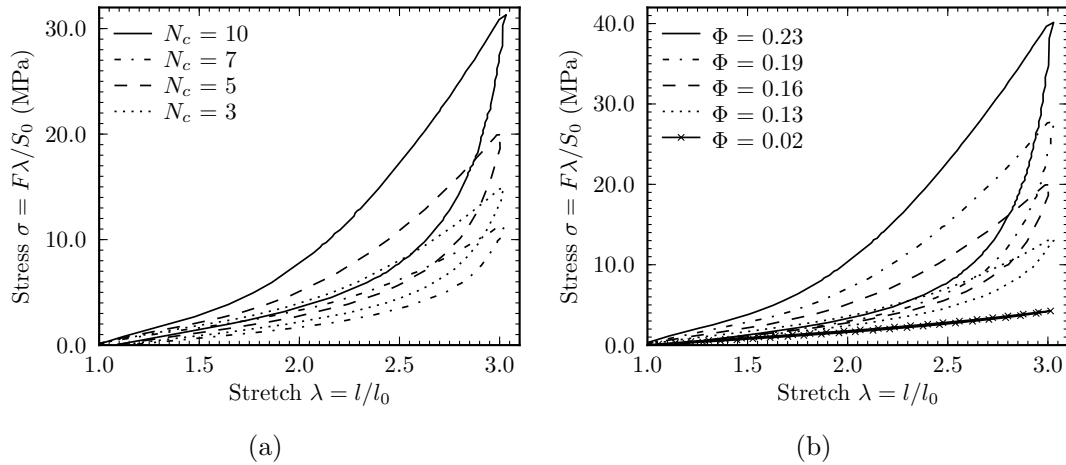
Figure 6.1: Material stress-stretch responses during the first cycle. (a) Materials with similar filler volume fraction $\Phi \approx 0.16$ (40 phr) and different crosslink densities. (b) Materials with similar crosslink densities $N_c \approx 7 \times 10^{-5}$ mol/cm^3 and different amounts of fillers.

6.2.3 Decoupling the Mullins effect from the cyclic softening

Performing a cyclic loading with increasing the maximum stretch at each cycle highlights the strong stress-softening occurring at the first cycle when reaching a level of stretch never undergone by the material (Figure 6.2a). This softening is attributed to the Mullins effect. Then, performing cyclic loadings by repeating cycles with set constant maximum stretch, provides evidences of a secondary cyclic softening that depends on the number of cycles (Figure 6.2b). In order to isolate the cyclic softening, we limit our study to the mechanical responses after the first cycle. Therefore, in the sequel, we designate the second loading-unloading as the cycle ($N = 1$).

The following section presents an original characterization of cyclic softening for proportional cyclic loadings.
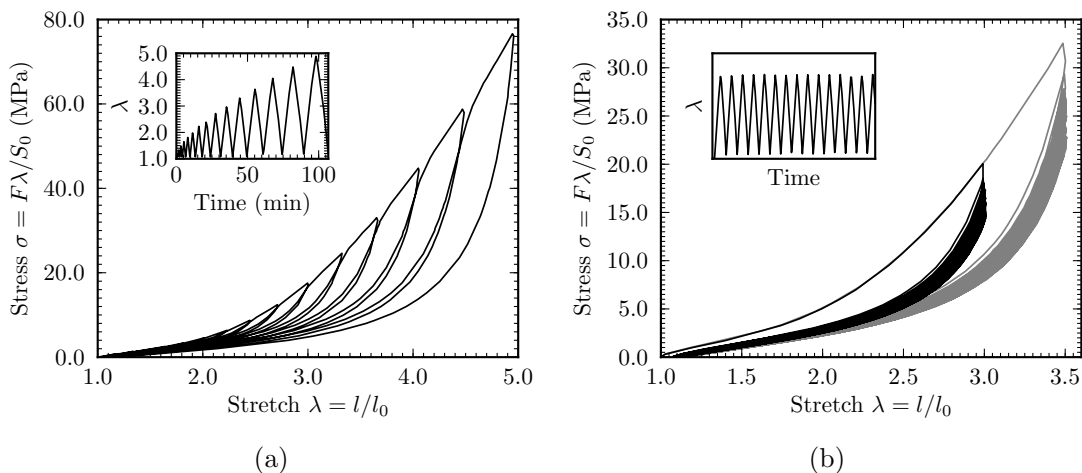
Figure 6.2: Material C4 stress-stretch responses to a uniaxial tensile cyclic tests. (a) With the maximum stretch increasing at each cycle. (b) With the maximum stretch remaining constant at each cycle.

6.3 Original characterization of cyclic softening

6.3.1 Softening standard parameter

Commonly used in continuum mechanics for metallic materials (Lemaitre and Chaboche, 1985), the concept of continuum damage variable (Kachanov, 1958), was extended to rubber-like materials by Simo (1987). In order to account for the cyclic stress-softening, Simo (1987) proposed a penalization of the initial elastic strain energy density $\mathcal{W}_0$ by a damage parameter D,

$$\mathcal{W} = (1 - D) \, \mathcal{W}_0 \tag{6.1}$$

Let us note that Eq. (6.1) leads to $\sigma = (1 - D) \, \sigma_0$. This kind of penalization has been used many times to model the stress-softening occurring during the first cycle (Simo, 1987; Govindjee and Simo, 1991; Miehe, 1995; Ogden and Roxburgh, 1999; Beatty and Krishnaswamy, 2000; Chagnon et al., 2004; Elías-Zúñiga, 2005; Guo and Sluys, 2006; Li et al., 2008) before being extended to cyclic softening modeling (Shen et al., 2001; Gentot et al., 2004),

$$\sigma^N = (1 - D_N) \, \sigma^{N=1} \tag{6.2}$$

where N is the number of cycles.

In order to characterize the stress-softening according to the number of cycles, a method based on the Eq. (6.2) is frequently used (Shen et al., 2001; Gentot et al., 2004; Mars and Fatemi, 2004b; Asare et al., 2009; Berrehili et al., 2010; Brieu et al., 2010; Yan et al., 2010; Saintier et al., 2011). The authors follow the decrease of the maximum stress $\sigma_{\max}$, or equivalently of the maximum force, measured at the peak stretch with respect to the number of cycles. The softening parameter may be defined as,

$$D_N = 1 - \frac{\sigma_{\max}^N}{\sigma_{\max}^{N=1}} \tag{6.3}$$

Unfortunately, one may notice that such a parameter characterizes the material softening by focusing on one point of the stress-stretch response only, which particular point concentrates most of the viscoelastic response of the material (Diani et al., 2006b). Moreover, knowing that the material response is nonlinear, using such a parameter will not provide access to an accurate

estimate of the entire softened stress-stretch responses. Therefore, the next section introduces an alternative softening parameter.

6.3.2 A new parameter for the estimate of the cyclic softening

As mentioned above, the material softening between two successive cycles may be characterized by the comparison of the stress at a given stretch, an alternative way is to consider the stretch for a given stress value. Thus a simple interpretation is that the softening is responsible for an amplification of the stretch at a given stress. Moreover, looking at the similar stress-stretch response shape curve for every cycle, we may expect the existence of a constant stretch amplification factor, α, for the entire stress-stretch response. Defining the stress-stretch response at cycle N for an applied maximum of stretch $\lambda_{\max}$, by $\mathcal{S}^N(\lambda, \sigma)$ the softening parameter $\alpha(N)$ is expressed by

$$\mathcal{S}^N(\lambda, \sigma) = \mathcal{S}^1(\alpha\lambda, \sigma) \tag{6.4}$$

with $\alpha \geq 1$. This parameter will prove to be valuable when every cyclic stress-stretch responses collapse on the first cycle stress-stretch response with $\alpha(N)$ being constant. Therefore, let us estimate α for material C4.

Figures 6.1 and 6.2 show that every material exhibits a significant hysteresis during the first cycle, but once the softening occurring during this cycle is evacuated, the loading and the unloading responses are fairly close and both responses may be used to characterize the material softening (Diani et al., 2006b). Figure 6.3a shows the loading responses corresponding to material C4 submitted to a cyclic loading with a maximum stretch $\lambda_{\max} = 3$. This Figure illustrates the ability of the loading responses to capture the cyclic softening, and in the following, we limit our study to the loading stress-stretch responses only. Let us notice that one could choose to use the unloading stress-stretch responses without changing the result general trends and conclusions that are presented in what follows.
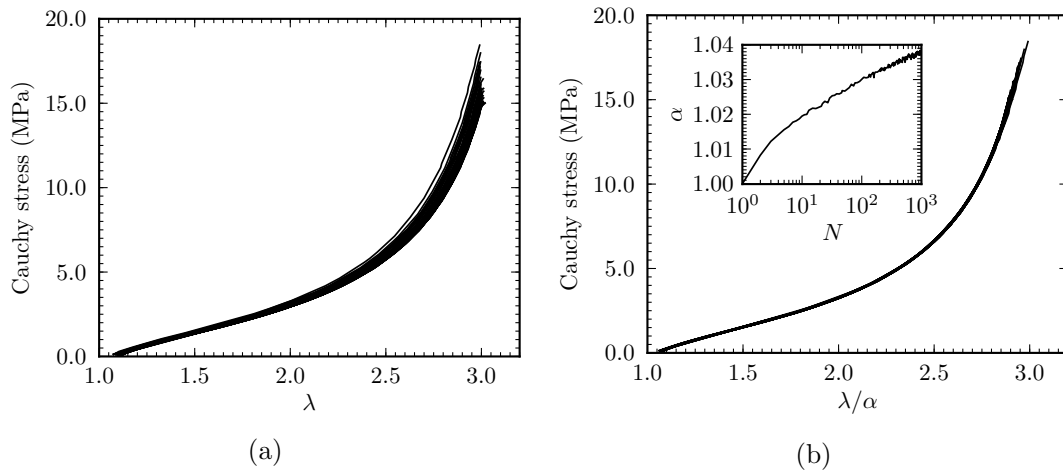
Figure 6.3: Material C4 softening parameter identification. (a) Loading stress-stretch responses for 1000 uniaxial tension cycles from zero stress up to $\lambda_{\max} = 3$. (b) Stress-stretch loading responses superimposition; in the inset graph, values of $\alpha(N)$ providing the displayed superimposition.

According to Eq. (6.4), the softening parameter $\alpha(N)$ relates the mechanical behavior at the cycle N to the mechanical behavior at the first cycle. For each loading curve, its best superimposition on the first loading curve ($N = 1$) provides a value for $\alpha(N)$, which is computed by least squares minimization. Material C4 loading curves superimposition is shown in Figure

6.3. The inset graph (Figure 6.3b) displays the values of α with the number of cycles. A good superimposition of every loading curve is obtained, which supports the concept of a stretch amplification factor as introduced in Eq. (6.4). Moreover due to the nonlinear behavior of our materials, the existence of the parameter α entails the non existence of a dual parameter defined by $\mathcal{S}^N(\lambda, \sigma) = \mathcal{S}^1(\lambda, \beta(N)\sigma)$, and sustains the interest of characterizing the softening on a change in stretch for a given stress rather than the opposite as defined in Eq. (6.2).

The major interest of the parameter α stands in its ability to provide information on the entire stress-stretch response of the material. Using the first loading response and the change of α according to the number of cycles, it is possible to estimate the stress-stretch response of a material at any cycle. Therefore, it is also possible to access to the changes of the material properties at the lower and the upper boundaries of the cyclic loading, which is equivalent to estimate the resulting residual stretch and the parameter D_N, respectively. The residual stretch is obtained straightforward as $\lambda_{\mathrm{res}}^N = \alpha\,\lambda_{\mathrm{res}}^{N=1}$ while D_N is estimated by calculating the ratio $\sigma(\alpha(N)\lambda_{\max})/\sigma(\lambda_{\max})$. Figure 6.4 shows a comparison of λ_{res} and D_N provided by the experimental data and estimated thanks to the values of α identified as Figure 6.3 shows. One may notice that both quantities λ_{res} and D_N are well estimated when considering the stress-stretch softening on the entire stress-stretch responses as α does. After all, the introduced parameter α seems to offer an attractive potential not only to study but also to model the cyclic softening of filled rubbers.
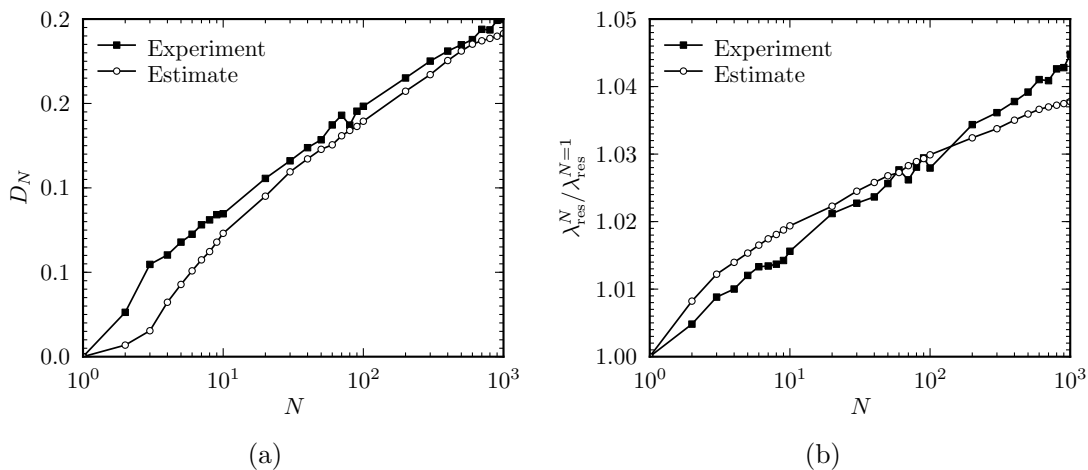
Figure 6.4: Comparison of the experimental data with the estimate given by using the stretch amplification concept for material C4 with a $\lambda_{\max} = 3$ cyclic loading amplitude. (a) Evolution of the parameter D_N. (b) Evolution of the residual stretch ratio $\lambda_{\mathrm{res}}^N/\lambda_{\mathrm{res}}^{N=1}$.

In the next section, we compute and examine the values of α for various maximum stretches and for the various materials presented in Figure 2.1.

6.4 Experimental results and analysis

6.4.1 Effect of material viscoelasticity

We ran tests at a constant moderately high crosshead speed of 180 mm/min as a compromise to reduce viscoelastic effects without taking too long to conduct the tests. In order to assess the impact of the viscoelasticity on our results, we have submitted material C4 to 100 cycles up to $\lambda_{\max} = 3$ at a slower constant crosshead speed of 18 mm/min. The parameter α was computed for both crosshead speed tests according to the procedure explained in the previous section and

results are presented in Figure 6.5. The stretch amplification factor shows identical values for both tests and therefore prove to be unaffected by the viscoelasticity at the moderate crosshead speed chosen in this study.
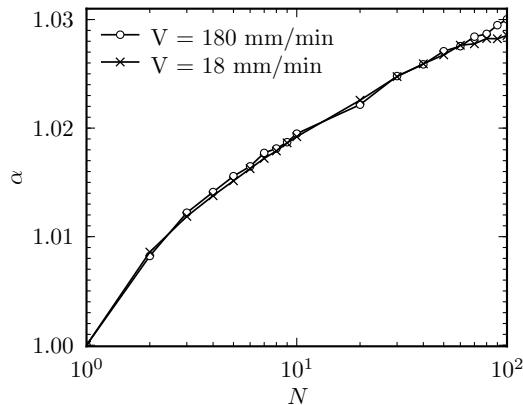
Figure 6.5: Effect of material C4 viscoelasticity on the cyclic softening during a 100-cycle test up to λ_{max}.

6.4.2 Effect of the cyclic stretch intensity on the cyclic softening

This section aims at investigating the impact of the chosen peak stretch on the cyclic softening. For this purpose, mechanical tests described in section 6.2.2 were conducted for several maximal stretch $\lambda_{\mathrm{max}} = \{2, 2.5, 3, 3.5, 4\}$ on material C4 ($\Phi \approx 0.16$ and $N_c \approx 7 \times 10^{-5}$ mol/cm^3). Figure 6.6a shows the change of the softening parameter α according to the number of cycles N for various λ_{max}. For the highest peak stretch, $\lambda_{\mathrm{max}} = 4$, the sample failure happened before the end of the test.

First, one may notice that the stress-softening increases slowly and the evolution rate decreases rapidly with the number of cycles. Similar observations about the cyclic softening have been reported in the literature (Gentot et al., 2004; Mars and Fatemi, 2004b; Brieu et al., 2010), although noticed on parameter D_N. Second, there is a noticeable impact of the maximum stretch on the softening evolution and an increase of the softening rate with the maximum stretch. This effect was also reported by Brieu et al. (2010). In the latter study, the authors showed that the cycle amplitude had no impact on the softening of non crystallizing rubbers and that the key parameter was the maximum stretch. We challenged this result on material C4, and we observed similar results, α is not significantly affected by the cycle amplitude but depends on the λ_{max} value.

Figure 6.6b is another illustration of the evolution of α with respect to the number of cycles N and to the maximum stretch. Interestingly, one may notice that the rate $\partial \alpha / \partial \lambda_{\mathrm{max}}$ is relatively independent of N. Let us mention that similar results were obtained on materials C5 ($\Phi \approx 0.19$ and N_c identical to C4) and D4 (Φ identical to C4 and $N_c \approx 5 \times 10^{-5}$mol/cm^3).

6.4.3 Effect of the material compositions on the cyclic softening

In order to study the effect of the crosslink density N_c and of the fillers volume fraction Φ, cyclic tests were performed for each material at the same maximum stretch, $\lambda_{\mathrm{max}} = 3$. First, we compared the evolution of the softening parameters α obtained for materials containing the same amount of fillers, 40 phr ($\Phi \approx 0.16$) and different crosslink densities from 3.65 to 10.55×10^{-5} mol/cm^3 (see Tables 2.1 and 2.2). Results are shown in Figure 6.7a. Material B4 (highest N_c) failure occurred before the end of the test.
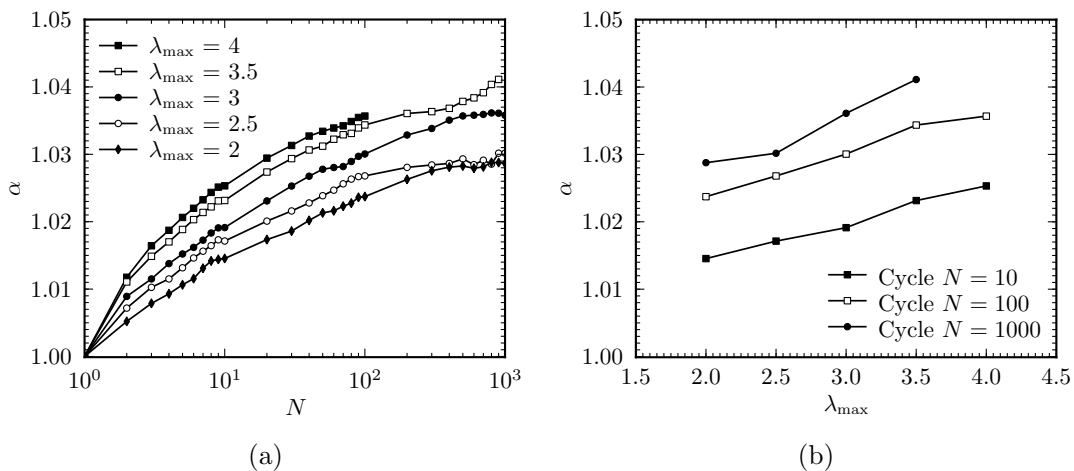
Figure 6.6: Effect of the maximum stretch $\lambda_{\max}$ on the cyclic softening for the material C4. (a) Evolution of the cyclic softening parameter α with respect to the number of cycles. (b) Evolution of the cyclic softening parameter α with respect to the maximum stretch.

The parameter α appears to increase with the crosslink density decrease with reaching a plateau for high crosslink densities. It seems that the material ability to soften delays its catastrophic failure which is consistent with previous results (Auer et al., 1957; Beatty, 1964; Zhao and Ghebremeskel, 2001; Mars and Fatemi, 2004b). A physical interpretation of the softening that may be proposed is a re-organization of the chain network, which is certainly easier when chains are long (low N_c) due to the enhancement of the chain mobility. Such an interpretation would match with our experimental observations
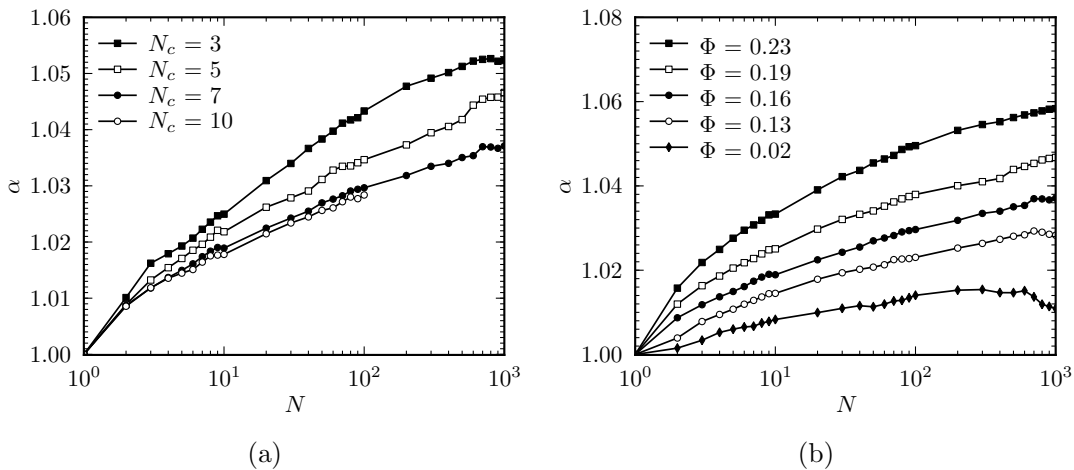
Figure 6.7: Effects of the material composition on the cyclic softening parameter α. (a) Effect of the crosslink density for materials with various N_c and a similar filler volume fraction $\Phi \approx 0.166$ (40 phr). (b) Effect of the filler volume fraction for material with a similar crosslink density $N_c \approx 7 \times 10^{-5}$ mol/cm^3 and different amounts of carbon-black.

We confronted materials with similar crosslink densities, approximately 7×10^{-5} mol/cm^3, and various filler volume fractions from 2 to 23%. One may notice the strong impact of the amount of fillers on the rate of cyclic softening in Figure 6.7b.

Results presented in Figure 6.7 are original and give access for the first time to the effect of some of the parameters characterizing the material physical properties on the mechanical cyclic softening, the softening increasing with the increase of the amount of fillers. Actually, the presence of fillers introduces strain field heterogeneities and creates highly stretched zones. Damage develops more easily in these regions, therefore damage and damage rate should raise in highly filled rubbers. In the present contribution, only the filler fraction and the crosslink density varied. The cyclic softening of filled rubbers is probably also dependent of other material parameters, like the nature of gum, the nature, geometry and distribution of fillers... and future work remains to complete the microstructure impact on the cyclic softening.

6.5 Cyclic softening modeling

This section aims at proving the relevance of the parameter α when modeling the stress-stretch responses of filled rubbers submitted to proportional cyclic loadings at a constant maximum stretch. For this purpose, we are considering the stress-stretch responses of virgin samples submitted to 1000 cycles from zero stress up to $\lambda_{\max}$ stretch. As previously, we will neglect the filled rubbers viscoelasticity and assume that the loading stress-stretch responses are representative of the material responses during the cyclic loadings. The material responses after the first cycle are affected by the maximum stretch intensity due to the Mullins softening. modeling the Mullins softening is out of the scope of this chapter and therefore we will assume that the maximum stretch dependent 2nd-cycle ($N = 1$) stress-stretch responses are known. Then, the Nth-cycle stress-stretch response should be reproduced thanks to parameter α for any value of N.

6.5.1 General constitutive equations

Filled rubber loading responses are typically reproducible with a hyperelasticity framework within the residual stretch correction. Filled rubbers may reasonably assumed incompressible in uniaxial tension and hyperelastic constitutive equations writes as,

$$\boldsymbol{\sigma} = \frac{\partial \mathcal{W}(\boldsymbol{F})}{\partial \boldsymbol{F}} \boldsymbol{F}^t - p\boldsymbol{I} \tag{6.5}$$

where $\boldsymbol{\sigma}$ is the Cauchy stress, $\mathcal{W}$ the strain energy density, $\boldsymbol{F}$ the deformation gradient, and p an arbitrary hydrostatic pressure. The material stress-stretch nonlinearity demands the use of a phenomenological strain energy density for an accurate fit. A strain energy density dependent of the right Cauchy green tensor ($\boldsymbol{C} = \boldsymbol{F}^t \boldsymbol{F}$) first invariant I_1 and introduced by Lambert-Diani and Rey (1999) is used for its ability to provide very good fits for a wide class of filled rubbers,

$$\frac{\partial \mathcal{W}(I_1)}{\partial I_1} = \exp\left(\sum_{i=0}^{n} \gamma_i \left(I_1 - 3\right)^i\right) \tag{6.6}$$

In the case of uniaxial tension, Eqs. (6.5) and (6.6) combine into,

$$\sigma = 2 \, \exp\left(\sum_{i=0}^{n} \gamma_i \left(\lambda^2 + \frac{2}{\lambda} - 3\right)^i\right) \left(\lambda^2 - \frac{1}{\lambda}\right) \tag{6.7}$$

with λ, the effective stretch which is defined by correcting the measured stretch by the residual set (stretch at zero stress), $\lambda = \lambda^{N=1}/\lambda_{\text{res}}^{N=1}$.

Once the material has undergone an initial loading cycle up to a given $\lambda_{\max}$, the first softened response ($N = 1$) is approximated by Eq. (6.7). Then the Nth-cycle stress-stretch response is estimated using Eq. (6.4) where parameter α still requires a mathematical expression. In the next section such an expression is proposed with some interesting parameter analysis.

6.5.2 Softening parameter equation

The analysis of Figures 6.6 and 6.7 shows that the parameter α dependence to the number of cycles N may be well reproduced by a simple mathematical expression of the form,

$$\alpha = 1 + a \left(\ln N \right)^b \tag{6.8}$$

with parameters a and b depending on the material physics (type of gum, type and amount of fillers, microstructure...) and on the loading intensity.

In order to better understand the contribution of each parameter a and b in the representation of α, Figure 6.8 presents estimates of α provided by Eq. (6.8) obtained for an identical parameter b ($b = 0.57$) and a material-dependent parameter a. Such a procedure supplies relatively good fits, that cannot be obtained by setting a constant and by varying b according to the material. In the present study, all materials were made of the same type of gum, the same type of fillers and using the same process, which certainly favor a weak dependence of α to the parameter b, but it cannot be expected that b remains constant for all filled rubbers. Setting b to a constant value, the changes of the cyclic softening are captured by a only. Values of the latter parameter are displayed in Figure 6.9 with respect to the crosslink density, the amount of fillers and the stretch intensity.
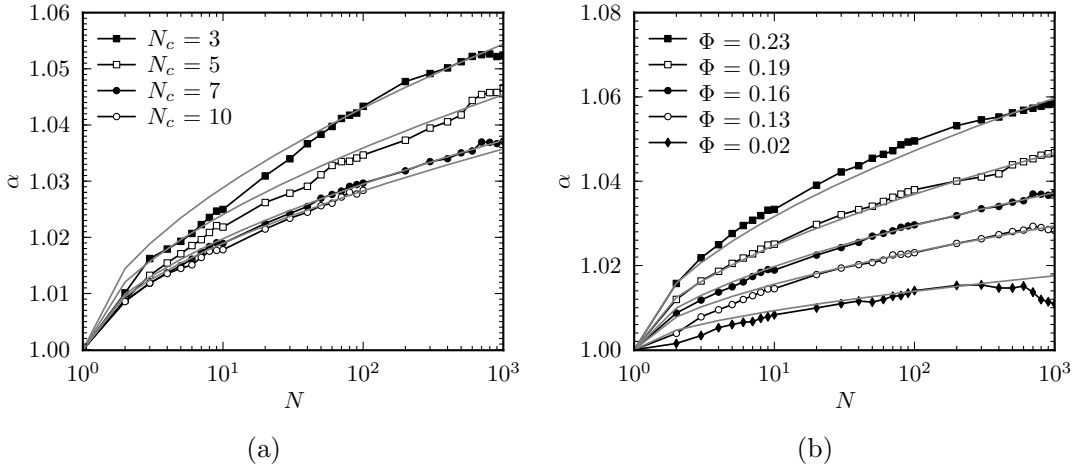
Figure 6.8: Fit of the cyclic softening parameter α shown in Figure 6.7 by the mathematical relation Eq. (6.8) with $b = 0.57$ and material-dependent values of a.

The parameter a trends are representative of the softening trends that were discussed earlier in section 6.4, when a increases the softening (or equivalently the rate of α) increases. One may notice in Figure 6.9 that a varies with the stretch intensity according to a similar trend for the tested materials C4 ($\Phi = 0.16$, $N_c = 7.38 \times 10^{-5}$ mol/cm^3), C5 ($\Phi = 0.19$, $N_c = 8.26 \times 10^{-5}$ mol/cm^3) and D4 ($\Phi = 0.16$, $N_c = 5.42 \times 10^{-5}$ mol/cm^3). Thus, it was shown here that in a modeling effort, b could be set to a constant value for the all set of materials and for any maximum stretch $\lambda_{\max}$.

In order to propose not only descriptive modeling but also predictive modeling, parameters a and b were computed for each materials on a reduced set of data obtained on a limited number of cycles. Then, the values of α obtained with Eq. (6.8) and the fitting parameters were confronted to the experimental data on 1000 cycles. When considering the first 50 cycles only, one obtains a very good estimate of α for the entire 1000-cycle test as it is shown in Figure 6.10. This reveals the strong potential of monitoring cyclic softening by the combination of Eqs. (6.4) and (6.8),
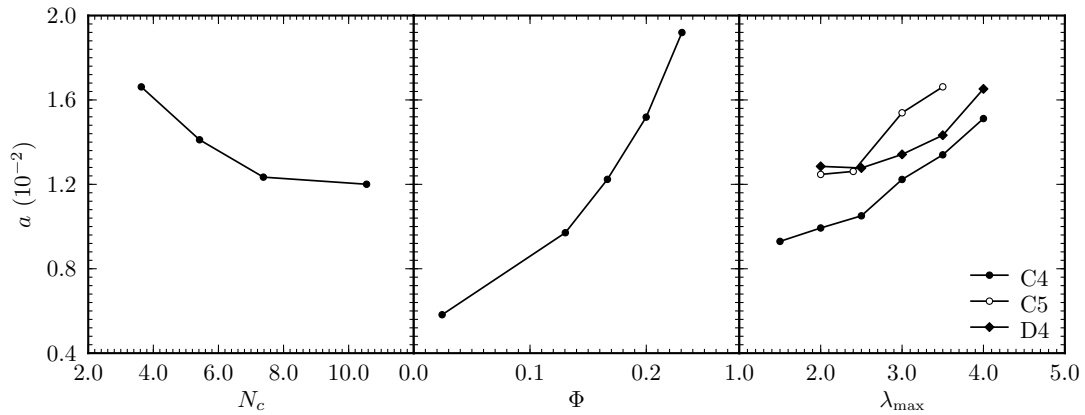
Figure 6.9: Effects on the cyclic softening of the crosslink density (left), the filler volume fraction (center) and the peak stretch value of the cycles (right) as pictured by the parameter a providing the fits presented in Figure 6.8.

such equations providing tools for predicting the material softening for a large number of cycles (1000) while testing it for a relatively low number of cycles (50 here).

As mentioned in the introduction, our tests are representative of the high stretch during a moderate number of cycles undergone by filled rubbers near a crack tip during the crack propagation. Actually, at high stretches it is more likely that samples will break after a moderate number of cycles, and some of our samples fractured before completing a thousand cycles (see material C4 in Figure 6.6 or material B4 in Figure 6.7). Nonetheless, the modeling presented here could probably applied over a larger number of cycles at moderate stretches. Additional fatigue tests, difficult to run in uniaxial tension due to the test duration required by such a loading condition, would be interesting to carry in order to prove it.
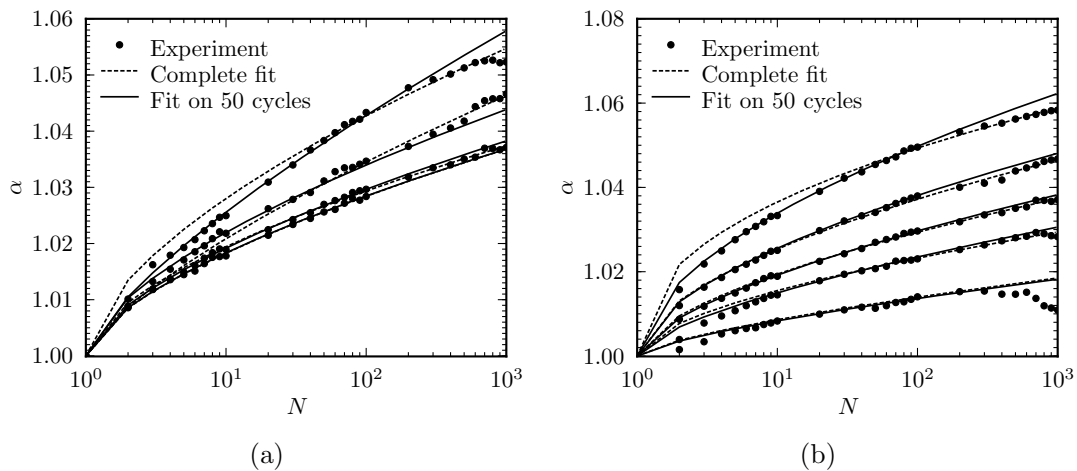
Figure 6.10: Fit of the cyclic softening parameter α shown in Figure 6.7 by the mathematical relation Eq. (6.8) using free parameters a and b. Fit obtained using the first 50 cycles (solid line) and fit obtained using all the cycles (dashed line).

In the next section the modeling presented here and defined by Eqs. (6.7), (6.4), and (6.8) is confronted to the cyclic stress-stretch representation.

6.5.3 Comparison between the model and the experimental data

For each maximum stretch, the parameters γ_i from Eq. (6.7) are computed on the $N = 1$ loading responses by a least squares minimization. Values of these parameters appear in table 6.1 and the comparison of the model with the experimental data is shown in Figure 6.11. For every $\lambda_{\max}$, the entire stress-stretch responses (from $\lambda = 1.1$ to $\lambda_{\max}$) are estimated within an average error of 5%, which is satisfactory for nonlinear large strain fits.

$\lambda_{\max}$	γ_0	γ_1	γ_2	$\lambda_{\mathrm{res}}^{N=1}$
2.0	$-2.24 \ .10^{-1}$	$-4.49 \ .10^{-1}$	$2.66 \ .10^{-1}$	1.052
2.5	$-3.20 \ .10^{-1}$	$-2.47 \ .10^{-1}$	$1.04 \ .10^{-1}$	1.071
3.0	$-4.22 \ .10^{-1}$	$-1.58 \ .10^{-1}$	$5.35 \ .10^{-2}$	1.085
3.5	$-4.73 \ .10^{-1}$	$-1.20 \ .10^{-1}$	$3.22 \ .10^{-2}$	1.109

Table 6.1: Model parameters for the fit of the maximum stretch dependent stress-stretch responses of material C4 after one cycle at $\lambda_{\max}$.
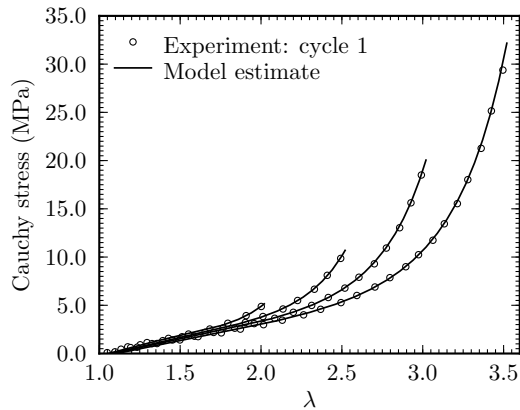
Figure 6.11: Material C4 first maximum stretch dependent stress-stretch response at the $N = 1$ cycle and model fit using parameters in Table 6.1.

In order to estimate the Nth-cycle stress-stretch responses, parameters a and b from Eq. (6.8), could be calculated for each cyclic tests. Nonetheless, we noticed in section 6.5.2 that b could be chosen constant for every test ($b = 0.57$), then values of a may be optimized for each $\lambda_{\max}$. The limit of such a procedure stands in the necessity to test the material at every stretch level before estimating its softening. Another interesting procedure is to test the material at a mean maximum stretch, $\lambda_{\max} = 3$ for instance, and estimate a and b on this test only. We then expect to predict reasonably well the stress-stretch responses for any cycle and any $\lambda_{\max}$ knowing the stress-stretch response at cycle $N = 1$ for any $\lambda_{\max}$. We have applied this procedure to C4, the mean squares minimization resulting parameter is $a = 0.0125$. Then, estimates of the Nth cycle stress-stretch responses for $\lambda_{\max} \in \{2, 2.5, 3, 3.5\}$ were computed with parameters from table 6.1, and $a = 0.0125$ and $b = 0.57$. The mean error between the experimental data and the model estimates ranged between 3% and 6%, which is similar to the error generated by the hyperelasticity fit of cycle 1. A very satisfying comparison between the model and the experimental data stress-stretch responses for the 10th and the 1000th cycle is shown in Figure 6.12. Similar results were obtained for materials C5 and D4 which were tested at various $\lambda_{\max}$ too.

Finally, for proportional loadings, we propose to account for filled rubbers cyclic softening by introducing a stretch amplification factor Eq. (6.4) revealing the material softening occurring
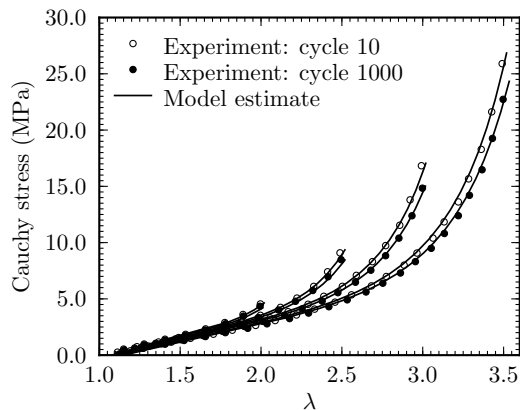
Figure 6.12: Material C4 10th-cycle and 1000th-cycle stress-stretch responses for cyclic loadings at various maximum stretch and model estimates of the stress-stretch responses.

after an initial pre-loading cycle. This stretch amplification factor may be formulated by the simple mathematical expression Eq. (6.8) and therefore may be characterized by two parameters a and b. These parameters can be evaluated on a limited number of cycles and then successfully extended to a larger number of cycles (Figure 6.10). In this study, we were able to set constant the parameter b for all materials and all maximum stretch level. Then, parameter a was shown to vary with the material composition and the loading conditions (Figure 6.9). Nonetheless, when considering a single value of a for a given material composition, defined by the mean of the best fit values obtained on the change of α measured at various stretch intensities, we showed a remarkable good prediction of entire stress-stretch responses measured after a large number of cycles (Figure 6.12) and for a large range of stretch intensities.

6.6   Conclusion

This chapter aimed at studying the softening of carbon-black filled styrene butadiene rubbers during cyclic uniaxial tension loadings at large strain. We focused our interest on the material mechanical responses once the first cycle already applied. In order to estimate how these responses evolved with the loadings, we introduced an original parameter characterizing the material softening with respect to the number of cycles applied. Unlike classic parameters found in the literature, the introduced parameter is estimated on the entire stress-stretch responses of the softened material. It is defined as a stretch amplification factor, evidencing the larger deformability of softened materials. This parameter was shown to provide a useful tool for a quantitative comparison of the softening of different materials or of the same material at various maximum cyclic stretches. The experimental results show that filled rubbers cyclic softening increases when adding fillers, decreasing the crosslink density and increasing the loading stretch intensity. In terms of modeling, the introduced parameter evolution with respect to the number of cycles is easily formalized by a 2-parameter ln function. Combined with a classic hyperelastic strain energy function, it was shown that testing the material during a limited number of cycles could be sufficient to predict its responses for a quite larger number of cycles.

Conclusion and future works

Summary

Chapter 1 reports and analyzes a literature review on the mechanical behavior of rubber-like material submitted to cyclic loading conditions. Significant modeling issues are noticed and the experimental strategy is established to assess all necessary experimental data. Testing devices and general experimental techniques, mostly developed within the thesis duration are also described. Chapter 2 introduces the studied materials. Various compounds were considered with changes in the filler amount and the crosslink density. Volume changes are investigated under uniaxial stretching. Results show that material incompressibility assumption seems unrealistic upon monotonous stretching but remains consistent when considering cyclic loading conditions. Then, material mechanical behaviors were characterized using uniaxial tension tests. Under monotonic loading conditions, the material stiffness increases with the increase of filler amount and of crosslink density. The stretch to failure increases with the decrease of the crosslink density but exhibits an optimum according to the amount of fillers. Basic features under cyclic loading conditions are illustrated and discussed in order to introduce the subsequent chapters. Chapter 3 proposes a method to characterize and quantify the Mullins softening in order to compare its dependence to the material composition. For this purpose, the strain amplification factor concept is revisited. A decomposition of the factor into a softening parameter and a reinforcing parameter is proposed. Samples were submitted to cyclic uniaxial tests and the softening parameter is computed for each material. Results highlight that the crosslink density has a negligible impact on the Mullins softening, and that increasing the filler amount increases the Mullins softening. Chapter 4 defines a Mullins softening activation criterion for filled rubbers submitted to general loading conditions. The criterion is grounded on an original analysis of unconventional experimental data. The experimental procedure aims at applying proportional and non-proportional loadings paths including cyclic uniaxial and biaxial tension tests. A softening evolution parameter is proposed in order to recognize the Mullins softening activation from a cyclic stress-stretch response with an increase of the maximum stretch. Results provide solid evidences for the definition of a Mullins softening activation criterion as the three-dimensional surface of the maximum directional stretches undergone by the material along its loading history. Chapter 5 proposes a constitutive model for the mechanical behavior of filled rubbers capturing the Mullins softening. The constitutive equations are grounded on a thorough analysis of original experimental data. The model is based on a directional approach. The Mullins softening is accounted for by the strain amplification concept and is activated by a directional criterion. The framework is developed in order to avoid any *a priori* assumption of the mathematical forms of the elementary strain energy density and of the Mullins softening evolution rule. An original identification procedure is proposed in order to build both functions from a cyclic tensile stress-stretch response. An accurate fit of the experimental data provided by a cyclic proportional uniaxial tensile test illustrates the model ability to capture the material stress-softening. Once identified on a proportional cyclic test, the model is shown to successfully and accurately predict uniaxial stress-stretch responses of non-proportional uniaxially or biaxially pre-stretched

samples. Chapter 6 studies the cyclic softening that evolves with the number of cycles. A parameter is introduced in order to characterize and quantify the material softening with respect to the number of cycles. It is defined as a stretch amplification factor. Proportional cyclic uniaxial tensile tests are considered. The results show that the cyclic softening increases when adding fillers, decreasing the crosslink density and increasing the loading stretch intensity. In terms of modeling, the introduced parameter is extended to accurately predict the stress-stretch responses of the softened material for any number of cycles.

Discussion

Many <u>experimental developments</u> were carried out during the thesis in order to apply the experimental strategy. The most significant additions are introduced in Chapter 1.

- A video extensometer system including an automatically controlled vertical motorized adjustable support has been entirely redesigned and rebuilt. The objectives were to improve the measurement of the strains and to increase the existing equipment versality and robustness in order to allow unconventional experiments. Along the thesis, this system was used for non-proportional loading paths, in order to study the material anisotropy evolution, to measure the material volume changes,...

- A planar biaxial testing device has been entirely engineered. This device was built with basic and standard technological components. Therefore, it was a value-priced efficient solution for applying complex loading conditions. A significant advantage of this device is the control in real time of the stretching by measurements of the sample local stretches. Such a control ensures accurate loading paths (differences between the local stretches and global strains estimated from the grip motions are large).

Both experimental solutions are currently in a finalization process in order to be easily transferred to other laboratories or research teams. A first transfer of the video extensometer system including the motorized adjustable support has already and successfully been performed to the laboratory PIMM of the ENSAM Paris.

Some original <u>experimental characterization methods</u> have been developed in order to fulfill the thesis objectives. These experimental methods may be extended for other analysis.

- The characterizations of the Mullins and the cyclic softening evolutions under proportional loading conditions proposed in Chapters 3 and 6, were used to quantify the effect of the stretching intensity, the fillers amount and the crosslink density. They may be used for studying other microstructure parameters such as the type of gum, the type and the nature of fillers, the effect of other additives,... They may also be extended for studying other phenomena such as the crystallization, the dependencies to thermal history, the oxidation, the effect of environmental agents,...

- The method defined in order to recognize the Mullins softening activation in Chapter 4 was used to study the effect of a non-proportional pre-loading. It may be used for studying other effects or phenomena, for instance the Mullins softening recovery. Moreover, the method may be used to assess the maximal loading history within a filled rubber structure undergoing loading conditions that cannot be observed *in situ*. By studying material sampled in various directions, the three-dimensional post-loading Mullins softening criterion can be computed. Such an experimental characterization may be useful in order to verify the results of complex structural analysis provided by finite element computation.

In term of <u>mechanical behavior modeling</u>, some developments have been proposed for the Mullins softening and for the cyclic softening in Chapters 5 and 6, respectively. Put together, they provide a model able to capture the material hyperelasticity, the stress-softening, the residual stretch and the induced anisotropy. Dependencies to the type of loadings, the loading intensity and to the number of cycles are accounted for. The model ability to accurately predict the mechanical behavior of non-proportional uniaxially or biaxially pre-stretched materials has been shown. Therefore, the main thesis objective, which is to provide a constitutive modeling able to predict the mechanical behavior of the material in the vicinity of a crack tip, is fulfilled.

Future works

In the previous section, some possible directions for future works have been discussed. They are based on a direct application of "tools" developed during the thesis. These tools were used in order to reach the thesis objective, but they may easily be extended for other purposes. This section focus now on future works regarding the modeling of the material behavior.

The constitutive model proposed in this thesis is grounded on a thorough analysis of original experimental data. However, the model is still phenomenological and the equations do not have any physical meaning. The framework is developed in order to avoid any *a priori* assumption of the mathematical forms of the elementary strain energy density, f, and of the Mullins softening evolution rule. Both functions are built from the experimental data according to the identification procedure proposed in Chapter 5. Let us note that the Mullins softening evolution rule is in perfect agreement with the experimental results shown in Chapter 3.

A possible opportunity for future works is given by the identification of f. The evolution of f is unaffected by the damage or by the material anisotropy. It captures the mechanical behavior of the virgin material along a single direction and Figure 5.12 illustrates its dependence to the amount of fillers. Some complementary investigations aiming at developing physically-based equations for f would be interesting. Moreover, once a satisfactory equation is built, the Mullins softening might be accounted for using a physical interpretation. Such a formalism will allow to relate the material behavior to its microstructure.

The large amount of experimental works performed during the thesis puts in light that the cyclic softening and the residual stretch can be characterized by a stretch amplification and accounted for in a tridimensional model by a decomposition of the deformation gradient tensor (*i.e.* $\boldsymbol{F} = \boldsymbol{F}_e \boldsymbol{F}_p$, see Chapter 5). Hence, the cyclic softening and the residual stretch are interpreted as a material flow. It worth notices that for filled rubber materials, the viscoelasticity is commonly accounted for with such a decomposition. Moreover, experimental evidences prove that the $\boldsymbol{F}_p$ flow is strongly dependent on viscoelasticity. Therefore, it seems interesting to account for both phenomena in a similar manner, even if various criteria and driving parameters may be expected.

The model develops during the thesis focus on the equilibrium responses only. Its efficiency has been demonstrated. It may now become essential to extend the constitutive equations in order to account for the material viscoelasticity.

There is still a major issue that needs to be addressed. The evolution of $\boldsymbol{F}_p$ (including both the residual stretch and the cyclic softening) is quite well established under proportional uniaxial tension loadings. However, the experimental evidences addressing the evolution of $\boldsymbol{F}_p$ under non-proportional loading conditions are very limited (if any).

A future works, with relatively long term perspectives, is to assess the evolutions of $\boldsymbol{F}_p$ valid for general loading conditions. For this purpose, significant experimental and numerical

developments are necessary. It is worth noticing that the procedure proposed for the Mullins softening criterion would not work for such a purpose due to the strong viscoelasticity dependence of $\boldsymbol{F}_p$. An original experimental procedure needs to be defined. This procedure should use the constitutive modeling introduced in Chapter 5 as a starting point. Then, evolution rules for $\boldsymbol{F}_p$ should be built by comparing the differences between the model predictions and the experimental data. However, modeling the mechanical behavior of a sample submitted to successive non-proportional loading conditions is not straightforward. During the experiments, the stresses and the stretches undergone by the samples are not homogeneous, since a structural problem exists. For such a problem, the constitutive equations should be implemented into a finite element code. The sample and the experimental boundary conditions should be modeled and implemented in order to perform some computations. The experimental displacement fields of the sample stress free face could be measured using digital image correlation. The experimental measured displacement fields and the numerical computed displacement fields should be compared. Finally, the dialogue between the experimental data and the model should be established. Once the experimental and numerical developments are completed, building relevant constitutive equations for $\boldsymbol{F}_p$ remains an interesting challenge.

Résumé étendu en français

Chapitre 1 : Revue de la littérature et méthodes expérimentales

Ce premier chapitre a pour objectif de fournir les bases qui seront utiles dans l'ensemble des chapitres suivants. Dans un premier temps, il présente une revue de la littérature sur le comportement mécanique des élastomères chargés lorsqu'ils sont soumis à des conditions de chargement cycliques. Une analyse de cette revue permet de mettre en évidence des lacunes dans les modèles de comportement actuellement proposés ainsi qu'un manque de données expérimentales. Cela permet alors de définir une stratégie expérimentale. La seconde partie de ce chapitre est consacrée à la présentation des méthodes expérimentales associées qui ont été développées.

Du fait de longues chaînes macromoléculaires réparties aléatoirement et réticulées, les élastomères possèdent des propriétés élastiques remarquables. Dans le but d'améliorer certaines propriétés mécaniques telles que la raideur ou la résistance à la propagation de fissures, des charges sont ajoutées à la gomme élastomère. Cependant, l'ajout de ces charges induit un inconvénient majeur, un adoucissement important de la contrainte suite au premier cycle de chargement. Cet adoucissement est communément nommé adoucissement Mullins du fait de l'important travail conduit sur le sujet par Mullins (1947, 1949, 1950, 1969). Les principales caractéristiques de l'adoucissement Mullins sont mises en évidence sur la Figure 1.2. Suite à une première charge, il se produit un adoucissement important de la contrainte. Quand des cycles sont répétés, avec une amplitude maximale inférieure à la déformation maximale vue au cours de l'histoire du chargement, alors l'évolution de l'adoucissement est très lente. Par contre, l'adoucissement évolue de façon importante si cette déformation maximale est franchie. Avec l'adoucissement, il se produit également une évolution de la déformation résiduelle à contrainte nulle. De plus, en appliquant des chargements non proportionnels, il apparaît que l'adoucissement Mullins induit une anisotropie du comportement mécanique. A ce jour, il n'y a toujours pas d'accord général sur la compréhension des phénomènes physiques conduisant à l'apparition de l'adoucissement Mullins, ni sur sa caractérisation, ni sur sa modélisation (Diani et al., 2009).

Quand des cycles sont répétés avec la même déformation maximale, il se produit une évolution de l'adoucissement avec le nombre de cycles. Cet adoucissement secondaire, mis en évidence sur la Figure 1.3, est désigné sous le terme "adoucissement cyclique" durant l'ensemble de cette thèse. L'évolution de l'adoucissement cyclique est très lente et elle devient rapidement imperceptible entre deux cycles successifs. Cependant, son effet ne peut pas être négligé si un grand nombre de cycles est considéré. Actuellement les contributions sur le problème des élastomères soumis à un grand nombre de cycles ont principalement pour objectif l'étude de la durée de vie ou de la propagation de fissures. Très peu s'intéressent à l'évolution du comportement mécanique.

La modélisation du comportement cyclique des élastomères chargés reste un problème majeur. Une revue de la littérature sur le sujet met en évidence que les lois de comportement actuellement proposées comportent des lacunes importantes. De plus, il apparaît que ces la-

cunes sont directement associées à un manque de données expérimentales rapportées. Afin de pallier ce manque de données expérimentales, une stratégie expérimentale est définie. Des moyens expérimentaux ainsi que des protocoles d'essais ont été développés dans ce but. Ils sont présentés et détaillés Section 1.6.

Chapitre 2 : Matériaux

Plusieurs élastomères chargés ont été utilisés durant cette thèse. Ils sont présentés et caractérisés dans ce chapitre. Tout d'abord, l'hypothèse d'incompressibilité est investiguée par des chargements de traction uniaxiale puis sa validité est discutée. Ensuite, l'effet de la microstructure sur les réponses en traction monotone est étudié. Finalement, des chargements cycliques sont appliqués afin d'illustrer des observations basiques de l'adoucissement Mullins et de l'adoucissement cyclique. Une partie des travaux présentés dans ce chapitre a été publiée et peut être trouvée dans la référence Merckel et al. (2011a).

Lors du Chapitre 1, une stratégie expérimentale a été définie. Ce second chapitre présente la composante matériau de celle-ci, c'est-à-dire le plan matériau.

Le comportement mécanique d'un élastomère chargé dépend très fortement de sa composition. Il en va de même pour l'évolution de l'adoucissement qu'il développe sous chargement cyclique. Dans le but d'étudier cette dépendance, plusieurs matériaux sont considérés et la stratégie utilisée a consisté à faire varier la fraction de charge et la densité pontale de la gomme. Comme l'anisotropie du comportement mécanique est un aspect majeur qui sera abordé dans la suite de cette thèse, l'anisotropie induite par le procédé de fabrication est étudiée par des essais de traction uniaxiale. Il apparaît que les matériaux présentent une anisotropie transverse. Une fois cette anisotropie mise en évidence, une caractérisation basique des matériaux est réalisée en utilisant des essais de traction uniaxiale.

Le premier objectif expérimental de ce chapitre est de valider, ou d'invalider, l'hypothèse d'incompressibilité qui est communément admise pour les matériaux élastomères. Cependant, plusieurs contributions rapportent des variations de volume importantes se produisant lors de chargements de traction (Le Cam, 2010). Des essais sont réalisés afin d'étudier la variation de volume se produisant pour les matériaux choisis et les conditions de chargement utilisées dans la suite. Les résultats mettent en évidence des variations de volumes importantes lors de chargements monotones. Dans ce cas, l'hypothèse d'incompressibilité est très discutable. Cependant, les résultats montrent également que cette hypothèse reste valide si des chargements cycliques sont considérés. Donc, pour la suite, la contrainte de Cauchy résultante d'un chargement de traction uniaxiale sera calculée en faisant l'hypothèse d'incompressibilité. Les modélisations du comportement et de l'endommagement des élastomères seront faites en utilisant une formulation incompressible.

Le second objectif expérimental est d'étudier les dépendances entre la réponse mécanique contrainte-élongation et la composition du matériau. Pour cela, des essais de traction uniaxiale monotone jusqu'à rupture sont réalisés. Les résultats mettent en évidence une forte dépendance de la raideur vis-à-vis de la densité pontale et du taux de charge, celle-ci augmentant avec le taux de charge et avec la densité pontale. Au contraire, il apparaît que l'élongation à rupture augmente fortement quand la densité pontale diminue alors qu'elle présente une valeur optimale en fonction du taux de charge.

Finalement, le troisième objectif expérimental est d'illustrer quelques caractéristiques basiques de l'adoucissement se produisant lorsqu'un matériau est soumis à un chargement cyclique. Les dépendances de l'adoucissement Mullins et de l'adoucissement cyclique vis-à-vis de la composition du matériau sont également étudiées dans le but d'introduire les travaux présentés dans

les chapitres suivants. Concernant tout d'abord l'adoucissement Mullins, les résultats mettent en évidence qu'il ne se produit pas d'adoucissement pour une gomme de SBR non chargée. De plus, il apparaît que "l'intensité" de l'adoucissement Mullins augmente fortement avec le taux de charge, cependant, l'effet de la densité pontale est quant à lui moins évident. Actuellement, il n'y a pas de méthode disponible dans la littérature permettant de quantifier cette "intensité" de l'adoucissement Mullins et donc de pouvoir comparer plusieurs mélanges. Ce problème sera traité dans le Chapitre 3. En ce qui concerne l'adoucissement cyclique, la diminution de la contrainte maximale et l'augmentation de la déformation résiduelle sont utilisées pour caractériser l'évolution de l'adoucissement avec le nombre de cycles. Les résultats mettent en évidence un effet important de la fraction de charge, cependant, l'effet de la densité pontale ne peut pas être clairement établi. Il semble donc que le paramètre couramment utilisé dans la littérature pour caractériser l'adoucissement cyclique soit discutable. Une solution plus fiable apparaît alors être nécessaire. Ce problème sera abordé dans le Chapitre 6.

Chapitre 3 : Caractérisation de l'adoucissement Mullins

Plusieurs élastomères chargés présentant des sensibilités différentes à l'adoucissement Mullins sont soumis à des chargements cycliques. Dans le but de quantifier l'adoucissement Mullins, un paramètre d'endommagement basé sur le concept d'amplification de la déformation est introduit. Ce paramètre est utilisé pour étudier l'effet de la composition des matériaux. Une grande partie des travaux présentés dans ce chapitre a été publiée et peut être trouvée dans les références Merckel et al. (2011c) et Merckel et al. (2011d).

En accord avec les résultats expérimentaux présentés Chapitre 2, l'introduction de charges dans une gomme élastomère conduit à augmenter la raideur et à produire un adoucissement Mullins. L'effet de renforcement induit par les charges est clairement établi, cependant, les interprétations physiques conduisant à l'apparition de l'adoucissement Mullins sont toujours débattues. D'après la revue de la littérature présentée Chapitre 1, les évidences expérimentales de l'adoucissement Mullins sont nombreuses et un nombre important de modèles sont développés dans le but de le prendre en considération. Cependant, il manque toujours un paramètre objectif permettant de quantifier l'adoucissement Mullins et donc de comparer l'influence de la composition des matériaux. Ce chapitre a pour objectif de proposer un tel paramètre.

Le concept d'amplification de la déformation pour représenter l'effet de renforcement des charges dans un élastomère a été introduit par Mullins and Tobin (1965). Pour cela, les charges et la gomme sont respectivement représentées par des phases rigide et souple. La phase rigide est supposée indéformable. La déformation dans la phase souple est égale à la déformation moyenne appliquée sur le matériau amplifiée par un facteur qui augmente avec la fraction volumique de phase rigide. Cette amplification de la déformation a été largement utilisée dans le contexte de l'hyperélasticité pour le renforcement induit par la présence des charges. Par la suite, il a été étendu pour représenter l'adoucissement Mullins en considérant une variation de la fraction de phase rigide avec l'historique de chargement. L'adoucissement Mullins est alors associé à une rupture irréversible des agrégats de charge conduisant à une diminution de la fraction "active" de charge. Cette représentation a également été largement utilisée dans la littérature avec un facteur d'amplification de la déformation qui décroît avec la déformation maximale appliquée.

Dans ce chapitre, le concept d'amplification de la déformation est utilisé afin de proposer un paramètre permettant de quantitativement caractériser l'adoucissement Mullins. Dans ce but, le facteur d'amplification usuellement utilisé dans la littérature est décomposé en deux parties afin de dissocier l'effet renforçant induit par les charges de celui associé à l'adoucissement Mullins. Le paramètre ainsi défini permet alors de quantifier l'adoucissement Mullins et donc

d'étudier sa dépendance à la microstructure du matériau en comparant différents mélanges. Dans ce but, des chargements cycliques de traction uniaxiale sont appliqués sur plusieurs matériaux ayant des compositions différentes afin d'étudier l'influence de la densité pontale et du taux de charge. Les résultats mettent en évidence que la densité pontale a une influence négligeable sur l'adoucissement Mullins alors que ce dernier augmente fortement avec le taux de charge. Finalement, il apparaît que le paramètre proposé présente une dépendance linéaire avec la fraction volumique de charge ainsi qu'avec la déformation maximale appliquée. Cela conduit donc à une expression très simple qui permet de prédire l'adoucissement Mullins se produisant pour des mélanges qui ne sont pas étudiés expérimentalement.

Ce chapitre a proposé une méthode de caractérisation de l'adoucissement Mullins. Cependant, il peut être noté que seulement des chargements de traction uniaxiale sont considérés. Pour ce type de chargement, il est clairement établi que l'adoucissement Mullins évolue avec l'élongation maximale appliquée. Dans le but de proposer une formulation tridimensionnelle pour modéliser le comportement mécanique, il est nécessaire de définir un "équivalent" de cette élongation maximale pour des conditions de chargement plus générales. Ce problème est traité dans le chapitre suivant.

Chapitre 4 : Critère de l'adoucissement Mullins pour des conditions générales de chargement

Afin de définir un critère général pour l'adoucissement Mullins, des échantillons d'élastomère chargés sont soumis à des chargements non proportionnels. Chaque échantillon est initialement soumis à un pré-chargement uniaxial ou biaxial suivi par une traction uniaxiale cyclique. Une analyse expérimentale originale permet de déterminer le seuil d'activation de l'adoucissement Mullins et conduit à la validation d'un critère général pour l'adoucissement Mullins. Une grande partie des travaux présentés dans ce chapitre a été publiée et peut être trouvée dans la référence Merckel et al. (2012a).

La revue de la littérature présentée au Chapitre 1 met en évidence que malgré un nombre important de contributions sur l'adoucissement Mullins, un critère d'activation de l'adoucissement Mullins valide pour des conditions de chargement générales n'est toujours pas clairement établi. L'objectif de ce chapitre est de définir un tel critère qui est essentiel pour la modélisation du comportement des élastomères chargés.

L'effet de l'adoucissement Mullins sur la réponse contrainte-élongation d'un élastomère chargé lors d'un chargement de traction uniaxiale proportionnel est illustré Figure 1.2. Il peut être noté sur cette figure que l'adoucissement Mullins et la déformation résiduelle augmentent conjointement avec la déformation maximale appliquée. Mullins (1947, 1949) a conduit une étude approfondie de ces deux phénomènes. En appliquant des chargements de traction non proportionnels, l'auteur a notamment mis en évidence l'anisotropie de l'adoucissement et de la déformation résiduelle. Par la suite, la majorité des études se sont limitées à des chargements proportionnels. Dans le cas d'un chargement proportionnel, l'adoucissement Mullins est piloté par l'intensité maximale du chargement appliqué. Un grand nombre de solutions a été proposé pour définir cette intensité (Diani et al., 2009). Jusqu'à maintenant, très peu de contributions ont utilisé des chargements non proportionnels pour étudier l'adoucissement Mullins et l'anisotropie qu'il induit. Cependant, de tels chargements sont nécessaires afin de produire les évidences expérimentales permettant de définir un critère général pour l'activation de l'adoucissement Mullins.

Ce chapitre propose la définition d'un critère d'activation de l'adoucissement Mullins pour des élastomères chargés soumis à des conditions de chargement générales incluant des chargements

non proportionnels. Le critère est fondé sur une analyse originale de données expérimentales non conventionnelles. En comparant les réponses contrainte-élongation d'un chargement cyclique de traction uniaxiale, un paramètre est défini afin de capturer l'évolution de l'adoucissement se produisant entre deux cycles. Ce paramètre permet de détecter une activation de l'adoucissement Mullins et de déterminer l'élongation nécessaire suivant la direction de traction afin d'obtenir une réactivation de l'adoucissement Mullins. La méthode est appliquée sur plusieurs échantillons ayant subi un pré-chargement uniaxial ou biaxial suivi d'un chargement cyclique de traction uniaxiale proportionnelle ou non proportionnelle. Les résultats permettre d'obtenir de solides évidences pour définir le critère de l'adoucissement Mullins comme étant la surface tridimensionnelle définie par l'élongation directionnelle maximale subie par le matériau au cours de son historique de chargement. Deux cas de chargements spécifiques comportant différents trajets non proportionnels sont considérés afin d'éprouver la capacité prédictive du critère proposé. Les prédictions du seuil d'activation de l'adoucissement Mullins sont satisfaisantes. La définition et la validation expérimentale d'un tel critère sont un point critique dans la modélisation de l'adoucissement Mullins et devraient ouvrir de nouvelles perspectives dans la modélisation du comportement mécanique des élastomères chargés. Dans le chapitre suivant, des telles perspectives sont exploitées afin de proposer une loi de comportement permettant de capturer l'anisotropie induite par l'adoucissement Mullins.

Chapitre 5 : Modélisation du comportement anisotrope d'élastomères chargés ayant subi un adoucissement Mullins

Un modèle original est proposé pour des élastomères chargés afin de capturer le comportement anisotrope adouci induit par des historiques de chargement non proportionnel. La formulation est fondée sur une analyse approfondie des données expérimentales. Dans le but de fournir un modèle facilement applicable à une large gamme de matériaux, le modèle proposé ne nécessite pas de postuler de formes mathématiques pour la densité d'énergie élémentaire ou pour la loi d'évolution de l'adoucissement Mullins. Une grande partie des travaux présentés dans ce chapitre a été soumise pour publication sous la référence Merckel et al. (2012b).

Les études expérimentales menées à l'issue des travaux de Mullins (1947, 1949) se sont focalisées sur des chargements proportionnels et l'anisotropie induite n'a pas été étudiée plus en détail durant plusieurs décades. C'est seulement très récemment que plusieurs travaux se sont à nouveau intéressés à l'anisotropie induite par l'adoucissement Mullins, qui ne peut s'observer que lorsque des chargements non proportionnels sont appliqués.

En terme de modélisation, un nombre important de modèles de l'adoucissement Mullins peuvent être trouvés dans la littérature. Cependant, la plupart d'entre eux sont proposés en faisant l'hypothèse d'isotropie de l'adoucissement Mullins. Très peu ont pour but de capturer l'anisotropie induite par l'adoucissement. Il apparaît que les lois à directions permettent de capturer une telle anisotropie sans grande difficulté et quelques modèles de ce type sont proposés dans la littérature. Cependant, tous ces modèles représentent également une déformation résiduelle qui est directement imposée et contrainte par la nature de l'anisotropie induite associée à l'adoucissement Mullins. Cela n'est pas en accord avec les observations expérimentales qui supportent un découplage des évolutions de ces deux phénomènes. Les modèles directionnels existants sont basés sur une interprétation physique de l'adoucissement Mullins. Généralement, ils dépendent d'une densité d'énergie élémentaire fondée sur de la physique et l'adoucissement Mullins est alors modélisé en considérant une altération des paramètres physiques de la densité d'énergie élémentaire. Dans le but de représenter de nouvelles données expérimentales, la densité

d'énergie élémentaire ainsi que la loi d'évolution de l'adoucissement Mullins doivent alors être modifiées afin d'être adaptées au nouveau matériau.

Ce chapitre propose une formulation générale pour modéliser le comportement hyperélastique des élastomères chargés avec une prise en considération réaliste de l'anisotropie induite par l'adoucissement Mullins. Pour cela, une approche directionnelle est utilisée avec le critère anisotrope d'activation de l'adoucissement Mullins présenté au Chapitre 4. Tout d'abord, en accord avec les évidences expérimentales, les évolutions de l'adoucissement Mullins et de la déformation résiduelle sont découplées. Ensuite, la prise en considération de l'adoucissement Mullins est faite afin d'éviter des hypothèses vis-à-vis des formes de la densité élémentaire d'énergie et de la loi d'évolution de l'adoucissement Mullins. Cela est possible en utilisant le concept d'amplification de la déformation initialement proposé par Mullins and Tobin (1957). Finalement, une procédure d'identification est proposée afin de construire la densité élémentaire et la loi d'évolution de l'adoucissement sans avoir besoin d'en postuler des formes mathématiques. Cette procédure nécessite les données expérimentales produites par un chargement de traction proportionnelle cyclique avec des cycles croissants. La capacité du modèle à représenter précisément les données expérimentales d'un chargement de traction uniaxiale proportionnelle est démontrée. De plus, une fois identifié sur un chargement cyclique proportionnel, le modèle permet de prédire avec succès les réponses contrainte-élongation en traction uniaxiale pour des échantillons ayant subi des pré-chargements non proportionnels de tractions uniaxiales ou bi-axiales. Finalement, le modèle et la procédure d'identification sont utilisés sur plusieurs mélanges afin de mettre en évidence la flexibilité de la méthode proposée.

Ce chapitre met fin au travail sur l'adoucissement Mullins rapporté durant cette thèse. Le Chapitre 3 a conduit à proposer un paramètre permettant de quantifier l'adoucissement Mullins. La quantité mécanique pilotant l'évolution de l'adoucissement Mullins pour des conditions générales de chargement a été déterminée dans le Chapitre 4. Finalement, le chapitre courant propose des équations permettant de modéliser le comportement anisotrope d'un élastomère chargé ayant subi un adoucissement Mullins. Dans le but de compléter notre étude, le chapitre suivant s'intéresse à l'adoucissement cyclique qui évolue avec le nombre de cycles.

Chapitre 6 : Caractérisation et modélisation de l'adoucissement cyclique

Plusieurs élastomères chargés sont soumis à des chargements cycliques de traction uniaxiale afin d'étudier l'adoucissement cyclique. Dans le but de déterminer l'effet de la composition du matériau et de l'intensité de la déformation appliquée, une méthode originale de caractérisation de l'adoucissement cyclique est proposée et un paramètre d'adoucissement est défini. Un modèle est écrit afin de prédire les réponses contrainte-élongation d'un élastomère chargé durant un chargement proportionnel de traction uniaxiale cyclique. Une grande partie des travaux présentés dans ce chapitre a été publiée et peut être trouvée dans la référence Merckel et al. (2011b).

Les élastomères sont utilisés dans un grand nombre d'applications industrielles et ils sont particulièrement adaptés pour les éléments destinés à être soumis à des conditions de chargements cycliques. Dans le but d'augmenter leur raideur et de ralentir la propagation de fissures, des charges sont ajoutées à la gomme élastomère. Cependant, l'ajout de ces charges conduit à produire l'adoucissement Mullins. Dans le cas d'un chargement proportionnel de traction uniaxiale, l'évolution de l'adoucissement Mullins est associée à celle de l'élongation maximale appliquée au cours de l'historique de chargement. Une fois que l'adoucissement Mullins s'est

produit, l'adoucissement de la réponse mécanique du matériau continue à évoluer doucement avec le nombre de cycles. Par contre, l'évolution du comportement entre deux cycles successifs devient rapidement imperceptible. L'adoucissement se produisant durant le premier cycle a été l'objet d'un nombre important de publications. Par contre, les contributions sur le sujet des élastomères soumis à un grand nombre de cycles se concentrent généralement sur l'étude de la durée de vie et très peu de travaux s'intéressent à l'évolution du comportement mécanique. Cependant, l'adoucissement cumulé induit par un grand nombre de cycles peut nécessiter d'être pris en considération dans le dimensionnement de structures soumises à des conditions de chargement cyclique.

Ce chapitre a pour objectif d'étudier l'adoucissement cyclique qui commence après le premier cycle, une fois que l'adoucissement Mullins s'est produit. Pour cela, une approche originale est proposée afin de caractériser l'effet de l'adoucissement cyclique sur les réponses contrainte-élongation. Un paramètre d'adoucissement basé sur un concept d'amplification de l'élongation est introduit afin de capturer l'évolution du comportement avec le nombre de cycles. Contrairement aux paramètres d'adoucissement classiquement trouvés dans la littérature, celui qui est introduit ici est défini sur la réponse contrainte-élongation complète. Une telle approche permet alors de quantifier l'adoucissement cyclique et de comparer son évolution soit pour des matériaux de composition différente, soit pour un même matériau soumis à différentes intensités de chargement. Les résultats montrent que l'adoucissement cyclique d'un élastomère chargé augmente avec le taux de charge, diminue quand la densité pontale augmente et augmente avec l'intensité du chargement. En terme de modélisation, l'évolution du paramètre introduit en fonction du nombre de cycles peut être représentée par une expression logarithmique et en le combinant avec une densité d'énergie classique, il permet alors de prédire les réponses contrainte-élongation en fonction du nombre de cycles.

Bibliography

F. Abraham, T. Alshuth, and S. Jerrams. The effect of minimum stress and stress amplitude on the fatigue life of non strain cyrstallising elastomers. Materials and Design, 26:239–245, 2005. (Cited on page 25.)

F. Addiego, A. Dahoun, C. G'Sell, and J.-M. Hiver. Characterization of volume strain at large deformation under uniaxial tension in high-density polyethylene. Polymer, 47:4387–4399, 2006. (Cited on page 44.)

A. P. Alexendrov and J. S. Lazurkin. Strength of amorphous and crystallizing rubber polymers. Doklady Akad. Nauk. SSSR, 45:291–294, 1944. (Cited on page 20.)

A. F. M. S. Amin, M. S. Alam, and Y. Okui. An improved hyperelasticity relation in modeling viscoelasticity response of natural and high damping rubbers in compression: experiments, parameter identification and numerical verification. Mech. Mater., 34(2):75–95, 2002. (Cited on page 20.)

A. F. M. S. Amin, L. A., and H. P. Effect of temperature history on the mechanical behaviour of a filler-reinforced nr/br blend: literature review and critical experiments. Zamm, 90:347–369, 2010. (Cited on page 67.)

A. Andriyana, N. Saintier, and E. Verron. Configurational mechanics and critical plane approach: Concept and application to fatigue failure analysis of rubberlike materials. Int. J. Fatigue, 32: 1627–1638, 2011. (Cited on page 25.)

G. Arfken. Spherical Harmonics, in Mathematical Methods for Physicists, 3rd ed. Orlando, FL: Academic Press, 1985. (Cited on pages 158 and 159.)

E. M. Arruda and M. C. Boyce. A three-dimensional constitutive model for the large stretch behavior of rubber elastic materials. J. Mech. Phys. Solids, 41:389–412, 1993. (Cited on page 18.)

S. Asare, A. G. Thomas, and J. J. C. Busfield. Cyclic stress relaxation (csr) of filled rubber and rubber components. Rubber Chem. Technol., 82:104–112, 2009. (Cited on pages 25, 55 and 113.)

E. E. Auer, K. W. Doak, and I. J. Schaffner. Factor affecting laboratory cut-growth resistance of cold SBR tread stocks. Rubber world, 135(6):876–885, 1957. (Cited on pages 16, 50, 111 and 117.)

Z. Bazănt and B. Oh. Efficient numerical integration on the surface of a sphere. Z. Angew. Math. Mech., 66:37–49, 1986. (Cited on page 97.)

J. R. Beatty. Fatigue of rubber. Rubber Chem. Technol., 37:1341–1364, 1964. (Cited on pages 25 and 117.)

M. F. Beatty and S. Krishnaswamy. A theory of stress-softening in incompressible isotropic materials. J. Mech. Phys. Solids, 48:1931–1965, 2000. (Cited on page 113.)

J. S. Bergström. Large strain time-dependent behavior of elastomeric materials. PhD thesis, Massachusetts institute of technology, 1999. (Cited on pages 61 and 64.)

J. S. Bergström and M. C. Boyce. Mechanical behavior of particle filled elastomers. Rubber Chem. Technol., 72:633–656, 1999. (Cited on pages 16, 49, 61, 68, 72 and 105.)

J. S. Bergström and M. C. Boyce. Large strain time-dependent behavior of filled elastomers. Mech. Mater., 32(11):627–644, 2000. (Cited on page 20.)

A. Berrehili, S. Castagnet, and Y. Nadot. Multiaxial fatigue criterion for a high-density polyethylene thermoplastic. Fatigue Fract. Engng. Mater. Struct., 33(6):345–357, 2010. (Cited on pages 25, 55 and 113.)

A. F. Blanchard and D. Parkinson. Breakage of carbon-rubber networks by applied stress. J. Appl. Polym. Sci., 44:799–812, 1952. (Cited on page 20.)

L. Bokobza. The reinforcement of elastomeric networks by fillers. Macromol. Mater. Eng., 289: 607–621, 2004. (Cited on pages 49 and 69.)

L. Bokobza. Multiwall carbon nanotube elastomeric composites: A review. Polymer, 48: 4907e4920, 2007. (Cited on pages 49 and 50.)

L. Bokobza and O. Rapoport. Reinforcement of natural rubber. J. Appl. Polym. Sci., 85: 2301–2316, 2002. (Cited on page 68.)

H. Bouasse and Z. Carrière. Sur les courbes de traction du caoutchouc vulcanisé. Ann. Fac. Sci. Toulouse, 3:257–283, 1903. (Cited on pages 18 and 19.)

M. C. Boyce and E. M. Arruda. Constitutive models of rubber elasticity: a review. Rubber Chem. Technol., 73:504–523, 2000. (Cited on page 17.)

M. Brieu, J. Diani, and N. Bhatnagar. A New Biaxial Tension Test Fixture for Uniaxial Testing Machine—A Validation for Hyperelastic Behavior of Rubber-like Materials. J. Test. Eval., 35 (4):364–372, 2007. (Cited on page 34.)

M. Brieu, J. Diani, C. Mignot, and C. Moriceau. Response of a carbon-black filled SBR under large strain cyclic uniaxial tension. Int. J. Fatigue, 32(12):1921–1927, 2010. (Cited on pages 25, 26, 55, 111, 113 and 116.)

F. Bueche. Tensile strength of filled sbr vulcanizates. Rubber Chem. Technol., 32:1269–1285, 1959. (Cited on page 50.)

F. Bueche. Molecular basis for the mullins effect. J. Appl. Polym. Sci., 4:107–114, 1960. (Cited on page 20.)

F. Bueche and J. C. Halpin. Molecular theory for the tensile strength of gum elastomers. J. Appl. Phys., 35:36–41, 1964. (Cited on page 50.)

W. E. Byerly. Spherical Harmonics, in An Elementary Treatise on Fourier's Series, and Spherical, Cylindrical, and Ellipsoidal Harmonics, with Applications to Problems in Mathematical Physics. New York: Dover, 1959. (Cited on page 158.)

G. Chagnon, E. Verron, L. Gornet, G. Marckmann, and P. Charrier. On the relevance of continuum damage mechanics as applied to the Mullins effect in elastomers. J. Mech. Phys. Solids, 52(7):1627–1650, 2004. (Cited on pages 22 and 113.)

L. Chazeau, C. Gauthier, and J. M. Chenal. Rubber Nanocomposites: Preparation, Properties and Applications. John Wiley & Sons, 2010. (Cited on page 49.)

J. M. Chenal, C. Gauthier, L. Chazeau, L. Guy, and Y. Bomal. Parameters governing strain induced crystallization in filled natural rubber. Polymer, 48:68–93, 2007. (Cited on page 44.)

M. Cheng and W. Chen. Experimental investigation of the stress–stretch behavior of epdm rubber with loading rate effects. Int. J. Solids Struct., 40:4749–4768, 2003. (Cited on page 67.)

F. Clément, L. Bokobza, and L. Monnerie. On the mullins effect in silica-filled polydimethyl-siloxane networks. Rubber Chem. Technol., 74:846–870, 2001. (Cited on page 20.)

A. Cohen. A padé approximant to the inverse langevin function. Rheol. Acta, 30:270–273, 1991. (Cited on page 154.)

E. Coquelle, G. Bossis, D. Szabo, and F. Giulieri. Micromechanical analysis of an elastomer filled with particles organized in chain-like structure. J. Mater. Sci., A1:5941–5953, 2006. (Cited on page 69.)

E. M. Dannenberg and J. J. Brennan. Strain-energy as a criterion for stress softening in carbon-black-filled vulcanizates. Rubber Chem. Technol., 39:597–608, 1965. (Cited on pages 19 and 20.)

R. Dargazany and M. Itskov. A network evolution model for the anisotropic Mullins effect in carbon black filled rubbers. Int. J. Solids Struct., 46(16):2967–2977, 2009. (Cited on pages 20, 24, 61, 77, 78, 84 and 151.)

O. De Almeida, F. Lagattu, and J. Brillaud. Analysis by a 3d dic technique of volumetric deformation gradients: Application to polypropylene/epr/talc composites. Composites: Part A, 39:1210–1217, 2008. (Cited on page 45.)

G. deBotton, I. Hariton, and E. A. Socolsky. Neo-hookean fiber reinforced composites in finite elasticity. J. Mech. Phys. Solids, 54:533–559, 2006. (Cited on page 151.)

C. J. Derham and A. G. Thomas. Creep of rubber under repeated stressing. Rubber Chem. Technol., 50(397–402), 1977. (Cited on pages 25 and 26.)

J. Diani and P. Gilormini. Combining the logarithmic strain and the full-network model for a better understanding of the hyperelastic behavior of rubber-like materials. J. Mech. Phys. Solids, 53(11):2579–2596, 2005. (Cited on page 86.)

J. Diani, M. Brieu, M. Vacherand, and A. Rezgui. Directional model for isotropic and anisotropic hyperelastic rubber-like materials. Mech. Mater., 36:313–321, 2004. (Cited on page 97.)

J. Diani, M. Brieu, and P. Gilormini. Observation and modeling of the anisotropic visco-hyperelastic behavior of a rubberlike material. Int. J. Solids Struct., 43(10):3044–3056, 2006a. (Cited on pages 19, 20, 22, 77, 78, 80, 84, 95, 151 and 155.)

J. Diani, M. Brieu, and M. Vacherand. A damage directional constitutive model for Mullins effect with permanent set and induced anisotropy. Eur. J. Mech. A Solids, 25:483–496, 2006b. (Cited on pages 20, 22, 24, 52, 77, 84, 93, 94, 95, 97, 98, 113, 114, 151 and 154.)

J. Diani, A. M. ortega, K. Gall, S. Kasprzak, and A. R. Greenberg. On the relevance of the 8-chain model and the full-network model for the deformation and failure of networks formed through photopolymerization of multifunctional monomers. J. Polym. Sci. Part B: Polym. Phys., 46:1226–1234, 2008. (Cited on page 49.)

J. Diani, B. Fayolle, and P. Gilormini. A review on the mullins effect. Eur. Polym. J., 45: 601–612, 2009. (Cited on pages 18, 19, 20, 21, 22, 26, 41, 61, 77, 111, 127, 130 and 151.)

K. A. Dijkhuis, J. W. Noordermeer, and W. K. Dierkes. The relationship between crosslink system, network structure and material properties of carbon black reinforced epdm. Eur. Polym. J., 45:3302–3312, 2009. (Cited on pages 49 and 50.)

A. Dorfmann and R. Ogden. A constitutive model for the mullins effect with permanent set in particle-reinforced rubber. Int. J. Solids Struct., 41(1855–1878), 2004. (Cited on pages 19, 23, 52, 53, 61, 68, 94, 105 and 151.)

A. Einstein. Eine neue bestimmung der molekuldimensionen. Ann. Phys. (Leipzig), 19:289, 1906. (Cited on page 105.)

A. Einstein. Berichtigung zu meiner arbeit: Eine neue bestimmung der molekuldimensionen. Annalen der Physik, 339:591–592, 1911. (Cited on page 63.)

A. Elías-Zúñiga. A phenomenological energy-based model to characterize stress-softening effect in elastomers. Polymer, 46(10):3496–3506, 2005. (Cited on pages 22 and 113.)

Q.-Z. Fang, T. J. Wang, H. G. Beom, and H. P. Zhao. Rate-dependent large deformation behavior of pc/abs. Polymer, 50:296–304, 2009. (Cited on page 45.)

R. F. Fedors and R. F. Landel. Statistical variability of ultimate properties of sbr gum vulcanizates. Rubber Chem. Technol., 39:712–725, 1966. (Cited on page 50.)

Y. Fukahori. Mechanism of the self-reinforcement of cross-linked nr generated through the strain-induced crystallization. Polymer, 51:1621–1631, 2010. (Cited on page 49.)

J. A. Gaunt. On the triplets of helium. Philos. Trans. Roy. Soc. (London) Ser. A, 228:151–196, 1929. (Cited on page 159.)

C. Gauthier, L. Chazeau, T. Prasse, and J. Y. Cavaille. Reinforcement effects of vapour grown carbon nanofibres as fillers in rubbery matrices. Comp. Sci. Technol., 65:335–343, 2005. (Cited on page 50.)

G. Gee, J. Stern, and L. R. G. Treloar. Volume changes in the stretching rubber. Trans. Faraday Soc., 46:1101–1106, 1950. (Cited on page 44.)

A. N. Gent, S. M. Lai, C. Nah, and C. Wang. Viscoelastic effects in cutting and tearing rubber. Rubber Chem. Technol., 67:610–619, 1994. (Cited on page 51.)

L. Gentot, M. Brieu, and G. Mesmacque. Modelling of stress-softening for elastomeric materials. Rubber Chem. Technol., 77:758–774, 2004. (Cited on pages 25, 26, 55, 111, 113 and 116.)

S. Gherib, L. Chazeau, J. M. Pelletier, and H. Satha. Influence of the filler type on the rupture behavior of filled elastomers. J. Appl. Polym. Sci., 118:435–445, 2010. (Cited on page 49.)

J. M. Gloaguen and J. M. Lefebvre. Plastic deformation behaviour of thermoplastic/clay nanocomposites. Polymer, 42:5841±5847, 2001. (Cited on page 45.)

S. Göktepe and C. Miehe. A micro-macro approach to rubber-like materials. Part 3: The microsphere model of anisotropic Mullins-type damage. J. Mech. Phys. Solids, 53(10):2259–2283, 2005. (Cited on pages 22, 24, 77, 93, 97 and 151.)

S. Govindjee and J. Simo. A micro-mechanics to computationally efficient phenomenology: carbon black-filled rubbers incorporating mullins effect. J. Mech. Phys. Solids, 40:213–233, 1992. (Cited on page 151.)

S. Govindjee and J. C. Simo. A micro-mechanically based continuum damage model for carbon black-filled rubbers incorporating Mullins'effect. J. Mech. Phys. Solids, 39(1):87–112, 1991. (Cited on pages 24, 61, 113 and 151.)

F. Grytten, H. Daiyan, M. Polanco-Loria, and S. Dumoulin. Use of digital image correlation to measure large-strain tensile properties of ductile thermoplastics. Polymer Testing, 28:653–660, 2009. (Cited on page 45.)

C. G'Sell, J.-M. Hiver, A. Dahnoun, and A. Souahi. Video-controlled tensile testing of polymers and metals beyond the necking point. J. Mat. Sci., 27:5031–5039, 1992. (Cited on page 44.)

Z. Guo and L. J. Sluys. Computational modelling of the stress-softening phenomenon of rubberlike materials under cyclic loading. Eur. J. Mech. A Solids, 25(6):877–896, 2006. (Cited on pages 113 and 151.)

E. Guth and O. Gold. On the hydrodynamical theory of the viscosity of suspensions. Phys. Rev., 53:322, 1938. (Cited on pages 49, 72 and 105.)

G. R. Hamed. Molecular aspects of the fatigue and fracture of rubber. Rubber Chem. Technol., 67:529–537, 1994. (Cited on page 50.)

D. E. Hanson, M. Hawley, R. Houlton, K. Chitanvis, P. Rae, B. E. Orler, and D. A. Wrobleski. Stress softening experiments in silica-filled polydimethylsiloxane provide insight into a mechanism for the Mullins effect. Polymer, 46(24):10989–10995, 2005. (Cited on pages 19, 20, 77, 78 and 151.)

R. Harbour, A. Fatemi, and W. Mars. Fatigue life analysis and predictions for nr and sbr under variable amplitude and multiaxial loading conditions. Int. J. Fatigue, 30:1231–1247, 2008. (Cited on page 25.)

J. A. C. Harwood and A. R. Payne. Stress softening in natural rubber vulcanizates iii. carbon black filled vulcanizates. J. Appl. Polym. Sci., 10:315–323, 1966a. (Cited on pages 19, 20, 21, 22 and 68.)

J. A. C. Harwood and A. R. Payne. Stress softening in natural rubber vulcanizates. iv. unfilled vulcanizates. J. Appl. Polym. Sci., 10:1203–1211, 1966b. (Cited on pages 19, 20 and 21.)

J. A. C. Harwood, L. Mullins, and A. R. Payne. Stress softening in natural rubber vulcanizates. part ii. stress softening effects in pure gum and filler loaded rubbers. J. Appl. Polym. Sci., 9: 3011, 1965. (Cited on pages 19, 20, 22, 68 and 69.)

G. Heinrich, M. Klüppel, and T. A. Vilgis. Reinforcement of elastomers. Curr. Opin. Solid State Mat. Sci., 6:195–302, 2002. (Cited on pages 23 and 49.)

W. Holt and A. McPherson. Change of volume of rubber on stretching: Effects of time, elongation and temperature. J. Res. Natl. Bur. Stand., 17:657– 678, 1936. (Cited on page 44.)

R. Houwink. Slipping of molecules during the deformation of reinforced rubber. Rubber Chem. Technol., 10:229–240, 1956. (Cited on page 20.)

M. Itskov and N. Aksel. A class of orthotropic and transversely isotropic hyperelastic constiutive models based on polyconvex strain energy function. Int. J. Solids and struct., 41:3833–3848, 2004. (Cited on page 151.)

M. Itskov, E. Halberstroh, A. E. Ehret, and M. C. Vöhringer. Experimental Observation of the Deformation Induced Anisotropy of the Mullins Effect in Rubber. Kaut. Gummi. Kunstst., pages 93–96, 2006. (Cited on pages 20, 77 and 78.)

M. Itskov, A. Ehret, R. KazakevicÃŰiutė-Makovska, and G. Weinhold. A thermodynamically consistent phenomenological model of the anisotropic Mullins effect. Zamm, 90(5):370–386, 2010. (Cited on pages 23, 77 and 84.)

A. G. James and A. Green. Strain Energy Functions of Rubber. II. The Characterization of Filled Vulcanizates. J. Appl. Polym. Sci., 19:2319–2330, 1975. (Cited on page 20.)

M. A. Johnson and M. F. Beatty. The Mullins effect in uniaxial extension and its influence on the transverse vibration of a rubber string. Continuum Mech. and Thermodyn., 5:83–115, 1993. (Cited on pages 23 and 61.)

M. A. Johnson and M. F. Beatty. The Mullins effect in equibiaxial extension and its influence on the inflation of a balloon. Int. J. Engng. Sci., 33(2):223–245, 1995. (Cited on page 20.)

H. Jones and H. Yiengst. Dilatometer studies of pigment-rubber systems. Rubber Chem. Technol., 14:113–124, 1941. (Cited on page 44.)

L. Kachanov. Time of the rupture process under creep conditions. Izv. Akad. Nauk. S.S.R. Otd. Tech. Nauk., 8:26–31, 1958. (Cited on pages 22 and 113.)

H. Kahraman, G. W. Weinhold, E. Haberstroh, and M. Itskov. Experimental and phenomenological description of the anisotropic mullins effect for carbon black reinforced elastomers. KGK Kautschuk Gummi Kunststoffe, 63:64–69, 2010. (Cited on page 151.)

K. K. Kar and A. K. Bhowmick. Effect of holding time on high strain hysteresis lost of carbon black filled rubber vulcanizates. Polym. Eng. Sci., 38:1927–1945, 1998. (Cited on page 68.)

H. G. Killian, M. Strauss, and W. Hamm. Universal properties in filler-loaded rubbers. Rubber Chem. Technol., 67:1–16, 1994. (Cited on page 24.)

J. Kim and H. Jeong. A study on the material properties and fatigue life of natural rubber with different carbon blacks. Int. J. Fatigue, 27:263–272, 2005. (Cited on page 25.)

M. Klüppel. Hyperelasticity and stress softening of filler reinforced polymer networks. Macromol. Symp., 200:31–43, 2003. (Cited on page 23.)

M. Klüppel and J. Schramm. A generalized tube model of rubber elasticity and stress softening of filler reinforced elastomer systems. Macromol. Theory. Simul., 9:742–754, 2000. (Cited on pages 19, 21, 23, 52, 61, 63, 65, 68, 98, 102 and 105.)

D. Kohls and G. Beaucage. Rational design of reinforced rubber. Curr. Opin. Solid State Mat. Sci., 6(3):183–194, 2002. (Cited on pages 41, 49, 61 and 111.)

G. Kraus, W. Childers, and K. W. Rollmann. Stress softening in carbon black reinforced vulcanizates. strain rate and temperature effects. J. Appl. Polym. Sci., 10(229), 1966. (Cited on pages 20, 21, 47 and 67.)

G. Krauss. A carbon black structure-concentration equivalence principle. application to stress-strain relationships of filled rubbers. Rubber Chem. Technol., 44:199–114, 1971. (Cited on page 50.)

S. Krishnaswamy and M. F. Beatty. The Mullins effect in compressible solids. Int. J. Engng. Sci., 38:1397–1414, 2000. (Cited on page 22.)

W. Kuhn and F. Grün. Beziehungen zwischen elastischen konstanten und dehnungsdoppel-brechung hochelastischer stoffe. Kolloidzeitschrift, 101:248–271, 1942. (Cited on pages 18 and 153.)

P. Kumar, A. G. Thomas, Y. Fukahori, and J. J. C. Busfield. Cavitation in granulate filled rubber materials. In A. Boukamel, L. Laiarinandrasana, S. Méo, and E. Verron, editors, Proceedings of the Fifth European Conference on Constitutive Models for Rubber, Paris, France, pages 157–163, 2007. (Cited on page 44.)

L. Laiarinandrasana, R. Piques, and A. Robinsson. Visco-hyperelastic model with internal state variable coupled with discontinuous damage concept under total Lagrangian formulation. Int. J. Plast., 19(7):977–1000, 2003. (Cited on page 22.)

G. J. Lake. Fatigue and fracture of elastomers. Rubber Chem. Technol., 68:435–460, 1995. (Cited on page 51.)

G. J. Lake and A. G. Thomas. The strength of highly elastic materials. Philos. Trans. R. Soc. London, Ser. A, 300:108–119, 1967. (Cited on pages 9, 25 and 51.)

J. Lambert-Diani and C. Rey. New phenomenological behavior laws for rubbers and thermo-plastic elastomers. Eur. J. Mech. A Solids, 18:1027–1043, 1999. (Cited on page 118.)

A. Lapra, F. Clément, L. Bokobza, and L. Monnerie. Straining effects in silica-filled elastomers investigated by atomic force microscopy: from macroscopic stretching to nanoscale strainfield. Rubber Chem. Technol., 76:60–81, 2003. (Cited on page 69.)

F. Laraba-Abbes, P. Ienny, and R. Piques. A new 'Tailor-made' methodology for the mechanical behaviour analysis of rubber-like materials: 2. Application to the hyperelastic behaviour characterization of a carbon-black filled natural rubber vulcanizate. Polymer, 44(3):821–840, 2003. (Cited on pages 20, 77, 78 and 151.)

K. Layouni, L. Laiarinandrasana, and R. Piques. Compressibility induced by damage in carbon black reinforced natural rubber. In J. Busfield and A. H. Muhr, editors, Proceedings of the Third European Conference on Constitutive Models for Rubber, London, UK, pages 273–281, 2003. (Cited on page 44.)

J. B. Le Cam. A review of the volume changes in rubbers: The effect of stretching. Rubber Chem. Technol., 83(3):247–269, 2010. (Cited on pages 26, 41, 44 and 128.)

J. B. Le Cam and E. Toussaint. Cyclic volume changes in rubber. Mech. Mater., 41:898–901, 2009. (Cited on pages 44 and 47.)

J. B. Le Cam, B. Huneau, and E. Verron. Description of fatigue damage in carbon black filled natural rubber. Fatigue Fract. Engng. Mater. Struct., 31:1031–1038, 2008. (Cited on pages 25 and 44.)

J. L. Leblanc. Rubber-filler interactions and rheological properties in filled compounds. Prog. Polym. Sci., 27:627–687, 2002. (Cited on page 16.)

J. Lemaitre and J. Chaboche. Mécanique des Matèriaux Solides. Dunod, Paris, 1985. (Cited on page 113.)

J. Li, D. Mayau, and V. Lagarrigue. A constitutive model dealing with damage due to cavity growth and the Mullins effect in rubber-like materials under triaxial loading. J. Mech. Phys. Solids, 56(3):953–973, 2008. (Cited on pages 20 and 113.)

G. Limbert and J. Middlenton. A transversely isotropic viscohyperelastic material, application to the modeling of biological soft connective tissues. Int. J. Solids Struct., 41:4237–4260, 2004. (Cited on page 151.)

A. Lion. A constitutive model for carbon black filled rubber: experimental investigations and mathematical representation. Continuum Mech. Thermodyn, 8:153–169, 1996. (Cited on page 22.)

J. Lu and L. Zhang. Physically motivated invariant formulation for transversely isotropic hyperelasticity. Int. J. Solids and struct., 42:6015–6031, 2005. (Cited on page 151.)

H. Luo, M. Klüppel, and H. Schneider. Study of filled sbr elastomers using nmr and mechanical measurements. Macromolecules, 37:8000–8009, 2004. (Cited on pages 19, 23, 52, 61 and 68.)

G. Machado. Contribution à l'étude de l'anisotropie induite par l'effet Mullins dans les élastomères silicone chargés. PhD thesis, Université de Grenoble, 2011. (Cited on pages 77, 78 and 95.)

G. Machado, G. Chagnon, and D. Favier. Experimental observation of induced anisotropy of the mullins effect in particle-reinforced silicone rubber. In G. Heinrich, M. Kaliske, A. Lion, and S. Reese, editors, Proceedings of the sixth European Conference on Constitutive Models for Rubber, Dresden, Germany, pages 511–515, 2009. (Cited on page 77.)

G. Machado, G. Chagnon, and D. Favier. Analysis of the isotropic models of the Mullins effect based on filled silicone rubber experimental results. Mech. Mater., 42(9):841–851, 2010. (Cited on pages 20 and 22.)

G. Marckmann and E. Verron. Comparison of hyperelastic models for rubber-like materials. Rubber Chem. Technol., 79:835–858, 2006. (Cited on page 17.)

G. Marckmann, E. Verron, L. Gornet, G. Chagnon, P. Charrier, and P. Fort. A theory of network alteration for the mullins effect. J. Mech. Phys. Solids, 50:2011–2028, 2002. (Cited on pages 24, 61 and 154.)

W. Mars and A. Fatemi. A literature survey on fatigue analysis approaches for rubber. Int. J. Fatigue, 24:949–961, 2002. (Cited on pages 25 and 111.)

W. Mars and A. Fatemi. Observations of the constitutive response and characterization of filled natural rubber under monotonic and cyclic multiaxial stress states. J. Eng. Mater. Technol., 126:19–28, 2004a. (Cited on pages 16, 24, 25, 26 and 111.)

W. Mars and A. Fatemi. Multiaxial stress effects on fatigue behavior of filled natural rubber. Int. J. Fatigue, 28:521–529, 2006. (Cited on page 25.)

W. V. Mars and A. Fatemi. Factors that affect the fatigue life of rubber: a literature survey. Rubber Chem. Technol., 77:391–408, 2004b. (Cited on pages 25, 55, 111, 113, 116 and 117.)

A. Medalia. Morphology of aggregates. iv. effective volume of aggregates of carbon black from electron microscopy; application to vehicle adsorption and to die swell of filled rubber. J. Colloid. Interface Sci., 32:115–131, 1970. (Cited on pages 16 and 49.)

A. I. Medalia. Effect of carbon-black on dynamic properties of rubber vulcanizates. Rubber Chem. Technol., 51:437–523, 1978. (Cited on page 49.)

B. Meissner and L. Matějka. A structure-based constitutive equation for filler-reinforced rubber-like networks and for the description of the mullins effect. Polymer, 47:7997–8012, 2006. (Cited on pages 23 and 61.)

B. Meissner and L. Matějka. Constitutive equation describing the biaxial stress-strain behavior of poly(dimethylsiloxane) networks reinforce with silica generated in situ. Eur. Polym. J., 44: 1940–1948, 2008. (Cited on pages 23 and 61.)

A. Menzel and P. Steinmann. Permanent set in vulcanized rubber. Int. J. Solids and struct., 38:9505–9523, 2001. (Cited on page 151.)

Y. Merckel, M. Brieu, J. Diani, and D. Berghezan. Effect of material and mechanical parameters on the stress-softening of carbon-black filled rubbers submitted to cyclic loadings. In Proceedings of the 7th European Conference on Constitutive Models for Rubber, Dublin, Ireland, pages 253–257, 2011a. (Cited on page 128.)

Y. Merckel, J. Diani, M. Brieu, and D. Berghezan. Experimental characterization and modelling of the cyclic softening of carbon-black filled rubbers. Mater. Sci. Eng. A, 528:8651–8659, 2011b. (Cited on pages 94 and 132.)

Y. Merckel, J. Diani, M. Brieu, and J. Caillard. Characterization of the mullins effect of carbon-black filled rubbers. Rubber Chem. Technol., 84(3), 2011c. (Cited on pages 81, 98, 102, 105 and 129.)

Y. Merckel, J. Diani, M. Brieu, P. Gilormini, and J. Caillard. Effect of the microstructure parameters on the mullins softening in carbon-black filled styrene–butadiene rubbers. J. Appl. Polym. Sci., 123:1153–1161, 2011d. (Cited on page 129.)

Y. Merckel, J. Diani, S. Roux, and M. Brieu. A simple framework for full-network hyperelasticity and anisotropic damage. J. Mech. Phys. Solids, 59:75–88, 2011e. (Cited on pages 84, 159 and 160.)

Y. Merckel, M. Brieu, J. Diani, and J. Caillard. A mullins softening criterion for general loading conditions. J. Mech. Phys. Solids, 60:1257–1264, 2012a. (Cited on pages 98 and 130.)

Y. Merckel, J. Diani, M. Brieu, and J. Caillard. Constitutive modeling of the anisotropic behavior of mullins softened filled rubbers. Submitted to Mech. Mater., 2012b. (Cited on page 131.)

L. Meunier, G. Chagnon, D. Favier, L. Orgéas, and P. Vacher. Mechanical experimental characterisation and numerical modelling of an unfilled silicone rubber. Polymer Testing, 27:765–777, 2008. (Cited on page 19.)

K. H. Meyer and C. Ferri. Sur l'élasticité du caoutchouc. Helv. Chim. Acta., 18:570–589, 1935. (Cited on page 17.)

K. H. Meyer, G. v. Susich, and E. Valkó. Die elastischen eigenschaften der organischen hochpolymeren und ihre kinetische deutung. Kolloidzsch, 59:208–216, 1932. (Cited on page 17.)

C. Miehe. Discontinuous and continuous damage evolution in ogden-type large-strain elastic materials. Eur. J. Mech. A Solids, 14:697–720, 1995. (Cited on page 113.)

C. Miehe and J. Keck. Superimposed finite elastic-viscoelastic-plastoelastic stress response with damage in filled rubbery polymers. experiments, modelling and algorithmic implementation. J. Mech. Phys. Solids, 48:323–365, 2000. (Cited on page 102.)

C. Moreau, S. Thuillier, G. Rio, and V. Grolleau. The mechanical behavior of a slightly compressible rubber-like material: correlation of simulations and experiments. Rubber Chem. Technol., 72, 1999. (Cited on page 20.)

A. H. Muhr. Modeling the stress-strain behavior of rubber. Rubber Chem. Technol., 78:391–425, 2005. (Cited on page 26.)

L. Mullins. Effect of stretching on the properties of rubber. J. Rubber Res., 16(12):275–289, 1947. (Cited on pages 10, 18, 19, 20, 77, 94, 127, 130, 131 and 151.)

L. Mullins. Permanent set in vulcanized rubber. India Rubber World, 120:63–66, 1949. (Cited on pages 10, 18, 19, 20, 24, 77, 80, 94, 127, 130, 131 and 151.)

L. Mullins. Thixotropic behavior of carbon black in rubber. J. Phys. and Col. Chem., 54(2): 239–251, 1950. (Cited on pages 10, 18 and 127.)

L. Mullins. Softening of rubber by deformation. Rubber Chem. Technol., 42:339–362, 1969. (Cited on pages 10, 15, 18, 20, 21, 22, 61, 64, 111, 127 and 151.)

L. Mullins and N. Tobin. Theoretical model for the elastic behavior of filler-reinforced vulcanized rubber. Rubber Chem. Technol., 30:555–571, 1957. (Cited on pages 19, 20, 21, 23, 44, 45, 47, 52, 61, 68, 93, 98, 105 and 132.)

L. Mullins and N. Tobin. Carbon-black loaded rubber vulcanizates: Volume changes in stretching. Rubber Chem. Technol., 31:505–512, 1958. (Cited on pages 21 and 47.)

L. Mullins and N. R. Tobin. Stress softening in natural rubber vulcanizates. Part 1. Use of a strain amplification factor to describe elastic behavior of filler-reinforced vulcanized rubber. J. Appl. Polym. Sci., 9:2993–3009, 1965. (Cited on pages 16, 49, 61, 63, 111 and 129.)

S. Mzabi. Caractérisation et analyse des mécanismes de fracture en fatigue des élastomères chargés. PhD thesis, Université Pierre & Marie Curie, 2010. (Cited on pages 9, 16 and 111.)

S. Mzabi, D. Berghezan, S. Roux, F. Hild, and C. Creton. A critical local energy release rate criterion for fatigue fracture of elastomers. J. Polym. Sci. Part B: Polym. Phys., 49:1518–1524, 2011. (Cited on pages 25 and 111.)

R. W. Ogden and D. G. Roxburgh. A pseudo-elastic model for the Mullins effect in filled rubber. Proc. Roy. Soc. Lond., pages 2861–2877, 1999. (Cited on pages 22, 23, 102 and 113.)

A. M. Ortega, S. E. Kasprzak, C. M. Yakacki, J. Diani, A. R. Greenberg, and K. Gall. Structure–property relationships in photopolymerizable polymer networks: Effect of composition on the crosslinked structure and resulting thermomechanical properties of a (meth)acrylate-based system. J. Appl. Polym. Sci., 110:1559–1572, 2008. (Cited on page 50.)

G. Palmieri, M. Sasso, G. Chiappini, and D. Amodio. Mullins effect characterization of elastomers by multi-axial cyclic tests and optical experimental methods. Mech. Mater., 41:1059–1067, 2009. (Cited on page 20.)

E. Parsons, M. C. Boyce, and D. Parks. An experimental investigation of the large-strain tensile behavior of neat and rubber-toughened polycarbonate. Polymer, 45:2665–2684, 2004. (Cited on page 45.)

E. Parsons, M. C. Boyce, D. Parks, and M. Weinberg. Three-dimensional large-strain tensile deformation of neat and calcium carbonate-filled high-density polyethylene. Polymer, 46: 2257–2265, 2005. (Cited on page 45.)

H. Pawelski. Softening behaviour of elastomeric media after loading in changing directions. In D. Besdo, R. H. Schuster, and J. Ihleman, editors, Proceedings of the Second European Conference of the Constitutive Models for Rubber, Balkema, pages 27–34, 2001. (Cited on page 93.)

H. Qi and M. Boyce. Constitutive model for stretch-induced softening of the stress stretch behavior of elastomeric materials. J. Mech. Phys. Solids, 52:2187–2205, 2004. (Cited on pages 23, 61, 72, 98 and 102.)

H. J. Qi and M. C. Boyce. Stress-strain behavior of thermoplastic polyurethanes. Mech. Mater., 37(8):817–839, 2005. (Cited on page 20.)

J. Ramier, L. Chazeau, C. Gauthier, L. Stelandre, L. Guy, and E. Peuvrel-Disdier. In situ sals and volume variation measurements during deformation of treated silica filled sbr. J. Mater. Sci., 42:8130–8138, 2007. (Cited on page 44.)

Z. Rigbi. Reinforcement of rubber by carbon black. Adv. Polym. Sci., 36:21–68, 1980. (Cited on page 19.)

R. S. Rivlin. Large elastic deformations of isotropic materials. iv. further developments of the general theory. Philos. Trans. R. Soc. London, Ser. A, 241:379–397, 1948. (Cited on page 17.)

N. Saintier, G. Cailletaud, and R. Piques. Multiaxial fatigue life prediction for a natural rubber. Int. J. Fatigue, 28:530–539, 2006. (Cited on page 25.)

N. Saintier, G. Cailletaud, and R. Piques. Cyclic loadings and crystallization of natural rubber: An explanation of fatigue crack propagation reinforcement under a positive loading ratio. Mater. Sci. Eng. A, 528(3):1078–1086, 2011. (Cited on pages 25 and 113.)

Y. Shen, F. Golnaraghi, and A. Plumtree. Modelling compressive cyclic stress-strain behaviour of structural foam. Int. J. Fatigue, 23:491–497, 2001. (Cited on pages 25, 26, 55, 111 and 113.)

T. Shinomura and M. Takahashi. Volume change measurements of filled rubber vulcanizates under stretching. Rubber Chem. Technol., 43:1025–1035, 1970. (Cited on pages 44 and 45.)

J. C. Simo. On a fully three-dimensional finite-strain viscoelastic damage model: formulation and computational aspects. Comput. Methods Appl. Mech. Eng., 60:153–173, 1987. (Cited on pages 22, 26, 61, 113 and 155.)

H. M. Smallwood. Limiting laws of the reinforcement of rubber. J. Appl. Phys., 15:758–766, 1944. (Cited on pages 63 and 72.)

T. L. Smith. Ultimate tensile properties of elastomers. iii. dependence of the failure envelope on crosslink density. Rubber Chem. Technol., 40:544–555, 1967. (Cited on page 50.)

T. L. Smith. Strength of elastomers - a perspective. Polym. Eng. Sci., 17:129–143, 1977. (Cited on pages 49, 50 and 51.)

T. L. Smith and A. B. Magnusson. Diisocyanate-linked polymers. iii. relationships between the composition and ultimate tensile properties of some polyurethane elastomers. J. Appl. Polym. Sci., 5:218–232, 1961. (Cited on page 50.)

O. Starkova and A. Aniskevich. Poisson's ratio and the incompressibility relation for various strain measures with the example of a silica-filled sbr rubber in uniaxial tension tests. Polymer Testing, 29:310–318, 2010. (Cited on page 44.)

N. Suzuki, M. Ito, and F. Yatsuyanagi. Effects of rubber/filler interactions on deformation behavior of silica filled sbr systems. Polymer, 46:193–201, 2005. (Cited on page 20.)

S. Trabelsi, P. A. Albouy, and J. Rault. Crystallization and melting processes in vulcanized stretched natural rubber. Macromolecules, 36:7624–7639, 2003a. (Cited on page 19.)

S. Trabelsi, P. A. Albouy, and J. Rault. Effective local deformation in stretched filled rubber. Macromolecules, 36:9093–9099, 2003b. (Cited on pages 19 and 54.)

L. R. G. Treloar. Crystallization phenomena in raw rubber. Trans. Faraday Soc., 37:84–97, 1941. (Cited on page 54.)

L. R. G. Treloar. The elasticity and related properties of rubbers. Rep. Prog. Phys., 36:755–826, 1973. (Cited on pages 18 and 49.)

L. R. G. Treloar. The Physics of Rubber Elasticity. Oxford University Press, 1975. (Cited on pages 18 and 50.)

L. R. G. Treloar and G. Riding. A non-gaussian theory for rubber in biaxial strain - 1. mechanical properties. Proc. Roy. Soc. London, 369(ser. A):261–280, 1979. (Cited on pages 18, 96, 97 and 152.)

K. Tsunoda, J. J. C. Busfield, C. K. L. Davies, and A. G. Thomas. Effect of materials variables on the tear behaviour of a non-crystallising elastomer. J. Mater. Sci., 35:5187–5198, 2000. (Cited on page 51.)

V. Vahapoğlu and S. Karadeniz. Constitutive equations for isotropic rubber-like materials using phenomenological approach: A bibliography (1930–2003). Rubber Chem. Technol., 79:489–500, 2006. (Cited on page 17.)

E. Verron and A. Andriyana. Definition of a new predictor for multiaxial fatigue crack nucleation in rubber. J. Mech. Phys. Solids, 56:417–443, 2008. (Cited on page 25.)

Q. Wang, F. Wang, and K. Cheng. Effect of crosslink density on some properties of electron beam-irradiated styrene–butadiene rubber. Rad. Phys. Chem., 78:1001–1005, 2009. (Cited on page 50.)

R. E. Webber, C. Creton, H. R. Brown, and J. P. Gong. Large Strain Hysteresis and Mullins Effect of Tough Double-Network Hydrogels. Macromolecules, 40(8):2919–2927, 2007. (Cited on page 20.)

A. Weiss, B. Maker, and S. Govindjee. Finite element implementation of incompressible, transversely isotropic hyperelasiticity. Comput. Methods Appl. Mech. Eng., 135:107–128, 1979. (Cited on pages 93 and 151.)

J. Wu and K. M. Liechti. Multiaxial and time-dependent behavior of a filled rubber. J. Time-Dependent Mater., 4:293–331, 2000. (Cited on page 44.)

Y. L. Xu. Fast evaluation of the gaunt coefficients. Math. Comput., 65:1601–1612, 1996. (Cited on page 160.)

L. Yan, D. A. Dillard, R. L. West, L. D. Lower, and G. V. Gordon. Mullins Effect Recovery of a Nanoparticle-Filled Polymer. J. Polym. Sci. Part B: Polym. Phys., 48:2207–2214, 2010. (Cited on pages 25, 55 and 113.)

W. Yu, X. Chen, Y. Wang, L. Yan, and N. Bai. Uniaxial ratchetting behavior of vulcanized natural rubber. Polym. Eng. Sci., 48:191–197, 2008. (Cited on page 25.)

H. Zhang, A. K. Scholz, J. de Crevoisier, F. Vion-Loisel, G. Besnard, A. Hexemer, H. R. Brown, E. J. Kramer, and C. Creton. Nanocavitation in carbon black filled styrene-butadiene rubber under tensiondetected by real time small angle x-ray scattering. Macromolecules, 45:1529–1543, 2012. (Cited on page 46.)

J. Zhao and G. N. Ghebremeskel. A review of some of the factors affecting fracture and fatigue in SBR and BR vulcanizates. Rubber Chem. Technol., 74(3):409–425, 2001. (Cited on pages 50 and 117.)

Appendix A

A simple framework for full-network hyperelasticity and anisotropic damage

A formulation of a constitutive behavior law is proposed for hyperelastic materials, such that damage induced anisotropy can be accounted for continuously. The full-network approach with directional damage is adopted as a starting point. The full-network law with elementary strain energy density based on the inverse Langevin is chosen as a reference law which is cast into the proposed framework. This continuum formalism is then rewritten using spherical harmonics to capture damage directionality. The proposed formalism allows for an efficient (and systematic) expansion of complex non-linear anisotropic constitutive laws. A low order truncated expression of the resulting behavior is shown to reproduce accurately the stress-strain curves of the exact behavior laws.

Contents

A.1 Introduction

Particle filled rubber-like materials combine large elastic deformations due to the macro-molecular network structure, and high strain at failure properties due to the filler contents. These remarkable mechanical properties contribute to their extensive use in various applications such as tires, shock absorbers, gaskets...

One of the main drawbacks to the use of filler-gum microstructures is the stress softening occurring during the first loading and referred as the Mullins effect (see reviews (Mullins, 1969; Diani et al., 2009)). This damage is irreversible under current use conditions. Along with stress softening, materials evidence induced anisotropy and residual strains, also known as permanent set. First mentioned by Mullins (1947, 1949), experimental evidences of the induced anisotropy were later reported (Laraba-Abbes et al., 2003; Hanson et al., 2005; Diani et al., 2006a; Kahraman et al., 2010). In particular, small specimens cut out of large pre-stretched samples show a direction-dependent behavior induced by the pre-stretch.

Among recent contributions on anisotropic hyperelasticity, let us cite Weiss et al. (1979), who defined, implemented and tested a 4 invariant strain energy density for transversely isotropic soft biological tissues. This density designed for transversely isotropic soft biological tissues, depends on 4 invariants, instead of 3 for isotropic materials. Using the same invariant approach, other strain energy densities were proposed serving the representation of transversely anisotropic hyperelastic materials (Itskov and Aksel, 2004; Limbert and Middlenton, 2004; Lu and Zhang, 2005; Guo and Sluys, 2006; deBotton et al., 2006). Dorfmann and Ogden (2004) also defined a 4-invariant strain energy density to model the Mullins induced anisotropy. The invariant approach may be used for simple anisotropy like transverse isotropy or orthotropy, but becomes tedious for general anisotropies such as the one induced by the Mullins effect (Menzel and Steinmann, 2001). In order to circumvent this difficulty, Göktepe and Miehe (2005) and Diani et al. (2006a) formulated a directional damage behaviour law, all directions of the space being approximated by a discrete set of 42 and 32 directions respectively. Also, Dargazany and Itskov (2009) adopted the same idea of directional damage with a partial 42-direction representation of the unity sphere, to introduce an anisotropic hyperelastic strain energy which supports a physical interpretation of the roles of the filler particles and the macromolecular chains (Govindjee and Simo, 1991, 1992).

Thus, there is now ample evidences, and a general consensus, for the need to resort to anisotropic damage in order to realistically account for the mechanical behaviour of rubber with fillers. However, the combined occurrence of various non-linearities, anisotropic damage and hyperelasticity, calls for complex formulations of the constitutive law, and leads to practical limitations in the identification of the constitutive law parameters and above all in numerical modeling implementation. The present work proposes a general framework using systematic series expansion for the previously introduced general directional damage law. Since the expansion is tailored to the expression of second order tensors such as stress and strain, low order truncations are expected to allow for an adjustable compromise between simplicity of the formulation (aiming at numerical implementation) and fidelity to the complex observed mechanical behaviour. This is our main motivation. In the current work, we will not account for the viscoelastic aspect of the stress-strain response of filled rubbers. Actually, filled rubbers may exhibit some hysteresis during the first cycle, even at moderate strain rates, but once the Mullins softening evacuated, the unloading and the reloading responses are fairly close and the hysteresis may be neglected. In such a case, the unloading stress-strain curve provides a good estimate of the softened material hyperelastic behaviour (Diani et al., 2006b). Here we will focus on the material behaviour after Mullins softening only.

Section A.2 defines the notations and basic concepts used in the sequel. The concept of directional damage in all space directions is introduced into the full-network hyperelastic model in Section A.3. This provides a continuous anisotropic hyperelastic behaviour whose strain energy

involves quadratures over the unit sphere. In Section A.4, a spherical harmonics expansion is adopted to circumvent the computation of those integrals, and gain efficiency. The resulting formulation is compact and explicit. Its convergence properties are illustrated over different loadings (uniaxial and biaxial loadings as well as pure shear). It is shown in Section A.5 that a very low order of expansion is required in order to match the stress-strain response of the chosen reference law. Section A.6 summarizes the proposed approach.

A.2   Notations

For clarity, we introduce here the notations used in the sequel. As far as anisotropy and directional dependencies will be a central issue, the polar angles (θ, φ) are introduced to represent the orientation of unit vectors $\boldsymbol{u}$,

$$\boldsymbol{u} = (\cos(\theta), \sin(\theta)\cos(\varphi), \sin(\theta)\sin(\varphi)) \tag{A.1}$$

The unit sphere is denoted as $\mathcal{S}$, and a uniform measure over it, representing solid angle is denoted as $\mathrm{d}^2\Omega \equiv \sin(\theta)\mathrm{d}\varphi\mathrm{d}\theta$.

It will be useful to introduce the projection operator along $\boldsymbol{u}$ as the dyadic product, $\boldsymbol{f}^{(2)} = \boldsymbol{u} \otimes \boldsymbol{u}$. Similarly, higher order tensor products of $\boldsymbol{u}$ with itself, $\boldsymbol{f}^{(n)}$, will be used

$$\boldsymbol{f}^{(n)} = \bigotimes_{i=1}^{n} \boldsymbol{u} \tag{A.2}$$

In order to describe the material deformation, the deformation gradient $\boldsymbol{F}$ and the right Cauchy-Green deformation tensor, $\boldsymbol{C} = \boldsymbol{F}^t\boldsymbol{F}$, are introduced (superscript ^{t} denotes transposition). The elongation along direction $\boldsymbol{u}$, $\lambda(\boldsymbol{u})$, is simply obtained from the right Cauchy-Green tensor, $\boldsymbol{C}$, as

$$\lambda(\boldsymbol{u}) = \sqrt{\boldsymbol{u}.\boldsymbol{C}.\boldsymbol{u}} = \sqrt{\boldsymbol{C} : \boldsymbol{f}^{(2)}} \tag{A.3}$$

In all the sequel, the elastomer is assumed to be incompressible. The Cauchy stress tensor is obtained from the elastic energy density, $\mathcal{W}$, through

$$\boldsymbol{\sigma} = \frac{\partial \mathcal{W}(\boldsymbol{F})}{\partial \boldsymbol{F}} \boldsymbol{F}^t - p\boldsymbol{I} \tag{A.4}$$

where p is the hydrostatic pressure.

It is of interest to distinguish the intensity of the loading, and its multiaxiality. For this aim, Henky tensor, $\boldsymbol{h} \equiv \frac{1}{2}\ln\boldsymbol{F}\boldsymbol{F}^t$, is introduced and its sorted eigenvalues are denoted by h_i ($h_1 \geq h_2 \geq h_3$). The following invariants, ρ and h_{eq}, are defined as

$$h_{\mathrm{eq}} \equiv \sqrt{\frac{2}{3}\left(h_1^2 + h_2^2 + h_3^2\right)} \qquad \text{and} \qquad \rho \equiv \frac{3\,h_2}{h_3 - h_1} \tag{A.5}$$

$h_{\mathrm{eq}} \geq 0$ is indicative of the intensity of the loading. In contrast $-1 \leq \rho \leq 1$, is a dimensionless parameter ranging from -1, for equibiaxial tension, to 1 for uniaxial tension. For pure shear, $\rho = 0$. Those notations are convenient to explore (and compare) different types of loadings.

A.3   Full-network model with directional damage

A.3.1   Hyperelastic full-network

An elastomer is a complex polymer network constituted of long macromolecules, spread in all the directions of space, which contribute to the global elasticity of the material. A simple mean-field idealized representation, initially proposed by Treloar and Riding (1979), is the full network

model . At each spatial point, a continuous distribution of chain orientation is considered, with a density $n(\boldsymbol{u})\mathrm{d}^2\Omega$. The active chain density in the reference state, n_0[1] is obtained from a summation over all directions,

$$n_0 = \iint_{\mathcal{S}} n(\boldsymbol{u})\mathrm{d}^2\Omega \tag{A.6}$$

Along each direction, parameterized by $\boldsymbol{u}$, a chain is assumed to be subjected to the elongation $\lambda(\boldsymbol{u})$ (Eq. (A.3)), for a homogeneous deformation gradient, $\boldsymbol{F}$. Introducing $w(\lambda)$, the elastic energy of a single chain under an elongation λ, the full elastic energy density, $\mathcal{W}(\boldsymbol{F})$, is written

$$\mathcal{W}(\boldsymbol{F}) = \iint_{\mathcal{S}} w(\lambda(\boldsymbol{u}))\, n(\boldsymbol{u})\mathrm{d}^2\Omega \tag{A.7}$$

By substitution of (A.3) in (A.7), the elastic energy density partial derivative comes as,

$$\frac{\partial \mathcal{W}}{\partial \boldsymbol{F}} = \iint_{\mathcal{S}} \left.\frac{\partial w(x)}{\partial x}\right|_{x=\lambda(\boldsymbol{u})} \frac{1}{2\lambda(\boldsymbol{u})} \frac{\partial\,(\boldsymbol{u}.\boldsymbol{C}.\boldsymbol{u})}{\partial \boldsymbol{F}}\, n(\boldsymbol{u})\,\mathrm{d}^2\Omega \tag{A.8}$$

Then, one easily finds that

$$\frac{\partial\,(\boldsymbol{u}.\boldsymbol{C}.\boldsymbol{u})}{\partial \boldsymbol{F}} = 2\boldsymbol{F}(\boldsymbol{u}\otimes\boldsymbol{u}) \tag{A.9}$$

and substituting (A.8) and (A.9) in (A.4), provides us with the following expression of the Cauchy stress tensor

$$\boldsymbol{\sigma} = \boldsymbol{F}\left(\iint_{\mathcal{S}} \left.\frac{\partial w(x)}{\partial x}\right|_{x=\lambda(\boldsymbol{u})} \frac{\boldsymbol{u}\otimes\boldsymbol{u}}{\lambda(\boldsymbol{u})}\, n(\boldsymbol{u})\mathrm{d}^2\Omega\right) \boldsymbol{F}^t - p\boldsymbol{I} \tag{A.10}$$

and simplifies into

$$\boldsymbol{\sigma} = \boldsymbol{F}\boldsymbol{G}\boldsymbol{F}^T - p\,\boldsymbol{I} \tag{A.11}$$

with

$$\boldsymbol{G} = \iint_{\mathcal{S}} \left.\frac{\partial w(x)}{\partial x}\right|_{x=\lambda(\boldsymbol{u})} \frac{\boldsymbol{u}\otimes\boldsymbol{u}}{\lambda(\boldsymbol{u})}\, n(\boldsymbol{u})\mathrm{d}^2\Omega \tag{A.12}$$

A.3.2 Specific hyperelastic law

Most of the formalism that follows can be applied to an arbitrary non-linear $w(\lambda)$. However, in order to illustrate the proposed methodology, a specific form of w introduced by Kuhn and Grün (1942) is chosen. Let N be the number of bonds of the chain, k the Boltzman constant and T the temperature. w reads

$$w(x) = NkT\left[\beta\mathcal{L}(\beta) + \ln\left(\frac{\beta}{\sinh(\beta)}\right)\right] \tag{A.13}$$

where

$$\beta = \mathcal{L}^{-1}\left(\frac{x}{\sqrt{N}}\right) \tag{A.14}$$

and $\mathcal{L}(x) \equiv \coth(x) - 1/x$ is the Langevin function. The expression of the force-elongation law takes a simple form

$$\frac{\mathrm{d}w(x)}{\mathrm{d}x} = \sqrt{N}kT\beta \tag{A.15}$$

---

[1]Let us note, that this parameter corresponds to $\nu/4\pi$ in the usual full-network law notation, with ν the active chain density

The inverse Langevin function can be Taylor-expanded to provide the following approximation at order m_L

$$\mathcal{L}^{-1}(x) = x \sum_{i=0}^{m_L} L_i x^{2i} \tag{A.16}$$

where the coefficients L_i are listed in Table A.1.

The above expansion gives the following force-elongation relationship

$$\frac{\mathrm{d}w(x)}{\mathrm{d}x} = xkT \sum_{i=0}^{m_L} L_i \left(\frac{x^2}{N}\right)^i \tag{A.17}$$

L_0	L_1	L_2	L_3	L_4	L_5	L_6	L_7	L_8	L_9
3	$\frac{9}{5}$	$\frac{297}{175}$	$\frac{1539}{875}$	$\frac{126117}{67375}$	$\frac{43733439}{21896875}$	$\frac{231321177}{109484375}$	$\frac{20495009043}{9306171875}$	$\frac{1073585186448381}{476522530859375}$	$\frac{4387445039583}{1944989921875}$

Table A.1: Taylor-expansion coefficients for the inverse Langevin function

It is to be noted that the Taylor expansion by definition gives a strong weight to the behaviour of the function at the origin. Let us note that other simplifications may be preferred. Cohen (1991) introduced a Padé approximant which is often used for its ability to reproduce the divergence of the inverse Langevin function. The algebraic form of the Padé approximant is however not the best suited to the following development and hence will not be used in the sequel to keep integrations simple.

A.3.3 Anisotropic damage law

Damage induced by Mullins effect might be mainly due to desorption of macromolecular chains from reinforcements, disentanglement, few chain breakage... In order to account for the Mullins effect, Marckmann et al. (2002) introduced a damage model with a spherical symmetry which was extended to the anisotropic case by Diani et al. (2006b). The main idea is to allow chain length to grow under the maximum stretch that has been experienced along its history. Such a damage essentially produces a merging of chains leading to fewer and/or longer chains. Diani et al. (2006b) proposed to account for such an effect by keeping the product $n(\boldsymbol{u})N(\boldsymbol{u})$ constant for all directions $\boldsymbol{u}$. To apply this idea, a continuous distribution of the chain lengths is considered in the same way as $n(\boldsymbol{u})$ in Eq. (A.6). At each spatial point the density distribution is $N(\boldsymbol{u})\mathrm{d}^2\Omega$ and the reference state N_0 is obtained from a summation over all directions,

$$N_0 = \iint_{\mathcal{S}} N(\boldsymbol{u})\mathrm{d}^2\Omega \tag{A.18}$$

Starting from an isotropic elastomer where the $n(\boldsymbol{u})N(\boldsymbol{u})$ product is independent of the orientation, the chain density in direction $\boldsymbol{u}$ can be written

$$n(\boldsymbol{u}, \lambda_{\max}(\boldsymbol{u})) = \frac{n_0 N_0}{N(\boldsymbol{u}, \lambda_{\max}(\boldsymbol{u}))} \tag{A.19}$$

where $\lambda_{\max}(\boldsymbol{u})$ is the maximum elongation encountered over the past in the direction $\boldsymbol{u}$. Thus under any load path other than a purely hydrostatic pressure, an anisotropy is induced in the material by such an orientation dependent damage. The elastic energy density introduced in Eq. (A.7) remains valid, and the directional damage is encoded in $n(\boldsymbol{u})$ or equivalently in $N(\boldsymbol{u})$.

A directional damage is defined here as

$$\delta(\boldsymbol{u}, \lambda_{\max}(\boldsymbol{u})) = 1 - \frac{N_0}{N(\boldsymbol{u}, \lambda_{\max}(\boldsymbol{u}))} \tag{A.20}$$

leading to

$$n(\boldsymbol{u}, \lambda_{\max}(\boldsymbol{u})) = n_0 \left(1 - \delta(\boldsymbol{u}, \lambda_{\max}(\boldsymbol{u})) \right) \qquad (A.21)$$

Note that albeit damage is here a non-dimensional variable varying from 0 (initial state) to 1 (fully damaged), it cannot be simply related to the reduction in free energy of the material, as defined classically (Simo, 1987).

Introducing both the Taylor expansion for the inverse Langevin function Eq. (A.17) and the damage Eq. (A.21) into Eq. (A.12) yields :

$$\boldsymbol{G} = n_0 kT \boldsymbol{g} \qquad (A.22)$$

with

$$\boldsymbol{g} = \sum_{i=0}^{m_L} L_i \iint_{\mathcal{S}} \left(\frac{\lambda^2}{N} \right)^i (u \otimes \boldsymbol{u}) \, (1 - \delta(\boldsymbol{u})) \, \mathrm{d}^2\Omega \qquad (A.23)$$

Then, by substituting Eq. (A.20) and making use of the tensor $\boldsymbol{f}^{(2)}$ defined Eq. (A.2), $\boldsymbol{g}$ transforms into,

$$\boldsymbol{g} = \sum_{i=0}^{m_L} \frac{L_i}{N_0^i} \iint_{\mathcal{S}} (\boldsymbol{C} : \boldsymbol{f}^{(2)})^i \boldsymbol{f}^{(2)} (1 - \delta(\boldsymbol{u}))^{i+1} \, \mathrm{d}^2\Omega \qquad (A.24)$$

In the latter equation, contributions of the deformation and of the directional damage can be split

$$\boldsymbol{g} = \boldsymbol{K}_0 + \boldsymbol{C} : \boldsymbol{K}_1 + (\boldsymbol{C} \otimes \boldsymbol{C}) :: \boldsymbol{K}_2 + ... \qquad (A.25)$$

where

$$\boldsymbol{K}_i = \frac{L_i}{N_0^i} \iint_{\mathcal{S}} \boldsymbol{f}^{(2i+2)} (1 - \delta(\boldsymbol{u}))^{i+1} \, \mathrm{d}^2\Omega \qquad (A.26)$$

and where :: denotes the doubly contracted tensorial product defined by $(\boldsymbol{A} :: \boldsymbol{B})_{ij} = A_{ijklmn} B_{klmn}$. When damage is not increasing, the tensors $\boldsymbol{K}$ of all orders remain constant and hence they do not involve new computation. The behaviour law is completely characterized once the directional damage evolution law is specified. In order to illustrate the above formalism on a documented example which has been shown to account quite precisely for the softening induced by a uniaxial tension, the damage law proposed by Diani et al. (2006a) will be used. It is written with the above notations

$$\delta(\boldsymbol{u}, \lambda_{\max}(\boldsymbol{u})) = \frac{\alpha(\lambda_{\max}(\boldsymbol{u}) - 1)^2}{1 + \alpha(\lambda_{\max}(\boldsymbol{u}) - 1)^2} \qquad (A.27)$$

α is a damage parameter and the evolution of δ according to the maximum encountered elongation is shown in Figure A.1.

Up to now, no approximation has been introduced, and hence, provided the series is summed up to a sufficient order, the exact law is obtained. However, the interest of the proposed approach is its ability to account for the constitutive law for a low order truncation of the infinite series, Eq. (A.24). Hence, a loading history exploring larger and larger $\lambda_{\max}$ is considered, and solved by a classic numerical integration with an increasing number of terms in the series. Figure A.2 shows the hyperelastic stress-strain responses of a material already submitted to various maximum elongations in uniaxial tension. Note that for uniaxial tension, $h_{\mathrm{eq}} = 1.3$ corresponds approximately to a 3.7 elongation along the tension direction.

It is observed that the convergence rate is quite fast. To quantify this rate the relative difference between consecutive orders of the truncated series approximation, $\sigma^{(m_L)}$, is computed, $\eta_{m_L} = \langle (\sigma^{(m_L)} - \sigma^{(m_L-1)}) / \sigma^{(m_L-1)} \rangle$. This dimensionless difference term is reported in Table A.2 and shown in Fig. A.2(right). An exponential convergence is observed. In the following the maximum considered order will be limited to $m_L = 3$.
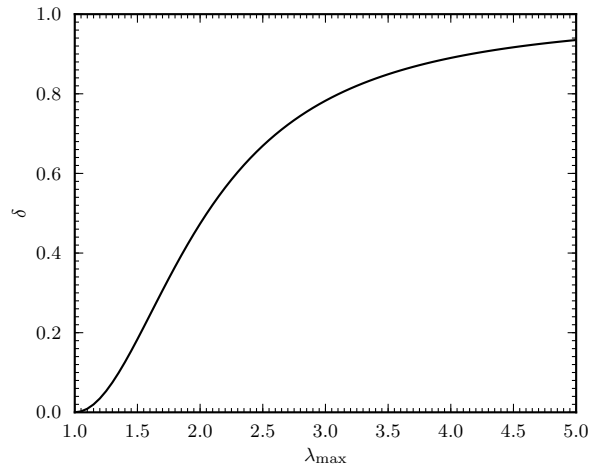
Figure A.1: Evolution of the directional damage δ according to the maximum applied elongation in this direction. The parameter α is set to 0.9.
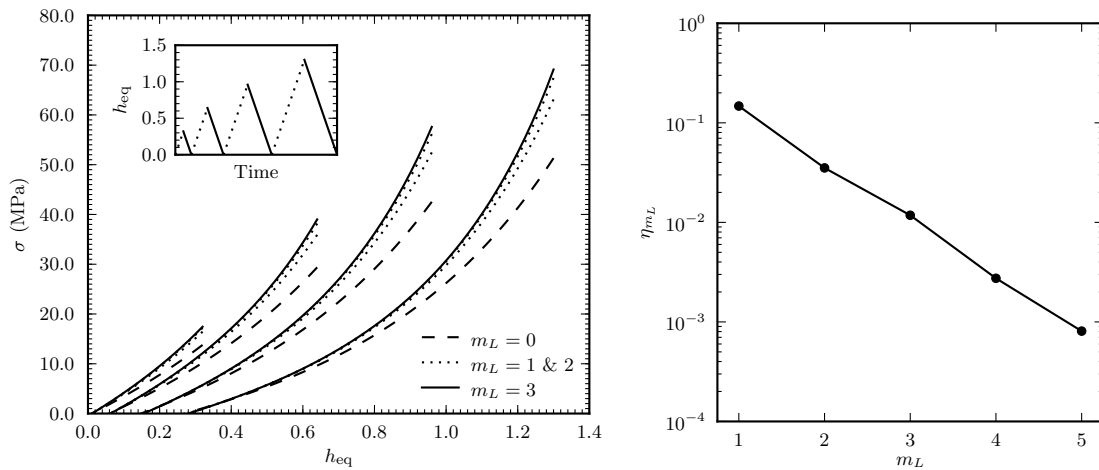

Figure A.2: Effect of the expansion order m_L of the inverse Langevin function, $\mathcal{L}^{-1}$. Left: Evolution of the stress-strain curves for uniaxial tension, following increasing values of $h_{\mathrm{eq}}^{\mathrm{max}}$. Right: Convergence as a function of the truncation order m_L. The quantity η is the mean absolute value of the relative difference in Cauchy stress for two consecutive truncation orders. The average is taken along the stress-strain curve followed after $h_{\mathrm{eq}}^{\mathrm{max}} = 1.3$. The used parameters are $N_0 = 5$, $\alpha = 0.9$ and $n_0 kT = 1$.

m_L	1	2	3	4	5
η_{m_L} (%)	15.	3.5	1.2	0.2	0.08

Table A.2: Relative error as a function of the truncation order, m_L.

It is worth noting that the directional damage introduces a residual strain after unloading to zero stress. At this rest state, a small strain approximation is valid as can be checked on Figure A.2. Hence, the stress can be approximated by its 0th order expansion, and hence $\boldsymbol{g} \approx K_0$. Exploiting the axisymmetry of the simple tension along the 1 axis, the diagonal components of

$\boldsymbol{g}$ can easily be computed

$$
\begin{aligned}
g_{11} &= 2\pi L_0 \int_{-1}^{1} \frac{c^2}{1+\alpha\left(\sqrt{1/a+(a^2-1/a)c^2}-1\right)^2} \, \mathrm{d}c \\
g_{22} = g_{33} &= \pi L_0 \int_{-1}^{1} \frac{(1-c^2)}{1+\alpha\left(\sqrt{1/a+(a^2-1/a)c^2}-1\right)^2} \mathrm{d}c
\end{aligned}
\tag{A.28}
$$

where a is the maximum elongation along the tensile axis.

At unloading, a zero stress implies that $\boldsymbol{F}\boldsymbol{g}\boldsymbol{F}^t$ is spherical. The residual strain is an isochoric elongation along the tension axis, and the elongation along the 1-axis is called λ_{res}. A simple computation yields

$$
\lambda_{\mathrm{res}} = \sqrt[3]{\frac{g_{22}}{g_{11}}}
\tag{A.29}
$$

Figure A.3 shows the stress-strain response after a uniaxial tension of the same intensity $h_{\mathrm{eq}} = 1.3$, for different values of α. The larger α is, the more pronounced the softening and the smaller the tangent modulus at zero stress are. Similarly, the residual deformation increases with α (Fig. A.3 right).
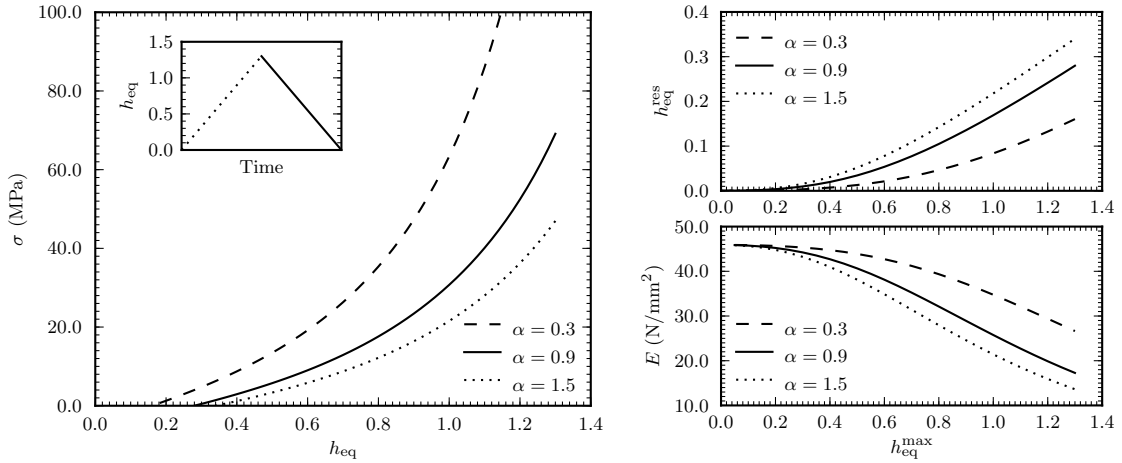

Figure A.3: Effect of the damage parameter α. Left: Model stress-strain responses for various values of α and a maximum strain history reaching $h_{\mathrm{eq}}^{\mathrm{max}} = 1.3$. Right: Evolutions of the residual deformation and the linear modulus at zero stress as a function of the maximum deformation intensity. The values of the model parameters are $N_0 = 5$, $n_0 kT = 1$, and the order of expansion of the inverse Langevin function is $m_L = 3$.

It is also of interest to compare the softening after different types of loading. The two extreme cases in terms of the dimensionless parameter ρ (A.5) are chosen, *i.e.* uniaxial versus equibiaxial tension. Figure A.4 shows the stress responses as a function of the loading intensity h_{eq}, together with the residual deformation $h_{\mathrm{eq}}^{\mathrm{res}}$ and the evolution of the tangent modulus at zero stress, E.

The presented approach thus allows to account precisely to a constitutive law which involves different non-linearities through the computation of different tensors which depends only on the maximum loading. However, the difficulty for its practical use is the computation of the different tensors which have to be evaluated numerically. Even for simple loadings, the number of such tensors increases quickly with the expansion order. The following section aims at reducing this computation task.
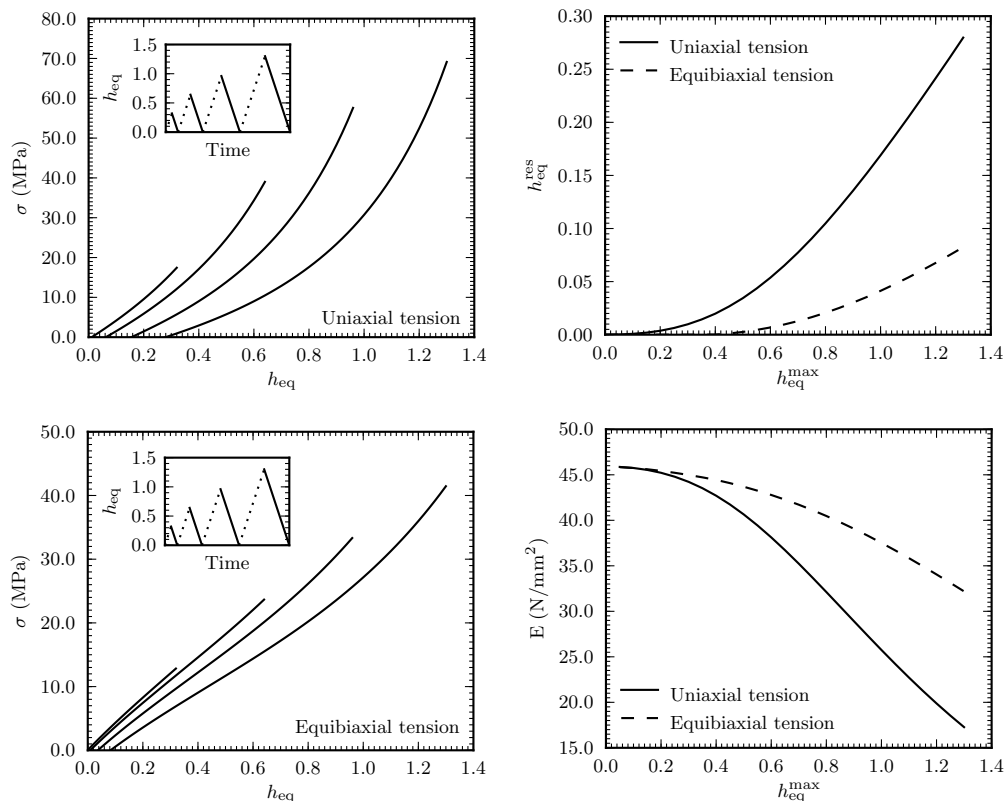
Figure A.4: Influence of loading type. Left: stress-strain curves after different maximum deformation characterized by the intensity h_{eq}. Right: evolution of the residual deformation and the linear modulus at zero stress, E, as a function of the maximum deformation intensity. The values of the parameters were $N_0 = 5$, $n_0 kT = 1$ and $\alpha = 0.9$, and the order of expansion of the inverse Langevin function is 3.

A.4 Spherical harmonic based damage definition

A.4.1 Constitutive equations

Spherical harmonics are the solution of the angular part of the Laplace equations in spherical coordinates (Byerly, 1959) and allows for the decomposition of an arbitrary scalar field on the surface of the unit sphere , $\mathcal{S}$. They are written as a double index series of functions $Y_l^m(\theta, \varphi)$ where the indices (l, m) are respectively called "order" and "degree" ($l \geqslant 0$ and $|m| \leqslant l$). They are conveniently expressed in terms of associated Legendre polynomials, P_l^m,

$$P_l^m(x) = \frac{(-1)^m}{2^l l!} \left(1 - x^2\right)^{l/2} \frac{\mathrm{d}^{l+m}}{\mathrm{d}x^{l+m}} \left(x^2 - 1\right)^l \tag{A.30}$$

and, as conventionally done in physics (Arfken, 1985), the following normalization is used

$$Y_l^m(\theta, \varphi) = \sqrt{\frac{(2l+1)(l-m)!}{4\pi(l+m)!}} \; P_l^m(\cos\theta) \; e^{im\varphi} \tag{A.31}$$

The spherical harmonics form an orthonormal basis of the Hilbert space of square-integrable functions. On the unit sphere, any square-integrable function can thus be expanded in spherical harmonic series. The expansion of $(1 - \delta(\boldsymbol{u}))$ on spherical harmonics introduces the double index

series of amplitudes ν_{lm}^{δ}

$$1 - \delta(\boldsymbol{u}) = \sum_{l=0}^{\infty} \sum_{m=-l}^{l} \nu_{lm}^{\delta} Y_l^m(\theta, \varphi) \tag{A.32}$$

where the amplitudes can be expressed as (Arfken, 1985)

$$\nu_{lm}^{\delta} = \iint_{\mathcal{S}} (1 - \delta(\boldsymbol{u})) \overline{Y}_l^m \mathrm{d}^2\Omega \tag{A.33}$$

where $\overline{Y}_l^m$ is the complex conjugate of Y_l^m. For symmetry reasons, only real parts of the coefficients of even orders and degrees are non-zero.

A spherical harmonic expansion of orientation tensors $\boldsymbol{f}^{(2n)}$ is performed in a similar way as in Eq. (A.33). This decomposition is finite and involves a maximum order of $2n$, without approximation. The amplitudes, denoted $\boldsymbol{\nu}_{lm}^{\boldsymbol{f}^{2n}}$ are tensors of order $2n$,

$$\boldsymbol{f}^{(2n)} = \sum_{l=0}^{2n} \sum_{m=-l}^{l} \boldsymbol{\nu}_{lm}^{\boldsymbol{f}^{2n}} Y_l^m \tag{A.34}$$

The expression of $\boldsymbol{f}^{(2)}$ and $\boldsymbol{f}^{(4)}$ expansions are given explicitly in Merckel et al. (2011e).

Tensors $\boldsymbol{K_p}$ (Eq. A.26) are thus expressed as

$$\boldsymbol{K}_p = \frac{L_p}{N_0^p} \iint_{\mathcal{S}} \left[\sum_{m=0}^{2p+2} \sum_{n=-m}^{m} \boldsymbol{\nu}_{mn}^{\boldsymbol{f}^{2p+2}} Y_m^n \right] \left[\sum_{q=0}^{\infty} \sum_{r=-q}^{q} \nu_{qr}^{\delta} Y_q^r \right]^{p+1} \mathrm{d}^2\Omega \tag{A.35}$$

Following the previous section, the inverse Langevin function is expanded up to order $m_L = 3$. Similarly, δ expansion is truncated at order $p_{\max}$. Hence 4 tensors, $\boldsymbol{K}_p$, are to be determined.

The integration of the product of several spherical harmonics is straightforward for two terms (spherical harmonics are orthonormal). For three terms, an analytical expression is available. A larger number of terms is more tedious to compute. It is worth devoting some discussion to the practical implementation of the above approach for low order elements. Let us emphasize that this procedure is independent of the type of loading and of its intensity.

The first term is $\boldsymbol{K}_0$ whose expression is

$$\boldsymbol{K}_0 = L_0 \sum_{\substack{0 \leq n \leq 2 \\ -n \leq m \leq n}} \sum_{\substack{0 \leq p \leq p_{\max} \\ -p \leq q \leq p}} \boldsymbol{\nu}_{nm}^{\boldsymbol{f}^2} \nu_{pq}^{\delta} \iint_{\mathcal{S}} Y_n^m Y_p^q \, \mathrm{d}^2\Omega \tag{A.36}$$

where the orthogonality properties of the spherical harmonics can be used to simplify

$$\iint_{\mathcal{S}} Y_n^m Y_p^q \, \mathrm{d}^2\Omega = (-1)^m \, \delta_{np} \delta_{m(-q)} \tag{A.37}$$

where the $(-1)^m$ factor can be dropped as only even values of m are to be considered. Finally,

$$\boldsymbol{K}_0 = L_0 \sum_{\substack{0 \leq n \leq 2 \\ -n \leq m \leq n}} \boldsymbol{\nu}_{n(-m)}^{\boldsymbol{f}^2} \nu_{nm}^{\delta} \tag{A.38}$$

For higher order terms, it is useful to resort to the Gaunt series (Gaunt, 1929), $G_{Lll'}^{Mmm'}$, which decomposes the product of two spherical harmonics into spherical harmonics

$$Y_l^m Y_{l'}^{m'} = \sum_{L,M} Y_L^M G_{Lll'}^{Mmm'} \tag{A.39}$$

where Gaunt coefficients can be expressed as

$$G_{Lll'}^{Mmm'} = \iint_{\mathcal{S}} \overline{Y}_L^M Y_l^m Y_{l'}^{m'} \, \mathrm{d}^2\Omega \tag{A.40}$$

Efficient numerical implementations of the Gaunt coefficient exist (see for instance Xu (1996)). Based on the Gaunt series, it is convenient to define the following "product", $\odot$,

$$(\nu \odot \nu)_{mn} \equiv \sum_{\substack{p \\ -p \leq q \leq p}} \sum_{\substack{r \\ -r \leq s \leq r}} G_{mpr}^{nqs} \nu_{pq} \nu_{rs} \tag{A.41}$$

Let us note that $\iint_{\mathcal{S}} Y_l^m d^2\Omega = \sqrt{4\pi}\delta_{l0}\delta_{m0}$, and hence $\boldsymbol{K}_0$ can be written as

$$\boldsymbol{K}_0 = \sqrt{4\pi} \, L_0 \left(\boldsymbol{\nu}^{\boldsymbol{f}^2} \odot \nu^\delta \right)_{00} \tag{A.42}$$

Let us now consider the next order tensor, $\boldsymbol{K}_1$

$$\boldsymbol{K}_1 = \frac{L_1}{N_0} \sum_{\substack{0 \leq n \leq 4 \\ -n \leq m \leq n}} \sum_{\substack{0 \leq p \leq p_{\max} \\ -p \leq q \leq p}} \sum_{\substack{0 \leq r \leq p_{\max} \\ -r \leq s \leq r}} \boldsymbol{\nu}_{nm}^{\boldsymbol{f}^4} \nu_{pq}^\delta \nu_{rs}^\delta \iint_{\mathcal{S}} Y_n^m Y_p^q Y_r^s \, \mathrm{d}^2\Omega \tag{A.43}$$

or

$$\boldsymbol{K}_1 = \sqrt{4\pi} \frac{L_1}{N_0} \left(\boldsymbol{\nu}^{\boldsymbol{f}^4} \odot (\nu^\delta \odot \nu^\delta) \right)_{00} \tag{A.44}$$

It is important to note that the inner "product" involves here squares ($\nu^\delta \odot \nu^\delta$). Similarly, higher order tensors, $\boldsymbol{K}_n$, will be computed from higher "powers" of ν^δ, which are to be constructed recursively from the operator $A \to \nu^\delta \odot A$ where A is a dummy spherical harmonic amplitude series.

The following orders do not introduce any new difficulties. Their expressions are given in Merckel et al. (2011e).

A.4.2 Convergence of the expansion

Figure A.5 shows the unloading responses of a body subjected to a uniaxial tension at different maximal extensions, for various order of the expansion of the damage δ. For a zeroth order expansion, the only spherical harmonic which is activated is Y_0^0, and hence damage is isotropic. Henceforth, no residual strain results. Higher orders lead to a non-zero residual strain as expected.

It is to be noted that the convergence is extremely fast. Expansions to order 2 and 4 are almost superimposed on the direct computation without spherical harmonics. In order to estimate the impact of subsequent orders, the computation was carried out up to order 6. The average of the absolute value of the difference between consecutive expansion orders all along the unloading path (from a maximum extension such that $h_{\mathrm{eq}}^{\max} = 1.3$, gives evaluations of the error η_p which are reported in Table A.3 for uniaxial tension. The accurate reproduction of the chosen law requires a fourth order expansion to reach a value less than 1%. However, in practice, the actual constitutive law is not known, and the proposed framework is to be fed by experimental observations in order to adjust the hyperelastic law and the damage growth law. Although such a procedure is not investigated in the present work, presumably a truncation to second order, $p_{\max} = 2$ should constitute a good compromise between sophistication of formulation and ease of implementation.

Damage is now defined through parameters ν_{lm}^δ which are dependent on the intensity and the type of loading. The next section is devoted to the comparison of these different loadings.
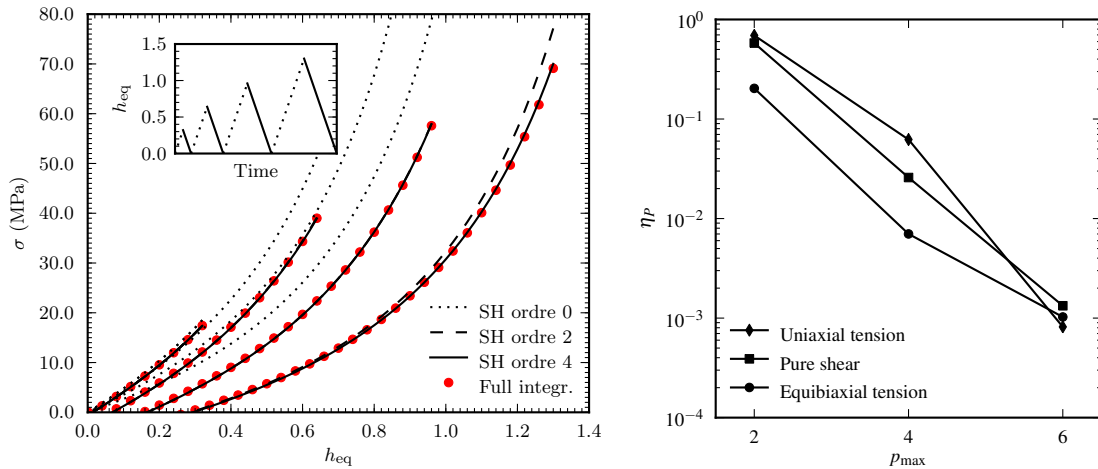
Figure A.5: Effect of spherical harmonics expansion order for the directional damage δ. Left: Evolution of the stress-extension in uniaxial tension following different maximum extensions $h_{\text{eq}}^{\max}$. The direct integration data is shown as a solid red curve. Right: Convergence rate as a function of the maximum spherical harmonics expansion order for δ for different types of loading. The parameter values are $N_0 = 5$, $\alpha = 0.9$ and $n_0 kT = 1$, and the order of expansion of $\mathcal{L}^{-1}$ is $m_L = 3$.

$p_{\max}$	$0 \to 2$	$2 \to 4$	$4 \to 6$
η_p (%)	69.	6.2	0.07

Table A.3: Relative error as a function of the truncation order $p_{\max}$.

A.5 Example of induced anisotropy

In order to illustrate the induced anisotropy as captured by the present framework, Figure A.6 shows the three dimensional surface of the spherical plot of $1 - \delta$ for three loadings (uniaxial tension, pure shear and equibiaxial tension) spanning the entire accessible range of the ρ parameter, Eq. (A.5). These damage surfaces were obtained for the same intensity, $h_{\text{eq}} = 1.3$ of loading, and a fourth order of the spherical harmonic expansion, $p_{\max} = 4$, was used.

These plots obtained with the spherical harmonic based damage model demonstrate the high level of anisotropy induced by the loading. They also show the dependence of the induced anisotropy on the type of loading. One notes that in terms of identification, the pure shear case looks similar to the uniaxial tension case, and hence carrying out tests for which ρ lies between 0 and 1 may not reveal helpful to discriminate among different anisotropic damage laws. In contrast, the equibiaxial loading appears to be significantly different.

In a similar spirit, one can evaluate the average value of $1 - \delta$ over all directions, as a function of the type and intensity of loading. The latter average is proportional to the amplitude of ν_{00}^{δ} since $Y_0^0 = (4\pi)^{-1/2}$ is constant over the unite sphere $\mathcal{S}$. Figure A.7 shows the progressive decrease of this coefficient with the intensity of loading, and compares different loading types through their ρ values. As in the previous figure, no much changes is observed as ρ varies from 0 to 1, again pointing to the similarity of pure shear and uniaxial tension loadings (in terms of the damage they induce). The α parameter controls the amplitude of damage: the higher α, the more damage for a given strain. Three values of α are shown in Figure A.7, and the graph shows that increasing α has the same qualitative influence as increasing h_{eq}.
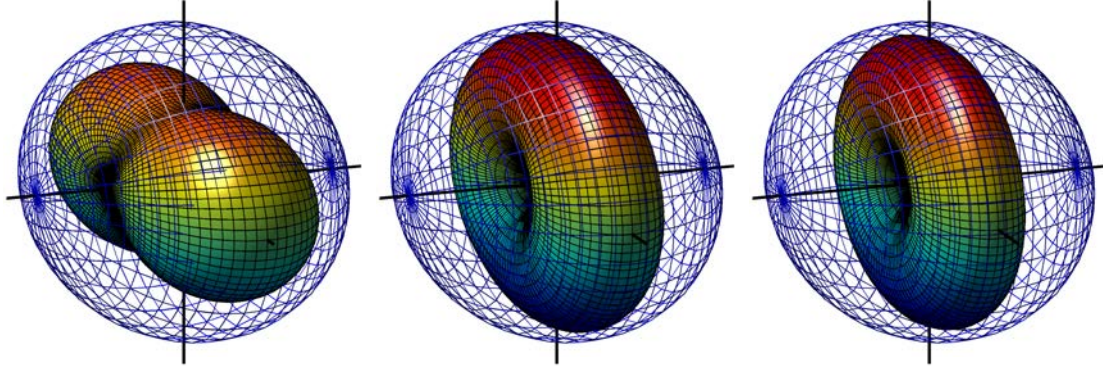
Figure A.6: 3D representation of $1 - \delta$ where δ is the directional damage for different types of loadings, $\rho = -1$, 0, and 1 respectively from left to right. The meshed unit sphere shows the initial (undamaged) state. The SH expansion order is limited to 4, and the loading intensity is $h_{\mathrm{eq}} = 1.3$. The damage parameter α is set to 0.9.
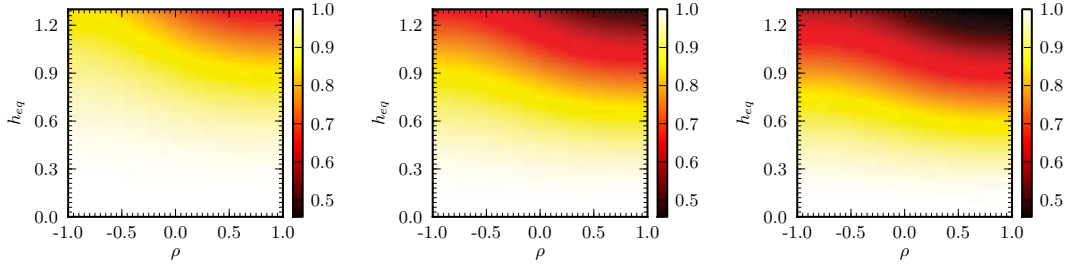

Figure A.7: Effect of the type, ρ, and intensity, h_{eq}, of loading on the spherical average of $(1 - \delta)$, equal to $(4\pi)^{-1/2}\nu_{00}^{\delta}$. The three plots shows the impact of the damage parameter $\alpha = 0.3$, 0.9 and 1.5 respectively from left to right.

A.5.1 Evolution of the ν_{lm}^{δ} parameters under loading

Figure A.8 shows for all types of loading, (indexed by ρ), and intensities, h_{eq}, ranging from 0 to 1.3, the evolution of all 10 non-zero amplitudes ν_{lm}^{δ}, for an expansion of δ up to order six. (At fourth order, the top 6 amplitudes ν_{lm}^{δ} would remain.)

Those graphs give the amplitude of variation of the amplitudes ν_{lm}^{δ} for realistic loadings. They can easily be ranked according to their order of magnitude, and hence their respective influence on the stress value. The amplitude ν_{00}^{δ} is the only one to be of order unity. The following ν_{20}^{δ}, ν_{22}^{δ} and ν_{40}^{δ} are about a factor 10 smaller. All others ν_{42}^{δ}, ν_{44}^{δ}, and all sixth order amplitudes are of order 10^{-2}. These observations are useful guidelines for a practical implementation when a minimum number of terms is sought.

A.6 Summary

Let us summarize the actual implementation of the above formulation for practical use. First, the two truncation orders, m_L and $p_{\max}$, are to be defined. Let us first assume that the local damage state is known under its spherical harmonics form, ν_{nm}^{δ}. The tensors $\boldsymbol{K}$ are computed recursively from the calculus of higher powers of ν^{δ}, $(\bigodot_1^p \nu^{\delta})$, and of the corresponding decomposition of $\boldsymbol{f}^{(2n)}$. The strain state being characterized by the right Cauchy-Green tensor, $\boldsymbol{C}$, the $\boldsymbol{g}$ tensor is obtained from Eq. (A.25). Hence the Cauchy stress, $\boldsymbol{\sigma}$, Eq. (A.11), is obtained for any deformation state.
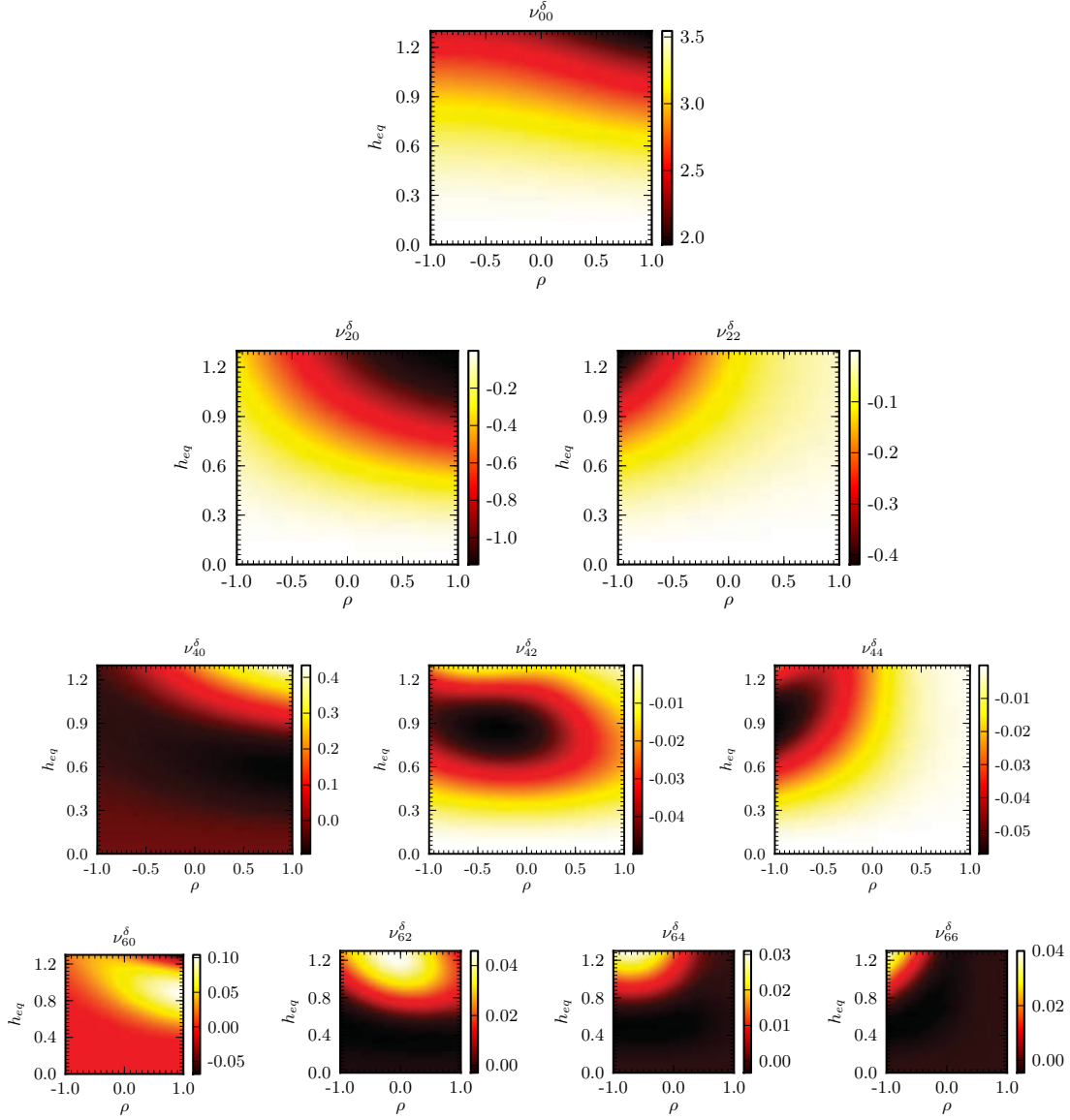
Figure A.8: Evolution of all non-zero amplitudes ν_{lm}^{δ} for an expansion of δ at the 6th order. The loading is parameterized in each graph by its type, ρ, and its intensity, h_{eq}. The damage parameter α is set to 0.9.

The only remaining difficulty is the updating of the damage. If all the information, $\delta(\boldsymbol{u})$, had been kept then this step would have been straightforward. Namely at time $t + \mathrm{d}t$, the directional damage is simply

$$\delta^{t+\mathrm{d}t}(\boldsymbol{u}) = \max\left(\delta^{t}(\boldsymbol{u}), \delta(\boldsymbol{u})\right) \tag{A.45}$$

where $\delta^{t}(\boldsymbol{u})$ is the actual damage in direction $\boldsymbol{u}$ at time t and $\delta(\boldsymbol{u})$ is the instantaneous directional damage along the same direction based on the deformation state at time $t + \mathrm{d}t$. The difficulty is that ν^{δ} is now known only from its truncated spherical expansion. Hence, a weak form of the above maximum law is needed. Note that a similar difficulty is present when ν^{δ} over the unit sphere is only characterized by a discrete set of directions. It is suggested to exploit the fact that the function $\Delta\delta(\boldsymbol{u}) = \delta^{t+\mathrm{d}t}(\boldsymbol{u}) - \delta^{t}(\boldsymbol{u})$ has to be positive over $\mathcal{S}$. Since only the spherical

harmonic decomposition is known, a possible weak form is that for any (l, m)

$$\iint_{\mathcal{S}} \Delta\delta(\boldsymbol{u}) Y_l^m \overline{Y_l^m} \, \mathrm{d}^2\Omega \geq 0 \tag{A.46}$$

This integral can be transformed using Gaunt's coefficients, so that for all pairs (l, m) (taken in the same set of indices as the considered non-zero amplitudes of ν^δ)

$$\sum_{pq} (-1)^m G_{pll}^{qm(-m)} \nu_{pq}^{\Delta\delta} \geq 0 \tag{A.47}$$

where $\nu^{\Delta\delta}$, the spherical harmonics amplitude of $\Delta\delta(\boldsymbol{u})$, is nothing but the difference of the spherical harmonics amplitude of $\delta^{t+\mathrm{d}t}(\boldsymbol{u})$ and $\delta^t(\boldsymbol{u})$.

Those elements provide a consistent framework to work directly with the spherical harmonics amplitudes ν^δ without having to revert to real space.

Further simplifications occurs when additional assumptions are proposed such as fixed principal axes (for strain and damage). In this case, a number of terms in the expansion cancel exactly due to symmetry. A more general case is also of interest when tests are carried out on thin rubber sheets. In this case, one principal axis (normal to the specimen), remains invariant. An appropriate choice consists in choosing the 1-axis along the normal. In this case, a rotation within the plane only affect the φ angle, and in the spherical harmonics case, it corresponds to a simple phase shift (for each θ angle, the SH transform is nothing but a Fourier transform).

A.7 Conclusion

Anisotropic damage and hyperelasticity related through an arbitrary directional law, have been cast into a tensorial formalism, accounting for a continuous distribution of direction orientations. Deformation and elastic properties are naturally split. This expansion which exploits a polynomial development of the stress/strech relation can be truncated to any desired order, m_L. The different tensors $\boldsymbol{K}$ (to be contracted with $\boldsymbol{C}$ to form the tangent elastic properties) can be further decomposed over a spherical harmonic basis, itself to be truncated to an arbitrary order, $p_{\max}$. The resulting formalism allows for a compact representation of a class of constitutive law which is intrinsically quite complex.

This representation has been applied to a specific law, already proposed in the literature, to show that a low order expansion (for m_L and $p_{\max}$) gives a very accurate account of stress-strain laws up to large strains. In practice, the hyperelastic and damage laws are to be identified from experimental tests, and hence it is important to have a given framework which can be either restricted or expanded at will, depending on the available information, so that identification can be treated as a well-posed problem. In particular, field measurements may provide the required experimental data for this purpose.

Caractérisation expérimentale et modélisation du comportement mécanique d'élastomères chargés sous conditions de chargement cycliques

Les applications pour lesquelles des élastomères sont soumis à des sollicitations cycliques sont nombreuses. Des charges sont généralement utilisées afin d'améliorer leurs propriétés, cependant, elles induisent également un adoucissement important de la contrainte lors de sollicitations cycliques. A ce jour, les phénomènes physiques conduisant à l'apparition de cet adoucissement ne sont pas clairement établis et sa modélisation demeure une difficulté majeure.

Afin d'étudier l'adoucissement, des élastomères chargés sont soumis à des chargements cycliques. Des méthodes de caractérisations originales sont proposées afin de quantifier les effets de l'intensité du chargement et du nombre de cycles. Pour faire le lien avec la microstructure du matériau, plusieurs mélanges de compositions différentes sont utilisés.

Des chargements non proportionnels de traction uniaxiale et biaxiale sont appliqués afin de mettre en évidence l'anisotropie induite par l'adoucissement. Ces données expérimentales non conventionnelles sont utilisées afin de définir un critère général pour l'activation de l'adoucissement Mullins. Une loi de comportement fondée sur une analyse approfondie des données expérimentales est proposée. La modélisation est basée sur une approche directionnelle. L'adoucissement Mullins est modélisé en utilisant le concept d'amplification de la déformation et son activation est pilotée par un critère directionnel. La capacité du modèle à prédire les réponses d'un matériau ayant subi un historique de chargement non proportionnel est validée.

Mots clés : Elastomères chargés - Caractérisation expérimentale - Loi de comportement - Hyperélasticité - Adoucissement Mullins - Adoucissement cyclique - Anisotropie induite

Experimental characterization and modeling of the mechanical behavior of filled rubbers under cyclic loading conditions

Rubber-like materials are submitted to cyclic loading conditions in various applications. Fillers are always incorporated within rubber compounds. They improve the mechanical properties but induce a significant stress-softening under cyclic loadings. The physical source of the softening is not yet established and its modeling remains a challenge.

For a better understanding of the softening, filled rubbers are submitted to cyclic loadings. In order to quantify the effects of the loading intensity and the number of cycles, original methods are proposed to characterize the softening. To study the influence of the material microstructure on the softening, compounds with various compositions are considered.

Non-proportional tensile tests including uniaxial and biaxial loading paths are applied in order to highlight the softening induced anisotropy. Such unconventional experimental data are used to provide a general criterion for the softening activation. A constitutive modeling grounded on a thorough analysis of experimental data is proposed. The model is based on a directional approach. The Mullins softening is accounted for by the strain amplification concept and is activated by a directional criterion. The model ability to predict non-proportional softened material responses is demonstrated.

Key words: Filled rubber - Experimental characterization - Constitutive modeling - Hyperelasticity - Mullins softening - Cyclic softening - Induced anisotropy